frontiers | Research Topics

Advances in nutrition, food processing and monitoring

Edited by
Zoltan Kovacs, John-Lewis Zinia Zaukuu, George Bazar and László Abrankó

Published in
Frontiers in Nutrition

ISSN 1664-8714
ISBN 978-2-8325-2239-4
DOI 10.3389/978-2-8325-2239-4

About Frontiers

Frontiers is more than just an open access publisher of scholarly articles: it is a pioneering approach to the world of academia, radically improving the way scholarly research is managed. The grand vision of Frontiers is a world where all people have an equal opportunity to seek, share and generate knowledge. Frontiers provides immediate and permanent online open access to all its publications, but this alone is not enough to realize our grand goals.

Frontiers journal series

The Frontiers journal series is a multi-tier and interdisciplinary set of open-access, online journals, promising a paradigm shift from the current review, selection and dissemination processes in academic publishing. All Frontiers journals are driven by researchers for researchers; therefore, they constitute a service to the scholarly community. At the same time, the *Frontiers journal series* operates on a revolutionary invention, the tiered publishing system, initially addressing specific communities of scholars, and gradually climbing up to broader public understanding, thus serving the interests of the lay society, too.

Dedication to quality

Each Frontiers article is a landmark of the highest quality, thanks to genuinely collaborative interactions between authors and review editors, who include some of the world's best academicians. Research must be certified by peers before entering a stream of knowledge that may eventually reach the public - and shape society; therefore, Frontiers only applies the most rigorous and unbiased reviews. Frontiers revolutionizes research publishing by freely delivering the most outstanding research, evaluated with no bias from both the academic and social point of view. By applying the most advanced information technologies, Frontiers is catapulting scholarly publishing into a new generation.

What are Frontiers Research Topics?

Frontiers Research Topics are very popular trademarks of the *Frontiers journals series*: they are collections of at least ten articles, all centered on a particular subject. With their unique mix of varied contributions from Original Research to Review Articles, Frontiers Research Topics unify the most influential researchers, the latest key findings and historical advances in a hot research area.

Find out more on how to host your own Frontiers Research Topic or contribute to one as an author by contacting the Frontiers editorial office: frontiersin.org/about/contact

Advances in nutrition, food processing and monitoring

Topic editors

Zoltan Kovacs — Hungarian University of Agricultural and Life Sciences, Hungary
John-Lewis Zinia Zaukuu — Kwame Nkrumah University of Science and Technology, Ghana
George Bazar — University of Kaposvár, Hungary
László Abrankó — Szent István University, Hungary

Topic coordinator

Isaac Amoah — Kwame Nkrumah University of Science and Technology, Ghana

Citation

Kovacs, Z., Zaukuu, J.-L. Z., Bazar, Z., Abrankó, L., eds. (2023). *Advances in nutrition, food processing and monitoring*. Lausanne: Frontiers Media SA.
doi: 10.3389/978-2-8325-2239-4

Table of contents

frontiers | Frontiers in Nutrition

TYPE Editorial
PUBLISHED 11 April 2023
DOI 10.3389/fnut.2023.1179597

OPEN ACCESS

EDITED AND REVIEWED BY
Elena Ibañez,
Institute of Food Science Research (CSIC), Spain

*CORRESPONDENCE
Zoltan Kovacs
✉ kovacs.zoltan.food@uni-mate.hu

SPECIALTY SECTION
This article was submitted to Nutrition and Food Science Technology, a section of the journal Frontiers in Nutrition

RECEIVED 04 March 2023
ACCEPTED 27 March 2023
PUBLISHED 11 April 2023

CITATION
Zaukuu J-LZ, Amoah I, Bazar G, Abrankó L and Kovacs Z (2023) Editorial: Advances in nutrition, food processing and monitoring. *Front. Nutr.* 10:1179597. doi: 10.3389/fnut.2023.1179597

Editorial: Advances in nutrition, food processing and monitoring

John-Lewis Zinia Zaukuu[1], Isaac Amoah[2], George Bazar[3], László Abrankó[4] and Zoltan Kovacs[5]*

[1]Department of Food Science and Technology, Faculty of Bio-sciences, College of Science, Kwame Nkrumah University of Science and Technology, Kumasi, Ghana, [2]Department of Biochemistry, Faculty of Bio-sciences, College of Science, Kwame Nkrumah University of Science and Technology, Kumasi, Ghana, [3]Adexgo Kft, Balatonfüred, Hungary, [4]Department of Food Chemistry and Analysis, Institute of Food Science and Technology, Hungarian University of Agriculture and Life Sciences, Budapest, Hungary, [5]Department of Measurements and Process Control, Institute of Food Science and Technology, Hungarian University of Agriculture and Life Sciences, Budapest, Hungary

KEYWORDS

modeling, nutritional intervention, functional foods, spectroscopy, NIRS

Editorial on the Research Topic
Advances in nutrition, food processing and monitoring

In recent decades, several efforts aimed at providing an understanding of the developing trends of nutrition in an ever-increasing population have been reported. This is mainly because there has been an increased consumer demand for enriched foods, special diets, and functional foods due to growing health concerns. Consumers have become more interested in foods with added value that can be used for nutritional interventions (1).

Consequently, there have been rapid advances in methodologies and technologies geared toward improving efficiency and outcomes in the field of nutrition and food processing. These advances have resulted in the development of several novel methods and portable point-of-care devices whose operations have largely depended on advances in science, involving a blend of biology, chemistry, and physics. Some of these methods and techniques include advanced drying techniques, chromatographic approaches, spectrometry and spectroscopy, sensor-based devices, and nanotechnologies (2).

This editorial provides details about the Research Topic which brought together a list of original papers published on advances made in nutrition, food processing, new food product development, and the use of spectroscopic-based devices for the monitoring of the attributes of these newly developed food products to combat nutritional deficiencies.

Globally, an estimated two billion people suffer from a chronic deficiency of micronutrients (3). Even deficiencies in a mild to moderate context have been reported to be capable of resulting in impaired physical and cognitive abilities, poor physical growth, and work impairments, which could all be considered as hidden hunger. Diet quality, therefore, is an important determinant of the development of diet-related chronic diseases (4). Consequently, there has been a need for the food industry to reformulate foods to improve their healthiness. Csurka et al. researched the prospect of valorizing powdered blood from livestock as a substitute for egg allergen in the preparation of sponge cakes and investigated the physicochemical properties of the cake. The authors reported that cakes enriched with blood products were not different in preference, compared to the control non-enriched counterparts. However, the addition of powdered blood products to cakes increased their hardness, compared to the control sample. The storability properties of the cakes were negatively affected after 3 days of storage. Food processing impacts the matrix composition, resulting in changes in physicochemical properties and could potentially improve the shelf-life of the food.

Tassy et al. investigated the nutritional quality of packaged foods launched globally between 2016 and 2018 and those launched between 2018 and 2020, as reported in the Mintel Global New Products Database. The authors compared these two time periods in order to determine whether there has been recent improvement in food reformulation to improve their healthiness using indicators including proteins, fibers, sugars, saturated fatty acids, and sodium. The authors pointed out that food reformulation to improve the healthiness of packaged food, especially through reductions in the sodium and sugar content was observed in the period under study.

The effect of the processing method on the nutritional composition of eggs produced by chickens has been investigated (Pirkwieser et al.). The authors investigated the effect of pasteurization and spray drying on the nutritional profile of eggs from hens. No changes in total fat content, amino acid profile, α- and δ-tocopherol, lutein, zeaxanthin, essential trace elements, and cobalamin following the use of the spray-drying method were observed. These highlights spray drying as an effective processing method to maintain the nutritional integrity of eggs.

The type of food processing method employed impacts the structural modification of the matrix of the food. This property can be exploited to improve the health-promoting properties of newly developed food products. The effect of the consumption of steamed potato flour used in composite formulation with wheat for bread development on metabolic indices has been investigated. Xu et al. conducted a randomized controlled trial that assessed the effect of the acute intake (4 weeks) of steamed potato-wheat bread on weight, lipids, glucose, and Na+/K+ concentrations. The authors observed significant reductions in body weight, lipid weight ($p = 0.016$), body mass index ($p = 0.020$), low-density lipoprotein cholesterol ($p = 0.035$), and the urinary level of Na+/K+ ($p = 0.007$).

In the food processing and product development space, the use of these devices has resulted in maintaining quality standards in the nutritional, physicochemical, and sensorial integrity of newly developed food products. Near-infrared spectroscopy (NIRS) is one common and essential technique that has been used to track food product quality in recent times. Largely, NIRS devices operate using spectroscopic principles and have a potential for non-invasive and on-field analysis using their handheld/portable versions or in-line setup when automated measurements can be performed. They can therefore serve as a buffer to keep pace with the novel trends of food fortification and product development.

For example, Li et al. established a deep neural network method to classify navel orange surface defects and subsequent automated classifications of fruits with a normal vs. defective surface. They used Standard Normal Variate (SNV) transformation to eliminate baseline drift and an independent component analysis-genetic algorithm to classify the defective surfaces. In their conclusion, wavelength selection was crucial in obtaining good classification accuracies. However, only images from the upper surface of the navel orange were collected, while lower surface images were not. Therefore, a major research focus includes capturing and analyzing images of the entire surface of navel oranges in subsequent online detection work.

Yali pears are fruits with high nutrients and sensory qualities but are often subjected to attacks by pests due to the improper nursing of pear trees. An online rapid non-destructive detection method for internal defects of Yali pears based on Vis-NIR was proposed based on a deep learning model for monitoring Yali pear quality in a bid to guarantee a high level of sorting of the fruits (Hao et al.). The results showed that the online discriminant model established based on spectra pretreated by Savitzky-Golay Smoothing combined with Convolutional Block Attention Module-Convolutional Neural Networks (CBAMCNN) deep learning method yielded the highest accuracy where the calibration set and validation set had values of 96.88 and 92.71%, respectively. The rapidness of the technique was also proven with a prediction time of 0.032 s for a single Yali pear. The deep learning method makes full use of its autonomous feature extraction and learning ability.

In advancing the scope of NIRS for the complex analysis of moist substances such as many foods and food raw materials, emerging data analysis techniques such as aquaphotomics have also been explored. Aquaphotomics is a technique that simply uses the electromagnetic spectrum of water as a molecular mirror for advanced analysis with NIRS. This method was recently applied to monitor the quality changes of the strawberry fruit during storage in a refrigerator with an electric field generator (supercooling fridge, SCF) and without it (control fridge, CF) (Muncan et al.). From their results, strawberries in CF and SCF showed that exposure to an electric field leads to a delay in ripening by around 3 days. This was evidenced by the increased amount of structural, strongly bound water and vapor-like trapped water in the strawberries stored in SCF.

Different regression techniques were compared for the prediction of the total acidity (TA) of intact mangos (5). It was observed that partial least squares regression, support vector machine, and artificial neural networking could all predict TA with good accuracy. However, the highest coefficient of the determination for TA prediction: 0.985 in calibration and 0.943 in prediction was achieved using the artificial neural networks (ANN) approach. ANN also proved to be the best in terms of the RPD index [Ratio of the standard error of Performance (or prediction) to standard Deviation] reaching 4.02.

In conclusion, designing and implementing nutrition-focused interventions have often involved the use of carefully designed methodologies such as randomized controlled trials, case-control studies, and cross-sectional studies. However, achieving good nutrition depends on and encompasses the entire food supply; this is the backbone of food processing and monitoring techniques. Nutrition, food processing, and monitoring have evolved significantly during the last decades in theory and practice, particularly due to urbanization and an increasing global population. NIRS has proven to be a powerful tool as acknowledged by numerous researchers for being non-invasive and non-destructive but still providing rapid feedback. The technique, when applied in tandem with the novel data analysis approaches, promises to be a good method for food quality evaluations. The editors would like to thank all authors and reviewers for their contributions to this Research Topic.

Author contributions

All authors listed have made a substantial, direct, and intellectual contribution to the work and approved it for publication.

Conflict of interest

GB was employed by Adexgo Kft.

The remaining authors declare that the research was conducted in the absence of any commercial or financial relationships that could be construed as a potential conflict of interest.

Publisher's note

All claims expressed in this article are solely those of the authors and do not necessarily represent those of their affiliated organizations, or those of the publisher, the editors and the reviewers. Any product that may be evaluated in this article, or claim that may be made by its manufacturer, is not guaranteed or endorsed by the publisher.

References

1. Topolska K, Florkiewicz A, Filipiak-Florkiewicz A. Functional food–consumer motivations and expectations. *Int J Environ Res Public Health*. (2021) 18:5327. doi: 10.3390/ijerph18105327

2. Valoppi F, Agustin M, Abik F, Morais de Carvalho D, Sithole J, Bhattarai M, et al. Insight on current advances in food science and technology for feeding the world population. *Front Sustain Food Syst*. (2021) 5:1–17. doi: 10.3389/fsufs.2021.626227

3. Nair MK, Augustine LF, Konapur A. Food-based interventions to modify diet quality and diversity to address multiple micronutrient deficiency. *Front Public Heal*. (2016) 3:1–14. doi: 10.3389/fpubh.2015.00277

4. Afshin A, Sur PJ, Fay KA, Cornaby L, Ferrara G, Salama JS, et al. Health effects of dietary risks in 195 countries, 1990–2017: A systematic analysis for the Global Burden of Disease Study 2017. *Lancet*. (2019) 393:1958–72.

5. Munawar AA, Zulfahrizal Meilina H, Pawelzik E. Near infrared spectroscopy as a fast and non-destructive technique for total acidity prediction of intact mango: comparison among regression approaches. *Comput Electron Agric*. (2022) 193:106657. doi: 10.1016/j.compag.2021.106657

frontiers | Frontiers in Nutrition

TYPE Original Research
PUBLISHED 25 August 2022
DOI 10.3389/fnut.2022.987285

OPEN ACCESS

EDITED BY
John-Lewis Zinia Zaukuu,
Kwame Nkrumah University of Science and Technology, Ghana

REVIEWED BY
Elisa Julianti,
Universitas Sumatera Utara, Indonesia
Souravh Bais,
Adina Institute of Science and Technology (AIST), India

*CORRESPONDENCE
Haiquan Xu
xuhaiquan@caas.cn
Junmao Sun
sunjunmao@caas.cn

SPECIALTY SECTION
This article was submitted to Nutrition and Food Science Technology, a section of the journal Frontiers in Nutrition

RECEIVED 06 July 2022
ACCEPTED 11 August 2022
PUBLISHED 25 August 2022

CITATION
Xu H, Guo Y, Cai S, Wang X, Qu J, Ma Y, Fang H and Sun J (2022) The effect of steamed potato-wheat bread intake on weight, lipids, glucose, and urinary Na^+/K^+: A randomized controlled trial in Chinese adults. *Front. Nutr.* 9:987285. doi: 10.3389/fnut.2022.987285

The effect of steamed potato-wheat bread intake on weight, lipids, glucose, and urinary Na^+/K^+: A randomized controlled trial in Chinese adults

Haiquan Xu[1]*, Yanzhi Guo[1], Shaolun Cai[1], Xiuli Wang[1], Junling Qu[1], Yunqian Ma[1], Hongyun Fang[2] and Junmao Sun[1]*

[1]Institute of Food and Nutrition Development, Ministry of Agriculture and Rural Affairs, Beijing, China, [2]National Institute for Nutrition and Health, Chinese Center for Disease Control and Prevention, Beijing, China

Steamed potato bread has received much attention from nutritionists and agriculturalists since it became a staple food of China in 2015. Epidemiological studies have indicated that potatoes may cause diabetes and hypertension, but few trials have evaluated this effect. Through a clinical trial, we evaluated the effect of steamed potato bread intake on adults. In total, 49 and 30 individuals were assigned to the intervention and control groups, respectively. Potato-wheat bread (raw wheat flour and cooked potato flour in the ratio 3:7) and steamed wheat bread (100% raw wheat flour) were provided to the intervention and control groups, respectively, once a day for 4 weeks. Compared with the control group, the intervention group showed significant net changes in weight (−0.6 kg; 95% confidence interval [CI]: −1.2, −0.1; $p = 0.016$), body mass index (BMI, −0.2 kg/m^2; 95% CI: −0.4, −0.1; $p = 0.020$), low-density lipoprotein cholesterol (LDL-c, −0.22 mmol/L; 95% CI: −0.49, −0.01; $p = 0.035$), and the urinary level of Na^+/K^+ (−2.4; 95% CI: −4.1, −0.7; $p = 0.007$). In conclusion, the steamed potato-wheat bread intake for 4 weeks resulted in decreases in weight, BMI, LDL-c, and the urinary Na^+/K^+ level among Chinese adults.

KEYWORDS

potato staple food, potato bread, glucose, lipids, BMI, urinary Na^+/K^+

Introduction

Potato is one of the most essential food crops, and more than 1 billion people consume it worldwide (1). Although potato consumption is currently the highest in Western countries, it is rapidly becoming a staple food in some other regions. For example, in China, potato has received much attention from nutritionists and agriculturalists recently. In 2015, potato was promoted as a staple food through a food policy and has been included in the Dietary Guidelines for Chinese Residents (2016 edition) (2).

Although potatoes are considered healthy and nutritious, they have a high glycemic index (GI) and glucose load (GL) (3, 4). Some studies have noted a significant association of high GI diet and GL with an increased risk of type 2 diabetes (T2D) (5–7). Furthermore, a meta-analysis revealed a significantly positive association between high consumption of potatoes and risk of T2D, especially through the consumption of French fries (8). Moreover, starch in potatoes becomes digestible on heating, which can raise glucose levels (9).

Since 2015, various food processing enterprises and scientific research institutes have actively invested in using potatoes in noodles, rice noodles, bread, biscuits, and other foods that are part of the Chinese diet. The production of staple foods with potatoes has increased to make foods nutritious. Since the potato staple food policy being proposed by China, many researches have demonstrated the feasibility of this policy (10, 11). However, the effect of potato as a staple food on Chinese people is lacking. Among adolescents, consumption of potato staple food positively affected the total cholesterol (CHO) and insulin profiles but negatively affected the systolic blood pressure (SBP) and high-density lipoprotein cholesterol (HDL-c) (12). However, no trial has been conducted to evaluate the effect of Chinese potato staple food intake among adults, especially in the form of secondary processing production. Hence, more studies are required to determine the effect of potato staple food on human health. Glucose and lipids were hypothesized to not increase abnormally and the urinary Na^+/K^+ levels were hypothesized to decrease after frequent intake of potato-wheat bread in adults. Then, this study assessed the effect of steamed potato-wheat bread intake on blood glucose, lipids, blood pressure, and urinary Na^+/K^+ in adults. So, this study may provide theoretical support for the policy from health effect perspective.

Materials and methods

Study design

An intervention trial was designed. Adult participants were recruited by using posters and social media (from September 26 to October 23, 2016) from Chinese Academy of Agricultural Science. The participants were allocated to either the intervention group (52 subjects) or control group (33 subjects) randomly in accordance with a random number table, 3 participants in intervention and 3 participants in control moved out during the study. In total, 79 participants were analyzed in the study (30 in the control group and 49 in the intervention group). The intervention group was provided steamed potato-wheat bread produced through blending raw wheat flour and cooked potato flour, and their counterparts in the control group were provided steamed bread produced by using raw wheat flour only. Dehydrated cooked potato flour was blended with wheat flour at 30% by weight to make steamed potato-wheat bread (raw wheat flour and cooked potato flour in the ratio 3:7). The baseline data was collected in 28 October 2016, and the final physical examination was performed after 4 weeks' intervention. During the intervention, steamed bread was consumed as staple food at lunch once every day. Other foods were provided to both groups as usual by the research group, both intervention and control participants could choose the vegetables from the supplied category except bread. Figure 1 illustrates the flow of the trial. This trial was registered with the Chinese Clinical Trial Registry (ChiCTR1900027027).

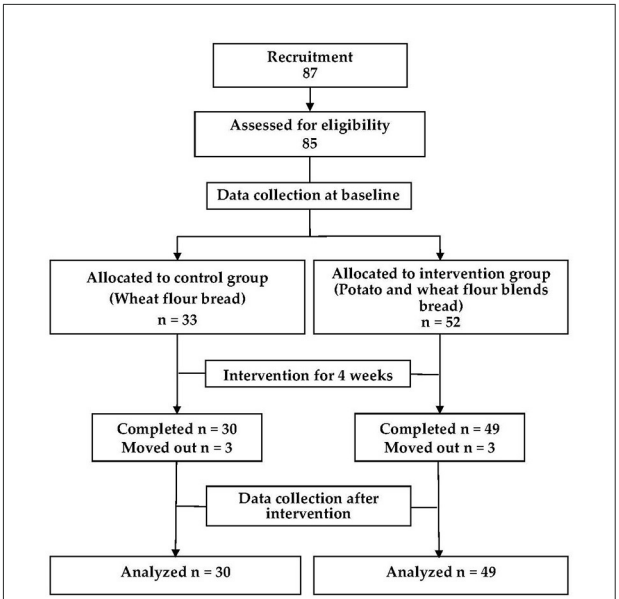

FIGURE 1
CONSORT flowchart of the study.

Participants were excluded from the study if (I) they had serious illnesses (e.g., congenital heart disease and kidney disease), (II) they had potato or wheat flour allergies, (III) they could not withstand daily steamed bread intake for 4 weeks, or (IV) they had recently participated in similar interventions.

This trial was conducted in accordance with the Declaration of Helsinki and was approved by the China Ethics Committee of Registering Clinical Trials (Approval Number: ChiECRCT20190210). The informed consent document was voluntarily signed by participants.

Assessment of intervention effects

Some anthropometric measurements were obtained and urine and blood indictors were evaluated both at baseline and at the end of the intervention. Fasting body weight was measured to the nearest 0.1 kg using a digital scale (RGT-140, Wujin Hengqi Co. Ltd., Changzhou, China), and height was

measured using a stadiometer HP-M (Tsutsumi, Tokyo, Japan). The participants did not wear shoes or overcoats during these measurements. Body mass index (BMI) was calculated as weight in kilograms divided by height in meters squared (kg/m^2). Blood pressure was measured by trained nurses to the nearest 2 mmHg using a mercury sphygmomanometer; during this measurement, patients were in sitting position with at least 10 min of rest before the measurement. SBP and diastolic blood pressure (DBP) were based on the first and fifth Korotkoff sounds, respectively. Two measurements were collected for all participants at 10 min intervals, and the average values were used for the analysis.

Fasting venous blood samples (5 mL) and urine samples (10 mL) were collected in the morning after 10–14 h of overnight fasting. Serum glucose (GLU) was determined through the glucose-oxidase method (Daiichi Pharmaceutical Co., Ltd, Tokyo, Japan) within 4 h after the sample was obtained. CHO, triglycerides (TG), low-density lipoprotein cholesterol (LDL-c), and HDL-c were determined through enzymatic methods by using commercial kits (Daiichi Pharmaceutical Co., Ltd, Tokyo, Japan). Serum insulin was determined through the AxSYM assay based on microparticle enzyme immunoassay technology. Urine samples were collected at the first voiding after waking in the morning for measuring urinary sodium and potassium concentrations. Urinary Na^+ and K^+ concentrations (mmol/L) were measured using an ion-specific electrode method, and then the Na^+/K^+ molar ratio was calculated.

Analytical methods for different nutrients in bread included direct drying (water), the Kjeldahl method (protein), the Soxhlet extractor method (fat), enzymatic gravimetry (fiber), fluorometry (vitamin C), high-performance liquid chromatography (β-carotene, vitamin E, vitamin B_1, and vitamin B_2), the ignition weight method (ash), inductively coupled plasma optical emission spectrometry (sodium, potassium, calcium, iron, and zinc), and the calculation method (energy and carbohydrate). The nutritional analysis indicated that steamed potato-wheat bread provided less energy, protein, fat, carbohydrate, sodium, and iron but more fiber, vitamin E, vitamin B_1, vitamin B_2, ash, potassium, calcium, and zinc than the wheat bread (Supplementary Table 1). The bread intake was measured using a daily food record. The diet and activities of the participants during the intervention period were collected with questionnaire including "whether there is any change in your diet?", "whether you have taken any measures to control your weight?" and "activities and exercises in your leisure time."

Statistical analysis

According to the power calculation, a minimum of 26 participants was required for each group for 90% power to detect the effect with a two-sided significance level of 0.05, which was based on the lipid parameter from an intervention study among adolescents (12).

The average daily bread intake was calculated as the indicator of bread intake for participants; then, the energy and nutrients provided by steamed bread were analyzed based on the average bread intake and nutritional content of the bread. The continuous variables (such as age, height, weight BMI and so on) were expressed as mean and standard deviation, and binary variables (such as proportion of sex, proportion of nation) were expressed as sample and percentage. The t and chi-square tests were used to compare differences in baseline characteristics between control and intervention groups. The paired t-test was used for within-group comparison. The linear mixed effects model was used to compare the changes in continuous variables from the baseline to the end of the study between the control and intervention groups overall after adjusting for confounding factors, including sex, energy intake and physical activity. The intervention effects values were estimated according to Beta values, and 95% confidence interval was then calculated. The effects in subgroups of males and females were analyzed with same model and method. The statistical significance level was set at $p < 0.05$. The SAS software package version 9.2 (SAS Institute Inc, Cary, NC, USA) was used for analysis.

Results

General characteristics

The average age of participants was 41.0 ± 8.6 years for the control group and 42.8 ± 8.2 years for the intervention group. The proportions of female participants were 53.3 and 71.4% in the control and intervention groups, respectively. Although the weight of the control group at baseline was more than that of the intervention group, no significant difference in BMI was observed between the two groups. The intervention group consumed significantly more bread than their counterparts did, but the energy provided by the steamed bread daily was not significantly different (Table 1). Compared with the control group, the intervention group received significantly more fiber, vitamin E, vitamin B_1, vitamin B_2, potassium, and calcium and less sodium than the control group (Table 2). There's no significant difference between intervention and control groups for the proportion of subjects without changes in diet (60.9% vs. 80.0%, $p = 0.181$), proportion of subjects with weight uncontrolled (80.4% vs. 93.3%, $p = 0.389$), and the average activity time (0.3 ± 0.3 vs. 0.4 ± 0.3, hours / day, $p = 0.411$) during the intervention period.

Physical measurement

At baseline, the weight and BMI were 64.7 kg and 23.4 kg/m^2, respectively, for the control group and 62.9 kg and 23.5 kg/m^2, respectively, for the intervention group. Compared with

TABLE 1 Characteristics of participants at baseline.

Characteristics	Control group	Intervention group
Total (*N*)	30	49
Sex [*N* (%)][#]		
Male	14 (46.7)	14 (28.6)
Female	16 (53.3)	35 (71.4)
Nation [*N* (%)][#]		
Han people	26 (86.7)	46 (93.9)
Minority	4 (13.3)	3 (6.1)
Age [year, Mean (SD)][†]	41.0 (8.6)	42.8 (8.2)
Height [cm, Mean (SD)][†]	165.7 (8.4)	163.1 (6.5)
Weight [kg, Mean (SD)][†]	64.7 (12.5)	62.9 (11.4) *
BMI [kg/m^2, Mean (SD)][†]	23.4 (3.0)	23.5 (3.3)
Bread intake [g/day, Mean (SD)][†]	113.8 (50.3)	136.9 (34.9) *

*$p < 0.05$. [#]Comparison based on chi-square test. [†]Comparison based on t-test. BMI, body mass index.

TABLE 2 Nutrients provided by the daily steamed breads (mean ± SD).

Nutrients	Control group	Intervention group	*P*-Value
Energy (kcal)	278.4 ± 123.1	301.2 ± 76.9	0.313
Protein (g)	9.5 ± 4.2	8.7 ± 2.2	0.355
Fat (g)	1.9 ± 0.8	1.7 ± 0.4	0.217
Carbohydrate (g)	54.6 ± 24.1	61.1 ± 15.6	0.194
Fiber (g)	0.6 ± 0.3	1.2 ± 0.3	<0.001
Vitamin E (mg)	0.80 ± 0.35	1.24 ± 0.32	<0.001
Vitamin B1 (mg)	0.08 ± 0.04	0.12 ± 0.03	<0.001
Vitamin B2 (mg)	0.02 ± 0.01	0.07 ± 0.02	<0.001
Sodium (mg)	223.76 ± 98.96	14.04 ± 3.58	<0.001
Potassium (mg)	148.94 ± 65.87	429.03 ± 109.47	<0.001
Calcium (mg)	16.81 ± 7.44	19.76 ± 5.04	0.062
Iron (mg)	1.13 ± 0.50	1.19 ± 0.30	0.582
Zinc (mg)	0.47 ± 0.21	0.64 ± 0.16	0.133

The t-test was used for the comparison between groups.

the control group, the net changes in weight and BMI for the intervention group after 4 weeks of bread intake were −0.6 kg (95% confidence interval [CI]: −1.2, −0.1; $p = 0.016$) and −0.2 kg/m^2 (95% CI: −0.4, −0.1; $p = 0.020$), respectively. The SBP and DBP were 121.6 and 75.1 mmHg, respectively, for the control group and 121.2 and 72.3 mmHg, respectively, for the intervention group. Net blood pressure changes in the intervention group were as follows: SBP increased by 0.1 mmHg (95% CI: −4.9, 5.1; $p = 0.967$) and DBP increased by 2.8 mmHg (95% CI: −0.6, 6.2; $p = 0.100$). For the sex-based subgroup analysis, net changes in SBP were 2.2 mmHg (95% CI: −4.9, 9.3; $p = 0.532$) and −0.7 mmHg (95% CI: −7.9, 6.5; $p = 0.851$) for male and female participants, respectively, and the net changes in DBP were 5.3 mmHg (95% CI: 0.4, 10.1; $p = 0.034$) and 1.2 mmHg (95% CI: −3.6, 6.0; $p = 0.624$) among male and female participants, respectively (Table 3, Figure 2).

Blood indicators

Compared with the control group, both lipid metabolic indicators (i.e., CHO, TG, HDL-c, and LDL-c) and blood glucose exhibited a decreasing trend in the intervention group, and a significant net change (mean between-group difference) of −0.22 mmol/L for LDL-c (95% CI: −0.49, −0.01; $p = 0.035$) was observed in the intervention group after 4 weeks of potato bread intake (Figure 2). After the sex-based subgroup analysis, a significant net change in LDL-c of −0.28 mmol/L (95% CI: −0.55, −0.01; $p = 0.049$) was observed in female participants, but male participants exhibited no significant changes. For GLU, a decreasing trend were observed −0.05 mmol/L (95% CI: −0.28, 0.19; $p = 0.689$) in intervention women (Table 3).

Urinary sodium and potassium

Compared with the control group, urinary Na^+ and K^+ excretions in the intervention group changed by −7.1 (95% CI: −29.1, 14.9; $p = 0.520$) mmol/L and 14.4 (95% CI: −4.7, 33.5; $p = 0.136$) mmol/L, respectively. Significant changes in the Na^+/K^+ ratio were observed of −2.4 (95% CI: −4.1, −0.7; $p = 0.007$) overall, −2.9 (95% CI: −5.6, −0.1; $p = 0.039$) among men, and −1.7 (95% CI: −4.0, 0.7; $p = 0.162$) among women (Table 3).

Discussion

To the best of our knowledge, this is the first trial to evaluate the effect of steamed potato-wheat bread intake on Chinese adults. The results revealed significant effects on weight, BMI, LDL-c, and the urinary Na^+/K^+ ratio after the intake of steamed potato-wheat bread as staple food once daily for 4 weeks in this study. Compared with the wheat bread group, the potato-wheat bread group showed a significant net decrease in weight, BMI, LDL-c, and the urinary Na^+/K^+ level.

Vitamin C is often lacking in the diet of individuals without access to fresh produce. Although vitamin C is destroyed during the cooking process and potatoes have a moderate content of vitamin C compared with some other fruits and vegetables, potatoes play a critical nutritional role as the primary source of vitamin C in many countries, as well as providing fiber, potassium, calcium, iron, vitamin B_6, niacin, and folate, which are related to a reduced risk of several chronic diseases (13). The importance of potatoes for vitamin C intake is partly because they can be stored, but the Chinese steamed potato-wheat bread was made from a mixture of cooked potato flour and wheat

TABLE 3 Outcomes of the intervention for groups and subgroups.

Subgroups	Variable	Control group		Intervention group		Effect	
		Baseline	End	Baseline	End	Beta (95% CI)	*P*-Value
Overall	Weight (kg)	64.7 ± 12.5	65.2 ± 12.7**	62.9 ± 11.4	62.6 ± 11	−0.6 (−1.2, −0.1)	0.016
	BMI (kg/m^2)	23.4 ± 3.1	23.5 ± 3.1**	23.5 ± 3.3	23.4 ± 3.1	−0.2 (−0.4, −0.1)	0.020
	SBP (mmHg)	121.6 ± 13.8	120.2 ± 14.9	121.2 ± 15.9	120 ± 16.3	0.1 (−4.9, 5.1)	0.967
	DBP (mmHg)	75.1 ± 11.1	70.3 ± 9.3**	72.3 ± 11.2	70.2 ± 10.8	2.8 (−0.6, 6.2)	0.100
	GLU (mmol/L)	5.29 ± 0.58	5.37 ± 0.55	5.10 ± 0.47	5.12 ± 0.50	−0.01 (−0.39, 0.07)	0.900
	INS (mIU/L)	11.19 ± 3.17	13.17 ± 3.81**	9.91 ± 6.18	12.94 ± 6.12**	1.22 (−0.49, 2.93)	0.158
	CHO (mmol/L)	4.8 ± 0.82	4.86 ± 0.89	4.71 ± 0.78	4.58 ± 0.80	−0.17 (−0.43, 0.09)	0.194
	TG (mmol/L)	1.29 ± 1.02	1.62 ± 2.33	1.07 ± 0.47	1.16 ± 0.54	−0.22 (−0.80, 0.35)	0.440
	LDL-c (mmol/L)	3.08 ± 0.87	3.15 ± 0.87	2.86 ± 0.8	2.67 ± 0.78**	−0.22 (−0.49, −0.01)	0.035
	HDL-c (mmol/L)	1.44 ± 0.28	1.47 ± 0.34	1.61 ± 0.36	1.58 ± 0.37	−0.24 (−0.77, 0.29)	0.371
	Urinary Na^+ (mmol/L)	129.4 ± 34.5	141.5 ± 43.4	134.3 ± 39.5	138.8 ± 35.7	−7.1 (−29.1, 14.9)	0.520
	Urinary K^+ (mmol/L)	39.7 ± 27.0	48.0 ± 33.5	31.5 ± 20.4	54.1 ± 35.5**	14.4 (−4.7, 33.5)	0.136
	Urinary Na^+/K^+	4.7 ± 2.8	4.3 ± 2.5	6.0 ± 3.6	3.3 ± 1.7**	−2.4 (−4.1, −0.7)	0.007
Male	Weight (kg)	74.5 ± 8.6	75.1 ± 8.7*	73.3 ± 11.8	73.0 ± 11.1	−0.7 (−1.9, 0.4)	0.178
	BMI (kg/m^2)	25 ± 2.4	25.2 ± 2.4*	25.6 ± 3.5	25.5 ± 3.3	−0.3 (−0.6, 0.1)	0.093
	SBP (mmHg)	126.1 ± 12.5	124.8 ± 13.4	124.3 ± 17.1	125.2 ± 12.2	2.2 (−4.9, 9.3)	0.532
	DBP (mmHg)	79.9 ± 10.5	73.7 ± 9.5**	74.5 ± 11.9	73.5 ± 10.2	5.3 (0.4, 10.1)	0.034
	GLU (mmol/L)	5.38 ± 0.38	5.44 ± 0.4	5.49 ± 0.39	5.5 ± 0.54	0.06 (−0.28, 0.40)	0.727
	INS (mIU/L)	11.57 ± 2.52	13.85 ± 3**	12.5 ± 8.71	16.49 ± 8.94*	1.72 (−2.29, 5.73)	0.386
	CHO (mmol/L)	4.88 ± 0.74	4.84 ± 0.78	4.82 ± 0.92	4.7 ± 0.85	0.01 (−0.42, 0.44)	0.955
	TG (mmol/L)	1.46 ± 1.14	1.38 ± 0.74	1.27 ± 0.61	1.34 ± 0.71	0.18 (−0.42, 0.77)	0.545
	LDL-c (mmol/L)	3.19 ± 0.78	3.22 ± 0.89	3.07 ± 0.97	2.87 ± 0.84	−0.14 (−0.65, 0.36)	0.567
	HDL-c (mmol/L)	1.39 ± 0.34	1.38 ± 0.32	1.44 ± 0.3	1.45 ± 0.25	0.02 (−0.13, 0.17)	0.778
	Urinary Na^+ (mmol/L)	135.3 ± 31.1	136.3 ± 44.7	140.8 ± 44.5	140.6 ± 44.5	−1.2 (−43.6, 41.2)	0.954
	Urinary K^+ (mmol/L)	48.5 ± 30.3	44.9 ± 37.1	31.8 ± 19.5	42.6 ± 19.6	14.4 (−17.6, 46.5)	0.364
	Urinary Na^+/K^+	3.9 ± 2.4	4.6 ± 2.6	5.9 ± 3.1	3.8 ± 1.8**	−2.9 (−5.6, −0.1)	0.039
Female	Weight (kg)	56.1 ± 8.3	56.5 ± 8.5	58.7 ± 8.2	58.4 ± 7.8	−0.5 (−1.1, 0)	0.072
	BMI (kg/m^2)	22 ± 2.9	22.1 ± 2.9	22.7 ± 2.9	22.6 ± 2.7	−0.3 (−0.6, 0)	0.048
	SBP (mmHg)	117.6 ± 14.1	116.2 ± 15.3	120 ± 15.5	117.9 ± 17.4	−0.7 (−7.9, 6.5)	0.851
	DBP (mmHg)	70.9 ± 10.1	67.3 ± 8.4*	71.4 ± 11	68.9 ± 11	1.2 (−3.6, 6.0)	0.624
	GLU (mmol/L)	5.22 ± 0.71	5.3 ± 0.66	4.94 ± 0.41	4.97 ± 0.39	−0.05 (−0.28, 0.19)	0.689
	INS (mIU/L)	10.86 ± 3.7	12.57 ± 4.41**	8.88 ± 4.58	11.52 ± 3.87**	0.99 (−0.44, 2.41)	0.171
	CHO (mmol/L)	4.74 ± 0.91	4.89 ± 0.99	4.66 ± 0.72	4.53 ± 0.78	−0.29 (−0.63, 0.05)	0.097
	TG (mmol/L)	1.15 ± 0.92	1.83 ± 3.15	0.99 ± 0.38	1.08 ± 0.44	−0.58 (−1.44, 0.29)	0.184
	LDL-c (mmol/L)	2.98 ± 0.96	3.09 ± 0.88	2.78 ± 0.72	2.59 ± 0.75*	−0.28 (−0.55, −0.01)	0.049
	HDL-c (mmol/L)	1.49 ± 0.21	1.54 ± 0.34	1.68 ± 0.36	1.64 ± 0.4	−0.10 (−0.25, 0.05)	0.176
	Urinary Na^+ (mmol/L)	123.9 ± 37.6	146.4 ± 43.1	131.5 ± 37.6	137.9 ± 31.7	−14.7 (−41, 11.6)	0.265
	Urinary K^+ (mmol/L)	31.5 ± 21.3	50.9 ± 30.8*	31.5 ± 21.1	59.4 ± 40.0**	8.9 (−15.7, 33.5)	0.470
	Urinary Na^+/K^+	5.4 ± 3.0	4.2 ± 2.5	6.0 ± 3.8	3.1 ± 1.6**	−1.7 (−4.0, 0.7)	0.162

The linear mixed effects model was used for comparing the groups. The comparison of overall participants was adjusted for sex, energy intake and physical activity. The paired t-test was used for within-group comparison; $^{**}p < 0.01$; $^{*}p < 0.05$. BMI, body mass index; CI, confidence interval; SBP, systolic blood pressure; DBP, diastolic blood pressure; GLU, serum glucose; INS, serum insulin; CHO, total cholesterol; HDL-c, high-density lipoprotein cholesterol; LDL-c, low-density lipoprotein cholesterol; TG, triglycerides.

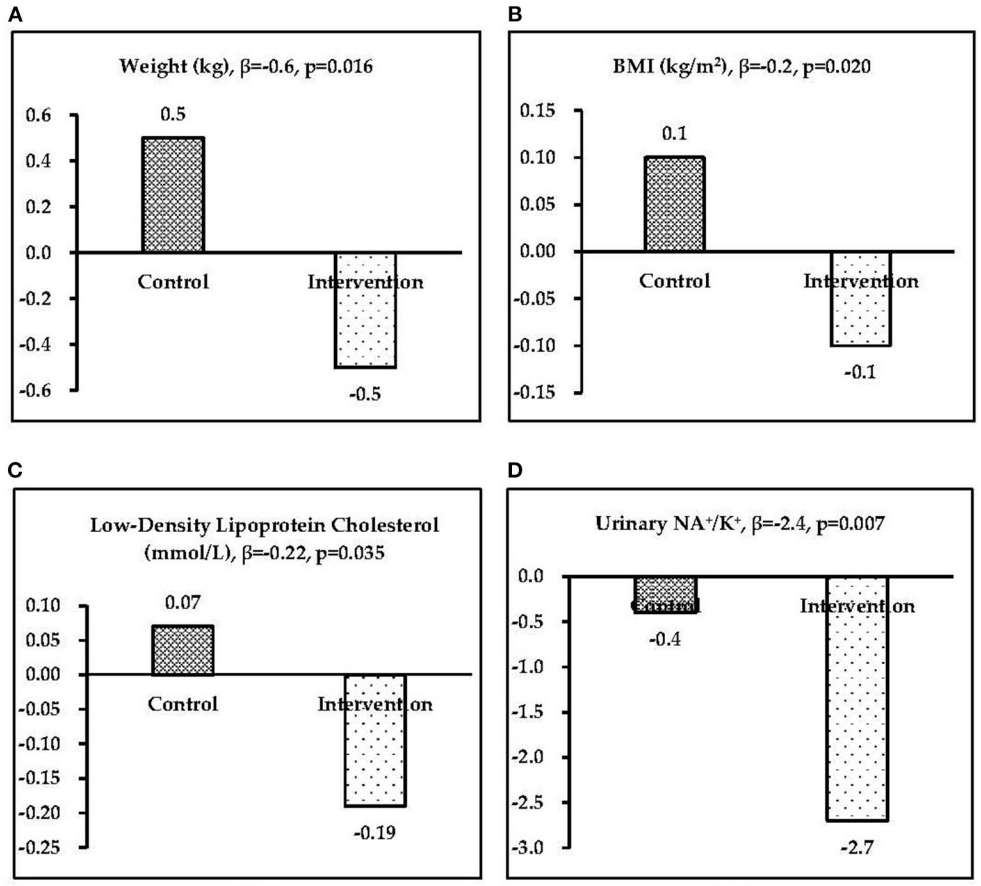

FIGURE 2
Significant intervention effects (β) in the two groups: **(A)** weight, **(B)** body mass index, **(C)** low-density lipoprotein cholesterol, and **(D)** urinary Na^+/K^+.

flour, and most vitamin C was destroyed while processing the bread; thus, little vitamin C was left in the steamed potato bread (<0.044 mg/100 g). Compared with wheat staple food, potato staple bread contains more potassium and less sodium, which is associated with cardiovascular health, may control hypertension, and decreases the urinary Na^+/K^+ level.

Adiposity and potato consumption have been positively associated in previous trials (14, 15); more specifically, the intake of boiled, baked, and mashed potatoes was associated with a slight increase in body weight in both sexes (14) and an increase in waist circumference in women (15). However, in this trial, compared with the wheat bread group (control group), the weight and BMI decreased in potato-wheat bread group (intervention group). The positive associations between potatoes and body weight from cohort studies may have been confounded by unmeasured factors of unhealthy lifestyle (16). Furthermore, French fries showed a stronger association with weight gain than intake of other potato foods (14, 17). This may be due to the higher energy density of French fries compared with baked, boiled, and mashed potatoes (18) and the unhealthy lifestyle that may be related to the intake of French fries (19). Another study reported that consumption of French fries is associated with a higher mortality risk, but total potato consumption was not associated with mortality (20). For the Chinese staple potato bread was processed by using the steaming method, and the potato bread provided less energy than the wheat bread (230.8 kcal/100 g vs. 248.5 kcal/100 g). Although the intervention group received more energy than the control group, the weight of the intervention group appeared to relatively decrease.

Beyond the nutritional properties of a quality staple food, potato may have a role to play in human health over a lifetime of consumption. Potato has been implicated in contributing to diabetes because of its high GI and GL (5, 21). Studies on potatoes have shown GI values as high as 118 (22) and have associated high GI and GL with an increased risk of several chronic diseases (23–25). Moreover, diets rich in potatoes are commonly unhealthy (20). The nutrient content of potatoes is dependent on the cooking method (26, 27). Fried potatoes typically contain high amounts of fats and salts. Boiling, baking, and microwaving can reduce vitamin C, thiamin, riboflavin,

niacin, folic acid, and vitamin B_6 in potatoes. Roasting or baking could enhance the availability of minerals in potatoes. Heating potatoes converts their native starch granules to rapidly digestible starch (28). Hence, boiled potatoes have higher GI than potatoes cooked using other methods. Therefore, the effects of potato consumption are greatly dependent on the type of potato product consumed.

Some epidemiological studies have shown that potatoes are positively associated with T2D (6, 7) and gestational diabetes mellitus (29). In a cross-sectional study involving 4,774 Iranian adults, the frequency of potato consumption was associated with high fasting blood glucose level (30) and T2D. Moreover, three prospective studies in the USA have reported that high potato consumption was associated with a high risk of diabetes mellitus and hypertension (31, 32). Thus, potato consumption has a significant role in the progression of T2D. Unlike other vegetables, potatoes have a high GI and are rich in starch, which is absorbed rapidly (22, 33). High potato consumption may lead to a sharp increase in postprandial blood glucose concentrations, resulting in β-cell dysfunction or exhaustion and T2D (34–36). However, some prospective studies have reported that potato consumption is not associated with the risk of incident cardiovascular disease (37) and hypertension (38). One prospective cohort consisting of 64,227 Chinese women without a history of T2D found that the risk of T2D was reduced by 28% in the category with the highest consumption of potatoes versus the category with the lowest potato consumption (39). Increased potato consumption during a 20-year follow-up study was inversely related to 2-h glucose level (40). Furthermore, the increasing effect on glucose level was not observed in this trial, possibly because the processed method was used for the potato staple bread. The potato flour used to produce the steamed potato bread was made from cooked potato. Previous researches indicated that repeated cooking can increase the resistant starch in potato by 10% (41, 42). After a secondary heating treatment with a cooling interval, the proportion of resistant starch in steamed potato bread might increase. Resistant starch reportedly plays a role in controlling blood glucose and insulin levels (43, 44). Additionally, the different potato cultivars from different areas may play a role.

The Chinese potato stapling strategy is closely related to agriculture, nutrition, and public health. A novel potato cultivar was needed for the staple bread. A novel potato cultivar for potato staple food should be bred and selected based on certain traits, such as high dry weight, which is one of the most essential traits for staple food processing. However, based on the possible relationship between potato consumption and T2D, a high resistance starch cultivar maybe one target. Biotechnology-based tools are now widely used to enhance and expand the traditional remit of potatoes in food production. Enabling potatoes to produce therapeutic compounds through modification of their functionality is now a reality. In this review, strong corporation from nutritionists, agriculturalists, and public health researchers will be needed to improve this crop. Moreover, potatoes could be genetically modified to improve the functional properties of tuber-derived flour through the expression of beneficial traits related to the gene (45).

This trial had also some limitations. Firstly, the duration of steamed potato bread intake was short; Secondly, there was a lack of dietary analysis and digestibility measures; Thirdly, though main confounding factors have been controlled, still some factors can't be controlled about the population, and subgroups were not considered in the sample design; Lastly, the concentration in a spot voiding urine not 24-h urinary excretion for sodium and potassium may cause the results inaccurate. All these factors may have affected the results. However, this is the first clinical trial to evaluate the effect of steamed potato bread on blood pressure, glucose, lipids, and urinary Na^+ and K^+ in healthy Chinese adults, and it could provide valuable evaluation data for the potato stapling strategy in China.

Conclusion

The intake of steamed potato bread, which was made from a blend of wheat flour and cooked potato flour, once daily for 4 weeks in adults could decrease weight, BMI, LDL-c, and the urinary Na^+/K^+ level, and especially increase DBP in male participants.

Data availability statement

The original contributions presented in the study are included in the article/Supplementary material, further inquiries can be directed to the corresponding author/s.

Author contributions

HX led the development of the manuscript and primary data analysis. HX, YG, HF, and JS contributed to the research design and trial methodology. HX, XW, YM, JQ, and SC contributed to the sample data collection. All authors contributed to the revision and approval of the final content of the manuscript.

Funding

This study was supported by the Special Research Grant for Nonprofit Public Service of China (Agriculture) (grant number 201503001) and Science and Technology Innovation Project of the Chinese Academy of Agricultural Science (grant number ASTIP2022).

Acknowledgments

We would like to acknowledge the support from all the team members and the participating subjects.

Conflict of interest

The authors declare that the research was conducted in the absence of any commercial or financial relationships that could be construed as a potential conflict of interest.

Publisher's note

All claims expressed in this article are solely those of the authors and do not necessarily represent those of their affiliated organizations, or those of the publisher, the editors and the reviewers. Any product that may be evaluated in this article, or claim that may be made by its manufacturer, is not guaranteed or endorsed by the publisher.

Supplementary material

The Supplementary Material for this article can be found online at: https://www.frontiersin.org/articles/10.3389/fnut.2022.987285/full#supplementary-material

References

1. Hermansen A, Lu D, Forbes G. Potato production in China and Norway: similarities, differences and future challenges. *Potato Res.* (2012) 55:197–203. doi: 10.1007/s11540-012-9224-7

2. Chinese Nutrition Society. *Dietary Guidelines for Chinese*. Beijing: People's Medical Publication House (2017). p. 362.

3. Nayak B, Berrios JJ, Tang J. Impact of food processing on the glycemic index (GI) of potato products. *Food Res Int.* (2014) 56:35–46. doi: 10.1016/j.foodres.2013.12.020

4. Kusnadi D, Barclay AW, Brand-Miller JC, Louie J. Changes in dietary glycemic index and glycemic load in Australian adults from 1995 to 2012. *Am J Clin Nutr.* (2017) 106:189–98. doi: 10.3945/ajcn.116.150516

5. van Bakel MM, Kaaks R, Feskens EJ, Rohrmann S, Welch AA, Pala V, et al. Dietary glycaemic index and glycaemic load in the European prospective investigation into cancer and nutrition. *Eur J Clin Nutr.* (2009) 63:188–205. doi: 10.1038/ejcn.2009.81

6. Salmerón J, Manson JE, Stampfer MJ, Colditz GA, Wing AL, Willett WC. Dietary fiber, glycemic load, and risk of non-insulin-dependent diabetes mellitus in women. *JAMA.* (1997) 277:472–7. doi: 10.1001/jama.277.6.472

7. Salmerón J, Ascherio A, Rimm EB, Colditz GA, Spiegelman D, Jenkins DJ, et al. Dietary fiber, glycemic load, and risk of NIDDM in men. *Diabetes Care.* (1997) 20:545–50. doi: 10.2337/diacare.20.4.545

8. Zhang Y, You D, Lu N, Duan D, Feng X, Astell-Burt T, et al. Potatoes consumption and risk of type 2 diabetes: a meta-analysis. *Iran J Public Health.* (2018) 47:1627–35.

9. Augustin L. Glycaemic index in chronic disease. *Nutrafoods.* (2013) 12:117–25. doi: 10.1007/s13749-013-0061-3

10. Gao B, Huang W, Xue X, Hu Y, Huang Y, Wang L, et al. Comprehensive environmental assessment of potato as staple food policy in China. *Int J Environ Res Public Health.* (2019) 16:2700. doi: 10.3390/ijerph16152700

11. Xu H, Wang X, Ma G. Nutrition feasibility analysis of development of potato as a staple food (in Chinese). *Food Nutr China.* (2015) 21:13–17.

12. Xu H, Guo Y, Lu S, Ma Y, Wang X, Zhao L, et al. Effect of steamed potato bread intake on glucose, lipids, and urinary Na+ and K+: a randomized controlled trial with adolescents. *Int J Environ Res Public Health.* (2020) 17:2096. doi: 10.3390/ijerph17062096

13. Darooghegi Mofrad M, Djafarian K, Mozaffari H, Shab-Bidar S. Effect of magnesium supplementation on endothelial function: a systematic review and meta-analysis of randomized controlled trials. *Atherosclerosis.* (2018) 273:98–105. doi: 10.1016/j.atherosclerosis.2018.04.020

14. Mozaffarian D, Hao T, Rimm E, Willett W, Hu F. Changes in diet and lifestyle and long-term weight gain in women and men. *N Engl J Med.* (2011) 364:2392–404. doi: 10.1056/NEJMoa1014296

15. Halkjær J, Tjønneland A, Overvad K, Sørensen TI. Dietary predictors of 5-year changes in waist circumference. *J Am Diet Assoc.* (2009) 109:1356–66. doi: 10.1016/j.jada.2009.05.015

16. Nicklas TA, O'Neil C, Fulgoni VL. Differing statistical approaches affect the relation between egg consumption, adiposity, and cardiovascular risk factors in adults. *J Nutr.* (2015) 145:170–6S. doi: 10.3945/jn.114.194068

17. Linde JA, Utter J, Jeffery RW, Sherwood NE, Pronk NP, Boyle RG. Specific food intake, fat and fiber intake, and behavioral correlates of BMI among overweight and obese members of a managed care organization. *Int J Behav Nutr Phys Act.* (2006) 3:1–8. doi: 10.1186/1479-5868-3-42

18. Camire ME, Kubow S, Donnelly DJ. Potatoes and human health. *Crit Rev Food Sci Nutr.* (2009) 49:823–40. doi: 10.1080/10408390903041996

19. Langsetmo L, Poliquin S, Hanley DA, Prior JC, Barr S, Anastassiades T, et al. Dietary patterns in Canadian men and women ages 25 and older: relationship to demographics, body mass index, and bone mineral density. *BMC Musculoskelet Disord.* (2010) 11:20. doi: 10.1186/1471-2474-11-20

20. Veronese N, Stubbs B, Noale M, Solmi M, Vaona A, Demurtas J, et al. Fried potato consumption is associated with elevated mortality: an 8-y longitudinal cohort study. *Am J Clin Nutr.* (2017) 106:162–7. doi: 10.3945/ajcn.117.154872

21. Wirfält E, McTaggart A, Pala V, Gullberg B, Frasca G, Panico S, et al. Food sources of carbohydrates in a European cohort of adults. *Public Health Nutr.* (2002) 5:1197–215. doi: 10.1079/PHN2002399

22. Atkinson FS, Foster-Powell K, Brand-Miller JC. International tables of glycaemic index and glycaemic load values. *Diabetes Care.* (2008) 31:2281–3. doi: 10.2337/dc08-1239

23. Fan J, Song Y, Wang Y, Hui R, Zhang W. Dietary glycemic index, glycemic load, and risk of coronary heart disease, stroke, and stroke mortality: a systematic review with meta-analysis. *PLoS ONE.* (2012) 7:e52182. doi: 10.1371/journal.pone.0052182

24. Mirrahimi A, Chiavaroli L, Srichaikul K, Augustin LS, Sievenpiper JL, Kendall CW, et al. The role of glycemic index and glycemic load in cardiovascular disease and its risk factors: a review of the recent literature. *Curr Atheroscler Rep.* (2014) 16:381. doi: 10.1007/s11883-013-0381-1

25. Sieri S, Krogh V, Agnoli C, Ricceri F, Palli D, Masala G, et al. Dietary glycemic index and glycemic load and risk of colorectal cancer: results from the EPIC-Italy study. *Int J Cancer.* (2015) 136:2923–31. doi: 10.1002/ijc.29341

26. Siri-Tarino PW, Sun Q, Hu FB, Krauss RM. Meta-analysis of prospective cohort studies evaluating the association of saturated fat with cardiovascular disease. *Am J Clin Nutr.* (2010) 91:535–46. doi: 10.3945/ajcn.2009.27725

27. Augustin J, Johnson SR, Teitzel C, True RH, Hogan JM, Toma RB, et al. Changes in the nutrient composition of potatoes during home preparation: II. Vitamins. *Am J Pota Res.* (1978) 55:653–62. doi: 10.1007/BF02852138

28. García-Alonso A, Goñi I. Effect of processing on potato starch: *in vitro* availability and glycaemic index. *Die Nahrung.* (2000) 44:19–22. doi: 10.1002/(SICI)1521-3803(20000101)44:1<19::AID-FOOD19>3.0.CO;2-E

29. Bao W, Tobias DK, Hu FB, Chavarro JE, Zhang C. Pre-pregnancy potato consumption and risk of gestational diabetes mellitus: prospective cohort study. *BMJ.* (2016) 352:h6898. doi: 10.1136/bmj.h6898

30. Khosravi-Boroujeni H, Mohammadifard N, Sar-rafzadegan N, Sajjadi F, Maghroun M, Khosravi A, et al. Potato consump-tion and cardiovascular disease risk factors among Iranian population. *Int J Food Sci Nutr.* (2012) 63:913–20. doi: 10.3109/09637486.2012.690024

31. Muraki I, Rimm EB, Willett WC, Manson JE, Hu FB, Sun Q. Potato consumption and risk of type 2 diabetes: results from three prospective cohort studies. *Diabetes Care.* (2016) 39:376–84. doi: 10.2337/dc15-0547

32. Borgi L, Rimm EB, Willett WC, Forman JP. Potato intake and incidence of hypertension: results from three prospective US cohort studies. *BMJ.* (2016) 353:i2351. doi: 10.1136/bmj.i2351

33. McGill CR, Kurilich AC, Davignon J. The role of potatoes and potato components in cardiometabolic health: a review. *Ann Med.* (2013) 45:467–73. doi: 10.3109/07853890.2013.813633

34. Riccardi G, Rivellese AA, Giacco R. Role of glycemic index and glycemic load in the healthy state, in prediabetes, and in diabetes. *Am J Clin Nutr.* (2008) 87:269–74S. doi: 10.1093/ajcn/87.1.269S

35. Bhupathiraju SN, Tobias DK, Malik VS, Pan A, Hruby A, Manson JE, et al. Glycemic index, glycemic load, and risk of type 2 diabetes: results from 3 large US cohorts and an updated meta-analysis. *Am J Clin Nutr.* (2014) 100:218–32. doi: 10.3945/ajcn.113.079533

36. Ceriello A, Esposito K, Piconi L, Ihnat MA, Thorpe JE, Testa R, et al. Oscillating glucose is more deleterious to endothelial function and oxidative stress than mean glucose in normal and type 2 diabetic patients. *Diabetes.* (2008) 57:1349–54. doi: 10.2337/db08-0063

37. Larsson SC, Wolk A. Potato consumption and risk of cardiovascular disease: 2 prospective cohort studies. *Am J Clin Nutr.* (2016) 104:1245–52. doi: 10.3945/ajcn.116.142422

38. Hu EA, Martinez-Gonzalez MA, Salas-Salvado J, Corella D, Ros E, Fito M, et al. Potato consumption does not increase blood pressure or incident hypertension in 2 cohorts of Spanish adults. *J Nutr.* (2017) 147:2272–81. doi: 10.3945/jn.117.252254

39. Villegas R, Liu S, Gao YT, Yang G, Li H, Zheng W, et al. Prospective study of dietary carbohydrates, glycemic index, glycemic load, and incidence of type 2 diabetes mellitus in middle-aged Chinese women. *Arch Intern Med.* (2007) 167:2310–6. doi: 10.1001/archinte.167.21.2310

40. Feskens EJ, Virtanen SM, Rasanen L, Tuomilehto J, Stengård J, Pekkanen J, et al. Dietary factors determining diabetes and impaired glucose tolerance. A 20-year follow-up of the Finnish and Dutch cohorts of the seven countries study. *Diabetes Care.* (1995) 18:1104–12. doi: 10.2337/diacare.18.8.1104

41. Meng T, Yan Y, Zhao C, Ye X. Effect of Chinese cooking on the resistant starch and other main nutrient elements in potatoes (in Chinese). *Sci Technol Food Industry.* (2012) 33:86–9.

42. Berry CS. Resistant starch: formation and measurement of starch that survives exhaustive digestion with amylolytic enzymes during the determination of dietary fibre. *J Cereal Sci.* (1986) 4:301–14. doi: 10.1016/S0733-5210(86)80034-0

43. Raigond P, Ezekiel R, Raigond B. Resistant starch in food: a review. *J Sci Food Agric.* (2015) 95:1968–78. doi: 10.1002/jsfa.6966

44. Tian J, Chen J, Ye X, Chen S. Health benefits of the potato affected by domestic cooking: a review. *Food Chem.* (2016) 202:165–75. doi: 10.1016/j.foodchem.2016.01.120

45. Mullins E, Milbourne D, Petti C, Doyle-Prestwich BM, Meade C. Potato in the age of biotechnology. *Trends Plant Sci.* (2006) 11:254–60. doi: 10.1016/j.tplants.2006.03.002

frontiers | Frontiers in Nutrition

TYPE Original Research
PUBLISHED 29 August 2022
DOI 10.3389/fnut.2022.979594

OPEN ACCESS

EDITED BY
John-Lewis Zinia Zaukuu,
Kwame Nkrumah University of Science and Technology, Ghana

REVIEWED BY
Raquel Braz Assunção Botelho,
University of Brasilia, Brazil
Mohammad Hojjatoleslamy,
Islamic Azad University of Shahrekord, Iran

*CORRESPONDENCE
Tamás Csurka
csurka.tamas@uni-mate.hu

SPECIALTY SECTION
This article was submitted to Nutrition and Food Science Technology, a section of the journal Frontiers in Nutrition

RECEIVED 27 June 2022
ACCEPTED 28 July 2022
PUBLISHED 29 August 2022

CITATION
Csurka T, Varga-Tóth A, Kühn D, Hitka G, Badak-Kerti K, Alpár B, Surányi J, Friedrich LF and Pásztor-Huszár K (2022) Comparison of techno-functional and sensory properties of sponge cakes made with egg powder and different quality of powdered blood products for substituting egg allergen and developing functional food. *Front. Nutr.* 9:979594. doi: 10.3389/fnut.2022.979594

Comparison of techno-functional and sensory properties of sponge cakes made with egg powder and different quality of powdered blood products for substituting egg allergen and developing functional food

Tamás Csurka[1,2]*, Adrienn Varga-Tóth[1], Dorottya Kühn[1], Géza Hitka[3], Katalin Badak-Kerti[4], Boglárka Alpár[1,2], József Surányi[1,2], László Ferenc Friedrich[1] and Klára Pásztor-Huszár[1]

[1]Department of Livestocks Products and Food Preservation Technology, Institute of Food Science and Technology, Hungarian University of Agriculture and Life Sciences, Budapest, Hungary, [2]Doctoral School of Food Sciences, Hungarian University of Agriculture and Life Sciences, Budapest, Hungary, [3]Department of Postharvest, Commerce, Supply Chain and Sensory Science, Institute of Food Science and Technology, Hungarian University of Agriculture and Life Sciences, Budapest, Hungary, [4]Department of Grain and Industrial Plant Processing, Institute of Food Science and Technology, Hungarian University of Agriculture and Life Sciences, Budapest, Hungary

Animal blood is a valuable resource, which is usually not utilized in a value-added way by the industry like other animal by-products, even though it has plenty of benefits in terms of sustainability and human health, particularly against iron deficiency anemia. Animal blood is perfectly suitable for providing special functions, which are necessary for functional foods, and improving techno-functional properties based on the previous reports published in the literature. In this paper, egg powder was substituted by powdered animal blood products (whole blood powder, blood plasma powder, and hemoglobin powder) in sponge cake. Techno-functional and sensory properties (texture by texture profile analysis and three-point breaking test, water activity, dry matter content, and color) were instrumentally measured and then a sensory evaluation was carried out by unskilled panelists. Quality characteristics (texture, color, and dry matter content) were daily measured on the day of baking and then every 24 h for 3 additional days because freshly baked cakes are usually consumed within 3 days. Based on the results, powdered blood products are suitable for substituting the egg powder in sponge cakes and developing functional foods. Blood powders can increase the hardness, chewiness, and breaking force of cakes, giving them the ability to be stuffed with more fillings and molded into special shapes without compromising on

the sensory characteristics. They can also increase the intensity of the cocoa flavor, which results in a richer, darker color without deceiving the consumers.

KEYWORDS

animal blood, by-product, functional food, iron, iron deficiency anemia, sensory properties, sustainability, techno-functional properties

Introduction

Animal blood is usually handled as hazardous waste and annihilated or in the best case used for producing feed raw material. However, it may play a role in sustainability in value-added further processing, and more sustainable products are preferred by consumers (1). Blood, which is obtained during the bleeding process when animals are slaughtered, accounts for a significant proportion of their live weight depending on the muscle mass: 7.6–8.3% in the case of cattle, 4.5–6% in the case of pig, 7.6–8.3% in the case of sheep, average 6.6% in the case of horse, and 5–10% in the case of poultry. Blood is a liquid connective tissue. Plasma is the intercellular part, in which the red blood cell (RBC) fraction or hemoglobin fraction is suspended. The RBC fraction attains its name from red blood cells because they make up the majority of this fraction, but it contains other blood cells like leucocytes, lymphocytes, and macrocytes, as well as many thrombocytes (2). Two-thirds of the blood take part in the circulatory system, and the residual one-third is present in the resting state and stored in organs like the spleen, liver, lungs, and other tissues (e.g., capillaries of skin). These blood storage organs are able to supply blood to the circulatory system in special cases (e.g., large blood loss). In many ways, animal blood can be an excellent raw material for the development and production of common and functional foods (3–7), and it is also suitable for the development of functional foods for allergen replacement purposes, as it is hypoallergenic (8, 9).

Functional foods are foods that contain higher than average amounts of ingredients, often artificially added, that have been shown to have a positive effect on health at the average normal consumption of the food (e.g., vitamin-enriched foods), or foods that contain lower than expected amounts of harmful ingredients at the average normal consumption of each food product (e.g., reduced-fat products). A functional food may also be a food intended for a specific group of consumers (e.g., people who suffer from a food allergy and bodybuilders). Functional foods are economically competitive and acceptable products that can be enriched with, for example, blood-derived bioactive peptides, protein (with good gelling and foaming properties), or hem-iron. Functional foods can play a major role in human nutrition during the current pandemic (10–13). A functional food can be a food that serves a specific need, such as the needs of consumers with egg allergies. IgE-mediated egg allergy affects up to 8.9% of children in developed countries (14).

It is hard to substitute egg white in bakery products because of its solubility, heat coagulation, foaming, and emulsifying properties (15). Animal blood plasma has already been used in bakery products and shown a similar effect to egg white in texture and appearance of cakes when blood plasma is used as an egg white alternative if blood plasma and egg white were in similar form (e.g. powder or liquid) and amount (16, 17). Plasma proteins contain mostly globular proteins (about 60 w/w% albumins and 40 w/w% globulins) and around 3–4 w/w% fibrinogen (18). According to recent studies, these are better for developing binding than meat powders, gelatin, wheat gluten, isolated soy proteins, and sodium alginate with calcium carbonate (19). In addition, other blood protein fractions (globulins, serum albumin, and hemoglobin) are better emulsifiers than an egg (20), in which egg white proteins contain 54–55 w/w% albumin, and egg yolk proteins contain 14 w/w% serum albumin, 41 w/w% glycoproteins, and 45 w/w% immunoglobulins (21). Investigating the effect of blood proteins on texture is important not only for substituting egg-allergenic ingredients or developing a harder, better texture, but also for improving the sustainability of animal slaughter and preventing or treating iron deficiency anemia.

The prevalence of anemia caused by iron deficiency is around 30% globally. Symptoms of anemia include physical and mental decline and miscarriage in pregnant women. Non-hem-iron absorption is <10%, but hem-iron absorption is 15–35%, and non-hem-iron is much more exposed to inhibitory effects due to the different metabolic pathways (22, 23).

A 100 g of porcine whole blood powder is able to cover the daily essential amino acid needs of an average 70 kg adult male with the exception of methionine (24), which can be supplemented with cereals. The iron content of porcine blood is 1,490.14 mg/kg, and in bovine blood, the iron content is 2,810.62 mg/kg expressed in terms of blood matter content (25, 26). In Russia and other post-Soviet states, blood chocolates and blood-colored candies are popular, especially for iron-deficient children. It is a good idea to give natural, well absorbable iron to children in the form of sweets or cakes. Due to our culture and trends, by-products such as blood are unlikely to become a major product in the foreseeable future, and the direct use of by-products on their own should not be forced. Therefore, the impact of blood and blood fractions on the techno-functional

and organoleptic properties of foods should be investigated, and the results should be used to support and motivate industrial use.

Proteins have several different techno-functional properties. Hydration properties (water–protein interactions, such as hydration, water-holding capacity, dispersibility, solubility, and swelling) and surface properties (such as emulsification and foaming capacity) are very important basic properties. Rheological properties (protein–protein interactions, such as precipitation, gelation, and texturization) and sensory properties (such as taste (first of all, umami), texture, and color) are also basic properties but are affected by much more synergistic and divergent effects. Besides, techno-functional properties have a fifth category: the other properties (like adhesion, cohesion, film formation, etc.), which cannot be clearly classified under the previous ones (27). Blood plasma proteins are perfect cold binder agents (28), which can be helpful in the forming and handling of the batter before the heat treatment. In different food products, plasma proteins could improve the heat stability of the colloid system and decrease the heat treating loss (29–33). Blood products were successfully used in Kenya and Chile for improving the iron content of bakery products and in Russia in the case of sweets (34, 35).

The purpose of this paper was to briefly summarize the importance and role of blood in the development of functional (enriched with iron and/or protein and allergen-free) foods and investigate the effect of egg powder substitution in sponge cake with several types of blood powders (whole blood powder, hemoglobin powder, and plasma powder) on instrumentally measured sensory properties (color and texture) and techno-functional properties (pH, water activity, and dry matter content). Results were validated by a sensory evaluation of developed cakes. The objectives of this research were to compare the effect of egg powder, blood powder, blood plasma powder, and hemoglobin powder in cakes on quality-determining techno-functional and sensory properties (texture by texture profile analysis and three-point breaking test, water activity, dry matter content, color, appearance, taste and smell intensity, and liking) for substituting egg allergen by these valuable animal by-products.

Materials and methods

Materials

Whole blood powder and the powdered form of two main blood products (plasma powder and hemoglobin powder) were investigated for substituting egg powder and for developing functional product features (iron content). Thus, the protein content of the cake matrix was closely the same as the basic egg powdered in each sample type. Raw material specifications and a food nutrition database (26) were used for calculating the recipe. The amount of egg powder was calculated from average M-sized eggs, which is 58 g of weight. The cocoa-flavored sponge cake was prepared based on a common mix recipe, in which the protein content of the egg was substituted by different powdered blood products. The fat content of the egg was substituted by sunflower oil. Recipes are shown in Table 1. The water content of the egg was replaced by just water in case of each recipe. Determinative special ingredients, which were used during this investigation, were the follows:

- Hemoglobin powder 92B (Sonac Burgum B.V., Netherlands).
- Plasma powder 70B (Sonac Burgum B.V., Netherlands).
- Vepro 95 phf whole blood powder (Solvent Kereskedoház Zrt., Hungary).
- Egg powder (Capriovus Kft., Hungary).

Replacement of fat in egg yolk is also necessary because fats and oils are important ingredients of bakery products. The major functions of lipids are to soften and tenderize the texture of the product by adding moisture, to make it richer and to improve the retention of quality. Sunflower oil was used in our research because it has no effect on the taste and smell of the product.

Methods

Experimental design

In this paper, the results are presented according to a 4 × 4 full factorial experimental design for comparison of the effect of four different protein raw materials (egg powder, whole blood powder, blood plasma powder, and hemoglobin powder) with the same protein quantity and sample groups with four different storage times (0, 1, 2, and 3 days). The aim of the research plan was to detect the effect of different factors (sample type and storage time) on several techno-functional and sensory properties to investigate the quality of cakes.

Sample preparation

The batter was prepared in a bowl. Dry ingredients were mixed well, and then melted margarine was added into the dry mix, and all these were mixed thoroughly. Finally, the milk and water were added to the mix and then were further mixed using a household mixer. The raw foamy batter was filled into a metal tray and then heat-treated in a combined oven/steamer (Lainox VE051P Type LX, Italy) at 180°C with air mixing for 20 min. The sponge cake was sliced and stored for 3 additional days after the day of baking, because a fresh cake is expected to be stored for a maximum of 3–4 days before consumption.

The development of nutritional properties for the whole mass of all ingredients can be calculated according to the specifications and nutritional facts of ingredients. This theoretical development was only mathematically calculated in

TABLE 1 Ingredients [g or ml] in recipes of different investigated products.

Ingredients	Cocoa flavored sponge with egg powder (control)	Cocoa flavored sponge with whole blood powder	Cocoa flavored sponge with hemoglobin powder	Cocoa flavored sponge with plasma powder
Wheat plain flour (g)	300	300	300	300
Powdered sugar (g)	250	250	250	250
Margarin (g)	120	120	120	120
Milk with 2.8% fat (ml)	100	100	100	100
Cocoa powder with 15–16 w/w% fat content (g)	40	40	40	40
Baking powder (g)	12	12	12	12
Vanilla aroma (g)	2	2	2	2
Egg powder / Whole blood powder / Hemoglobin powder / Plasma powder (g)	28	14,16	13,8	18
Water (g)	88	92,06	92,66	88,8
Sunflower oil (g)	-	10,64	10,64	10,64

the case of 1% whole blood powder without any measurement, and no decomposition was assumed.

Storage experiment

It was also intended to carry out a storage experiment. From the day of production, the change in the quality of the sponge cake was examined during storage at room temperature for 3 days, since the product is expected to be consumed within this period of time at the latest in the case of fresh pastries and cakes. The storage conditions correspond to the average expected home storage conditions for the cakes, that is, at room temperature in imperfectly sealed (folded) plastic bags. In order to eliminate the effect of random changes in relative humidity in the air of the storage room, parallel samples were produced and sifted 1 day apart.

A 4-day storage period has been established because the texture and the dry matter content of the bakery products change in 4 days under room conditions according to the industrial experiments and previous studies (36, 37).

Texture measurement

The texture of sponge cakes was measured by using a Stable Micro System (SMS) TA. XT Plus texture analyzer (Stable Microsystem, United Kingdom). A computer controlled the movement of the upper rod. Different probes can be used to measure the different shear, compressive, and torsional stresses in different directions lasting for different time periods while investigating the behavior of the samples with this equipment.

Texture profile analysis (TPA) was carried out, and the following attributes were measured: (1) Hardness: the resistance [N] at maximum compression during the first compression. It is the force necessary to attain a given deformation. It represents the hardness of the sample at first bite. (2) Cohesiveness: The ratio [-] of positive force during the second compression cycle to that of the first one (downward strokes only). It indicates the strength of the internal bonds that make up the body of the sample. (3) Springiness: It is expressed as a ratio [mm mm-1] or percentage of a product's original height. Springiness is measured in several ways, but most typically, based on the distance of the detected height during the second compression divided by the original compression distance. (4) Chewiness: The force [N] required to chew a solid sample till a steady state of swallowing (hardness multiplied by cohesiveness multiplied by springiness) (38, 39). Sponge cake samples were sliced into sections with 40 × 40 mm square floor area and 20 mm height. The probe was a p/75v steel cylinder plate. The pre-test speed of the probe was 10 mm s^{-1}, and the test speed and post-test speed were 1 mm s^{-1}. Maximal compression was 50% of sample height (10 mm), and it lasted 1 s. Then the sample was allowed to relax. The sampling frequency was 50/s. Each sample was measured three times.

A fracture test was carried out, and the breaking force was measured, which is the peak force that can be measured when the cake dough sample is split into two portions. In the case of cakes with a hard crust, the peak force can be measured at the time of the breaking of crust instead of the full dough. HDP/3PB three-point bend rig probe was used. The probe started on the surface of the samples and then moved across the sample with a 1 mm s^{-1} test speed.

The limitation of this investigation is that lipids can affect the texture of gels and heat-treated gels (40). However, the aim of this research was the substitution of egg allergen in sponge

cake. This limitation was a compromise for the substitution of egg powder without any additives.

Color measurement

Minolta CR-400 (Konica Minolta, INC., Japan) chroma meter was used for the measurement of reflection colors. The measurement was based on the fact that any color can be generated by the mixture of three colors defined by light wavelength. The ratio of these three different wavelength lights is plotted in a coordinate system called CIELAB color space. The color coordinates can be numbered, facilitating the analysis of colors. In the case of blood, there is a relationship between the red color (and chroma) and the iron content and thereby between the physical and chemical attributes.

The instrument was calibrated with a standard white etalon. Each sample was measured three times on a white plate with the same illumination. The measured attributes were as follows: redness/greenness (a*), yellowness/blueness (b*), and brightness (L*). Chroma (C*) was calculated according to the following equation:

Equation (1): $C^* = \sqrt{a^{*2} + b^{*2}}$ (41).

Hue angle was also an important color attribute, which was calculated according to the following equation:

Equation (2): $h_{ab} = arctan\frac{b^*}{a^*}$ (42).

Water activity measurement

Water activity was measured by using Novasina LabMaster-aw neo-type instrument (Novasina AG, Switzerland) that requires a very small sample amount and can fully control the temperature between 0 and 60°C during the measurement. Measurements were performed at room temperature to control the integrity of samples for relevant data detection. Each sample group was measured two times.

Dry matter content measurement

About 3–5 g of sample was measured by using a Kern ABJ-NM/ABS-N (Kern & Sohn GmbH, Germany) analytical balance and placed in an open Petri dish. Then the samples were dried at 120°C until a constant mass was obtained in a laboratory drying oven (Labor Muszeripari Muvek, Hungary). The samples were cooled in a desiccator, and then their residual mass was measured by using an analytical balance. Each sample was measured three times.

Sensory evaluation

A sensory evaluation was carried out in a lab equipped with adequate facilities (without confounding factors and with panel members separated in time and/or space). An online questionnaire was filled out by the panel members during the evaluation. The samples for the evaluation of this parameter were the analytical samples with an extra "placebo" sample, which was the same as the egg powdered sample but was colored with activated carbon. Vegetable activated carbon is an allowed food additive marked by E 153 according to one of the strictest regulations for food additives (the Regulation (EC) No 1333/2008 of the European Parliament and of the Council of 16 December 2008 on food additives) (43). Thanks to the active carbon, this egg powdered sample group had the same color as the whole blood powdered and hemoglobin powdered samples for the naked eye. Thus, it was possible to examine the perception of the product texture and taste without influencing the preconceptions of the color. The latter condition was necessary because a placebo/nocebo effect was found in earlier investigations. It means that taste perception depends on visual perception. Specifically, darker and/or more saturated color can mean a stronger taste and higher nutrition content for consumers (44–46). Panel members were informed that sponge cakes, which they taste, may contain blood, blood plasma, or extra cocoa (There was no sample with extra cocoa). They were informed that they may have got similar samples or different samples, but each panel member got the same five samples in a different sequence. Samples were labeled by a random three-digit number code, and each panel member got the samples in a different sequence to eliminate the effect of successive tasting, because the previous sample can influence the opinion of the next sample. Panel members were provided water to naturalize between the samples. The panel consisted of 33 panelists: 17 men and 16 women. The average age of panelists was 29.8 years, while the minimum age was 20 years and the maximum age was 56 years. The panel members were common consumers and not experts. Panel members had to test the samples and rank objectively the flexibility, crumbling, stickiness, dryness, intensity of cocoa smell, and intensity of cocoa flavor, as well as subjectively the smell, taste, and texture in category scales with five levels in a descriptive test. They could write a comment about the samples and rank the samples based on their preferences.

Statistical analysis

The measurement results were evaluated by applying IBM SPSS statistic v25 (IBM Corp., Armonk, NY) (47) and Microsoft Excel 365 version: 2010 (build: 13328.20356) software. A full factorial design was used, and results were statistically evaluated in three parts to detect the effect of raw material and storage time 1) on instrumentally measured texture parameters in the first analysis, 2) on color parameters in the second analysis, and 3) on sensory attributes in the third analysis. Dry matter content and water activity provided trend-like results. These two attributes could not provide a statistically significant difference. Multivariate analysis of variance (MANOVA) was carried out, to compare the means of different sample groups of the related

variables (48). The normality of residuals was checked by Shapiro–Wilk test in the case of texture and color attributes and D'Agostino's K-squared test (49) in the case of sensory attributes. The normality of residuals for sensory attributes was not completely adequate for MANOVA, but in order to evaluate the results, MANOVA was carried out for all of the three attribute groups. According to Levene's test, the homogeneity of variances was adequate for the MANOVA in the case of color attributes and some texture attributes (hardness, chewiness, and breaking force). MANOVA is robust enough to test the equality of covariance matrices; hence, in the case of attributes with no adequate homogeneous covariance matrices according to the results of Levene's test, Box's M test (50) was carried out. In the case of each measured attribute analyzed in one MANOVA, the degree of freedom was the same, and differences in the maximal and minimal standard deviation values of the compared sample groups to the power of two were <2. So, homoscedasticity was adequate for MANOVA in the case of each texture, color, and sensory attribute. The value of the unexplained variance rate (Wilks's lambda) was evaluated. The homogeneous groups were separated by Tukey's HSD *post-hoc* test.

Results and discussion

The effect of cereal proteins on the amino acid composition of blood and their worldwide consumption makes a sponge cake a perfect model product to study the effect of powdered blood products that are used as a substitute for egg powder in batter and cakes. In order to technologically design the structure of the cake, it is essential to understand the structure of the foams. As a result of mechanical stress (mixing), the foaming agents (protein emulsifiers) create a foam with an airy structure, the volume of which increases rapidly in the first stage of the whipping, and then gradually this growth slows down; finally, the air bubbles grow and merge when exceeding the critical value and the foam collapses (51, 52). Air absorption of batter depends on beater speed, geometric properties, surface tension, and viscosity of the batter (53). The amount and type of emulsifiers affect the bubble structure and distribution, which influence the quality of the final bakery product (54). Generally, emulsifiers may be proteins or lipids. Protein emulsifiers are responsible for mechanically strong viscoelastic films, and lipids enable weaker films to counteract changes in interfacial tension when the interface is perturbed (52). Protein-emulsifier interactions affect the rheology of emulsions according to recent studies (55–57). The dispersion medium of the foams can be liquid or solid, while the dispersed phase can only be gaseous. In the case of sponge cake batter, the proteins of the egg white (ovalbumin, conalbumin, ovomucoid, globulin, and ovomucin) are usually responsible for the formation of the foam structure. Under strong mechanical action, gas bubbles are dispersed in the liquid egg, the water-soluble proteins are denatured and then adsorbed on the surface of the colloidal solution, and the bubbles are surrounded by the formed film layer. Since albumin-type proteins typically make up the majority of proteins in the blood, especially in plasma, the blood is similarly capable of forming a colloidal structure. Foaming is affected by the following factors: pH and salinity. Flour and sugar are responsible for foam stability and foam hardness of bakery products. The discharged sponge flan is essentially a solid (58, 59). If the egg is substituted in a bakery product, the fat content of the egg also needs to be substituted.

Texture

The normality of residuals was checked by Shapiro–Wilk test [hardness: $W(160) = 0.993$, $p = 0.65$; springiness: $W(160) = 0.967$, $p = 0.05$; cohesiveness: $W(160) = 0.977$, $p = 0.08$; chewiness: $W(160) = 0.994$, $p = 0.734$; breaking force: $W(160) = 0.986$, $p = 0.102$], and the homogeneity of variances was checked by Levene's test attributes [hardness: $F_{(15,144)} = 2.137$, $p = 0.011$; chewiness: $F_{(15,144)} = 1.272$, $p = 0.227$; breaking force: $F_{(15,144)} = 1.904$; $p = 0.027$] and Box's M test (springiness, cohesivity: $n = 10$, $N = 160$) to confirm that MANOVA could be carried out.

Sponge cakes were made with egg powder, whole blood powder, hemoglobin powder, and blood plasma powder as a protein source and stored for 3 days. The texture of the cakes in all the sample groups was similar to a common sponge cake. The nominal differences between the results of different sample groups were not significant, but a significant difference was found in the case of each measured texture attribute. The effect of the raw material and storage time on texture attributes was investigated by the first MANOVA. The overall MANOVA result was significant for the sample type, that is, the protein source in the used raw material, (Wilks's lambda: 0.009, $p < 0.001$) and the storage time (Wilks's lambda: 0.028, $p < 0.001$). The two-way interaction between the sample type and storage time was also significant (Wilks's lambda: 0.054, $p < 0.001$). The results of Wilks's lambda tests indicate a strong relationship between the factors and dependent variants, but the effect for the sample type was the strongest.

Different sample types could be separated from each other. Tukey's *post-hoc* test could significantly ($p = 0.05$) separate three groups based on hardness: the cakes with egg powder were the softest with an average hardness value of 6.92 N, cakes with whole blood powder and blood plasma powder were similar with average hardness values of 9.1 and 9.4 N, respectively, and cakes with hemoglobin powder were the hardest with the average hardness value of 11.9 N. It can be explained by the fact that albumin content is similar in egg and blood plasma and can develop a lighter batter with more air bubbles due

to their foaming properties. Whole blood powder contains plasma proteins, but hemoglobin powder does not. If the aim of product development is a harder cake, which can show, for instance, a greater weight of filling or higher iron content, hemoglobin powder enrichment is an ideal choice. But, if the aim of product development is a nearly common sponge cake texture without egg allergen, blood plasma powder or whole blood plasma powder is the best choice. The hardness values of cakes made with 20– 40 g kg^{-1} egg in other studies were below these values, and were closer to the values of the cake made with egg powder (60–62). Based on springiness, Tukey's *post-hoc* test could significantly ($p = 0.05$) separate two different groups with nominally not much significant difference. The samples prepared with whole blood powder and egg powder were similar with average springiness values of 0.69 and 0.71, respectively, and these were different from samples prepared with hemoglobin powder and blood plasma powder which showed average springiness values of 0.75 and 0.77, respectively. Springiness values of cakes made with the egg from the previous studies were found to be 0.82, 0.56, and 0.85. The second result was closer to the value of the cake made with plasma powder and egg powder. The higher springiness values can be explained by the fact that using fresh eggs makes a better foam than using a powdered egg (60–62). In the case of chewiness, there was a significant difference ($p = 0.05$) between all sample groups, but the difference was not statistically significant. The samples with egg powder were less chewable with an average chewiness value of 4.01 N. Then the samples with whole blood powder showed an average chewiness value of 4.43 N. Cakes with blood plasma powder had a greater chewiness value (average 5.24 N), and cakes with hemoglobin powder was the most chewable (average 6.18 N). There was one comparable chewiness result, that is, 5.17 N (Rodriguez-García). It was closer to the cakes made with blood plasma powder. There was a significant difference ($p = 0.05$) between all sample groups with regard to the breaking force. This value best reflected the foaming ability of different protein sources because air bubbles in the cake dough weaken the structure of cakes and make it easier to break it. The results of chewiness and breaking force may play a role in product development like hardness values. Samples with egg powder were the easiest breakable with an average of 5.42 breaking force. Breaking force values (average 6.08 N) of samples with blood plasma powder were close to the values of egg powdered samples. The breaking force of samples with whole blood powder (average 7.31 N) and hemoglobin powder (average 8.17 N) was also significantly different ($p = 0.05$).

Storage time also had a significant effect on texture. However, this change was a nominally small difference between the texture attributes of different sampling times. Consumers often eat the cakes only 2 or 3 days after purchase. Based on these results, each cake composition can guarantee a constant quality until the third day after the baking day. In the case of hardness, a nominally significant change could be observed only between the samples prepared from blood plasma powder on the second and third storage days. Thus, the average hardness value of sample groups on the third day was 32% greater than the average hardness value of sample groups on the first and second days. Chewiness results were similar: There was a significant difference ($p = 0.05$) between the chewiness of sample groups on the third day and sample groups on other days, and there was no significant difference between the chewiness values of the sample groups from the starting day, and the first and second storage days. Average chewiness values increased by 34% for the third storage day from the average value of sample groups with 0, 1, and 2 days of storage time. Increasing hardness and chewiness and nearly stagnant springiness values during storage were reported in other studies as well (63–66). It can be explained by syneresis caused by drying, which had been significant on the second and third days. In the case of springiness and cohesiveness, there was no significant difference between the sample groups with different storage time periods. The effect of storage time is the clearest in the case of breaking force, which is related to the drying of the crust. Increasing crust hardness caused an increasing breaking force. There was a significant difference ($p = 005$) between all the sample groups with different storage time periods in case of breaking force, which is similar to the common cakes. The values of color attributes of sponge cake sample groups made with different protein raw material and stored for different times can be seen in Figure 1.

Color

The normality of residuals was checked by Shapiro–Wilk test [a*: W(60) = 0.98, $p = 0.442$; b*: W(60) = 0.984, $p = 0.644$; L*: W(60) = 0.989, $p = 0.878$; C*: W(60) = 0.968, $p = 0.121$; Hue angle: W(60) = 0.978, $p = 0.367$], and the homogeneity of variances was checked by Levene's test attributes [a*: $F_{(19, 40)} = 2.172$, $p = 0.222$; b*: $F_{(19, 40)} = 1.809$, $p = 0.057$; L*: $F_{(19, 40)} = 1.370$, $p = 0.197$; C*: $F_{(19, 40)} = 2.982$, $p = 0.002$; Hue angle: $F_{(19, 40)} = 1.916$, $p = 0.042$] to confirm that MANOVA could be carried out.

As it was expected, the colorization of heat-treated hemoglobin had the main effect on the color attributes, which could be observed in all the color attributes (L*, a*, b*, and C*). The color difference between the different sample types could be seen by the naked eye, and a significant difference was found based on the calculated total color differences. The values of color attributes of sponge cake sample groups made with different protein raw materials can be seen in Figure 2. The effect of the raw material and storage time on color attributes was investigated by the first MANOVA. The overall MANOVA

10.3389/fnut.2022.979594

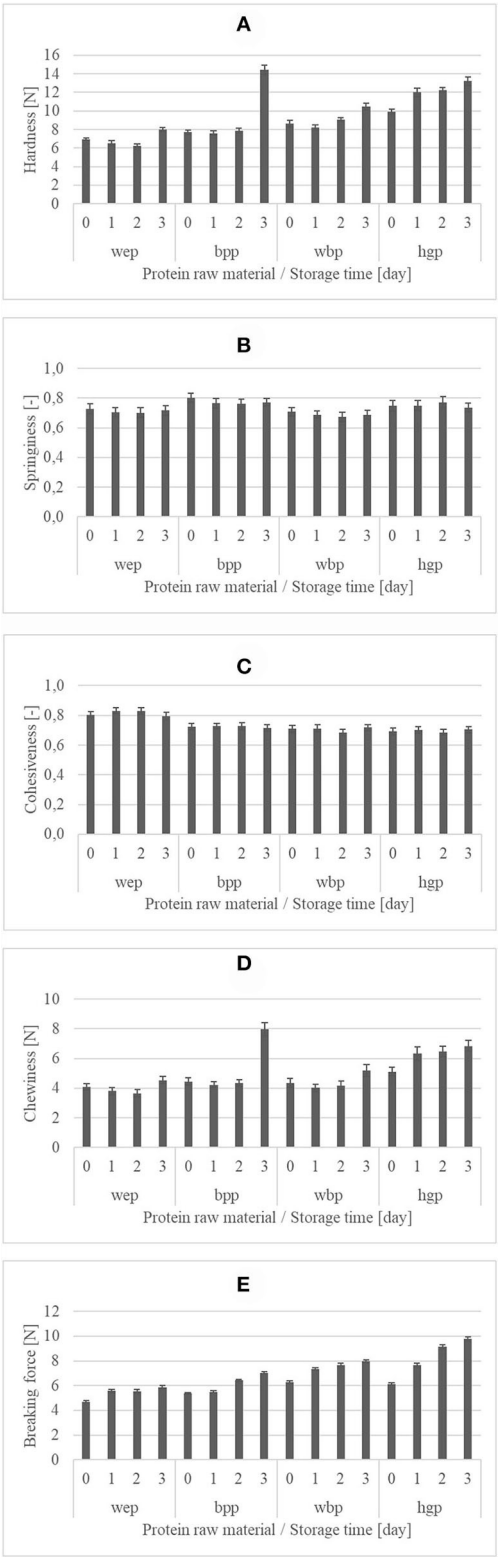

FIGURE 1
Texture attributes [**(A)** hardness [N]; **(B)** springiness [-]; **(C)** cohesiveness [-]; **(D)** chewiness [N]; **(E)** breaking force [N]] of sponge cake sample groups with different protein raw materials (wep, whole egg powder; bpp, blood plasma powder; wbp, whole blood powder; hgb, hemoglobin powder) and stored for different time periods (0 day – day of baking after cooling, 1 day, 2 days, and 3 days).

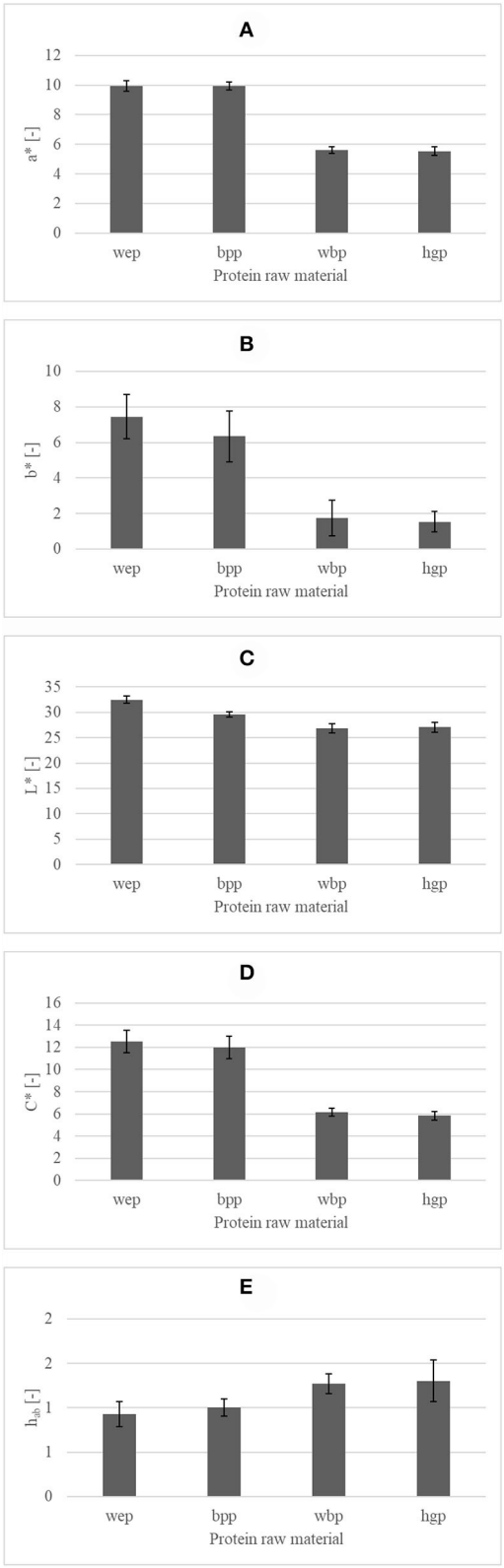

FIGURE 2
Color attributes [**(A)** a* - redness-greenness [-]; **(B)** b* - yellowness-blueness [-]; **(C)** L* - lightness [-]; **(D)** C* - chroma [-]; **(E)** h_{ab} - hue angle] of sponge cake sample groups with different protein raw materials (wep, whole egg powder; bpp, blood plasma powder; wbp, whole blood powder; hgb, hemoglobin powder).

result was significant for the sample type, that is, used protein source raw material (Wilks's lambda: 0.004, $p < 0.001$), and the storage time (Wilks's lambda: 0.012, $p < 0.001$). The protein raw material better determined the dependent variables. The effect of storage time also was significant, but the nominal differences between the average color values of different sample groups were very small (1-2 values on the color coordinate scales), while some color values were doubled between two different sample types. Furthermore, a particular pattern could not be observed in the color result based on the storage time, since color attributes fluctuated in different ways. The two-way interaction between the sample type and storage time was also significant (Wilks's lambda: 0.019, $p < 0.001$). The effect of interaction was weaker, but relatively stronger. According to the results of Tukey's *post-hoc* test, two different groups could be significantly ($p = 0.05$) separated based on redness-greenness coordinates; egg powdered and plasma powdered samples were redder with an average 9.94 a* value, while the whole blood powdered and hemoglobin powdered samples, which contained hem-iron, were less red with 5.74 a* value. Three groups could be significantly ($p = 0.05$) separated based on lightness; the lightest samples were the egg powdered samples with 32.5 L* value, the next ones were the plasma powdered samples with 29.59 L* value, and the darkest were the whole blood powdered and hemoglobin powdered samples with an average of 26.97 L* value. These results clearly indicate that the addition of hem-iron can cause black colorization in the heat-treated products rather than red colorization. In the case of other types of the food matrix, non-linear darkening was observed as a result of hemoglobin addition (67).

Because of this, hem-iron can be utilized in originally dark-colored products or beside adequate marketing tools for marketing the high nutritional value of the product. Based on yellowness-blueness coordinates, three groups could be significantly ($p = 0.05$) separated. The hemoglobin powdered and whole blood powdered samples were less yellow with a 1.63 b* value, the plasma powdered samples were more yellow with a 6.34 b* value, and the egg powdered samples were the most yellow with a 7.44 b* value. Two groups could be significantly ($p = 0.05$) separated based on chroma: one group contained the samples with hem-iron with an average 6.11 C* value and the other group contained the plasma powdered and egg powdered samples with a 12.24 C* value. Two groups could be significantly ($p = 0.05$) separated based on Hue angle: one group contained the samples with hem-iron with an average 1.33 Hue angle value, and the other group contained the plasma powdered and egg powdered samples with a 0.99 Hue angle value. Hue angle and chroma have two factors: redness-greenness and yellowness-blueness coordinates. The significant differences observed in the Hue angle reflect redness-greenness. It could be said that sample groups, which contained hem-iron, were globally similar, and egg powdered and blood plasma powdered sample groups were also slightly similar in the case of color attributes.

Water activity and dry matter content

The results of water activity measurement (not shown) were difficult to evaluate because of the large standard deviation. Water activity results of crumb (inner side of cake) from samples on the day of baking and on the first day of storage were between 0.52 and 0.66 in the case of all products and depended on the distance of the analytical sample part from the crust.

The dry matter content of sample groups with different raw materials was not significantly different. The average dry matter content of each sample group was nearly 25 w/w%, except for the sponge cakes made with blood plasma powder which showed 23 w/w% dry matter content. Although the difference was not significant, it can be explained by the outstandingly good foaming and water binding capacity of blood plasma, and this foam structure may lose less water during the baking process. Most of the sample groups typically changed similarly: cakes became wetter from the humidity of the air between the day of baking and the first storing day and then started to dry until the second day because of the syneresis, due to the aging of colloid systems. It was interesting that dry matter content continuously increased in the case of the samples with whole blood powder from the first storing day, but it decreased again in the case of other sample groups from the second storing day, as these got more wetter. This observation may be connected with the syneresis of different types of colloid systems.

Sensory evaluation

The normality of residuals was checked by D'Agostino's K-squared test, and the homogeneity of variances was checked by Box's M test (objective flexibility, objective crumbing, objective stickiness, objective dryness, objective cocoa smell intensity, objective cocoa flavor intensity, preference smell, preference color, preference taste, preference texture, and preference overall impression: $n = 33$, $N = 165$) to confirm that MANOVA could be carried out.

The results of sensory evaluation had a relatively great standard deviation, so these were hard to statistically evaluate in case of objective as well as subjective properties. The descriptive statistics of sensory properties is listed in Table 2. Significant differences and lack of significant differences between sample groups are marked in Table 2. Based on the results of MANOVA, the effect of the sample type on the dependent variables was not significant (Wilks's lambda: 0.587, $p < 0.001$). It means that a greater part of the dependent variables could not be explained by the differences in the sample types than part could be. The panel could not identify the differences between the different sample groups, except for a few properties according to Tukey's *post-hoc* test. The few exceptions, in which different groups could be significantly ($p = 0.05$) separated, were the following: (1) based on objective

TABLE 2 Descriptive statistics (mean [-], standard deviation [-], and sample number [-]) and homogeneous subsets of results of sensory properties (objective flexibility, objective crumbing, objective stickiness, objective dryness, objective cocoa smell intensity, objective cocoa flavor intensity, preference smell, preference color, preference taste, preference texture, and preference overall impression) of different sample groups (samples with blood plasma powder, samples with egg powder, black colored samples with egg powder, samples with hemoglobin powder, and samples with whole blood powder).

Sample type		Mean	Std. deviation	N	Homogeneous subsets
Flexibility - objective	Samples with blood plasma powder	3.67	1.19	33	b
	Samples with egg powder	3.24	1.06	33	a,b
	Black colored samples with egg powder	3.73	0.91	33	b
	Samples with hemoglobin powder	2.88	1.24	33	a
	Samples with whole blood powder	3.09	0.84	33	a,b
	Total	3.32	1.10	165	
Crumbing - objective	Samples with blood plasma powder	2.52	1.00	33	a
	Samples with egg powder	3.03	1.05	33	a
	Black colored samples with egg powder	2.61	1.06	33	a
	Samples with hemoglobin powder	3.18	1.10	33	a
	Samples with whole blood powder	3.24	1.23	33	a
	Total	2.92	1.12	165	
Stickiness - objective	Samples with blood plasma powder	2.58	0.94	33	a
	Samples with egg powder	2.67	0.99	33	a
	Black colored samples with egg powder	2.64	0.96	33	a
	Samples with hemoglobin powder	2.52	0.94	33	a
	Samples with whole blood powder	2.85	0.91	33	a
	Total	2.65	0.94	165	
Dryness - objective	Samples with blood plasma powder	2.21	0.99	33	a
	Samples with egg powder	2.52	1.03	33	a
	Black colored samples with egg powder	1.97	1.05	33	a
	Samples with hemoglobin powder	2.12	0.99	33	a
	Samples with whole blood powder	2.03	0.99	33	a
	Total	2.17	1.01	165	
Cocoa smell - objective	Samples with blood plasma powder	3.00	0.87	33	a
	Samples with egg powder	2.97	0.98	33	a
	Black colored samples with egg powder	3.30	1.26	33	a
	Samples with hemoglobin powder	3.27	1.01	33	a
	Samples with whole blood powder	2.97	1.21	33	a
	Total	3.10	1.07	165	
Cocoa flavor - objective	Samples with blood plasma powder	2.94	1.17	33	a
	Samples with egg powder	3.09	0.98	33	a,b
	Black colored samples with egg powder	3.73	0.94	33	b
	Samples with hemoglobin powder	3.36	1.19	33	a,b
	Samples with whole blood powder	3.03	1.24	33	a,b
	Total	3.23	1.13	165	
Smell - preference	Samples with blood plasma powder	3.09	1.13	33	a
	Samples with egg powder	3.24	0.87	33	a
	Black colored samples with egg powder	3.58	1.12	33	a
	Samples with hemoglobin powder	3.33	1.05	33	a
	Samples with whole blood powder	3.12	1.08	33	a
	Total	3.27	1.06	165	

(Continued)

TABLE 2 (Continued)

Sample type		Mean	Std. deviation	N	Homogeneous subsets
Color - preference	Samples with blood plasma powder	3.42	1.17	33	a,b
	Samples with egg powder	3.06	1.06	33	a
	Black colored samples with egg powder	4.09	0.84	33	b,c
	Samples with hemoglobin powder	4.03	0.95	33	b,c
	Samples with whole blood powder	4.12	1.02	33	c
	Total	3.75	1.09	165	
Taste - preference	Samples with blood plasma powder	3.12	1.11	33	a
	Samples with egg powder	3.33	1.05	33	a
	Black colored samples with egg powder	3.55	1.09	33	a
	Samples with hemoglobin powder	3.36	1.06	33	a
	Samples with whole blood powder	2.82	1.18	33	a
	Total	3.24	1.11	165	
Texture - preference	Samples with blood plasma powder	3.24	1.17	33	a,b
	Samples with egg powder	3.18	0.85	33	a,b
	Black colored samples with egg powder	3.73	1.07	33	b
	Samples with hemoglobin powder	2.97	1.19	33	a
	Samples with whole blood powder	3.03	0.92	33	a,b
	Total	3.23	1.07	165	
Overall impression - preference	Samples with blood plasma powder	3.42	1.20	33	a
	Samples with egg powder	3.33	0.92	33	a
	Black colored samples with egg powder	3.82	1.01	33	a
	Samples with hemoglobin powder	3.45	1.06	33	a
	Samples with whole blood powder	3.24	1.06	33	a
	Total	3.45	1.06	165	

flexibility, two groups were identified (group 1: hemoglobin powdered, whole blood powdered, and egg powdered samples; group 2: whole blood powdered, egg powdered, blood plasma powdered, and black colored egg powdered samples); (2) based on objective cocoa flavor, two groups were identified (group 1: blood plasma powdered, whole blood powdered, egg powdered, and hemoglobin powdered samples; group 2: whole blood powdered, egg powdered, hemoglobin powdered, and black colored egg powdered samples); (3) based on color preference, three groups were identified (group 1: egg powdered and blood plasma powdered samples; group 2: blood plasma powdered, hemoglobin powdered, and black colored egg powdered samples; group 3: hemoglobin powdered, black colored egg powdered, and whole blood powdered samples); and (4) based on texture preference, two groups were identified (group 1: hemoglobin powdered, whole blood powdered, egg powdered, and blood plasma powdered samples; group 2: whole blood powdered, egg powdered, blood plasma powdered, and black colored egg powdered samples). This result can be explained by the fact that panelists probably defined the perceived softness (inversely proportional to hardness) as the flexibility of the sponge cake samples. So, differences in the hardness of different sponge cake types, which were instrumentally measured by TPA, could be slightly detected by the unskilled panelists. It was interesting that sample groups made with egg powder were slightly different. This difference is due to the preconception caused by the color difference. Interestingly, the results of objectively evaluated flexibility were not fully expressed in the preference for texture. In contrast to TPA, this can hardly be explained by the similar foaming and texturizing properties of plasma and egg only. The small difference in objective cocoa flavor and color preference can be explained by the instrumentally measured color results, because the color of foods can influence consumers. This assumption could be confirmed by the fact that control egg powdered sponge cakes and "placebo" black colored egg powdered samples were assessed differently in the case of each sensory property. This difference was self-evidently completely significant ($p = 0.05$) in case of color preference, for a part of the panel members significant ($p = 0.05$) in case of objective flexibility, objective cocoa flavor and texture preference, and trend-like in case of other sensory attributes. According to the comments of panelists, sometimes extra cocoa flavor or blood taste and/or smell could be noticed in the "placebo" samples. The majority

of panelists could notice the blood or iron flavor in sponge cakes made with whole blood powder. It was interesting that sponge cakes made with blood plasma powder were recognized as control samples or more sweet egg powdered samples by a few panelists. It could be explained by the light color and higher salt content of these cakes, because salt has a synergist effect on sweetness.

This assumption could be confirmed by the fact that control egg powdered sponge cakes and "placebo" black colored egg powdered samples were assessed differently in the case of each sensory property. This difference was self-evidently completely significant ($p = 0.05$) in case of color preference, for a part of the panel members significant ($p = 0.05$) in case of objective flexibility, objective cocoa flavor and texture preference, and trend-like in case of other sensory attributes.

Development of nutritional properties

In addition to the effect of egg allergen substitution by powdered blood products on techno-functional and sensory properties, the development of nutritional properties has to be mentioned. The added iron content in the case of porcine/bovine whole blood powder was 1.5 mg / 2.9 mg. Iron added with 1 w/w% whole porcine/bovine blood powder covers 18.8% / 36.3% of the iron requirement of an average man, or 8.3% / 16.1% of the iron requirement of an average woman. So, an increase in iron content was also significant in the case of whole blood powder and hemoglobin powder enrichment. Hemoglobin powder contains almost just hemoglobin from blood proteins. Hem-origin iron content of sponge cake made with whole blood powder and hemoglobin powder can help to prevent and may play a role in the treatment of childhood iron deficiency anemia in an acceptable form for children.

Pure plasma powder does not contain hem-iron, but it contains the albumin fraction of blood proteins, which is responsible for the texture developing effect of whole blood powder. To further investigate this effect, a separate examination with plasma powder is preferred.

Conclusion

Based on the results of this study, powdered blood products are suitable substituents for the egg in cakes. Although the difference between sponge cakes made with egg powder and blood products is measurable and perceptible. Some quality attributes of the product rather improved as well as the new products were completely egg-free. A good example of the improved properties is that the texture was harder and more chewable in case of cakes made with blood products instead of egg as well as the color was darker and more saturated in case of cakes made with whole blood and hemoglobin powder. The darker and more saturated colors made the samples appear to contain more cocoa. Sponge cakes made with blood plasma powder are more similar to common sponge cakes made with egg powder, thanks to the similar albumin content and being free from hem-iron, but this benefit also means a great disadvantage in the view of nutritional value. Dry matter content and water activity were at a desirable level in all the sample groups. Due to drying and changes in colloidal structure, all the sample groups became harder and more chewable during storage. However, this change was so small that it can only be determined with instrumental measurement. It did not affect the final quality of the product. The differences between texture and sensory properties of sponge cakes made with egg powder and different blood origin powders could not or could just barely be noticed by unskilled panelists (consumers). An interesting finding was that the unskilled panelists have a different perception of the whole sample because of the different preconceptions based on the different appearances in the case of two sample groups with the same ingredients. Concerning all attributes, there was no best cake, but only cakes which fit better for purpose. If the purpose is substituting egg powder with the smallest color and texture change, the best choice is the blood plasma powder based on the results of this study. But besides coloring matters, egg powder can be substituted by whole blood powder and hemoglobin powder because consumers cannot feel the difference between the different cakes. If the purpose is to develop a harder, less breakable cake, which can take more fillings or can stand rougher handling, the best choice would be the cake made with hemoglobin powder. Whole blood and hemoglobin enrichments may be acceptable in cakes and sweetness by children, and a harder, less breakable sponge cake can stand special formatting in case of production of desserts for children.

Data availability statement

The raw data supporting the conclusions of this article will be made available by the authors, without undue reservation.

Ethics statement

Ethical review and approval was not required for the study on human participants in accordance with the local legislation and institutional requirements. Written informed consent from the participants or participants legal guardian/next of kin was not required to participate in this study in accordance with the national legislation and the institutional requirements.

Author contributions

TC and AV-T contributed to conception. TC conceived and designed the analysis, contributed to statistical analysis, and wrote the first draft of the manuscript. TC and DK collected the data and performed the analysis. AV-T and KP-H contributed to manuscript revision, read, and approved the submitted version. GH supervised the storage technology aspect of the work. KB-K supervised the bakery science aspect of the work. BA supervised the nutritional science aspect of the work. JS and LF supervised the livestock science and technology aspect of the work. All authors contributed to the article and approved the submitted version.

Funding

This research was supported by the Hungarian University of Agriculture and Life Sciences, Doctoral School of Food Sciences (Budapest, Hungary). This research was funded by the Ministry of Innovation and Technology within the framework of the Thematic Excellence Program 2021, National Defense, National Security Subprogram (TKP2021-NVA-22).

Conflict of interest

The authors declare that the research was conducted in the absence of any commercial or financial relationships that could be construed as a potential conflict of interest.

Publisher's note

All claims expressed in this article are solely those of the authors and do not necessarily represent those of their affiliated organizations, or those of the publisher, the editors and the reviewers. Any product that may be evaluated in this article, or claim that may be made by its manufacturer, is not guaranteed or endorsed by the publisher.

References

1. Floros JD, Newsome R, Fisher W, Barbosa-Cánovas GV, Chen H, Dunne CP, et al. Feeding the world today and tomorrow: the importance of food science and technology. *Compr Rev Food Sci Food Saf.* (2010) 9:572–99. doi: 10.1111/j.1541-4337.2010.00127.x

2. Liu XQ, Yonekura M, Tsutsumi M, Sano Y. Physicochemical properties of aggregates of globin hydrolysates. *J Agric Food Chem.* (1996) 44:2957–61. doi: 10.1021/jf9505786

3. Duarte RT, Carvalho Simões MC, Sgarbieri VC. Bovine blood components: fractionation, composition, and nutritive value. *J Agric Food Chem.* (1999) 47:231–6. doi: 10.1021/jf9806255

4. Hsieh YHP, Ofori JA. Blood-derived products for human consumption. *Revel Sci*. (2011) 1:14.21.

5. Ofori JA, Hsieh YHP. *The Use of Blood and Derived Products as Food Additives*. In Food additive. New York, NY; San Francisco, CA; London: Intech Open Access Publisher (2012). p. 299–56.

6. Toldrá F, Aristoy MC, Mora L, Reig M. Innovations in value-addition of edible meat by-products. *Meat Sci.* (2012) 92:290–6. doi: 10.1016/j.meatsci.2012.04.004

7. Bah CS, Bekhit AEDA, Carne A, McConnell MA. Slaughterhouse blood: an emerging source of bioactive compounds. *Compr Rev Food Sci Food Saf.* (2013) 12:314–31. doi: 10.1111/1541-4337.12013

8. Csurka T, Szücs F, Csehi B, Friedrich LF, Pásztor-Huszár K. Substitution of milk allergen ingredient by blood plasma powder in custard with different sweeteners. *Prog Agric Eng Sci.* (2021) 17:77–85. doi: 10.1556/446.2021.30010

9. Csurka T, Szücs F, Csehi B, Friedrich LF, Pásztor-Huszár K. Analysis of several techno-functional and sensory attributes upon egg allergen ingredient substitution by blood plasma powder in sponge cake. *Prog Agric Eng Sci.* (2021) 17:87–98. doi: 10.1556/446.2021.30011

10. Galanakis CM. Separation of functional macromolecules and micromolecules: from ultrafiltration to the border of nanofiltration. *Trends Food Sci Technol.* (2015) 42:44–63. doi: 10.1016/j.tifs.2014.11.005

11. Galanakis CM. The food systems in the era of the coronavirus (COVID-19) pandemic crisis. *Foods.* (2020) 9:523. doi: 10.3390/foods9040523

12. Galanakis CM, Aldawoud T, Rizou M, Rowan NJ, Ibrahim SA. Food ingredients and active compounds against the Coronavirus disease (COVID-19) pandemic: a comprehensive review. *Foods.* (2020) 9:1701. doi: 10.3390/foods9111701

13. Galanakis CM. Functionality of food components and emerging technologies. *Foods.* (2021) 10:128. doi: 10.3390/foods10010128

14. Osborne NJ, Koplin JJ, Martin PE, Gurrin LC, Lowe AJ, Matheson MC. HealthNuts Investigators. Prevalence of challenge-proven IgE-mediated food allergy using population-based sampling and predetermined challenge criteria in infants. *J Allergy Clin Immunol.* (2011) 127:668–76. doi: 10.1016/j.jaci.2011.01.039

15. Shepherd IS. Yoel RW. "Cake emulsions". Ch. 5. In: Friberg S, editor. *Food Emulsions*. New York, NY, USA: Marcel Dekker. (1976). p. 215–75.

16. Johnson LA, Havel EF, Hoseney RC. Bovine plasma as a replacement for egg in cakes. *Cereal Chem.* (1979) 56:339–42.

17. Lee CC, Johnson LA, Love JA, Johnson S. As an egg white substitute in cakes'. *Cereal Chem.* (1991) 68:100–4.

18. Putnam F. *The Plasma Proteins V3: Structure, Function, and Genetic Control, 2nd ed. Volume III*. Bloomington, IN: Elsevier (2012).

19. Lu GH, Chen TC. Application of egg white and plasma powders as muscle food binding agents. *J Food Eng.* (1999) 42:147–51. doi: 10.1016/S0260-8774(99)00112-0

20. Caldironi HA, Ockerman HW. Incorporation of blood proteins into sausage. *J Food Sci.* (1982) 47:405–8. doi: 10.1111/j.1365-2621.1982.tb10091.x

21. Jolivet P, Boulard C, Chardot T, Anton M. New insights into the structure of apolipoprotein B from low-density lipoproteins and identification of a novel YGP-like protein in hen egg yolk. *J Agric Food Chem.* (2008) 56:5871–9. doi: 10.1021/jf800321m

22. Liberal Â, Pinela J, Vívar-Quintana AM, Ferreira IC, Barros L. Fighting iron-deficiency anemia: innovations in food fortificants and biofortification strategies. *Foods.* (2020) 9:1871. doi: 10.3390/foods9121871

23. Egyed A. Carrier mediated iron transport through erythroid cell membrane. *Br J Haematol.* (1988) 68:483–6. doi: 10.1111/j.1365-2141.1988.tb04241.x

24. Ockerman HW, Hansen CL. *Animal Byproduct Processing and Utilization*. Boca Raton, London, New York, Washington, D.C: CRC Press. (2000) doi: 10.1201/9781482293920

25. Sorapukdee S, Narunatsopanon S. Comparative study on compositions and functional properties of porcine, chicken and duck blood. *Korean J Food Sci Anim Resour.* (2017) 37:228. doi: 10.5851/kosfa.2017.37.2.228

26. USDA, *United States Department of Agriculture, Agricultural Research Service, Nutrient Data Laboratory*. (2018). USDA National Nutrient Database for Standard

Reference, Release 29. Available online at: https://fdc.nal.usda.gov/ (accessed November 17, 2018).

27. Yada RY, Jackman R, Smith JL. *Protein Structure-Function Relationships in Foods*. Glasgow: Blackie Academic and Professional (1994). doi: 10.1007/978-1-5904615-2670-4

28. Herrero AM, Cambero MI, Ordonez JA, De la Hoz L, Carmona P. Plasma powder as cold-set binding agent for meat system: Rheological and Raman spectroscopy study. *Food Chem.* (2009) 593: 493–9. doi: 10.1016/j.foodchem.2008.07.084

29. Cofrades S, Guerra MA, Carballo J, Martin F, Colmenero FJ. Plasma protein and soy fiber content effect on bologna sausage properties as influenced by fat level. *J Food Sci.* (2000) 65:281–27. doi: 10.1111/j.1365-2621.2000.tb15994.x

30. Jarmoluk A, Pietrasik Z. Response surface methodology study on the effects of blood plasma, microbial transglutaminase and κ-carrageenan on pork batter gel properties. *J Food Engg.* (2003) 60:327–34. doi: 10.1016/S0260-8774(03)00055-4

31. Pietrasik Z, Jarmoluk A, Shand P.J. Effect of non-meat proteins on hydration and textural properties of pork meat gels enhanced with microbial transglutaminase. *LWT Food Sci Technol.* (2007) 40:915–20. doi: 10.1016/j.lwt.2006.03.003

32. Seideman SC, Smith GC, Carpenter ZL, Dill CW. Plasma protein isolate and textured soy protein in ground beef formulations. *J Food Sci.* (1979) 44:1032–5. doi: 10.1111/j.1365-2621.1979.tb03439.x

33. Suter DA, Sustek E, Dill CW, Marshall WH, Carpenter ZL. A method for measurement of the effect of blood protein concentrates on the binding forces in cooked ground beef patties. *J Food Sci.* (1976) 41:1428–32. doi: 10.1111/j.1365-2621.1976.tb01188.x

34. Andago A, Lamuka JIAMP, Nduati R, Kangemi K. *Development of A Bovine Blood Enriched Porridge Flour for Alleviation of Anaemia Among Young Children in Kenya*. (2015).

35. Walter T, Hertrampf E, Pizarro F, Olivares M, Llaguno S, Letelier A, et al. Effect of bovine-hemoglobin-fortified cookies on iron status of schoolchildren: a nationwide program in Chile. *Am J Clin Nutr.* (1933) 57:190–4. doi: 10.1093/ajcn/57.2.190

36. Soukoulis C, Yonekura L, Gan HH, Behboudi-Jobbehdar S, Parmenter C, Fisk I. Probiotic edible films as a new strategy for developing functional bakery products: The case of pan bread. *Food Hydrocol.* (2014) 39:231–42. doi: 10.1111/j.1750-3841.2006.00005.x

37. Pohjanheimo TA, Hakala MA, Tahvonen RL, Salminen SJ, Kallio HP. Flaxseed in breadmaking: Effects on sensory quality, aging, and composition of bakery products. *J Food Sci.* (2006) 71:343–8. doi: 10.1016/j.foodhyd.2014.01.023

38. De Huidobro FR, Miguel E, Blázquez B, Onega E, A. comparison between two methods (Warner–Bratzler and texture profile analysis) for testing either raw meat or cooked meat. *Meat Sci.* (2005) 69:527–36. doi: 10.1016/j.meatsci.2004.09.008

39. Nishinari K, Fang Y, Rosenthal A. Human oral processing and texture profile analysis parameters: Bridging the gap between the sensory evaluation and the instrumental measurements. *J Texture Stud.* (2019) 50:369–80. doi: 10.1111/jtxs.12404

40. Paraskevopoulou A, Kiosseoglou V. Texture profile analysis of heat-formed gels and cakes prepared with low cholesterol egg yolk concentrates. *J Food Sci.* (1997) 62:208–11. doi: 10.1111/j.1365-2621.1997.tb04401.x

41. Tomasevic I, Tomovic V, Ikonic P, Rodriguez JML, Barba FJ, Djekic I. Evaluation of poultry meat colour using computer vision system and colourimeter: is there a difference? *Br Food J.* (2019) 121:1078–87. doi: 10.1108/BFJ-06-2018-0376

42. Anese M, Sovrano S, Bortolomeazzi R. Effect of radiofrequency heating on acrylamide formation in bakery products. *European Food Research and Technology*. (2008) 226:1197–203 doi: 10.1007/s00217-007-0693-x

43. European Union. *Regulation (EC) No 1333/2008 of the European Parliament and of the Council of 16 December 2008 on Food Additives*. 1078–87.

44. Forgács A, Bóna E, Csíkos T. Az ízpreferenciák, ízaverziók és ételfóbiák pszichológiai vonatkozásai. *Magyar Belorvosi Archívum*. (2017) 70:300–10. Available online at: http://real-j.mtak.hu/11358/6/MBA%202017%206.pdf

45. Földváry M. *Színkommunikáció: Élelmiszer és színe*. (2015) 1.4.3. Available online at: http://www.szinkommunikacio.hu/14_07.htm (accessed September 21, 2021).

46. Spence C. On the psychological impact of food colour. *Flavour.* (2015) 4:21. doi: 10.1186/s13411-015-0031-3

47. *IBM SPSS Statistics for Windows, Version 25.0*. Armonk, NY: IBM Corp.

48. Huberty CJ, Olejnik S. *Applied MANOVA and discriminant analysis (Vol. 498)*. Hoboken, NJ: John Wiley & Sons. (2006).

49. D'Agostino RB. Transformation to normality of the null distribution of g1. *Biometrika.* (1970) 57:679–81. doi: 10.1093/biomet/57.3.679

50. Box GE. A general distribution theory for a class of likelihood criteria. *Biometrika.* (1949) 36:317–46. doi: 10.1093/biomet/36.3-4.317

51. Carlin GT. A microscopic study of the behavior of fats in cake batters. *Cereal Chem.* (1944) 21:189–99.

52. Coke M, Wilde PJ, Russell EJ, Clark DC. The influence of surface composition and molecular diffusion on the stability of foams formed from protein/surfactant mixtures. *J Colloid Interface Sci.* (1990) 138:489–504. doi: 10.1016/0021-9797(90)90231-C

53. Handelman AR, Conn JF, Lyons JW. Bubble mechanics in thick foams and their effects on cake quality. *Cereal Chem.* (1961) 38:294–305.

54. Brooker BE. The stabilisation of air in cake batters-the role of fat. *Food Struct.* (1993) 12:285–96.

55. Dickinson E, Hong ST. Influence of water-soluble nonionic emulsifier on the rheology of heat-set protein-stabilized emulsion gels. *J Agric Food Chem.* (1995) 43:2560–6. doi: 10.1021/jf00058a002

56. Dickinson E, Yamamoto Y. Viscoelastic properties of heat-set whey protein-stabilized emulsion gels with added lecithin. *J Food Sci.* (1996) 61:811–6. doi: 10.1111/j.1365-2621.1996.tb12208.x

57. Chen J, Dickinson E. Viscoelastic properties of protein-stabilized emulsions: Effect of protein– surfactant interactions. *J Agric Food Chem.* (1998) 46:91–7. doi: 10.1021/jf970536c

58. Awuchi CG, Igwe VS, Echeta CK. The functional properties of foods and flours. *Int J Adv Acad Res.* (2019) 5:139–60.

59. Turbin-Orger A, Della Valle G, Doublier JL, Fameau AL, Marze S, Saulnier L. Foaming and rheological properties of the liquid phase extracted from wheat flour dough. *Food Hydrocoll.* (2015) 43:114–24. doi: 10.1016/j.foodhyd.2014.05.003

60. Rodríguez-García J, Puig A, Salvador A, Hernando I. Optimization of a sponge cake formulation with inulin as fat replacer: structure, physicochemical, and sensory properties. *J Food Sci.* (2012) 77:C189–97. doi: 10.1111/j.1750-3841.2011.02546.x

61. Guadarrama-Lezama AY, Carrillo-Navas H, Pérez-Alonso C, Vernon-Carter EJ, Alvarez-Ramirez J. Thermal and rheological properties of sponge cake batters and texture and microstructural characteristics of sponge cake made with native corn starch in partial or total replacement of wheat flour. *LWT*. (2016) 70:46–54. doi: 10.1016/j.lwt.2016.02.031

62. Hosseini H, Bolourian S, Shahidi F. Extending the shelf-life of sponge cake by an optimized level of jujube fruit flour determined using custom mixture design. *Br Food J.* (2019) 121:12. doi: 10.1108/BFJ-07-2019-0489

63. Salehi F, Kashaninejad M. Texture profile analysis and stress relaxation characteristics of quince sponge cake. *J Food Meas Charact*. (2018) 12:1203–10. doi: 10.1007/s11694-018-9734-3

64. Sahi SS, Alava JM. Functionality of emulsifiers in sponge cake production. *J Sci Food Agric.* (2003) 83:1419–29. doi: 10.1002/jsfa.1557

65. Gupta M, Bawa AS, Semwal AD. Effect of barley flour incorporation on the instrumental texture of sponge cake. *Int J Food Prop.* (2009) 12:243–51. doi: 10.1080/10942910802312082

66. Salehi F, Kashaninejad M. Modeling of moisture loss kinetics and color changes in the surface of lemon slice during the combined infrared-vacuum drying. *Inf Proc Agric.* (2018) 5:516–23. doi: 10.1016/j.inpa.2018.05.006

67. Oellingrath IM, Sslinde E. Color, pigment and iron content of meat loaves with blood, blood emulsion, or mechanically deboned meat added. *J Food Sci.* (1985) 50:1551–5 doi: 10.1111/j.1365-2621.1985.tb10531.x

frontiers | Frontiers in Nutrition

TYPE Original Research
PUBLISHED 02 September 2022
DOI 10.3389/fnut.2022.984715

OPEN ACCESS

EDITED BY
John-Lewis Zinia Zaukuu,
Kwame Nkrumah University of Science and Technology, Ghana

REVIEWED BY
Iriani Rodrigues Maldonade,
Brazilian Agricultural Research Corporation (EMBRAPA), Brazil
Charles Odilichukwu R. Okpala,
Wroclaw University of Environmental and Life Sciences, Poland

*CORRESPONDENCE
Veronika Somoza
v.somoza.leibniz-lsb@tum.de

SPECIALTY SECTION
This article was submitted to Nutrition and Food Science Technology, a section of the journal Frontiers in Nutrition

RECEIVED 02 July 2022
ACCEPTED 15 August 2022
PUBLISHED 02 September 2022

CITATION
Pirkwieser P, Grosshagauer S, Dunkel A, Pignitter M, Schneppe B, Kraemer K and Somoza V (2022) Evaluation of spray-dried eggs as a micronutrient-rich nutritional supplement. *Front. Nutr.* 9:984715. doi: 10.3389/fnut.2022.984715

Evaluation of spray-dried eggs as a micronutrient-rich nutritional supplement

Philip Pirkwieser[1], Silke Grosshagauer[2], Andreas Dunkel[1], Marc Pignitter[2], Bernard Schneppe[3], Klaus Kraemer[4,5] and Veronika Somoza[1,2,6]*

[1]Leibniz Institute for Food Systems Biology at the Technical University of Munich, Freising, Germany, [2]Department of Physiological Chemistry, Faculty of Chemistry, University of Vienna, Vienna, Austria, [3]OVOBEST Eiprodukte GmbH & Co. KG, Neuenkirchen-Vörden, Germany, [4]Sight and Life Foundation, Basel, Switzerland, [5]Department of International Health, Johns Hopkins Bloomberg School of Public Health, Baltimore, MD, United States, [6]School of Life Sciences Weihenstephan, Technical University of Munich, Freising, Germany

Regular consumption of hen eggs can help to prevent deficiencies of essential nutrients, such as essential amino acids, vitamin A and E or trace elements zinc and selenium, for vulnerable populations. This study focused on assessing the nutritional value of spray-dried eggs, favored by their manufacturability, storability and ease of addition to (complementary) foods. Using a wide range of analytical techniques, we recorded and compared the nutrient profiles of commercially produced pasteurized whole eggs and their respective powder samples spray-dried at 160°C. Important nutrients that were not significantly affected by spray-drying include total fat content, several amino acids, α- and δ-tocopherol, lutein, zeaxanthin, essential trace elements and cobalamin. The most notable mean losses were found for unsaturated fatty acids, e.g., linoleic (by −38.7%, from 4.11 ± 0.45 to 2.52 ± 0.75 g/100 g DM) and linolenic acid (by −60.8%, from 0.76 ± 0.05 to 0.30 ± 0.04 g/100 g DM). Despite recording significant retinol losses in two out of three batches, the overall low reduction of −14% recommend spray-dried eggs as a valuable source of vitamin A. A daily intake of spray-dried egg powder corresponding to one medium sized egg meets dietary reference values for children, e.g., by 100% for vitamin E, by 24% for retinol, by 61% for selenium and by 22% for zinc. In conclusion, even though a dry weight comparison favors supplementation with pasteurized whole eggs, our results demonstrate a high potential for spray-dried eggs as nutritional supplement. However, the spray-drying process should be optimized toward higher retentions of unsaturated fatty acids and retinol.

KEYWORDS

food quality and safety, nutritional supplement, nutrient adequacy, chicken egg, spray-drying

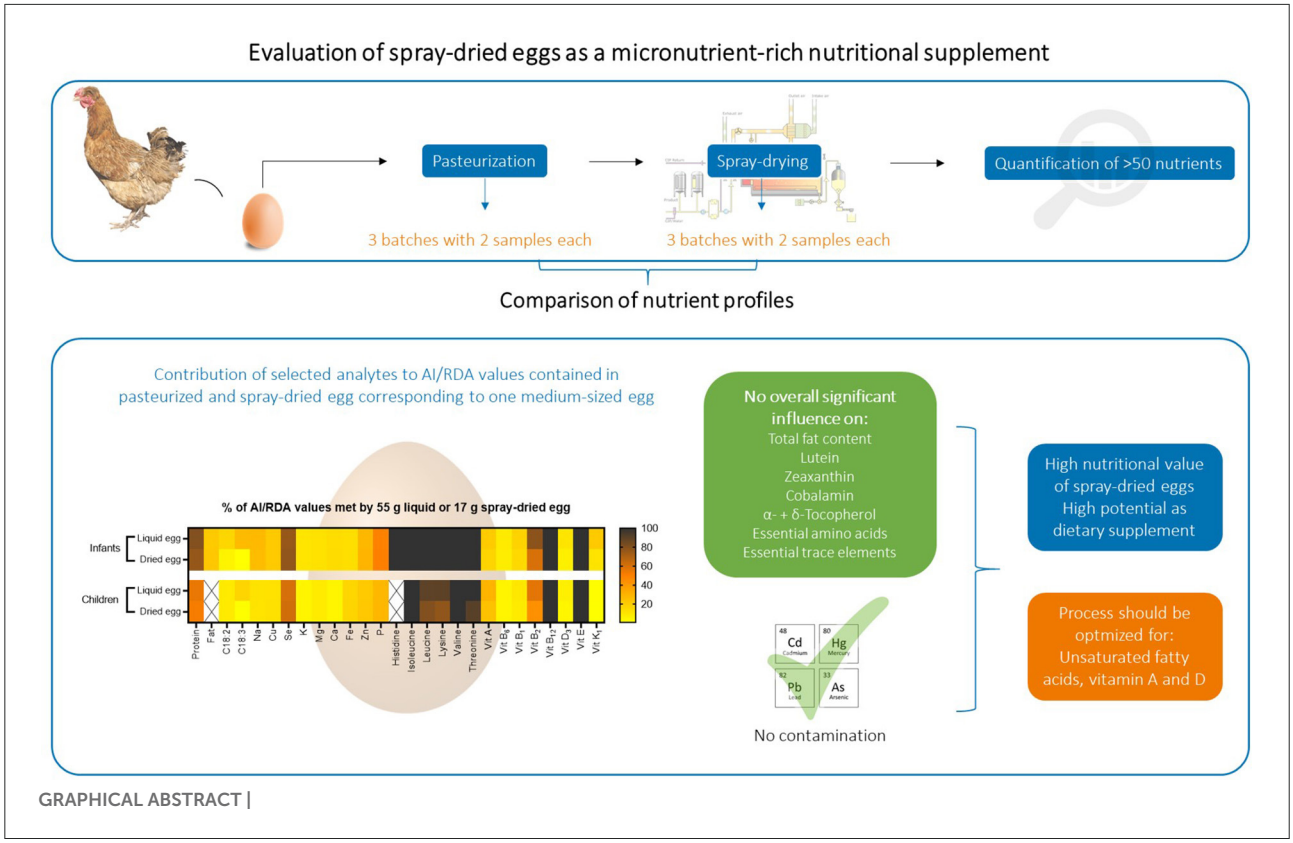

GRAPHICAL ABSTRACT |

Introduction

Hen eggs are appreciated globally as inexpensive, nutritious and technologically versatile foods. Steadily increasing production numbers over the past years, approaching 80 million tons per year, and a thereby calculated global average per capita of ∼161 eggs demonstrate their growing demand. Naturally, consumption greatly varies regionally, with annual per capita numbers ranging from 300 g in several African countries up to 19.1 kg in Japan (1, 2). The fact that whole egg is a valuable source of protein is made clear above all by its defined biological value of 100% (3). With this biological value, egg serves as a reference value for other foods and indicates how efficiently the dietary protein can be utilized as the body's own protein. With the exception of vitamin C, hen eggs contain all vitamins and represent an important source of nutrients. All fat-soluble vitamins A, D, E and K are found in the egg's yolks, with an average content per 100 g egg of 276 µg vitamin A (as retinol), 2.3 mg vitamin E (as total tocopherols), 2.9 µg vitamin D and 8.9 µg vitamin K. With these contents, eggs make an important contribution to meeting daily vitamin requirements of 0.8–1 mg of vitamin A, 12–15 mg of vitamin E, 20 µg of vitamin D and 60–70 µg of vitamin K (4).

The increasing knowledge on the efficient enrichment of fat-soluble vitamins in egg yolk ensued the idea of using hen eggs as an effective measure against dietary deficiencies, especially in developing countries (5, 6). For instance, this approach could be of importance for sub-Saharan African regions, where vitamin A deficiency is widespread and leads to a high prevalence of vision losses (7). Promising results on the supplementation with eggs could already be shown in intervention studies, e.g., regarding child growth by Iannotti et al. (8), where the addition of one egg a day to complementary foods of older infants reduced stunting and underweight by 47 and 74%, respectively. However, nutrition surveys from Europe and America also revealed that a sufficient vitamin E intake should not be taken for granted in developed countries (9). Since eggs are consumed regularly by a majority of the worldwide population, they can make an important contribution to meeting the requirements of fat-soluble nutrients. Yet, implementing strategies of increasing the consumption of hen eggs as sources of valuable essential nutrients requires both knowledge of the efficiency and technological implementation of nutrient fortification and consideration of economic and cultural factors. Particularly in areas where malnutrition is part of everyday life, availability and affordability of eggs is severely limited, with only two eggs monthly per person (10).

For technological as well as safety reasons, dried egg in all its variants—whole egg powder, egg yolk powder, egg white powder—is increasingly used in the food industry. In contrast

to dried eggs, shell eggs are not only fragile, they also require far more storage space, are more susceptible to microbial spoilage and carry a higher risk of salmonella (11). For food technology use, shell eggs are therefore often homogenized and pasteurized, which reduces the risk of salmonella transmission. Subsequent drying of the eggs also provides the advantage of reducing the water content to a minimum, thereby achieving a longer shelf life. Another benefit is that dried eggs offer a more convenient utilization, especially on a large industrial scale. Above all, drying reduces both weight and volume, resulting in a concentration of nutrients (12), suggesting a significant potential as nutritional supplement to effectively prevent malnutrition in vulnerable populations.

Another crucial point to consider for nutritional supplements is consumer acceptance—fortified foods or alternative sources of nutrients are often restrained by off-flavors (13, 14), whereas eggs are widely accepted and versatile.

Spray-drying is a common technique for dehydration of foods, in which droplets of the liquid food are formed by, e.g., a nozzle or an atomizer, and then transferred to a drying chamber, where incoming hot air causes the water to evaporate. The high-throughput process guarantees relatively low heat-spoilage and yields products of constant, pre-determined characteristics, ready for packaging (15). Although further processing of eggs to powder *via* spray-drying (usually at 160° or 180°C) is gaining more and more importance in the food industry, mirrored in several studies on the functional properties after drying (16, 17), little knowledge of how this process actually affects the eggs' entire nutrient profile exists. This obviously represents a major knowledge gap regarding the use of spray-dried eggs as nutritional supplement. A recent study by Abreha et al. (18) compared the fat and protein content of egg powder produced from eggs of two chicken breeds and attributed a high potential to its use as supplementary food. However, even though several key parameters were determined, analyses of the impact of spray-drying on, e.g., the contents of fatty acid and vitamins or the formation of peroxides were not included. Other reported influences of spray-drying on nutrients include losses of carotenoids, e.g., a reduction of lutein during pasteurization and further deterioration after spray-drying in egg yolk from carotenoid-enriched eggs (19). By contrast, Caboni et al. (20) found no significant difference in retinol contents of pasteurized whole egg and spray-dried egg powder. Additional storage experiments of these whole egg samples yielded only a slight decrease of fat-soluble vitamins at 4°C for 12 months, as opposed to a significantly greater deterioration when stored at 20°C over the same period of time (20).

Nevertheless, fortified hen's diet, a limited number of analytes or a spray-drying process incomparable to industrial scale reported impede general statements on the suitability of the spray-drying process for eggs from a nutritional point of view. To further elucidate the viability of spray-drying as a suitable method for the use of eggs as nutritional supplements, we performed a comprehensive analysis of food quality and safety related key analytes, using commercially produced pasteurized whole eggs and their respective spray-dried egg powder. Besides investigating the desirable preservation of nutrients, including vitamins A, D, E and unsaturated fatty acids, a putative enrichment of anti-nutrients or potential toxicants, such as non-essential trace elements, was monitored as well. Since higher temperatures and contact with oxygen favor lipid oxidation, the peroxide value was also part of the chemical-analytical examination. In this regard, e.g., Verardo et al. (21) found a twofold increase in peroxide content from 2.6 ± 0.3 meq O_2/kg fat in pasteurized eggs to 5.3 ± 0.4 meq O_2/kg fat in spray-dried samples. Ultimately, the purpose of the here presented work was to display whether spray-dried eggs have the potential to contribute to daily nutrient requirements as a supplement to fat-based complementary foods or whether the consumption of pasteurized whole eggs would be more beneficial to meet the dietary reference intakes (DRI). Therefore, the effect of spray-drying was studied in-depth for key nutrients of relevance regarding the use of spray-dried eggs as nutritional supplement. Obtained results were translated to their contribution to reference intakes [Adequate Intakes (AI) and Recommended Dietary Allowances (RDA)] for infants and children. The data presented herein forms the most complete assessment on the effect of industrial spray-drying on the nutritional value of eggs to date. The findings should help improve the spray-drying process for the subsequent use of eggs as high quality nutritional supplement in the future, especially as an effective measure against malnutrition in vulnerable populations of low- and middle-income countries."

Materials and methods

Chemicals

Chemicals and reagents used for sample preparation, instrument calibration and analysis were the following. Ultrapure water of resitivity >18.2 MΩ*, ethanol 96% (VWR), ethanol (absolut Emsure®, Merck), methanol (HPLC grade ≥ 99.9%, Sigma-Aldrich), n-hexane (Emplura® ≥ 95%, Merck), toluene (for analysis, Emsure® ACS Merck), chloroform (≥99% for synthesis, Carl Roth), tert.-Butylmethylether (EMSURE® ACS, for analysis, Merck), acetic acid (glacial, EMSURE® ACS Merck), nitric acid (ROTIPURAN®Supra 69%, Carl Roth), hydrochloric acid (≥37%, ACS, Sigma-Aldrich), hydrogen peroxide (trace metal grade, Sigma-Aldrich), pyrogallol (ACS reagent, ≥99% ,Sigma-Aldrich), sodium sulfate (anhydrous powder, ≥99% ACS reagent, Sigma-Aldrich), sodium sulfide (reagent grade, Sigma-Aldrich), sodium-L-ascorbate (crystalline, ≥98%, Sigma Aldrich), sodium hydroxide (≥85% p.a., Carl Roth), monopotassium phosphate (ACS, ≥9% Carl Roth), barium chloride-dihydrate (Emsure®, ACS

Merck), iron(II)sulfate-hydrate (86.0–89.0%, $FeSO_4$ basis) and iron(III)chloride-hexahydrate (97%, ACS, Sigma-Aldrich), sodium chloride (≥99.5%, p.a. ACS, Carl Roth), sodium methoxid (purum, ≥97.0%, Sigma-Aldrich) and xylenol orange tetrasodium salt (ACS, Sigma-Aldrich). Standard solutions retinol (powder), (±)-α-tocopherol, (±)-γ-tocopherol and (±)-δ-tocopherol, Butylhydroxytoluene, zeaxanthine (≥95%), methyl heptadecanoate (all HPLC standards, Sigma-Aldrich), lutein (≥96%, Merck), Instrumental Calibration Standard 2 and Alternate Metals solution (PerkinElmer), single standard solutions for mercury (PurePlus, PerkinElmer) and phosphorus (Aristar, VWR). The internal standard solution contained Sc, Rh, Ge and Re.

Instrumentation

The following instruments haven been used in this study. Ultrapure water system Arium 611 UF (Sartorius), centrifuge 5804 R and 5810 R (Eppendorf AG), concentrator 5301 (Eppendorf AG), gas chromatograph GC-2010 Plus, AOC 20is (Shimadzu), incubator INCU-Line ILS4 (VWR International), photometer Infinite M200 (Tecan), rotavapor R210 (Büchi), reflux condenser DIN NS29/32; 400 mm (Lenz Laborglasinstrumente), (U)HPLC-DAD UltiMate 3000RS (Dionex), Exion LC UHPLC system (Sciex, Darmstadt, Germany) connected to a QTRAP 6500^+ mass spectrometer (Sciex) using atmospheric pressure chemical ionization (APCI), bead-beater homogenizer (Precellys Evolution, Bertin Technologies), ICP-MS Nexion 5000 (PerkinElmer), microwave digestion system Multiwave 5000 (Anton Paar) and ultrasonic bath USC TH (VWR International). The respective application of these instruments is given in the following Methods section.

Methods

Study design and egg treatment

In order to investigate the influence of spray-drying on the nutrient profile of hen eggs, samples from three different batches of pasteurized whole egg as well as their respective spray-dried whole egg powder were analyzed. Processing of the eggs was kindly conducted by OVOBEST Eiprodukte GmbH & Co KG as follows: Fresh eggs were washed, automatically broken, filtered and homogenized. The contents were then conveyed to pasteurization at 62.2°C. Since the eggs were subsequently to be processed into powder, they were additionally pre-dried in the evaporator, yielding an average dry matter content of 30.3%, as opposed to 23.5–24% usual for shell eggs. At this stage, two samples were taken from each batch. For the powder, the liquid whole eggs were taken to the spray-drying plant (Sanovo Technology Group), where they were finely atomized through a nozzle and the resulting spray cone of fine egg droplets was sprayed into the box of the dryer. The inflow of hot air at 160°C caused the water to evaporate rapidly and the dry particles to fall to the bottom. The temperature of the outflowing air was kept between 80 and 90°C. The applied pressure ranged between 10,000 and 14,500 kPa, adjusted depending on outflowing air temperature and sample water content. The obtained powder was transported out of the spray-drying system, where two samples were taken from each batch and then aliquoted and stored at−80°C until analysis. An additional batch was prepared with an inflow temperature of 180°C and pressure ranging between 12,500 and 16,000 kPa, in order to monitor the influence of increased temperature on selected analytes. A simplified flow sketch of this procedure is illustrated in Figure S1 in Supplementary material.

Analytical methods

For fat extraction, the well-known and still commonly used (22) method according to Folch et al. (23) was chosen. The fat content was determined by differential weighing and the extracted fat was used immediately afterwards to measure the peroxide value.

Fatty acids were determined in the form of their fatty acid methyl esters as described by Aparicio and Aparicio-Ruíz (24) and Lall et al. (25) The measurement was performed by means of Gas chromatography (GC) followed by flame ionization detection (FID).

For quantitation of vitamin E, tocopherols were first extracted from the liquid egg and dried egg and separated by HPLC with reversed phase chromatography (RP). Here, separation of α-tocopherol, γ-tocopherol as well as δ-tocopherol was achieved. The β-homolog, which occurs in comparatively smaller amounts than the other homologs, could not be separated and thus quantitatively determined. Detection was performed by UV at a wavelength of 295 nm. The preparation of the sample was based on the description of Meluzzi et al., (26) which was modified as follows. From the thawed liquid egg, 5 g or, from the egg powder, 1–2 g were weighed into a 100 ml Erlenmeyer flask and used for extraction and saponification with 30 ml ethanol:potassium hydroxide solution (1:1 vol/vol). The samples were gassed with nitrogen and stirred for 30 mins. After the addition of 20 ml hexane (+1 g/L butylhydroxytoluene) and 20 ml of a saturated potassium dihydrogen phosphate (KH_2PO_4) solution, the sample was stirred for an additional 5 mins and transferred to a separating funnel. After separation, the organic phase (∼20 ml) was collected in 50 ml centrifuge tubes. The aqueous phase in the Erlenmeyer flask was transferred back to the funnel and extracted again with 20 ml hexane (+1 g/L butylhydroxytoluene). The combined organic phase (about 40 ml in total) was concentrated over nitrogen. After complete constriction, the sample was taken up in 2 ml of ethanol and transferred *via* syringe filter into an HPLC vial. The tocopherols were then measured by HPLC-UV with the

following conditions: Kinetex 5 µm EVO C18, 150 × 4.6 mm column, H_2O and methanol as mobile phases, 0.5 ml/min flow rate, 20 µl injection volume, a temperature of 10°C and detection by diode array detector (Dionex DAD-3000).

For quantification of the carotenoids lutein and zeaxanthin, LC–MS/MS analysis was performed using an Exion LC UHPLC system (Sciex, Darmstadt, Germany) connected to a QTRAP 6500^+ mass spectrometer (Sciex) using atmospheric pressure chemical ionization (APCI) in positive mode. The UHPLC systems consisted of two Exion LC AD pumps, an Exion LC degasser, an Exion LC AC column oven, an Exion LC AD autosampler, and an Exion LC controller. Chromatographic separation was achieved using a C30 Carotenoid column (250 × 4.6 mm, particle size 3 µm; YMC Europe GmbH, Dinslaken, Germany) and methanol/methyl tert-butyl ether(MTBE)/water (81/15/4, v/v/v, solvent A) and methanol/ MTBE/water (7/90/3, v/v/v, solvent B) as solvents at 40°C column temperature. The following binary gradient was applied using a total flow rate of 0.4 ml/min: 0 min 0% B, 5 min 0% B, 20 min 20% B, 22 min 100% B, 25 min 100% B, 28 min 0% B, 35 min 0%B. The mass spectrometer was operated in MRM mode, zero grade air served as the nebulizer (55 psi) and as nebulizer gas (450°C, 65 psi) and nitrogen as a curtain (35 psi) as well as collision gas. Data acquisition and instrumental control was performed using Analyst 1.6.3 software (Sciex), while quantitative data evaluation was completed with MultiQuant software (Sciex, version 3.02). To optimize the MS/MS detection for high sensitivity quantification, standard solutions of the analytes were infused into the MS instrument by the integrated syringe pump at a flow rate of 7 µl/min. The optimization of ion path parameters yielded the following values, that were applied for lutein and zeaxanthin, respectively: quantifier transition: Q1 m/z 569.3, Q3 m/z 569.2, dwell time 25 ms, declustering potential (DP) 106 V, collision energy (CE) 9 V, collision cell exit potential (CXP) 16 V, Qualifier transition: Q1 m/z 569.3, Q3 m/z 135.0, dwell time 25 ms, DP 106 V, CE 29 V, CXP 16 V. For sample preparation, egg samples were weighed into bead beater tubes (2 ml, CKMix, Bertin Technologies, Montigny Le Bretonneux, France) followed by addition of 500 µL extraction buffer containing a 1+1 mixture of MTBE and hexane and 100 µL of absolute ethanol containing butylated hydroxytoluene (BHT, 500 mg/L). Homogenization and extraction was performed using a bead-beater homogenizer (9,000 rpm for 3 × 30 and 30 s breaks). After equilibration (60 min, 10°C) and centrifugation (15 min, 12,000 rpm), the supernatant was membrane-filtered (Minisart RC 15, 0.45 µM, Sartorius, Goettingen, Germany) and directly injected (1 µl) into the LC-MS/MS instrument.

Retinol in whole egg samples was determined using the method of Pignitter et al. (27) For this purpose, the sample was saponified with KOH, followed by the addition of sodium ascorbate and sodium sulfide, extraction with hexane and measurement by HPLC-UV at 325 nm.

Regarding information on lipid oxidation, measurement of the peroxide value was considered sufficient, as the eggs used for this study did not have a long storage time and were analyzed soon after the laying date or after further processing into whole egg powder. The peroxide content in foods with a high fat content, such as cooking oil, is often determined by the Wheeler (28) method. Since hen eggs have a fat content of ∼10 g/ 100 g and thus a larger sample quantity would be required to extract enough fat, the peroxide number was determined using the FOX (ferrous oxidation-xylenol orange) assay (29).

For quantitative multi-elemental analysis by ICP-MS, approximately 250 mg of homogenized sample were prepared *via* microwave assisted digestion, using a solution consisting of 2 ml ultrapure water, 3 ml HNO_3 (69%) and 1 ml H_2O_2, heated at 190°C for 40 min. After digestion, samples were transferred to 25 ml volumetric flasks and filled with ultrapure water. Calibration standards were prepared from multi-elemental standards Instrumental Calibration Standard 2 and Alternate Metals as well as from single standard solutions for mercury and phosphorus. The internal standard solution contained Sc, Rh, Ge and Re. Reference materials used for method validation were skimmed milk powders ERM®-BD150 and ERM®-BD151 [European Commission, Joint Research Centre (JRC)] as well as TYG093RM [Heavy Metals in Infant Cereal (rice based), FAPAS].

Analysis of the remaining parameters were conducted by accredited laboratory Chemisches Institut Burkon, Nuremburg (Germany) based on ISO standards. In detail, dry matter was determined using method L 06.00-3: 2014-08*, amino acids according to methods EU 152/2009, ISO 13903: 2005, using IC-UV. For the vitamin B group, the following methods were used: BS EN 14122: 2014 mod. by LC-FLD for B_1, EN 14152: 2006 mod. using LC-FLD for B_2, EN 14164: 2014 by LC-FLD for B_6 and J.AOAC 2008, vol 91 No 4 by LC-UV/DAD, for B_{12}. Vitamin D_3 analysis was conducted according to EN 12821: 2009-08 by LC-DAD and vitamin K_1 according to EN 14148: 2003 by LC-FLD.

Statistical evaluation

Three batches of the pasteurized whole egg samples and the respective spray-dried samples were analyzed, each with two samples per batch that were then prepared and measured at least in duplicates. The measured data was prepared in Microsoft Excel (Office 365). Any outliers were excluded from the subsequent analysis with GraphPad Prism (9.3.1) using the Nalimov outlier test. Using a single factor analysis of variance as a non-parametric test (Welch's ANOVA), statistical significance ($p < 0.05$) was tested and reported in terms of mean (MW) ± standard deviation (SD). Figures were generated using GraphPad Prism (9.3.1).

Results and discussion

The obtained data was prepared and illustrated in three ways for the following discussion: (I) In mass of a nutrient per 100 g sample for comparing with results found in literature. (II) Absolute masses of a nutrient found in the respective masses of liquid egg and spray-dried egg powder corresponding to one medium-sized 60 g egg, given in mass per egg, where the relation was determined by measuring dry matter contents of all samples, thus revealing any losses that may have occurred during further processing. (III) How the consumption of spray-dried egg powder corresponding to the mass of one egg helps to achieve dietary reference intakes for infants aged 7–12 months and children aged 1–8 years, calculated in percentage. In addition to the illustrated and discussed results, all obtained mean values are summarized in Supplementary Tables S1, S2.

Dry matter

The dry weight of shell eggs normally ranges between 23 and 24% (30), but as the eggs used for this study were concentrated after pasteurization using a vacuum evaporator, an average dry matter of 31.5% was obtained, which was also taken into account in the interpretation and comparison with results of other studies. The mean values for liquid eggs were 32.4, 29.3 and 32.9% for the three investigated batches, respectively, and 97.7, 97.3 and 97.5% for the respective spray-dried samples. These results lead to factors of 3.02, 3.33 and 2.97 for calculating from fresh weight (FW) to dry matter (DM) for the individual batches and to masses of 55 g pasteurized whole egg and 17 g spray-dried egg equaling one 60 g medium-sized whole egg.

Total fat content and fatty acid distribution

The average total fat content of all pasteurized eggs analyzed was 11.3 ± 0.4 g/ 100 g whole egg (FW) or 35.2 ± 2.0 g/ 100 g DM, which amounts to 6.23 ± 0.22 g per egg. Spray-dried samples averaged at 38.7 ± 2.3 g/ 100 g DM or 6.57 ± 0.39 g per egg, showing a slight yet significant increase in the total fat content (Figure 1A).

Compared with the total fat content and fatty acid pattern from a previous analysis by Akpinar-Bayizit et al. (31), the concentrations obtained in the present study were in a similar range for both pasteurized and dried eggs. In detail, the average total fat content of liquid eggs determined by Akpinar-Bayizit et al. (31) was 10.04 g/ 100 g. This number corresponds well with that from the German Institute of Nutritional Information, reporting 9.3 g/ 100 g (32). After taking into account the drying factor of 3.84, a content of 38.6 ± 0.0 g/ 100 g can be calculated for Akpinar-Bayizit et al. (31), which would be slightly higher than the content determined in this study. The Souci-Fachmann-Kraut database states an average total fat content of 11.4 g/ 100 g FW (33), which is also in agreement with our values. For spray-dried eggs, Akpinar-Bayizit et al. (31) reported a mean total fat content of 40.4 ± 0.0 g/ 100 g, which was significantly higher than that of liquid whole eggs. It should be noted that the concentrations of the liquid egg products reported by Akpinar-Bayizit et al. (31) were compared with those of the spray-dried products without considering the drying factor, and no indication of the spray-drying temperature could be found for further clarification. That said, the higher fat content reported by these authors was probably largely due to a concentration during the drying process. Abreha et al. (18), who investigated the fat contents of spray-dried egg powder from eggs of two different chicken breeds, reported mean total fat contents of 36 g/ 100 g and 39 g/ 100 g. The recommendation of Lutter and Dewey (34) to meet a dietary intake of 6.3 g total fat by means of one daily portion of a fortified supplementary food (50 g) for infants aged 12–23 months, could be met by 71 and 77%, respectively, when 12.5 g of the whole egg powder is administered. With respect to the results presented in our study, consumption of 12.5 g whole egg powder would meet these recommendations by 71–80%.

Our analysis of fatty acids in pasteurized whole eggs yielded a homogenous distribution in all samples, with an average content of 10.1 ± 1.0 g/ 100 g and monounsaturated oleic acid accounting for 29% of total fatty acids. A higher proportion of saturated fatty acids (SFA, 19.4%) was analyzed compared to that of polyunsaturated fatty acids (PUFA, 13.9%). Palmitic acid was the most abundant saturated fatty acid, accounting approximately for 14% of the total fatty acids. Linoleic acid, an omega-6 fatty acid, was quantified with a mean content of 4.1 ± 0.5 g/ 100 g DM or 0.73 ± 0.06 g per egg, accounting for 11.6% of the total fatty acid content. The average concentration of the omega-3 fatty acid alpha-linolenic acid was 0.76 ± 0.05 g/ 100 g whole egg DM or 0.13 ± 0.01 g per egg, which corresponds to 2.5% of the total fatty acid content.

Oleic acid was also found to be the dominant fatty acid in spray-dried samples (Figure 1A). Nevertheless, in all egg powder samples, an average reduction of 34.8% compared to the liquid product was observed. The absolute contents shown in Figure 1B likewise highlighted greater losses for PUFAs than for SFAs. Linoleic acid decreased from 4.11 ± 0.45 to 2.52 ± 0.75 g/ 100 g DM and alpha-linolenic acid from 0.76 ± 0.05 to 0.30 ± 0.04 g/ 100 g DM. The discrepancy between similar total fat contents and losses of fatty acids after spray-drying can be explained by complete lipid extraction on one side and the selective quantification of specific compounds, deteriorated due to lipid oxidation, by GC-FID on the other. In the literature, reported by Stadelman and Cotterill (35), e.g., fat and fatty acid contents of the egg powder were often calculated only on the basis of the drying factor and not determined experimentally. Therefore, these values do not consider possible losses due to spray-drying.

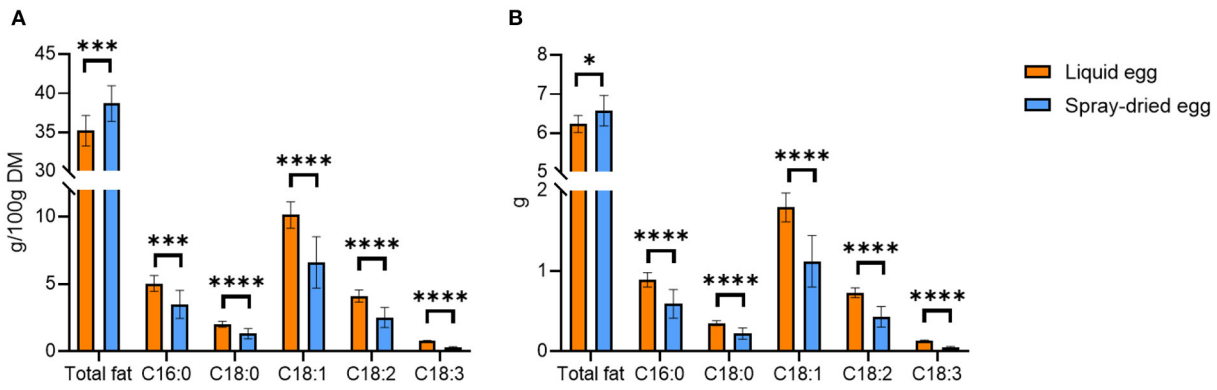

FIGURE 1
Average total fat content and fatty acid distribution of liquid eggs (orange bars) and egg powder (blue bars) in g/100 g DM **(A)** and g/egg **(B)**. Mean values ± SD ($n = 12$). Statistical significance between the egg powders and pasteurized whole egg displayed as: * $p \leq 0.05$; *** $p \leq 0.001$; **** $p \leq 0.0001$.

Javed et al. (36) examined fatty acid profiles using various spray-drying parameters on liquid and spray-dried eggs from hens fed with PUFA fortified designer feed. The authors reported slight DHA losses from 20.17 ± 0.67 mg/ 50 g egg to 17.65 ± 0.78 mg/ 50 g egg, showcasing that PUFA preservation can be achieved through optimization of the spray-drying process at least on a laboratory scale. In contrast, we could only record DHA in pasteurized liquid samples, with a mean DHA content of 120.5 ± 37.3 mg/ 100 g FW or 66.3 ± 6.3 mg per egg. All spray-dried egg samples were under the limit of quantification (<0.01 g/ 100 g), again confirming the high loss of PUFAs observed throughout this study.

Regarding the nutritional value, Figure 1B illustrates the absolute amounts of total fat content and fatty acids that can be delivered by pasteurized or spray-dried egg equaling one medium-sized egg. In detail, the intake of 55 g of fresh egg provides an average of 6.23 g of fat, of which 1.25 g are SFAs, 1.79 g monounsaturated (MUFAs) and 0.86 g PUFAs. The amount of 0.86 g PUFAs includes 0.73 g linoleic acid and 0.13 g alpha-linolenic acid. An adequate amount of dried egg (17 g) contains an average of 6.57 g of fat, of which 0.82 g accounts for SFAs, 1.12 g for MUFAs, and 0.48 g for PUFAs, the latter including 0.43 g of linoleic and 0.05 g of alpha-linolenic acid. Notably, as summarized in the conclusion of the Discussion section, for a selection of nutrients for infants aged 7–12 months and for children aged 1–8 years (Figure 8), these values meet the AI summarized by the National Academies Food and Nutrition Board (37) of linoleic acid by 9 and 5% and 10 and 6% for alpha linolenic acid, respectively.

Peroxide value

Peroxide values of <10 meq O_2/ kg fat for edible oils and fats, with the exception of up to 20 meq O_2/ kg fat for virgin olive oil, are considered acceptable, while a higher value represents the progress of oxidation (38). Since eggs are also a source of dietary fat, this value was used as a reference point for lipid oxidation in the present study. For the pasteurized samples, an average peroxide content of 1.05 ± 0.17 meq O_2/ kg fat ($n = 19$) could be determined. Spray-drying resulted in a significant increase to 1.68 ± 0.12 meq O_2/ kg fat ($p < 0.0001$). Inflow temperature of 180°C led to a further increase, with 1.81 ± 0.06 meq O_2/ kg fat.

In the study by Galobart et al. (39), the main cause of peroxide formation in dried eggs was attributed to the heat treatment. The larger surface area of the egg powder also provides a good surface for attack by oxygen and can thus start the radical chain reaction during storage or allow it to progress more rapidly. Therefore, special care was taken in our study during sample work-up, leaving as little head space as possible in the sample vessel. In order to minimize other influencing factors, such as storage time, peroxide analysis was performed immediately after sample collection. Lower values for egg powder were reported by Koç et al. (16), with 0.320–0.799 meq O_2/ kg fat. Notably, Koç et al. (16) determined the peroxide value by a different analytical method, the official method according to Wheeler AOAC 2000 (28). Wheeler's method would require an amount of about 5 g of extracted fat. Since hen eggs have a fat content of approximately 10 g/ 100 g, a larger sample size would have been required to extract enough fat, which is why we chose the FOX assay for determination. Moreover, the study reported by Koç et al. (16) is lacking a comparison to pasteurized egg samples and is generally focused on optimizing the spray-drying process by preserving the functional properties while keeping the peroxide value low (16). The authors also showed that the outlet temperature had a significant effect on the peroxide value. The lowest peroxide value of 0.320 meq O_2/ kg fat was obtained with 180°C inlet, 60°C outlet temperature and an atomization pressure of 392 kPa (16). Similarly, Javed et al. (36) examined the influence of various spray-drying and

storage parameters on the peroxide value using a laboratory scale spray-dryer. The authors obtained peroxide values of 0.324 meq O_2/ kg fat for normal eggs, 0.418 meq O_2/ kg fat for PUFA fortified designer eggs and of 0.45–0.65 meq O_2/ kg fat for spray-dried eggs, positively correlating with applied air temperatures. In addition, the authors reported significantly higher peroxide values when the samples were stored for up to 60 days at 25°C when compared to storage at 4°C. Nonetheless, in order to make a clear recommendation of the temperature conditions, it is also necessary to monitor other parameters, such as the changes in the concentrations of antioxidants in controlled studies.

Amino acids

The fact that water-soluble nutrients generally were not influenced considerably by spray-drying also is reflected in our results of amino acids. Nonetheless, reductions due to spray-drying, especially in lysine content, have been reported for infant formula in the past (40), warranting in-depth analysis of other spray-dried foods. Even though reaching significance in most cases, the commercial egg processing investigated in our study did not result in great reductions (4–10%) in the content of lysine or other essential amino acids. In detail, the lysine content recorded for pasteurized eggs, 1.20 ± 0.09 g/ 100 g FW, is in agreement with USDA data on fresh whole egg (0.91 g/ 100 g) (30). Our result equals 3.86 ± 0.13 g/ 100 g DM, with 3.47 ± 0.13 g/ 100 g found for spray-dried eggs, thus only displaying a slight, however significant ($p < 0.0001$) reduction of 10%. In this regard, Vargas-del-Río et al. (41) recently demonstrated that the addition of sucrose prior to spray-drying could give further control over amino acid preservation. A complete comparison of amino acid contents before and after spray-drying is depicted in Figure 2.

Amino acid requirements and recommended dietary allowances (RDA) for selected amino acids are given in mg/ kg body weight per day in literature (42, 43). Hence, we used weight-for-age charts provided by the World Health Organization, choosing body weights of 7.6 kg for infants aged 6 months and 11.9 kg for 2 year old children (44). Converting the per egg values depicted in Figure 2B to the percent contribution to required intakes for both age groups, 17 g of spray-dried egg account for 100% each for isoleucine and valine, 100% and 80% for leucine or 100 and 77% for lysine, respectively. Thus, it can be concluded that eggs remain an excellent source of essential amino acids even after pasteurization and spray-drying.

In addition, we determined N(6)-Carboxymethyllysine (CML) contents to monitor slight reductions of essential amino acids caused by Maillard reactions during spray-drying. CML is used as marker for the increasingly studied group of advanced glycation end products (45, 46) and heat treatment has been reported to increase CML contents of egg white and yolk significantly (47). In accordance with the lysine measurement, however, we did not record a significant increase of CML contents due to spray-drying, with a value of 614.2 ± 142.2 mg/ 100 g DM for the spray-dried samples. Another marker for amino acid degradation, hydroxyproline, could not be detected in any of the samples (LOD = 0.05 g/ 100 g).

Fat-soluble vitamins

Vitamin E

Analysis of the pasteurized whole eggs revealed a mean total tocopherol content of 13.3 ± 0.6 mg/100 g FW, which corresponds to a mean content of 41.2 ± 2.2 mg/ 100 g DM. Quantitatively, α-tocopherol accounted for the largest proportion with 22.0 ± 1.9 mg/ 100 g DM. As shown in Figure 3A, spray-drying of eggs did not result in significant reductions of the overall tocopherol compounds, with mean total tocopherol contents of 39.3 ± 4.9 mg/ 100 g DM and 21.9 ± 3.9 mg/ 100 g DM for α-tocopherol. With regard to the discussed results of fatty acids, vitamin E plays an important role in preventing and delaying lipid oxidation, driven by the formation of oxygen radicals (48). This, however, could not be observed in our study. In detail, the oxygen radical scavenging ability is strongly dependent on the tocopherol homolog distribution (γ + δ)/α (48). Higher ratios such as a value of 4.77 reported for soybean oil lead to more pronounced delays in lipid oxidation and therefore higher storability when compared to canola oil (1.39) or sunflower oil (0.06) (48). The results obtained in our study yield ratios of 0.88 for liquid and 0.80 for spray-dried eggs, with the difference not reaching statistical significance. To counteract the peroxidation of PUFAs during production and storage, a higher vitamin E content in the feed should be considered for future optimizations (6).

Previously published data on the effect of the spray-drying process on the vitamin E content in eggs showed a wide range of results. In the analysis by Caboni et al. (20), no significant difference was found between pasteurized liquid eggs (20.4 mg/ 100 g DM) and spray-dried eggs (20.3 mg/ 100 g DM) with respect to α-tocopherol. Meynier et al. (19) reported slight losses of 10% during spray-drying at 160°C for α- and γ-tocopherol. In contrast, Galobart et al. (39) reported vitamin losses due to drying when applying similar spray-drying parameters as we did (160°C input and 90°C output temperature). The authors reported the highest vitamin E loss for eggs where hens had not received vitamin E fortified feed: compared to raw liquid eggs, the α-tocopherol content of the spray-dried egg powder was reduced by 48.2%. However, when the hens were supplemented with 50, 100, and 200 mg α-tocopherol acetate/kg feed, the α-tocopherol loss in spray-dried eggs was only 37.7, 33.5 and 31.1%, respectively. Worth mentioning is that Galobart et al. (39) reported storage in glass jars at room temperature until analysis: these conditions might have an impact on the results. How many days elapsed between spray-drying and analysis, or

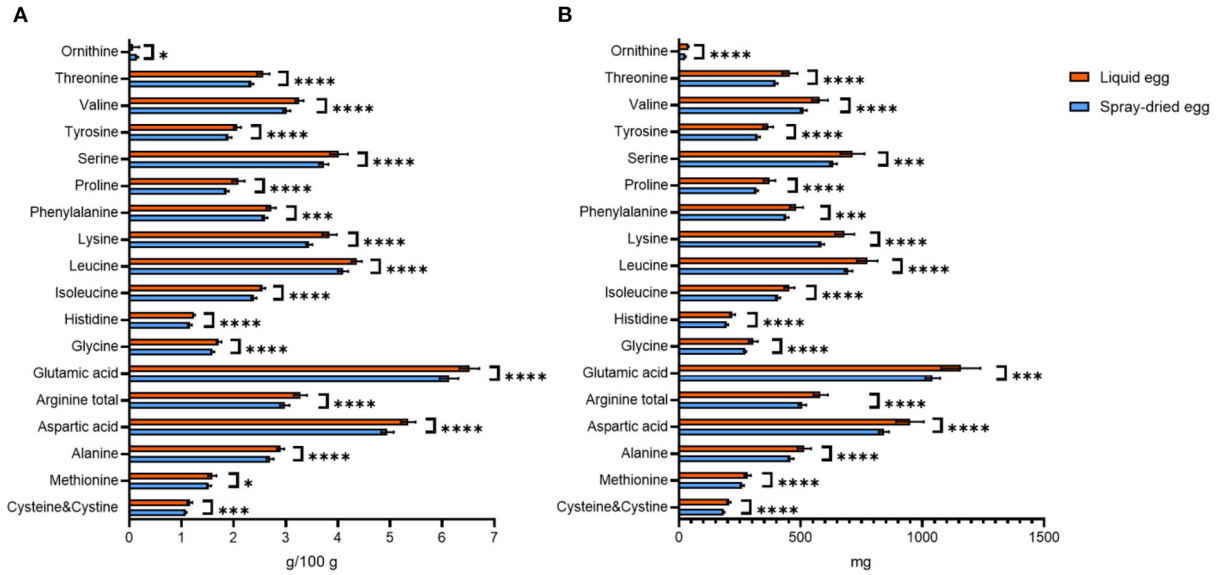

FIGURE 2
Contents of amino acids found in liquid eggs (orange bars) and egg powder (blue bars) in g/ 100 g **(A)** and mg per egg **(B)**. Results are presented as mean values ± standard deviation ($n = 12$). Statistical significance between the egg powders and pasteurized whole egg displayed as: * $p \leq 0.05$; *** $p \leq 0.001$; **** $p \leq 0.0001$.

how much oxygenated headspace was present in the glass vessels used could not be determined from the publication. In contrast, we stored both pasteurized and spray-dried samples at −80°C until analysis, which might explain why we did not record a significant decrease in α-tocopherol. Apart from exposure to light, contact with oxygen and temperature also play a decisive role in vitamin E stability (49).

As depicted in Figure 3B, 55 g of pasteurized egg approximately provides 3.7 mg α-, 2.2 mg γ-, and 1.2 mg δ-tocopherol, whereas an equivalent amount of dried egg (17 g) provides 3.6 mg α-, 1.9 mg γ-, and 1.1 mg δ-tocopherol. Regarding the DRIs, 17 g of the spray-dried egg examined in this study would therefore completely cover the required daily intake for both infants and children, demonstrating an excellent nutritional source.

Vitamin A

The retinol contents we determined, averaging at 184.9 ± 22.6 µg/ 100 g FW or 576.0 ± 89.7 µg/ 100 g DM (Figure 4A), are in agreement with those published by the DHSC (50), the USDA (51), and Miranda et al. (52) In detail, the DHSC reported an average vitamin A concentration of 120 µg/ 100 g in raw eggs, while Miranda et al. (52) noted a retinol content of 227 µg/ 100 g FW. The USDA, in turn, cited a mean retinol content in fresh eggs of 179 µg/ 100 g. These values are based on standard addition of vitamin A to the feed.

As shown in Figure 4A, spray-drying caused slight vitamin A losses to a mean value of 495.2 ± 66.2 µg/ 100 g DM, only reaching significance in two of the three batches. These variations between different batches suggest that spray-drying cannot be the sole cause of retinol loss. Generally, it is important to minimize oxidation-driving factors, such as oxygen or light, already at the feed level as well as during egg transport and storage. However, increasing the inflow temperature above 160°C proved unfavorable. We recorded a deterioration of 33.6% compared to the pasteurized whole egg sample for the 180°C batch.

To date, only a limited number of studies have investigated the effects spray-drying on the vitamin A content of eggs. Although the analysis by Caboni et al. (20) yielded an equally high total retinol content of 510 µg/ 100 g DM in pasteurized as well as spray-dried eggs, a more detailed observation showed a trans-cis shift of retinol. While pasteurized eggs had 440 µg/ 100 g of all-trans retinol content and 70 µg/ 100 g of cis retinol, this shifted to 420 µg/ 100 g of all-trans retinol and 90 µg/ 100 g of cis retinol in spray-dried eggs. This publication pointed out that a quantitatively detectable amount of cis-retinol isomers in the raw egg is rather uncommon and that this was probably due to differences in the metabolism of the chicken breed and/or occurrences in the feed. Notably, the lack of information regarding the spray-drying temperature limits a direct comparison with our results. Caboni et al. (20) also examined the influence of different storage temperatures. One-year storage of egg powder at 4°C did not result in a significant decrease in all-trans retinol, with a content of 380 µg/ 100 g DM. In contrast, storage at 20°C during the same period caused a decrease to 170 µg/ 100 g DM (20). These results highlighted

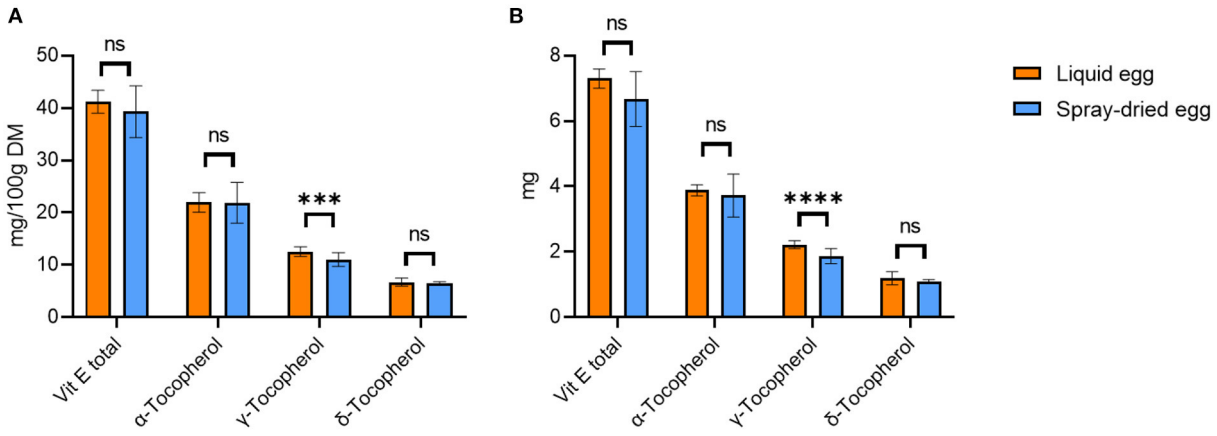

FIGURE 3
Tocopherol contents of liquid egg (orange bars) compared to spray-dried egg eggs (blue bars) in mg/ 100 g DM **(A)** and mg per egg **(B)**. Results are presented as mean values ± standard deviation ($n = 15$). Statistical significance between the egg powders and pasteurized whole egg displayed as: ns $p > 0.05$, *** $p \leq 0.001$, **** $p \leq 0.0001$.

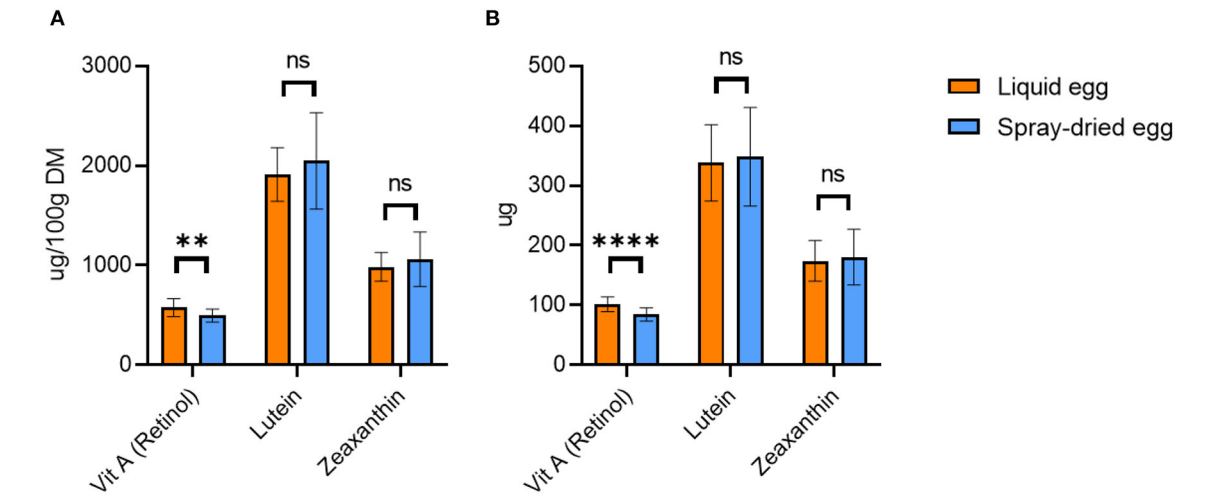

FIGURE 4
Retinol, lutein and zeaxanthin contents of liquid egg (orange bars) and egg powder (blue bars) in μg/ 100 g DM **(A)** and μg per egg **(B)**. Results are presented as mean values ± standard deviation ($n = 18$ for retinol, $n = 6$ for lutein and zeaxanthin). Statistical significance between the egg powders and pasteurized whole egg displayed as: ns $p > 0.05$, ** $p \leq 0.01$, **** $p \leq 0.0001$.

that the storage temperature of the egg powder is quite relevant for the preservation of vitamin A. Although the shelf life of dried egg is definitely longer compared to fresh egg, a timely consumption should still be aimed at in order to avoid losses of vitamin A.

Figure 4B illustrates the amount of retinol ingested with 55 g pasteurized egg and 17 g spray-dried egg, respectively. While pasteurized egg contains an average of 101.7 μg retinol, a similarly high value of 84.2 μg can be achieved by the intake of 17 g powder. Thus, the recommended DRI for infants and children can be met by 17 and 24% respectively, again showcasing the high potential of spray-dried egg as a viable source of nutrients.

Carotenoids

Figure 4A also contains the mean content of important carotenoids lutein and zeaxanthin, with 1.9 ± 0.3 and 1.0 ± 0.1 mg/ 100 g DM for pasteurized and 2.0 ± 0.5 and 1.1 ± 0.3 mg/ 100 g DM for spray-dried eggs, respectively. This amounts to 348 μg lutein and 180 μg zeaxanthin after consumption of 17g of spray-dried egg (Figure 4B). Hence, no significant change in their concentrations after spray-drying was observed

in any of the three batches investigated. Previous studies came to different conclusions in this regard. A temperature of 61.5°C and a pasteurization time of 3.5 mins did not cause significant changes in lutein and zeaxanthin concentrations in the study by Wenzel et al. (53) However, significantly higher xanthophyll contents were determined after spray-drying at 72°C. Lutein and zeaxanthin increased respectively from 164.9 ± 3.2 µg/ 100 g (FW) whole egg to 210.4 ± 8.2 µg/ 100 g (FW) dry egg and from 102.4 ± 1.9 µg/ 100 g whole egg (FW) to 128.9 ± 6.7 µg/ 100 g (FW) dry egg. The authors attributed this result to the structural unfolding of lipoproteins and destabilization of the cell matrix caused by heat exposure. The lipids of the lipoproteins, which are associated with lutein and zeaxanthin, could thus be cleaved off, increasing the extractability of xanthophylls. However, compared to other studies, such as that of Caboni et al. (20), the authors chose a temperature of 72°C, which is uncharacteristically low for spray-drying and could be one reason why the carotenoids were largely retained. Moreover, there was no information on the duration of spray-drying or other conditions during processing. Another study by Meynier et al. (19) found no effect of pasteurization or of spray-drying at 160 and 180°C on lutein and zeaxanthin content in eggs from a control group of hens without feed fortification.

Vitamin D_3 and K_1

The mean values of cholecalciferol (vitamin D_3) in DM were 5.7 ± 2.7 µg/ 100 g for pasteurized and 3.5 ± 1.2 µg/ 100 g for spray-dried samples (Figure 5), which corresponds to a reduction of 33.8% due to further processing. However, homogenous results were only obtained for one batch, which is reflected in the otherwise high standard deviations and the difference not reaching significance based on g/ 100 g egg calculations. This observation can also be seen in databases, e.g., of the USDA, where values of whole eggs range from 0 to 8.19 µg/ 100 g, averaging at 2.46 µg/ 100 g (51). Only comparing the batch with more homogenous results within the subsamples yielded a reduction of 15.3%. Slight losses of 7% vitamin D during spray-drying of eggs have been reported as early as 1944 (54), and in general, vitamin D loss during food processing is a commonly known problem (55).

Concerning phytomenadione (vitamin K_1), overall comparisons are impeded as only three subsamples from two batches ($n = 6$) of the pasteurized eggs produced values above the LOD of 0.8 µg/ 100 g, resulting in 0.94 ± 0.01 µg/ 100 g FW or 2.84 ± 0.06 µg/ 100 g DM. The spray-dried samples all exceeded the LOD and averaged at 1.62 ± 0.37 µg/ 100 g DM (Figure 5A). This is in accordance with a content of 1.2 µg/ 100 g DM for dried eggs given by the USDA (56). Nonetheless, in the few cases where comparisons are possible, the reduction due to spray-drying ranged from 28 to 54%. Phytomenadione is repeatedly reported as being heat-stable and retained after most cooking processes (57), and at least for cow's milk, this could be shown for spray-drying as well (58). Hence, the overall low values we recorded cannot be explained entirely by processing of the eggs and may be accounted to the high photosensitivity of the compound. However, even contents for whole fresh eggs vary greatly in databases, ranging, for example, from 0.3 µg/100 g (30) to 8.9 µg/ 100 g (33).

Vitamin B group

Figure 6A illustrates the contents of several vitamin B compounds examined in this study. Generally, as we could demonstrate for other analytes, values for pasteurized eggs are well within reported ranges for fresh whole eggs. For instance, the fresh weight mean value for riboflavin (vitamin B_2) was 567.7 ± 43.1 µg/ 100 g, with 408 µg/ 100 g being reported in SFK (33) or 410–520 µg/ 100 g by the USDA for raw whole eggs (30).

Riboflavin was the only B vitamin for which a noteworthy reduction during spray-drying could be observed, from 1.76 ± 0.05 to 1.41 ± 0.19 mg/ 100 g DM. Similar results have been reported before, e.g., 1.36 mg/ 100 g DM by Cotterill et al. (59) A direct comparison between pasteurized and dried eggs, where no effect of processing was reported, dates back to 1944 in a study by Denton et al. (54), in which values before and after drying were identical to the contents we obtained, with 1.3–1.4 mg/ 100 g DM. Similar to phytomenadione, riboflavin is considered to be heat stable but quite photosensitive, with average losses in milk as high as 80% after 2 h in light, which may be an explanation for study results where contents before and after treatment differ significantly or contents are low throughout (57). Regarding DRI, spray-dried eggs meet the recommended contents exceptionally well—in the case of infants aged 7–12 months by 100% for B_{12}, by 60% for B_2, by 15% for B_1 and by 8% for B_6. In sum, spray-drying does not change the status of eggs as important vitamin B sources, and as drying has been deemed crucial to retain this high nutritional value in storage examinations, e.g., for thiamin, (60) spray-drying represents an adequate choice.

Mineral and trace element composition

ICP-MS measurements were carried out to examine the overall mineral composition of both products concerning nutritional quality and safety, as well as to compare possible losses of nutritive elements or concentration of potentially toxic non-essential trace elements during spray-drying. Regarding the former, data of the mineral and trace element composition of both products are in accordance with the respective data given by the USDA for whole, pasteurized (61) and dried egg (56). Contents for a selection of nutritionally relevant elements are illustrated in Figure 7A. The analysis generally yielded homogenous results between all batches with no significant differences between the respective samples before and

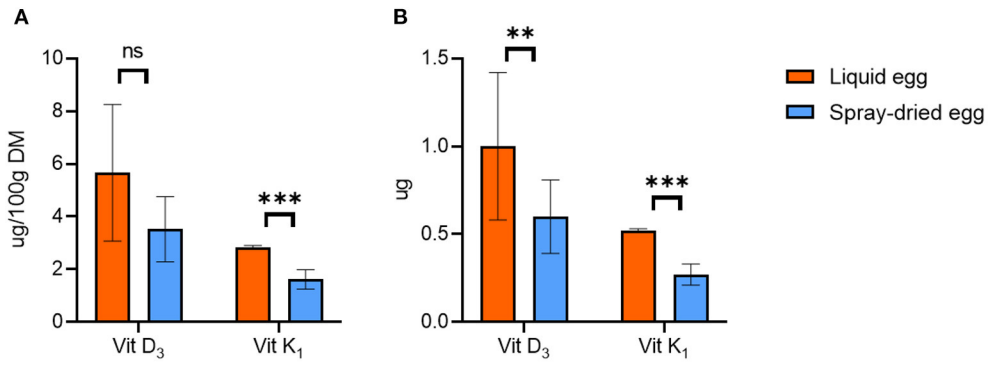

FIGURE 5
Contents of cholecalciferol (vitamin D_3) and phytomenadione (vitamin $_{K1}$) in pasteurized egg (orange bars) and egg powder (blue bars) in **(A)** µg/ 100 g dry matter and **(B)** µg per egg. Results are presented as mean values ± standard deviation ($n = 12$ for vit D_3 and $n = 6$ for vit K_1). Statistical significance between the egg powders and pasteurized whole egg displayed as: ns $p > 0.05$, ** $p \leq 0.01$, *** $p \leq 0.001$. To display the effect of spray-drying on vitamin K_1 content, only samples with contents in pasteurized eggs above the LOQ of 0.8 µg/100 g were considered for illustration.

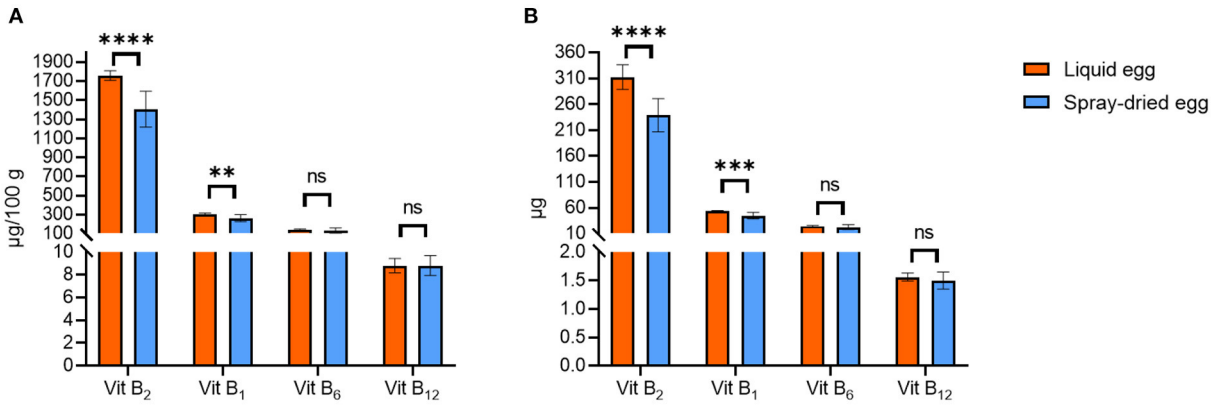

FIGURE 6
Contents of vitamin B compounds in pasteurized egg (orange bars) and egg powder (blue bars) in µg/ 100 g DM **(A)** and µg per egg **(B)**. Results are presented as mean values ± standard deviation ($n = 12$). Statistical significance between the egg powders and pasteurized whole egg displayed as: ns $p > 0.05$, ** $p \leq 0.01$, *** $p \leq 0.001$, **** $p \leq 0.0001$.

after spray-drying. Regarding the per egg intake depicted in Figure 7B, 17 g of spray-dried egg contained, e.g., 1.43 ± 0.07 mg iron and 0.88 ± 0.02 mg zinc. These values meet DRI for infants and children by 13 and 17% for iron and 29 and 22% for zinc, respectively, thus showing a high potential to aid in achieving the required total amounts. Two other noteworthy results not included in Figure 7 regard selenium and copper, of which 17 g spray-dried egg powder contain 15.1 ± 0.2 and 46.7 ± 6.5 µg, respectively, which amounts to 77 and 21% of the adequate intake for infants aged 7–12 months (37, 62).

In addition, a contamination with high levels of non-essential, potentially harmful trace elements mercury, lead, cadmium and arsenic can be excluded. Levels were well below the respective threshold values defined by the European Commission (63) and, except for Pb, under the level of quantification enabled by the highly sensitive technique in almost all cases. In detail, Pb levels in the egg powder samples were 7.74 ± 4.77 µg/ kg DM, whereas the threshold value of the European Commission for infant food marketed as powder is 20 µg/ kg FW (64), therefore approximately averaging to a tenfold ratio between our samples and the cutoff.

Hence, it can be summarized that both product groups, pasteurized whole eggs as well as spray-dried eggs, can be considered safe concerning non-essential, potentially harmful trace elements and that their consumption, even when applied as complementary food for infants, would not significantly contribute to overall heavy metal exposure. In addition, the high nutritional quality of eggs regarding their mineral and trace element content could be preserved in spray-dried eggs. These results further recommend a larger scale promotion of egg

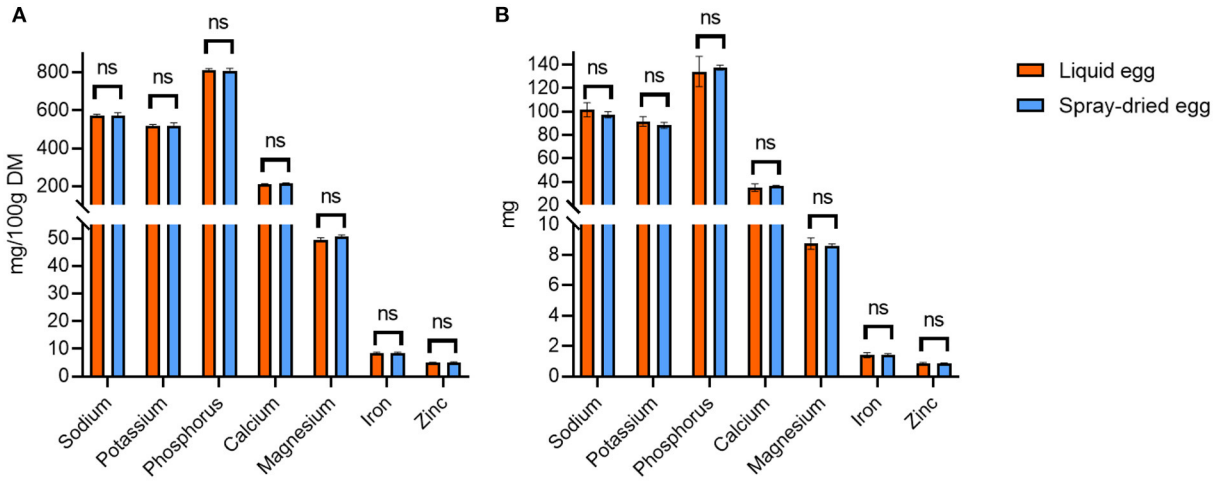

FIGURE 7
Selection of nutritionally relevant elements contained in liquid eggs (orange bars) and egg powder (blue bars) in mg/ 100 g **(A)** and mg per egg **(B)**. Results are presented as mean values ± standard deviation ($n = 12$). No statistical significant differences were found.

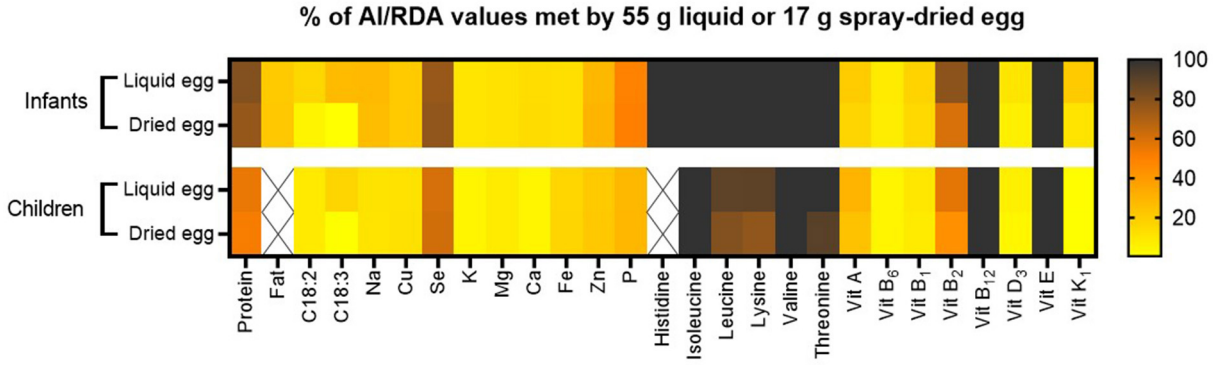

FIGURE 8
Percent of respective AI and RDA values met by consumption of 55 g pasteurized whole egg or 17 g spray-dried egg powder. RDA values for amino acids were calculated for infants aged 6 months with an average weight of 6.4 kg and children aged 2 years with an average weight of 11.9 kg. Other RDA and AI values used are estimations for infants aged between 7 and 12 months and children between 1 and 8 years. Nutrients without respective reference value for this population are crossed out.

powder to prevent infant malnutrition in developing countries, as complementary food preparations in this sector have been reported to often lack essential elements such as zinc or iron (65).

Nutritional quality

Figure 8 summarizes the nutritional quality of both pasteurized whole egg and spray-dried egg, illustrating by which percentage 55 g of pasteurized whole egg or 17 g of egg powder meet AI (acceptable intakes) or RDA values of selected nutrients.

As discussed in the respective subsections, spray-drying could mostly retain the high nutritional quality of pasteurized whole eggs without accumulating potentially harmful compounds. Moreover, the potential of eggs in helping to prevent malnutrition in vulnerable population groups is further enhanced by their possible use in spray-dried, concentrated form, with easier storability, which both represent crucial factors for the application in low- and middle-income countries. Whereas the commercial spray-drying process with an inflow temperature of 160°C and outflow between 80 and 90°C proved to be an apt choice for the majority of nutrients, such as vitamins E, B or essential amino acids, the significant deterioration of unsaturated fatty acids demonstrated that the process still requires optimization. This is evident in content losses of 38.7% for linoleic and 60.8% for linolenic acid. Increasing antioxidant vitamin E levels in the feed

could potentially prevent high PUFA losses during drying. For infants, the consumption of 55 g pasteurized whole egg meets the AI of α-linolenic acid by 27%, which represents a desirable amount and benchmark for future adaptations to spray-drying. In this regard, published data on egg powder produced from designer eggs in a laboratory scale spray-dryer (36) could already reveal that the combination of PUFA supplemented chicken feed and optimized spray-drying conditions can yield egg powder significantly richer in PUFAs than normal eggs. These results now need to be translated to industrial scale, combining effective feed supplementation with LCPUFAs (EPA and DHA) as well as vitamins E, A and D, with the preservation of all nutrients highlighted in our study, thus exploiting the full potential of spray-dried eggs as nutritional supplement.

Data availability statement

The original contributions presented in the study are included in the article/Supplementary material, further inquiries can be directed to the corresponding author.

Author contributions

BS, KK, and VS designed research. PP, SG, AD, and MP conducted research and analyzed data. PP, SG, and VS wrote the paper. VS had primary responsibility for final content. All authors read and approved the final manuscript.

Acknowledgments

The authors would like to thank Sebastian Bayer, Vanessa Jalen and Luisa Backes as well as Alexander Burkon of Chemisches Institut Burkon (Nuremburg, Germany) for their respective experimental contributions to this manuscript.

Conflict of interest

Author BS was employed by OVOBEST Eiprodukte GmbH & Co. KG.

The remaining authors declare that the research was conducted in the absence of any commercial or financial relationships that could be construed as a potential conflict of interest.

Publisher's note

All claims expressed in this article are solely those of the authors and do not necessarily represent those of their affiliated organizations, or those of the publisher, the editors and the reviewers. Any product that may be evaluated in this article, or claim that may be made by its manufacturer, is not guaranteed or endorsed by the publisher.

Supplementary material

The Supplementary Material for this article can be found online at: https://www.frontiersin.org/articles/10.3389/fnut.2022.984715/full#supplementary-material

References

1. Chambers JR, Zaheer K, Akhtar H, Abdel-Aal E-SM. Chicken eggs. In *Egg Innovations and Strategies for Improvements*. New York, NY: Elsevier (2017). pp 1–9. doi: 10.1016/B978-0-12-800879-9.00001-9

2. *International Egg Commission Global Egg Production Continues to Grow* (2021).

3. Biesalski H, Grimm P, Nowitzki-Grimm S. *Taschenatlas Ernährung (7. unveränderte Auflage)*. Stuttgart, New York: Georg Thieme Verlag (2017). doi: 10.1055/b-005-143652

4. Deutsche Gesellschaft für Ernährung ÖGfE. *Schweizerische Gesellschaft für Ernährungsforschung,, a. S., Ernährung, V. f. Referenzwerte für die Nährstoffzufuhr* (2021).

5. Ara G, Sanin KI, Khanam M, Sarker SA, Khan SS, Rifat M, et al. Study protocol to assess the impact of an integrated nutrition intervention on the growth and development of children under two in rural Bangladesh. *BMC Public Health*. (2019) 19:1–10. doi: 10.1186/s12889-019-7777-y

6. Grune T, Krämer K, Hoppe PP, Siems W. Enrichment of eggs with n−3 polyunsaturated fatty acids: effects of vitamin E supplementation. *Lipids*. (2001) 36:833–8. doi: 10.1007/s11745-001-0792-7

7. World Health Organization. *Global Prevalence of Vitamin A Deficiency in Populations at Risk 1995–2005: WHO Global Database on Vitamin A Deficiency*. Geneva: WHO (2009).

8. Iannotti LL, Lutter CK, Stewart CP, Gallegos Riofrío CA, Malo C, Reinhart G, et al. Eggs in early complementary feeding and child growth: a randomized controlled trial. *Pediatrics*. (2017) 140:3459. doi: 10.1542/peds.2016-3459

9. Péter S, Friedel A, Roos FF, Wyss A, Eggersdorfer M, Hoffmann K, et al. A systematic review of global alpha-tocopherol status as assessed by nutritional intake levels and blood serum concentrations. *Int J Vitam Nutr Res*. (2016) 14:1–21. doi: 10.1024/0300-9831/a000102

10. Beesabathuni K, Lingala S, Kraemer K. Increasing egg availability through smallholder business models in East Africa and India. *Matern Child Nutr*. (2018) 14:e12667. doi: 10.1111/mcn.12667

11. Moore KJ, Warren MW, Davis DR, Johnson MG. Changes in bacterial cell and spore counts of reduced-fat egg products as influenced by pasteurization and spray drying. *J Food Protect*. (1988) 51:565–8. doi: 10.4315/0362-028X-51.7.565

12. Belyavin C. *Eggs: Use in the Food Industry*. Amsterdam: Elseiver (2016). doi: 10.1016/B978-0-12-384947-2.00245-2

13. Mittermeier-Kleßinger VK, Hofmann T, Dawid C. Mitigating off-flavors of plant-based proteins. *J Agric Food Chem*. (2021) 69:9202–7. doi: 10.1021/acs.jafc.1c03398

14. Bimbo F, Bonanno A, Nocella G, Viscecchia R, Nardone G, De Devitiis B, et al. Consumers' acceptance and preferences for nutrition-modified and

functional dairy products: a systematic review. *Appetite*. (2017) 113:141–54. doi: 10.1016/j.appet.2017.02.031

15. Bhandari BR, Patel KC, Chen XD. Spray drying of food materials-process and product characteristics. *Drying Technol Food Process.* (2008) 4:113–57. doi: 10.1016/j.ijfoodmicro.2008.12.004

16. Koç M, Koç B, Susyal G, Yilmazer MS, Ertekin FK, Bagdatlioglu N. Functional and physicochemical properties of whole egg powder: effect of spray drying conditions. *J Food Sci Technol.* (2011) 48:141–9. doi: 10.1007/s13197-010-0159-1

17. Medina-Torres L, Calderas F, Nunez Ramírez D, Herrera-Valencia E, Bernad Bernad M, Manero O. Spray drying egg using either maltodextrin or nopal mucilage as stabilizer agents. *J Food Sci Technol.* (2017) 54:4427–35. doi: 10.1007/s13197-017-2919-7

18. Abreha E, Getachew P, Laillou A, Chitekwe S, Baye K. Physico-chemical and functionality of air and spray dried egg powder: implications to improving diets. *Int J Food Prop.* (2021) 24:152–62. doi: 10.1080/10942912.2020.1867569

19. Meynier A, Leborgne C, Viau M, Schuck P, Guichardant M, Rannou C, et al. n-3 fatty acid enriched eggs and production of egg yolk powders: an increased risk of lipid oxidation? *Food Chem.* (2014) 153:94–100. doi: 10.1016/j.foodchem.2013.12.028

20. Caboni MF, Boselli E, Messia MC, Velazco V, Fratianni A, Panfili G, Marconi E. Effect of processing and storage on the chemical quality markers of spray-dried whole egg. *Food Chem.* (2005) 92:293–303. doi: 10.1016/j.foodchem.2004.07.025

21. Verardo V, Riciputi Y, Messia MC, Marconi E, Caboni MF. Influence of drying temperatures on the quality of pasta formulated with different egg products. *Eur Food Res Technol.* (2017) 243:817–25. doi: 10.1007/s00217-016-2795-9

22. Sârâcilâ M, Panaite TD, Untea A, Ropota M, Vlaicu PA, Olteanu M, ?oica C. Monitoring lipid peroxidation in eggs enriched in omega 3 polyunsaturated fatty acids (*Ω*-3 PUFA). In: *Scientific Papers: Series D, Animal Science-The International Session of Scientific Communications of the Faculty of Animal Science.* (2017). p. 60.

23. Folch J, Lees M, Stanley GS. A simple method for the isolation and purification of total lipides from animal tissues. *J Biol Chem.* (1957) 226:497–509. doi: 10.1016/S0021-9258(18)64849-5

24. Aparicio R, Aparicio-Ruiz R. Authentication of vegetable oils by chromatographic techniques. *J Chromatogr A.* (2000) 881:93–104. doi: 10.1016/S0021-9673(00)00355-1

25. Lall RK, Proctor A, Jain VP. A rapid, micro FAME preparation method for vegetable oil fatty acid analysis by gas chromatography. *J Am Oil Chem Soc.* (2009) 86:309–14. doi: 10.1007/s11746-009-1359-6

26. Meluzzi A, Sirri F, Manfreda G, Tallarico N, Franchini A. Effects of dietary vitamin E on the quality of table eggs enriched with n-3 long-chain fatty acids. *Poult Sci.* (2000) 79:539–45. doi: 10.1093/ps/79.4.539

27. Pignitter M, Dumhart B, Gartner S, Jirsa F, Steiger G, Kraemer K, Somoza V. Vitamin A is rapidly degraded in retinyl palmitate-fortified soybean oil stored under household conditions. *J Agric Food Chem.* (2014) 62:7559–66. doi: 10.1021/jf502109j

28. AOAC. *Peroxide Value of Oils and Fats* 965.33.12. 17 ed. Washington: AOAC (2000).

29. Wrolstad RE, Acree TE, Decker EA, Penner MH, Reid DS, Schwartz SJ, et al. Handbook of food analytical chemistry, volume 1: Water, proteins, enzymes, lipids, and carbohydrates. Hoboken, NJ: Wiley (2005).

30. USDA FoodData Central. *Egg, Whole, Raw, Fresh.* Available online at: https://www.ernaehrung.de/lebensmittel/en/E111100/Chicken-egg-whole-fresh.php (accessed August 23, 2022)

31. Akpinar-Bayizit A, Ozcan T, Yilmaz-Ersan L, Gurbuz O. Impact of processing methods on nutritive value and fatty acid profile of hen eggs. *Pak Vet J.* (2010) 30:219–22.

32. Ernährungsinformation If. *DEBInet Deutsches Ernährungsberatungs- & -informationsnetz* (2021).

33. Souci S, Fachmann W, Kraut H. *Food Composition and Nutrition Tables, 7th revised and completed*. Stuttgart: MedPharm (2008).

34. Lutter CK, Dewey KG. Proposed nutrient composition for fortified complementary foods. *J Nutr.* (2003) 133:3011S—20S. doi: 10.1093/jn/133.9.3011S

35. Stadelman WJ, Newkirk D, Newby L. *Egg Science and Technology*. Boca Raton: CRC Press (2017).

36. Javed A, Imran M, Ahmad N, Hussain AI. Fatty acids characterization and oxidative stability of spray dried designer egg powder. *Lipids Health Dis.* (2018) 17:1–13. doi: 10.1186/s12944-018-0931-1

37. Del Valle HB, Yaktine AL, Taylor CL, Ross AC. *Dietary Reference Intakes for Calcium and Vitamin D*. Washington, DC: National Academies Press (2011).

38. Konsumentenschutz BASGu. *Codexkapitel B30 Speisefette, Speiseöle, Streichfette und andere Fetterzeugnisse*. Österreichisches Lebensmittelbuch (2019). p. 1–16.

39. Galobart J, Barroeta A, Baucells M, Cortinas L, Guardiola F. α-Tocopherol transfer efficiency and lipid oxidation in fresh and spray-dried eggs enriched with ω3-polyunsaturated fatty acids. *Poultry Sci.* (2001) 80:1496–505. doi: 10.1093/ps/80.10.1496

40. Schmitz-Schug I, Foerst P, Kulozik U. Impact of the spray drying conditions and residence time distribution on lysine loss in spray dried infant formula. *Dairy Sci Technol.* (2013) 93:443–62. doi: 10.1007/s13594-013-0115-8

41. Vargas-del-Río LM, García-Figueroa A, Fernández-Quintero A, Rodríguez-Stouvenel A. Spray-drying hen eggs: effects of the egg yolk to egg white ratio and sucrose addition on the physicochemical, functional, and nutritional properties of dried products and on their amino acid profiles. *Appl Sci.* (2022) 12:4516. doi: 10.3390/app12094516

42. National Research Council. Protein and amino acids. In *Recommended Dietary Allowances: 10th Edition*. Washington, DC: National Academies Press (US) (1989).

43. World Health Organization. Protein and amino acid requirements in human nutrition. In: *World Health Organization Technical Report Series*. Geneva: WHO (2007).

44. World Health Organization (WHO). *Child Growth Standards: Length/Height-For-Age, Weight-For-Age, Weight-For-Length, Weight-For-Height and Body Mass Index-For-Age: Methods and Development.* Geneva: World Health Organization (2006).

45. Lin J-A, Wu C-H, Yen G-C. Perspective of advanced glycation end products on human health. *J Agric Food Chem.* (2018) 66:2065–70. doi: 10.1021/acs.jafc.7b05943

46. Nguyen HT, Van der Fels-Klerx H, Van Boekel M. N ϵ-(carboxymethyl) lysine: a review on analytical methods, formation, and occurrence in processed food, and health impact. *Food Rev Int.* (2014) 30:36–52. doi: 10.1080/87559129.2013.853774

47. Wu S, Huang Y, Chen M, Li X, Xiang X, Lai K. Protein-bound Nε-carboxymethyllysine and Nε-carboxyethyllysine in raw and heat treated whites and yolks of hen eggs. *J Food Compos Anal.* (2020) 90:103491. doi: 10.1016/j.jfca.2020.103491

48. Zaunschirm M, Pignitter M, Kienesberger J, Hernler N, Riegger C, Eggersdorfer M, et al. Contribution of the ratio of tocopherol homologs to the oxidative stability of commercial vegetable oils. *Molecules.* (2018) 23:206. doi: 10.3390/molecules23010206

49. Weber P, Birringer M, Blumberg JB, Eggersdorfer M, Frank J. *Vitamin E in Human Health*. Berlin: Springer. (2019). doi: 10.1007/978-3-030-05315-4

50. Department of Health. *Nutrient Analysis of Eggs: Summary Report*. London: Department of Health (2012).

51. USDA FoodData Central. *Eggs, Grade A, Large, Egg Whole* (2021). Available online at: https://fdc.nal.usda.gov/fdc-app.html#/food-details/748967/nutrients (accessed August 23, 2022).

52. Miranda JM, Anton X, Redondo-Valbuena C, Roca-Saavedra P, Rodriguez JA, Lamas A, et al. Egg and egg-derived foods: effects on human health and use as functional foods. *Nutrients.* (2015) 7:706–29. doi: 10.3390/nu7010706

53. Wenzel M, Seuss-Baum I, Schlich E. Influence of pasteurization, spray-and freeze-drying, and storage on the carotenoid content in egg yolk. *J Agric Food Chem.* (2010) 58:1726–31. doi: 10.1021/jf903488b

54. Denton CA, Cabell C, Bastron H, Davis R. The effect of spray-drying and the subsequent storage of the dried product on the vitamin A, D, and riboflavin content of eggs: one figure. *J Nutr.* (1944) 28:421–6. doi: 10.1093/jn/28.6.421

55. Maurya VK, Bashir K, Aggarwal M. Vitamin D microencapsulation and fortification: trends and technologies. *J Steroid Biochem Mol Biol.* (2020) 196:105489. doi: 10.1016/j.jsbmb.2019.105489

56. USDA FoodData Central. *Egg, Whole, Dried* (2021).

57. Ottaway PB. Stability of vitamins in food. In *The Technology of Vitamins in Food.* Berlin: Springer (1993). p. 90–113.

58. Indyk H, Woollard D. The endogenous vitamin K1 content of bovine milk: temporal influence of season and lactation. *Food Chem.* (1995) 54:403–7. doi: 10.1016/0308-8146(95)00091-V

59. Cotterill O, Glauert J, Froning G. Nutrient composition of commercially spray-dried egg products. *Poultry Sci.* (1978) 57:439–42. doi: 10.3382/ps.0570439

60. Hisil Y, Ötles S. Changes of vitamin B1 concentrations during storage of hen eggs. *LWT-Food Sci Technol.* (1997) 30:320–23. doi: 10.1006/fstl.1996.0177

61. USDA FoodData Central. *Egg, Whole, Raw, Frozen, Pasteurized* (2021).

62. Krinsky NI, Beecher G, Burk R, Chan A, Erdman J, Jacob R, et al. Dietary reference intakes for vitamin C, vitamin E, selenium, and carotenoids. *Inst. Med.* (2000) 2000: 95–185. doi: 10.17226/9810

63. European Commission. *Commission Regulation (EC) No 1881/2006 of 19 December 2006 Setting Maximum Levels for Certain Contaminants in Foodstuffs (Text With EEA Relevance)*. Available online at: https://eur-lex.europa.eu/legal-content/EN/TXT/?uri=CELEX%3A02006R1881-20220701 (accessed August 23, 2022).

64. European Commission. *Commision Regulation (EU) 2021/1317 of 9 August 2021 Amending Regulation (EC) No 1881/2006 as Regards Maximum Levels of Lead in Certain Foodstuffs (Text With EEA Relevance)*. (2021). Available online at: https://eur-lex.europa.eu/eli/reg/2021/1317/oj

65. Grosshagauer S, Milani P, Kraemer K, Mukabutera A, Burkon A, Pignitter M, et al. Inadequacy of nutrients and contaminants found in porridge-type complementary foods in Rwanda. *Matern Child Nutr.* (2020) 16:e12856. doi: 10.1111/mcn.12856

frontiers | Frontiers in Nutrition

TYPE Original Research
PUBLISHED 11 October 2022
DOI 10.3389/fnut.2022.940111

OPEN ACCESS

EDITED BY
John-Lewis Zinia Zaukuu,
Kwame Nkrumah University of Science and Technology, Ghana

REVIEWED BY
Gustavo F. Gutiérrez-López,
Instituto Politécnico Nacional (IPN), Mexico
Norawanis Abdul Razak,
Universiti Malaysia Perlis, Malaysia

*CORRESPONDENCE
Lahcen Hssaini
hssaiini@gmail.com;
lahcen.hssaini@inra.ma

†These authors have contributed equally to this work

SPECIALTY SECTION
This article was submitted to Nutrition and Food Science Technology, a section of the journal Frontiers in Nutrition

RECEIVED 09 May 2022
ACCEPTED 16 September 2022
PUBLISHED 11 October 2022

CITATION
Irchad A, Razouk R, Ouaabou R, Mouhib M and Hssaini L (2022) Effect of ^{60}Co γ-rays on dried figs adsorption isotherms and thermodynamic properties. *Front. Nutr.* 9:940111. doi: 10.3389/fnut.2022.940111

Effect of ^{60}Co γ-rays on dried figs adsorption isotherms and thermodynamic properties

Ahmed Irchad[1†], Rachid Razouk[2], Rachida Ouaabou[3], Mohamed Mouhib[2†] and Lahcen Hssaini[2*†]

[1]Faculty of Sciences and Technics, University of Comoros, Moroni, Comoros, [2]National Institute of Agricultural Research (INRA), Rabat, Morocco, [3]Faculty of Sciences Semlalia, Cadi Ayyad University, Marrakesh, Morocco

Irradiation is one of the promising food preservation techniques, but few are known about its impact on foods' water vapor change. In this research, the impact of gamma irradiation on moisture adsorption isotherms of dried figs, one of the most emblematic foods of the Mediterranean diet, at increasing doses (0, 1, 1.5, and 2 kGy) was investigated. The isotherms data of equilibrium points displayed a sigmoid-shaped curve of the type II pattern for both controlled and irradiated dried figs, with a notable effect of irradiation on equilibrium moisture content, which revealed a decreasing pattern as irradiation dose and temperature increase. This effect was also seen in data fitting, where GAB model showed the best prediction statistics for control samples, while Peleg model displayed the most suitable samples irradiated at 1 and 1.5 kGy, then the Enderby model for those treated with 2 kGy. Results of Net isosteric heat of adsorption suggested that high irradiation dose increases the spontaneity of moisture adsorption. Hence, gamma irradiation exhibited a significant effect on the water-specific surface area of which the magnitude was proportional to the increasingly applied doses. This effect was also visibly significant on the optimum water activity [a_w (op)] for proper dried fig storage. Indeed, a_w was about 0.4243 for control samples, which is much higher compared to irradiated ones ($a_w = 0.2$). Information from this research suggests that gamma irradiation at a dose up to 2 kGy extended the dried figs' shelf life. Since many aspects related to the impact of gamma irradiation on the moisture adsorption isotherms and thermodynamic properties of dried figs as well as in other foods have yet to be further investigated, this study provides interesting results that may be a useful reference for future research direction.

KEYWORDS

gamma irradiation, adsorption isotherms, thermodynamic properties, post-harvest storage, Cobalt radioisotopic source, *Ficus carica* L.

Introduction

Water plays a key role in food quality and stability during storage due to its ability to interact with other molecules and to affect their conformation, mobility, and functionality (1). Knowledge of the hygroscopic properties of foods is of great importance for their processing, in order to understand and predict the influence of variations in

ambient relative humidity on their water content during storage (1). Moisture adsorption isotherms are the first step in scientific understanding of the state of water in food and their derivative compounds, and its potential influence on the many spoilage reactions occurring during their preservation (2). It is an extremely useful tool as a quantitative approach to predicting the final water content to be reached at the end of the drying process. It also helps in the selection of the appropriate packaging materials, ingredients, and optimum storage conditions to ensure the physical, chemical, and microbial stability of the dried products during storage (3). Due to the very complex composition of food products, theoretical predictions are usually inaccurate. Therefore, adsorption isotherms must be established experimentally for each product (4). In this sense, several mathematical models based on more or less physical empirical and/or theoretical criteria can help to describe the relationship between equilibrium water content and equilibrium relative humidity along with temperature (5, 6). These are useful tools that allow a better valuation of the thermodynamic properties for optimal conservation (7).

Figs and particularly dried figs are a traditional pantry staple for healthy eating in Middle Eastern and North African countries as fig trees grow abundantly in such hot and dry climates (8, 9). Despite the importance of this food source, several problems are impacting the marketability of dried figs in markets, mainly insect infestation, microbial growth, and mycotoxin contamination alongside color degradation during storage. Most of the post-harvest chemical fumigants used for dried figs, such as ethylene dibromide, methyl bromide, and ethylene oxide, are either banned or phased out because of their serious adverse impacts on human health and the environment (10–12). As well, based on the health hazards and environmental effects of conventional chemical post-harvest treatments, such as CO_2 applied under atmospheric conditions and at high pressure (13), magnesium phosphide (Mg_3P_2) (14), sulfuryl fluoride (SO_2F_2) (15), sulfur dioxide (SO_2) (16), and phosphine (17), alternative processing techniques are always needed for preserving both dried figs nutritional quality and consumer health.

Studies on gamma irradiation processing at a low irradiation dose (1.0 kGy or less) have been reported to be a suitable quarantine technology for post-harvest pest control (18–20), especially for the disinfestation of dried figs (16). Kabak et al. (21) also reported that irradiation processing can be an effective alternative technology in post-harvest inhibition of microbial contamination and mycotoxin biosynthesis during storage, thus to extend the shelf life of food products. The application of gamma irradiation in the food industry is generally framed on each side by minimum value allowing the desired objective to be achieved, and a maximum value depending on the cost of treatment, and on the other hand, the product's tolerance to radiation (22). Several relevant studies suggest a dose of 1 kGy for killing microorganisms in dried fruits (16, 23), and other studies suggest a dose higher than 1 kGy to enhance its biochemical attributes and shelf life (24, 25). Additionally, as reported by Farkas (26), to achieve desired levels of microbial and parasite control on a commercial scale, it is desirable to use the lowest possible doses necessary, since maintaining organoleptic and nutritional qualities and keeping costs down are also important factors. The focus of the aforementioned studies was on the impact of ionizing radiation on biochemical properties, microbial growth, and post-harvest pest control. However, very few studies have looked at the effect of gamma irradiation processing on the adsorption isotherms of agri-food products. Among these very few studies, only the influence of a single dose (1 kGy or less) of irradiation was investigated (7, 27–29).

Depending on what has been mentioned above, especially according to Cetinkaya et al. (16), Stefanova et al. (22), Ahmed (23), Azelmat et al. (24), and Hussain et al. (25), and as no single previous study has been undertaken on gamma-irradiated dried figs moisture isotherms thus far, we thought to explore this aspect within the range of 1 and 2 kGy for quality maintenance and quarantine purposes. Thus, this research was conducted as the first study investigating the adsorption isotherms and the thermodynamic properties of dried figs, as treated using gamma irradiation processing at increasing doses (0, 1, 1.5, and 2 kGy). The main objective of this work is to report for the first time the thermophysical behavior of moisture adsorption isotherms of irradiated dried figs compared to control, especially the relationship between equilibrium moisture content and corresponding relative humidity at three constant temperatures of 30, 40, and 50°C. Also, to fit the experimental data using Peleg, Enderby, and GAB's mathematical models to determine the one providing the best throughput resolution of equilibrium points with regard to gamma irradiation. The comparison for both controlled and irradiated dried figs of the optimal water activity for storage [a_w (op)] and the major thermodynamic properties such as water-specific surface area (S_0), net isosteric heat (q_{st}), Gibbs free energy (ΔG_β), and differential entropy of adsorption (Delta S), which represent outstanding properties regarding the energy required for adsorption was reported. In addition, the enthalpy–entropy compensation theory for both controlled and irradiated samples was verified.

Materials and methods

Raw materials preparation

Fully ripened figs belonging to *Ficus carica* L. "El Qoti Lebied" cultivar, one of the most locally cultivated clones,

10.3389/fnut.2022.940111

were collected during the first week of September 2020 from an orchard in the rural township in Chefchaouen, northern Morocco. Selected fruits had uniform size and maturity, with no diseases and visual blemishes. Initial moisture content was determined using the oven-dried method as described by AOAC (30) and was noted to be 78 ± 1% wet basis (w.b.). Afterward, all figs were blanched by immersion in boiling water containing 1 kg Na Cl (99.5°C at normal atmospheric pressure) in 20 L for 15 s, 30 times; Blanching water to fruit ratio was 2 kg: 1 L. Subsequently, fruits were dried in an industrial hybrid dryer (50°C: 20–24% relative humidity; 4 h). The drying was stopped at a moisture content of 25% according to the dried fig commercial quality standards developed by the United Nations Economic Commission for Europe (31). All dried figs, with the same level of water activity of 0.42, were packaged and sealed in polyethylene terephthalate (PET) bags (size: 10 × 6 cm L/W; permeability: 50–100 and 245.83–408.64 $cm^3.\mu m/m^2.h.$ atm for O_2 and CO_2, respectively; permeability to water vapor: 16.25–21.25 $g.\mu m/m^2.h$) to serve as replicates; each bag was 250 g. All samples were stored at room temperature, ∼22°C before being treated by gamma irradiation and analyzed for their adsorption isotherms.

Gamma irradiation

Dried figs irradiation was carried out at the Ionization Center of Boukhalef relevant to the National Institute for Agricultural Research (INRA) of Tangier, Morocco. PET bags prepared as described above were divided into four groups each one placed inside a carton box (22.7 cm length by 19 cm width and 5 cm thickness), one of which was chosen as a control. The three boxes left were treated by gamma rays at increasing doses: 1.0, 1.5, and 2.0 kGy of Cobalt radioisotopic source (^{60}Co) with a maximum dose rate of 10.87 Gy/min and a minimum dose rate of 9.64 Gy/min. Each treatment was performed in triplicates. Immediately, after the end of the irradiation, control and irradiated samples were stored at room temperature, ∼22°C before the investigation of water adsorption isotherms and thermodynamic properties.

Prior to gamma irradiation, the dosimetry was carried out according to a specific protocol, in which the dried figs were presented as described above with four bags (250 g) in each box (1 kg). The source of irradiation is Cobalt 60 COB9 type. The active material is confined inside two successive stainless steel tubular envelopes. These cylinders with a diameter of 10 mm and an active length of 450 mm are closed by massive plugs welded at their ends. The source holder used is made of stainless steel and can hold 22 COB9-type source pens.

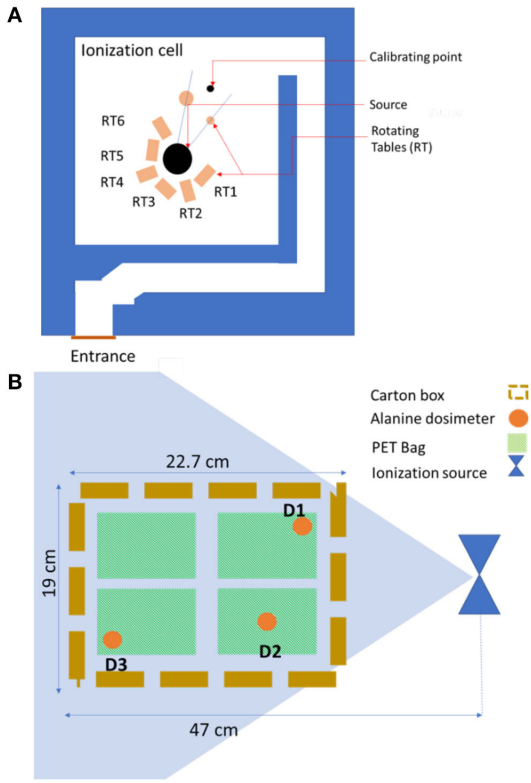

FIGURE 1
Ionization cell equipped with COB9-60 Cobalt source **(A)** and positioning of the alanine dosimeters in the box of dried figs **(B)**.

The unit sources are distributed over a diameter of 140 mm. This source holder allows reloading and use of the sources for several years. The storage container, which is used for the transport of the sources, is type B (U) with a diameter of 870 mm and a height of 1,160 mm. It is made of lead and provides the required protection during transport of the source and during the intervention inside the ionization room. The sources are stored in dry conditions. The ionization cell with a parallelepiped shape 6.1 m long, 5.8 m wide, and 2.6 m high is delimited by walls that ensure the biological protection of operators and the environment (Figure 1A). The concrete walls with a maximum thickness of 1.63 m make it possible to attenuate the radiation up to the limit required by the radiation protection regulations. The location of the three alanine dosimeters placed separately in randomly chosen carton boxes is shown in Figure 1B, which were placed within a 47-cm radius from the ionization source. To ensure that the irradiation of the dried figs was indeed homogeneous and uniform, so as not to have parts irradiated more than others, it was necessary to know the dose uniformity which is in our case 1.129.

10.3389/fnut.2022.940111

TABLE 1 Standard values of the water activities of the six saturated salts as a function of temperature used for the determination of the adsorption curves (35–37).

Temperatures	Values of the water activities					
30°C	0.0738	0.3238	0.4317	0.7275	0.8362	0.898
40°C	0.0626	0.3159	0.423	0.71	0.8232	0.891
50°C	0.0572	0.3054	0.4091	0.6904	0.812	0.8823
	KOH	$MgCl_2.6H_2O$	K_2CO_3	$NaNO_3$	KCl	$BaCl_2.2H_2O$

Determination of equilibrium moisture content

The procedures for obtaining absorption isotherms for agri-food products are described by several authors (32–34). In this study, the gravimetric static method at 30, 40, and 50°C with six saturated salt solutions (KOH, $MgCl_2$, K_2CO_3, $NaNO_3$, KCl, and $BaCl_2$) was used to determine the equilibrium moisture (X_{eq}) values of samples as described by Hssaini et al. (38) and Ouaabou et al. (35) (Table 1). One of the advantages of this procedure is that it allows these salt solutions to generate a well-defined surrounding relative humidity inside the experimental jars and continuously obtain all the relative humidity values in the range from 5 to 90% (36, 37). Each sample was weighted every 2 days until they reached a constant weight value recorded on two consecutive weightings, which were supposed to be the equilibrium. Ten days were required to reach the equilibrium state. The difference of mass before (M_i) and after equilibrium state (M_f) at 105°C (±0.1°C) during 24 h gives the equilibrium moisture content (EMC) at hygroscopic equilibrium (X_{eq}). It was determined using Equation (1) and reported on a dry weight basis (g water/g dry solid):

$$EMC = X_{eq} = \frac{M_i - M_f}{M_f} \quad (1)$$

Modeling of the adsorption isotherms

Although there are several mathematical models to describe the characteristics of moisture adsorption isotherm, Peleg (39), Enderby (40), and GAB's (41) mathematical models (Table 2) are among the most used in the literature and were retained to adjust the experimental data in this study to define the most suitable model, which describes the relationship between the equilibrium moisture content, the water activity, and the temperature. Generally, the problem of modeling the adsorption isotherms consists in finding a function checking the following Equations (2) and (3):

$$X_{eq} = f\left[\frac{P_{vp}}{P_{vs}}\right] = f(a_w, T) \quad (2)$$

$$a_w = \frac{P_{vp}}{P_{vs}} = \frac{RH\,(\%)}{100} \quad (3)$$

TABLE 2 Moisture sorption isotherm models selected to analyze data for dried figs.

Models	Mathematical expressions	References
Peleg	$X_{eq} = A(a_w)^C + B(a_w)^D$	(39)
Enderby	$X_{eq} = \left[\frac{A}{(1-Ba_w)} + \frac{C}{(1-Da_w)}\right] a_w$	(40)
Guggenheim–Anderson–De Boer (GAB)	$X_{eq} = \frac{ABC\,a_w}{[1-Ba_w][1-Ba_w-BCa_w]}$	(41)

A, B, C and D are the models constants.
X_{eq} : Equilibrium moisture content [dry basis (kg/kg d.b.)].
a_w : Water activity.

where P_{vp}: Partial pressure of water vapor in air (Pa), P_{vs}: Partial pressure of saturated vapor (Pa), and RH: Relative air humidity (%).

If the product is in hygroscopic equilibrium with the surrounding air, the water activity (a_w) is identical to the equilibrium relative humidity (a_w = ERH).

The aforementioned models are compared based on the correlation coefficient (R^2) and the standard error of estimated moisture (SE) (42). Curve Expert 3.1 and Originlab pro 8.1 software were used to determine the parameters of selected models using non-linear regression. R^2 (Equation 4) (27) and SE (Equation 5) (38) were used to determine the prediction accuracy of each model to the experimental equilibrium moisture content and water activity data. The best-fitted equation was considered to be the one giving the smallest SE coupled to the highest R^2 value (2, 38, 43–45):

$$R = \sqrt{\frac{\sum_{i=1}^{N}(MR_{pre,i} - \overline{MR}_{exp,i})^2}{\sum_{i=1}^{N}(MR_{exp,i} - \overline{MR}_{exp,i})^2}} \quad (4)$$

$$SE = \frac{\sum_{i=1}^{N}(MR_{pre,i} - MR_{exp,i})^2}{df} \quad (5)$$

where MR_{exp}: The i^{th} experimental equilibrium moisture content, Mi_{pre}: The i^{th} predicted equilibrium moisture content, N: The number of observations, and df: The number of degrees of freedom of regression model.

Adsorption-specific surface area (S_0)

By using the values of the monolayer moisture contents obtained by GAB model, the values of the water-specific surface area of adsorption can be calculated using Equation (6), and this is expressed in $m^2.g^{-1}$ of solids (4):

$$S_0 = M_m \times \frac{1}{PM_{H2O}} \times N_o \times A_{H2O} = 3.5 \times 10^3 \times M_m \quad (6)$$

where S_o: Water-specific solid surface area of adsorption ($m^2.g^{-1}$ solids); M_m: Monolayer moisture content (g/100 g, d.b); N_o: Number of Avogadro (6×10^{23} molecules per mole); A_{H2O}: Area of a water molecule (10.6×10^{-20} m^2); and PM_{H2O}: Molecular weight of the water (18 $g.mol^{-1}$).

Optimal water activity [a_w (op)] for storage

Food preservation by dehydration is based on the principle to maintain the water activity (a_w) below the critical threshold where microbial growth along with some undesirable chemical reactions occur (46). It is well-known that each microorganism has a critical a_w below which growth cannot occur. For instance, pathogenic microorganisms cannot grow at $a_w < 0.86$; yeasts and molds are more tolerant but usually, no growth occurs at $a_w < 0.62$. The so-called intermediate moisture foods (IMF) have aw values in the range of 0.65–0.90. Generally, with a_w between 0.4 and 0.2, the product is most stable with respect to lipid oxidation, non-enzymatic browning, and enzyme activity (41, 47). Among the objectives of the moisture isotherms study of a dehydrated agri-food product, is that it provides precise information on the equilibrium moisture content to be reached at the end of drying, and how to handle the product during packaging and storage for proper preservation. For this purpose, the optimal water activity values for conservation [a_w (op)] of irradiated and control dried figs were determined. Indeed, the adsorption isotherms curves can be described as a polynomial equation of the third degree (48). The zone of better stability of the products corresponds to the central part or "plate." This calculation method consists of making a polynomial decomposition of equilibrium moisture content, for all the experimental results of each sample, according to the water activity. Therefore, the optimum relative humidity for storage can be determined by calculating the value for which the second derivative of X_{eq} is canceled or "inflection point" (7, 49).

Net isosteric heat of adsorption (q_{st}) and differential entropy of adsorption (ΔS)

The calculation of the isosteric heat of adsorption is defined by the sum of the net isosteric heat of adsorption (q_{st}) and the latent heat of condensation of pure water vapor at system temperature (H_v) (50) and is given by Equation (7):

$$Q_s = q_s + H_v \quad (7)$$

From the experimental data of the adsorption isotherms, the net isosteric heat of adsorption at constant humidity (X_{eq}) can be calculated using the Clausius–Clapeyron equation (Equation 8) (51):

$$q_{st} = -R \left[\frac{d\,(\ln_{(a_w)})}{d(\frac{1}{\theta})} \right]_{X_{eq}} \quad (8)$$

where a_w: Water activity, θ: Absolute temperature (K), and R: Ideal gas constant ($8{,}314 \times 10^{-3}$ $kJ.mol^{-1}.K^{-1}$).

The value of water activity as a function of a fixed equilibrium moisture content can thus be determined from this equation using adsorption isotherms at different temperatures. For this, we assume that the net isosteric heat of adsorption is independent of temperature, and so Equation (8) can be integrated to give Equation (9):

$$\ln(a_w) = \frac{-q_{st}}{R}\frac{1}{T} + \frac{\Delta S}{R} \quad (9)$$

where ΔS : Differential entropy of sorption ($J.mol^{-1}.K^{-1}$).

Gibbs energy (ΔG_β)

From the slope of the curve $\ln_{(a_w)} = f(\frac{1}{T})$, the net isosteric heat of sorption (q_{st}) was determined. The deduced slope $\frac{q_{st}}{R}$ and the constant of $\frac{\Delta S}{R}$ displayed a linear relationship. Indeed, referring to Equation (10) below, Gibbs specific energy can be calculated:

$$\Delta G_\beta = -RTLn_{(a_w)} \quad (10)$$

Between q_{st} and ΔS, the theory of enthalpy–entropy compensation proposes a linear relationship given by Equation (11) (52):

$$q_{st} = T_\beta S + \Delta G_\beta \quad (11)$$

where T_β: Isokinetic temperature is the temperature at which all sorption reactions proceed at the same rate, ΔG_β : Gibbs energy which helps to determine whether the adsorption process is spontaneous or not. The system is spontaneous if ΔG_β is negative ($-\Delta G_\beta$) and conversely if ΔG_β is positive ($+\Delta G_\beta$).

The validation of the compensation theory is tested by comparing the isokinetic temperature to the harmonic mean temperature (T_{hm}). The T_{hm} was determined as follows:

$$T_{hm} = \frac{n}{\sum_1^n (\frac{1}{T})} \quad (12)$$

The enthalpy–entropy compensation theory can be applied only if $T_\beta \neq T_{hm}$.

10.3389/fnut.2022.940111

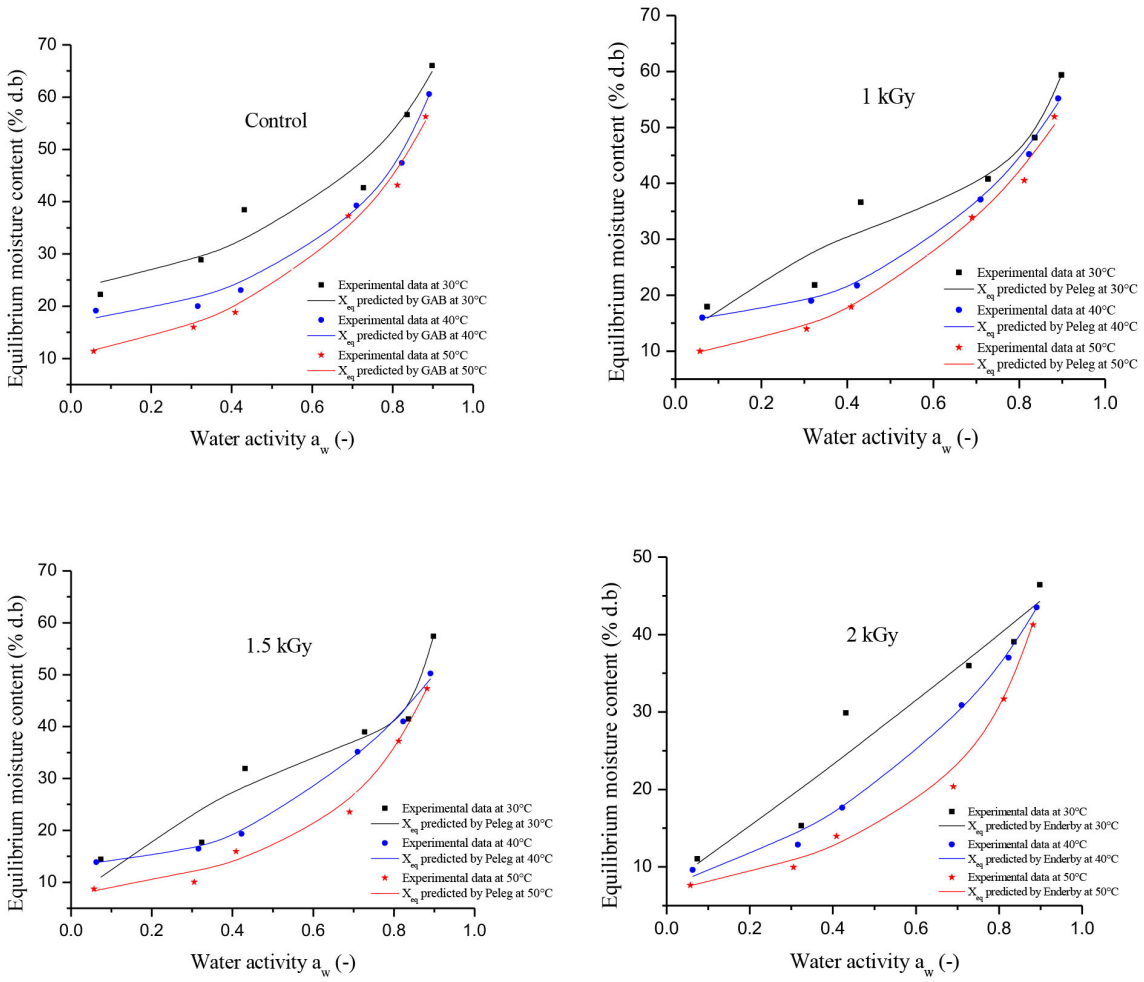

FIGURE 2
Adsorption isotherms of control and gamma irradiated (1, 1.5, and 2 kGy) at different temperatures.

Results and discussion

Moisture adsorption isotherms

Figure 2 illustrates the effect of temperature on the equilibrium moisture content (EMC) of control and irradiated dried figs. At each water activity, the EMC plotted in the Figure 2 represents the average of triplicate measurements. Since it was difficult to read the moisture equilibrium content kinetic as a function of aw (because of some overlapping points), we thought that it would be important to support that with numerical data. Thus, Table 3 reports the experimental data for the equilibrium moisture contents of control and gamma-irradiated dried figs. With the reference to the data reported in Table 3, we notice that at constant water activity, moisture adsorption at the different temperatures applied displayed significant decreases in equilibrium moisture levels X_{eq} (% d.b) for all dried fig samples as the temperature rises. This trend becomes more important as water activity decreases. For instance, at a constant a_w, the equilibrium moisture content for 1 kGy irradiated sample on a K_2CO_3 supersaturated saline solution were, respectively, 36.60, 21.71, and 17.89 g water/g d.b at 30, 40, and 50°C. Likewise, EMC levels for 1.5 kGy irradiated samples on $BaCl_2.2H_2O$ solution were, respectively, 57.41, 50.20, and 47.28 for the following a_w values 0.898, 0.891, and 0.882 (Table 4). However, it is noteworthy that, at 30°C it was observed a sharp increase in EMC within the range of a_w between 0.32 and 0.43, which is equivalent to 3 times the EMC increase that occurred under 40 and 50°C. This irregular increase trend was for both control and irradiated samples but was not observed under other temperatures. This could be linked probably to the higher active state of water molecules at high temperature levels, thus the attractive forces between them decreased. Thus, the EMC increased with decreasing

10.3389/fnut.2022.940111

TABLE 3 Equilibrium moisture content X_{eq} (% d.b) data of control and gamma irradiated (1, 1.5, and 2 kGy) dried figs in adsorption at 30, 40, and 50°C.

a_W	Control	1 kGy	1.5 kGy	2 kGy
Sorption isotherms at 30 °C				
0.0738	22.2300	17.9473	14.4153	11.0383
0.3238	28.8623	21.8213	17.6886	15.3081
0.4317	38.4398	36.6062	31.9034	29.8778
0.7275	42.6365	40.7842	38.9702	35.9780
0.8362	56.6191	48.1815	41.4434	39.0498
0.898	66.0061	59.3658	57.4161	46.4088
Sorption isotherms at 40°C				
0.0626	19.1460	15.9733	13.8532	9.5933
0.3159	20.0140	18.9915	16.4681	12.8722
0.423	23.0670	21.7163	19.3168	17.6189
0.71	39.2474	37.0987	35.1512	30.8564
0.8232	47.4143	45.1684	40.9511	37.0010
0.891	60.5485	55.1379	50.2033	43.5096
Sorption isotherms at 50°C				
0.0572	11.3813	9.9799	8.6962	7.6092
0.3054	15.9682	13.9664	10.0488	9.9535
0.4091	18.8157	17.8946	15.9337	13.9468
0.6904	37.2508	33.8758	23.5558	20.3438
0.812	43.1138	40.4748	37.1860	31.6761
0.8823	56.2481	51.8870	47.2790	41.2598

temperature at constant relative humidity. The same pattern was observed in the study by Hssaini et al. (38) over fig samples (c.v "Nabout" and "Sarilop"). Regarding the overall EMC trend following variant a_W and temperature, Hidar et al. (49) reported that it means that the material becomes less hygroscopic as the attraction strength between water molecules is reduced. Farahnaky et al. (2) reported with reference to Chowdhury et al. (44) and Jamali et al. (45) that as the temperature increases, water molecules become less stable and dissociate from the water binding sites of the food material, thus reducing the moisture content of the monolayer. Other similar investigations have reported that this is most often typical of agri-food materials (27, 28).

According to Brunauer's classification (53) and the International Union of Pure and Applied Chemistry (IUPAC) classification, data in this study obtained for both controlled and irradiated dried figs adsorption isotherms are classified as type II, which is most likely close to the sigmoidal shape. In this sense, Figure 3 illustrates the equilibrium moisture content of 1 kGy treated samples under all investigated temperatures and perfectly shows the s-shaped curve. More interesting, data in this study reported displayed a remarkable influence of gamma irradiation on the equilibrium moisture contents and the adsorption isotherms of samples within the entire range of water activity and temperature. In this sense, a boxplot graph of data under each tested temperature has been plotted and illustrated in Figure 4. Thus, gamma irradiation impacted very significantly the equilibrium moisture contents values and the adsorption isotherms, of which the equilibrium moisture content decreased proportionally as the irradiation dose increased. Indeed, irradiated samples had a smaller water adsorption capacity compared to control dried figs due to the possible influence of the gamma rays. This behavior can be explained by the fact that gamma rays probably interact with atoms and/or molecules in the cell considering the penetrating depth and radiolysis capabilities (27, 54, 55). In addition, it is possible that this interaction is a threshold event as a function of the gamma irradiation dose. As irradiation dose increases, water molecules and other structural macromolecules are affected. The less stable products break away from the water-binding sites of the food material, reducing the moisture content of the monolayer or even multilayer and interstitial (27).

However, because this is the first time that this very particular aspect has been highlighted and that unfortunately there is no report to our knowledge on irradiated dried figs isotherms or other similar biological commodities, the behavior and response to gamma irradiation of biological matrices different from dried figs were analyzed due the fact that the behavior and the response of these matrices could be likely to present similar behaviors vis-à-vis gamma irradiation. Thus, our

TABLE 4 Statistics (R^2 and SE) of sorption mathematical models (Peleg, Enderby and GAB) for control and gamma irradiated (1, 1.5, and 2 kGy) dried figs at 30, 40, and 50°C.

	Temperature		Models' constants				R^2	SE
			A	C	B	D		
Control	30	Peleg	57.95	8.0684	43.445	0.2659	0.9889	3.8785
	40		19.9258	0.01635	58.684	3.4451	0.993	2.2523
	50		54.4522	2.7454	16.192	0.1257	0.994	3.0817
	Average						0.99	3.07
	30	Enderby	6.1394	0.9392	862.6139	−26.5349	0.9872	4.1684
	40		−701.7006	0.1223	757.0997	0.1223	0.8888	12.3081
	50		−41.0987	0.3456	82.7602	0.3456	0.9642	7.4538
	Average						0.95	7.98
	30	GAB	0.07752	23.753	1.2795		0.9773	4.4762
	40		0.07602	14.6948	1.3403		0.9956	1.9706
	50		0.07594	207.4609	0.07877		0.9941	2.5029
	Average						0.99	2.98
1 kGy	30	Peleg	62.8452	12.3153	44.4566	0.3948	0.9708	5.9507
	40		19.2505	0.0684	50.5187	3.1025	0.9987	1.3014
	50		50.4786	2.7289	14.9247	0.1445	0.996	2.3435
	Average						0.99	3.2
	30	Enderby	510.321	−17.0761	5.87	0.9229	0.9678	6.2404
	40		750.4792	0.0744	−696.6964	0.0745	0.9206	9.8256
	50		16.4457	0.7485	11.3794	−13.4896	0.9965	2.1987
	Average						0.96	6.09
	30	GAB	0.0673	44.6348	0.6354		0.9605	5.638
	40		0.0659	20.9003	0.8509		0.9983	1.2072
	50		0.0662	11.9418	0.0693		0.9958	1.9601
	Average						0.98	2.94
1.5 kGy	30	Peleg	45.1958	0.5429	3034.3954	49.4879	0.9724	5.9059
	40		47.0705	2.4667	13.7966	0.000346	0.9972	1.7597
	50		15.5316	0.2158	58.7568	4.7689	0.9953	2.3641
	Average						0.99	3.34
	30	Enderby	2.9384	1.0098	258.1852	−7.9319	0.963	6.8213
	40		12.2867	−1.0405	13.7914	0.7609	0.9957	2.1719
	50		9.5263	0.8943	2.0563	−2.6424	0.9956	2.3038
	Average						0.98	3.77
	30	GAB	0.057249	29.7847	0.7092		0.9531	9.258
	40		0.052985	23.2266	0.3994		0.996	1.7271
	50		0.05061	12.8885	0.6863		0.9956	1.8753
	Average						0.98	4.29
2 kGy	30	Peleg	0.0003	−4.6034	48.1378	0.8078	0.9684	5.4669
	40		−0.7838	1.038	12.6242	1.038	0.9678	5.5225
	50		0.0152	0.2528	52.8631	5.4738	0.9975	1.4747
	Average						0.98	4.15
	30	Enderby	2.7997	−3.6677	37.4636	0.0925	0.9659	5.6752
	40		2.4187	−3.1361	16.6089	0.658	0.9978	1.4362
	50		7.142	0.9204	11.882	−0.148	0.9974	1.523
	Average						0.99	2.88
	30	GAB	0.04099	0.5241	0.0636		0.9491	5.6357
	40		0.03968	0.5189	0.0572		0.9961	1.5743
	50		0.03212	0.511	0.0089		0.9972	1.2712
	Average						0.98	2.83

10.3389/fnut.2022.940111

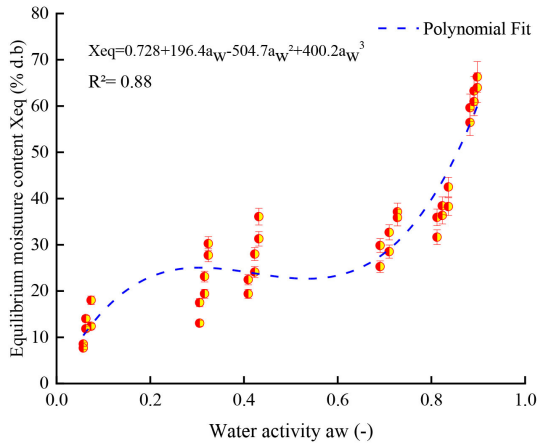

FIGURE 3
Equilibrium moisture content of 1 kGy treated samples under all investigated temperatures with the perfect s-shaped curve of adsorption isotherm.

results are slightly different from the study by Mghazli et al. (27), which reported that control and irradiated samples had the same hygroscopic behavior. Also, in that investigation, in water activity ranging between 0.2 and 0.7, the equilibrium moisture content of control samples was higher than the irradiated samples. Moussaoui et al. (7) and Lahnine al. (28) have observed the same findings. However, these results can be explained by the low ^{60}Co γ irradiation dose (<1 kGy) applied, which may have no significant impact on the stability of the product.

Adsorption isotherms modeling

The results of fitting the experimental data into Peleg, Enderby, and GAB sorption equations are shown in Table 4. The values of the correlation coefficient (R^2) and the standard error (SE) of estimated moisture are compared for each model to provide the best-fit model. From Table 4, tested models have generally expressed an average value of R^2 of 0.98 coupled with an average SE of 3.96 for all samples. According to SE, the values showed that the models used were in agreement with the experimental data with the exception of Enderby, which showed errors >5, with regard to equilibrium points of the control. After analyzing the statistical parameters in Table 4, the fit using GAB model was the most suitable for describing the adsorption isotherms of the control. On the one hand, the model has combined the highest R^2 (0.99) and the lowest SE (2.98) within the temperature range investigated in this study. On the other hand, the model Peleg displayed the best fit for irradiated dried figs at the first two irradiation doses 1 and 1.5 kGy. Obviously, this model displayed the highest R^2 (0.99), which was

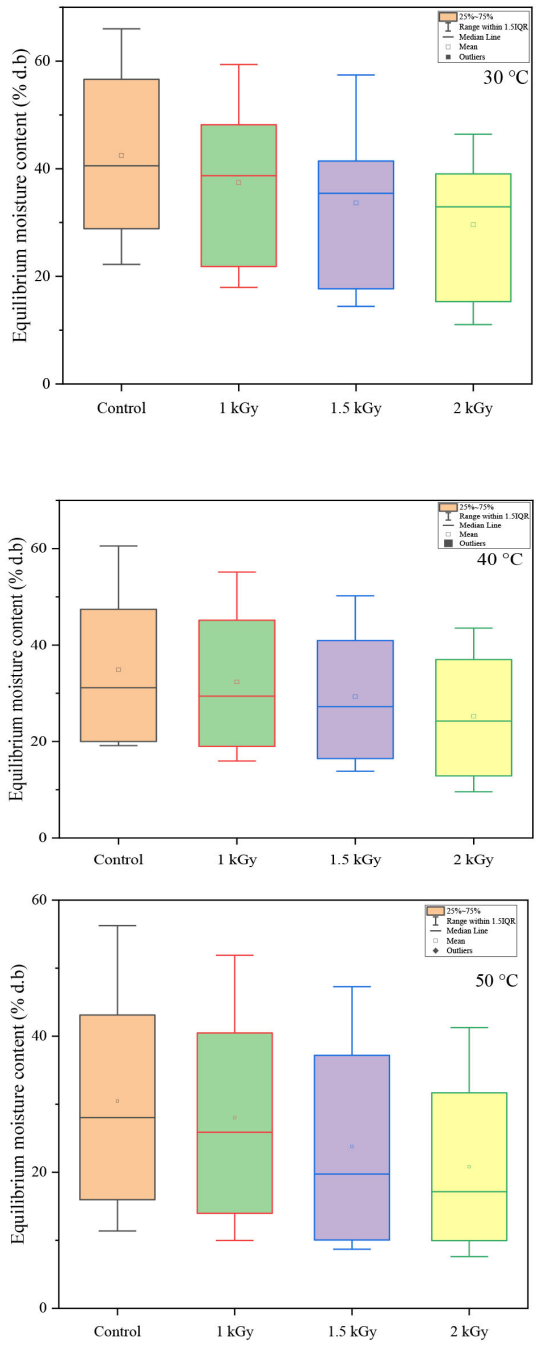

FIGURE 4
Boxplots showing the decreasing pattern of equilibrium moisture content (% d.b) with the increase of irradiation dose under each investigated temperature.

similar for both doses coupled with the lowest SE levels (3.2 and 3.34, respectively). The fit using the Enderby model was most appropriate to describe the adsorption isotherms for dried figs irradiated at the 2 kGy doses. The performance of the model selected for control and gamma-irradiated dried figs at different temperatures is illustrated in Figure 2.

These results join other previous studies which reported that from the criteria indices R^2 and SE, the aforementioned models could be useful for the ERH prediction of dried figs with the highest fit resolution (56). However, these results are slightly opposite to those reported by Hssaini et al. (38) who found that Enderby and Peleg showed the best prediction of adsorption isotherms for two varieties of figs "Kadota" and "Sarilop." In addition, the gamma irradiation used in this study displayed a remarkable effect on the fig adsorption isotherms modeling within the entire range of temperature investigated in this study. Thus, considering the fitting statistics parameters, it appears that at 50°C, R^2 increases and the SE decreases with increasing irradiation dose, particularly in the case of the GAB model experimental data. From the fact that the combination of higher R^2 and lower SE determines the goodness of data modeling, the quality of the fit of the three models was slightly greater than those of the control at 40 and 50°C considering increasing doses of irradiation. Nevertheless, despite the multitude of mathematical models used to describe the adsorption isotherms of several foods, none of them can accurately predict moisture isotherms over the entire range of water activity and for all food matrices (44, 57).

Water-specific surface area of adsorption (S_0)

Adsorption is the phenomenon of the attraction and retention of molecules from a liquid or gas "adsorbate" by a solid "adsorbent" at its surface, which leads to a higher concentration of molecules at the surface. Several factors will therefore influence this phenomenon, among others: particle size, mass of adsorbent, pH, and temperature of the solution. The particle size of the adsorbent is a parameter closely related to the specific adsorption surface area; small particles have a large specific adsorption surface area and therefore work much better than large particles. In addition, if the adsorption is favored by the low temperatures of the solution, it is exothermic, otherwise, it is endothermic (58). Table 5 reports the values of the water-specific surface area of adsorption calculated using Equation (6), and the monolayer moisture contents obtained by GAB model. According to the literature, the value of the water sorption–specific surface area of a food product is ranged between 100 and 250 $m^2.g^{-1}$ and is associated with the amount of polymers present in the food (4, 59). Considering those mentioned above, and after analyzing the statistical data in Table 5, we can conclude that the temperature significantly affects the interaction between the water and solid surface area. Indeed, most likely, the increase in temperature is able to change the structure of proteins and improve the interaction of proteins with other components, such as carbohydrates and fats; therefore, the available water adsorption sites have decreased due to the hydrophobicity of the proteins (60). Furthermore, based on the results, gamma irradiation has impacted very significantly the water-specific surface area between the control and treated samples. Thus, as the gamma irradiation dose increases, the effect tends to be more pronounced. Indeed, at a constant temperature, the S_0 has significantly decreased as the gamma irradiation dose increased, until it reaches approximately half the water-specific surface area of control samples. This trend becomes more important as the temperature increases. In fact, both temperature and gamma rays effectively contribute to dimmish the S_0 of dried figs in comparison to untreated samples.

TABLE 5 Water specific surface area (S_0) of control and gamma irradiated (1, 1.5, and 2 kGy) dried figs at 30, 40, and 50°C.

T (°C)	Control	1 kGy	1.5 kGy	2 kGy
30	271.32	235.55	200.3715	143.465
40	266.07	230.65	185.4475	138.88
50	265.79	231.7	177.135	112.42

These findings join the other previous studies reported by Lahnine et al. (28) and Moussaoui et al. (29), who stressed the same patterns as described above. Likewise, according to Calzetta Resio et al. (61), the existence of an intrinsic microporous structure in the matrix of many biopolymers is probably behind the large adsorption surface. As reported in Table 5, as the temperature increases the value of S_0 decreases. Considering this hypothesis mentioned by Calzetta Resio et al. (61), it can be assumed that gamma irradiation probably decreases intrinsic microporous structures depending on the intensity of the dose. Indeed, at higher temperatures, water molecules easily dissociate from water-binding sites. Moreover, the distance, attraction, and states of molecules also vary as the temperature changes (60). These behaviors could be more pronounced as the intensity of the irradiation dose increases assuming that physicochemical changes can occur strongly in the product, which very strongly reduces the number of active sites for the binding of the water. There is, however, great complexity in the response that a matrix can generate to gamma radiation. This can affect both the specific surface area and the cells to varying degrees depending on the dose of irradiation applied (62).

[a_W (op)] for storage conditions

Table 6 reports adsorption curves experimental data of control and gamma-irradiated dried figs according to a polynomial model of 3rd degree. The optimal water activity found in this study concords very slightly with the studies conducted by Moussaoui et al. (7), Mghazli et al. (27), and

10.3389/fnut.2022.940111

TABLE 6 Analysis of the curves of adsorption according to a polynomial model of 3rd degree.

Samples	$[a_w$ (op)]
Control	0.42
1 kGy	0.29
1.5 kGy	0.26
2 kGy	0.26

Lahnine et al. (28). Thus, the control sample presents the higher optimal water activity values (0.4243) compared to irradiated samples. Indeed, the irradiation dose significantly influenced the optimal values of water activity between the applied doses, particularly between 1 and 1.5 kGy treated figs, where the deduced values were 0.2865 and 0.2636, respectively. These doses were half those found in the control (0.4243). It is noteworthy that a very slight difference was spotted between 1.5 and 2 kGy irradiated, which a_w have barely changed (0.2636 and 0.2634, respectively). The findings are slightly different from the investigation conducted by Mghazli et al. (27) who reported opposite results. Thus, the control samples presented less water activity (0.39) than the irradiated samples (0.40). This behavior could be associated with the low gamma irradiation dose (<1 kGy) applied, which may have not expressed any significant impact on the stability of the product.

Among the main components of food matrices, besides water, carbohydrates, proteins, fats, vitamins, and minerals, also play a crucial role in human nutrition with essential major interest (63). For many years, the effects of irradiation on these components have been studied and are still explored today in a wide range of food products because the ionizing effects of radiation on food are highly dependent on the composition of the matrix and cannot be assumed similar to those observed in each individual component irradiated separately (64). This technology induces certain primary effects in food matrices that occur in particular due to the presence of water molecules by ionization and/or excitation, which increases exponentially by the secondary action of free radicals which can result from stress on the matrix (65). These chemically highly reactive species have the ability to interact with each other and/or with other food components, leading to the formation of new molecules which are not present in unirradiated foods (66).

In addition, among the various parameters which modify the radical species yield, probably the dose rate, the nature and energy of the irradiation, more generally the irradiation dose could hold a major role. Thus, these chemically highly reactive species are thus likely to add their effects to those of irradiation on cells and to modify probably the metabolism and the water retention capacity and potentially water activity on the matrix. As described by Farkas (67), food preservation is generally based on the removal of moisture which inhibits the development of pathogenic microorganisms and also minimizes fruit spoilage reactions triggered by moisture, among other enzymatic and Maillard browning reactions. However, the moisture content alone is not sufficient to predict the stability of foods, as it is not the total moisture content, but rather the water activity that determines the shelf life of food (47). Knowing as mentioned above that the a_w requirements of the various microorganisms vary considerably, our results in this study reported showed a significant effect of gamma irradiation on the decrease in the activity of water as a function of the dose absorbed, from 0.4 (untreated dried figs) to 0.2 (irradiated dried figs). This may suggest the preservative effect of the gamma irradiation technology in extending the shelf life of dried figs in relation to the water activity, since at a_w between 0.4 and 0.2, the product is also the most stable with regard to lipid oxidation, non-enzymatic browning, and enzymatic activity (41).

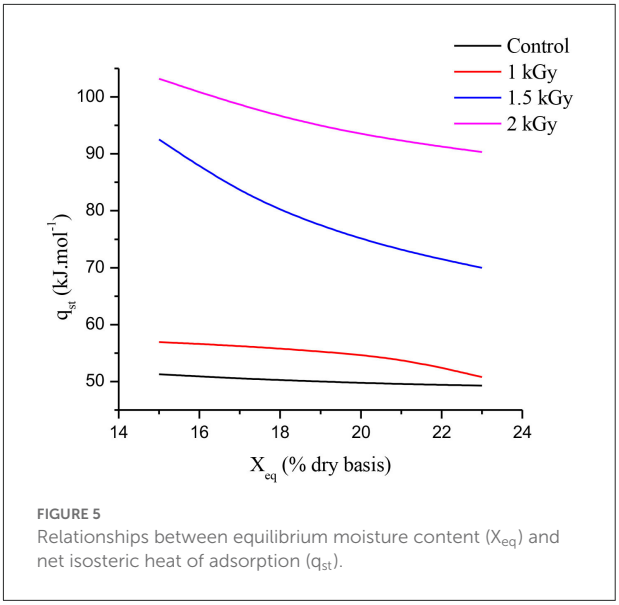

FIGURE 5
Relationships between equilibrium moisture content (X_{eq}) and net isosteric heat of adsorption (q_{st}).

Net isosteric heat of adsorption (q_{st})

To fix water molecules to the food product, net isosteric heat (q_{st}) represents the energy required at system temperature (68). Figure 5 illustrates the net isosteric heat of adsorption for control and gamma-irradiated dried figs and shows strong relationships between equilibrium moisture content (X_{eq}) and net isosteric heat of adsorption (q_{st}). Indeed, with increasing equilibrium moisture content, the strength of water molecules binding with the solid material decreases; therefore, as the moisture content increases, the net isosteric heat of adsorption decreases (69). As shown in Figure 5, at the lowest values of the X_{eq}, the q_{st} takes the highest values. Additionally, as the X_{eq} increases, the q_{st} decreases for all samples, illustrating the

10.3389/fnut.2022.940111

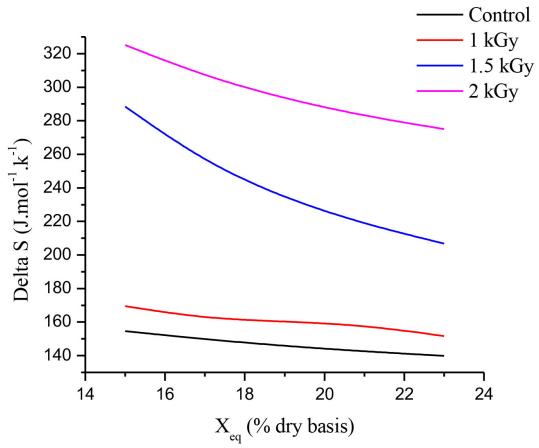

FIGURE 6
Relationships between equilibrium moisture content (X_{eq}) and differential entropy of adsorption (ΔS).

TABLE 7 Gibbs energy (ΔG_β) for control and gamma irradiated (1, 1.5, and 2 kGy) dried figs.

Samples	ΔG_β (J.mol^{-1})	T_β (K)
Control	137.1	326.41
1 kGy	498.4	310.59
1.5 kGy	277	300.45
2 kGy	259.4	297.12

strong bond of water with the matrix. This result is similar to that reported by Lahnine et al. (28). Once again, the gamma irradiation effect over dried fig net isosteric heat of adsorption displayed significant differences in q_{st} patterns following the increasing irradiation doses. Thus, at a constant temperature, as the gamma irradiation dose increase, the energy required for moisture adsorption increases, and therefore, the samples become more humidified. Nevertheless, the energy required for control samples is lower than for irradiated dried figs. This result is in agreement with the hypothesis of Moraes et al. (70), according to which the energy connecting water molecules to primary sorption sites becomes greater than the energy connecting water molecules when humidity is low. This behavior suggests that irradiated samples will have probably a great storage ability compared to control samples. Indeed, 2 kGy treated samples needed almost twice the energy needed by the control sample to absorb moisture.

Among the molecules of a plant matrix, those of water interact greatly with gamma rays due to the ubiquity of water in the plant cell (65, 71). Ionization, dissociation, and excitation are the main effects of gamma radiation. Low interaction can result from excitation, while ionization and dissociation are likely to result in strong interaction. This results in the production of radical species described as the primary effect of radiation (63). Due to the high reactivity of these chemicals' species, side effects will occur probably to potentially modify the structure and the stability of the matrix at different levels depending on the irradiation dose (64, 71). These radical species can damage or modify important components of the matrix, such as chloroplasts, and also modify biochemistry in carbohydrate transport mechanism (72), starch–sugar interconversion (73), dilation of thylakoid membranes and altered photosynthesis in cell structure (65), and texture change of some foods where polysaccharides such as pectin can be broken down leading to the release of calcium, causing the product softness increase (64, 65). Owing to these effects, alongside others, it is probably possible that the natural resistance of certain cells and irradiated membrane tissues increases, necessitating greater fixing energy for the water to the food matrix.

Differential entropy of adsorption (ΔS)

Figure 6 illustrates the relationships between equilibrium moisture content (X_{eq}) and differential entropy (ΔS) of control and gamma-irradiated dried figs at doses 1, 1.5, and 2 kGy. According to Madamba et al. (74), at a given energy level, the differential entropy of a material is proportional to the number of sorption sites available. From Figure 6, as the humidity increases, the differential entropy decreases for all samples. This behavior of the differential entropy shows once again, a strong dependence on humidity and on the dose of gamma irradiation applied. Thus, the differential entropy of 2 kGy treated samples is twice that of control samples. Obviously, further analysis is required to deepen our understanding of changes occurring at the molecular scale according to irradiation with regard to dried products' differential entropy of adsorption.

Gibbs energy (ΔG_β)

Within a confidence interval of 0.95, the Gibbs energy (ΔG_β) was determined from Equation (10) by linear regression. According to Alpizar-Reyes et al. (75), positive values of Gibbs energy ($+\Delta G_\beta$) are an indicative criterion that sorption is non-spontaneous, while negative values ($-\Delta G_\beta$) provide information on the spontaneity of sorption. Thus, the values of ΔG_β present in Table 7 suggest that the sorption process was non-spontaneity for all the samples. In addition, by analyzing the Gibbs energy data (ΔG_β) reported in Table 7, a significant effect of gamma irradiation remarkably appears. Indeed, the control samples presented lower free energy (ΔG_β) compared to the irradiated samples. In addition, as the irradiation dose increases, the free energy decreases. Whereas, high Gibbs free energy values indicate high availability of water adsorption and high hydrophilic properties, the study of thermodynamic

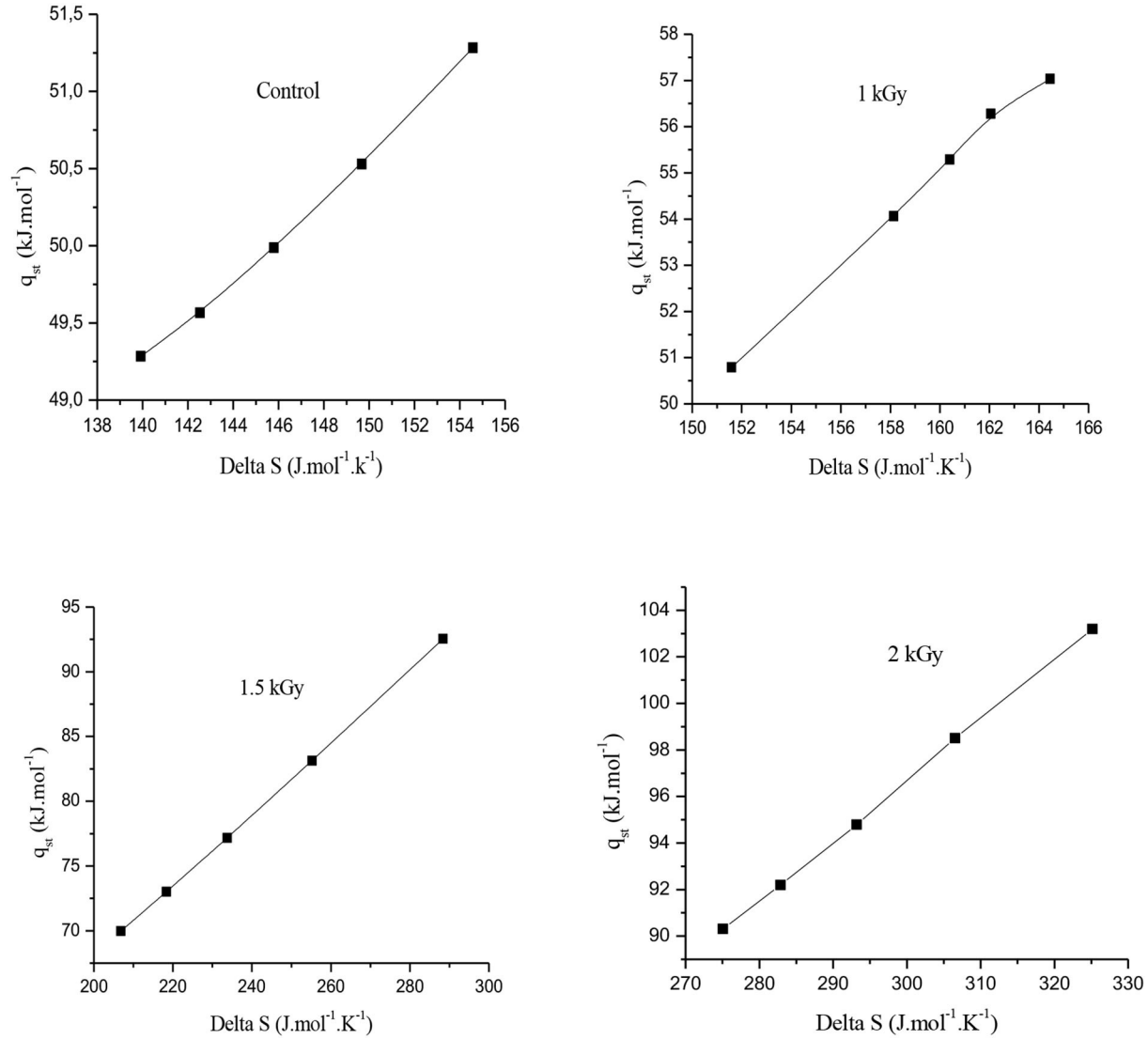

FIGURE 7
Enthalpy–entropy compensation theory for the water adsorption processes.

properties for agro-products such as the free energy (ΔG_β) is of major importance since it generally generates new data on the association and energy between water molecules in the system (76).

Enthalpy–entropy compensation theory

A simple thermodynamic argument suggests that the enthalpy–entropy compensation is a general property of weak intermolecular interactions and that the two free energy contributions should almost equilibrate for hydrogen bonding at 300 K. This statement from Dunitz (77) also drive him to ask how can we estimate the contributions of entropy and enthalpy to the free energy of association at varying binding forces. Thus, according to Liu and Guo (78), if there is a linear correlation between the logarithm of pre-exponential factors and activation energies, between enthalpies and activation entropies, or between changes in enthalpy and entropy of a series of similar reactions, the compensation effect is true. However, this definition is proposed based on the assumption that the data used in the correlation is error-free. Nevertheless, in real experiments, measurement errors are inevitable and the data used in the correlation are the estimators of the corresponding parameters. Therefore, it is possible that although the true values of the parameters do not correlate, their estimators do, and this is the cause of false compensation.

Figure 7 illustrates the graphs of net isosteric heat of sorption (q_{st}) vs. differential entropy (ΔS) for each sample category, control and irradiated. A high degree of linearity between (q_{st}) and (ΔS) is observed, which assumes that the theory of compensation exists (38, 74). By examining the illustrations in Figure 7, the realization of the compensation theory implies that a single reaction mechanism is followed by all members of the series of reactions; therefore, the existence of a single mechanism suggests that the microstructure of food is stable and does not undergo any change during moisture sorption (69, 79, 80). This observation joins that of Beristain et al. (81), concluding that the linear plot of compensation between q_{st} and ΔS correlates well with water adsorption in starchy and sugar-rich foods, such as dried figs. In addition, with our results, it can be assumed that the gamma irradiation treatment did not modify this compensation. With regard to the compensation enthalpy–entropy theory, the isokinetic temperature (T_β) and the harmonic temperature (T_{hm}) are significantly, at a certain distance, different from one another. The calculated harmonic temperature (T_{hm}) was 312.94 K, while the observed isokinetic temperature values were 310.59 K, 300.45 K, and 297.12 K for 1, 1.5, and 2 kGy, respectively. This difference supports the enthalpy–entropy compensation theory. Therefore, data, presented in this study, showed that (T_{hm}) is higher than (T_β), suggesting that the adsorption process of dried fig samples is entropy-driven (35, 38, 82, 83).

Conclusion

Stability of dried foods, as easily accessible snacks, continues to be a major concern for the agri-food industry. Therefore, studying the effect of gamma irradiation, as being a non-heating and non-toxic processing technology, and environmentally friendly, on dried food adsorption isotherms can be very useful to particularly assess it could probably modify the metabolism and the water retention capacity and potentially water activity of the matrix. In this study, the thermodynamic properties derived from dried figs' moisture adsorption isotherms provided relevant information about the influence of irradiation at increasing doses on samples' hygroscopic properties under different storage conditions. The magnitude of ^{60}Co γ-rays effect becomes more important as the irradiation dose increases. At the end of this study, gamma irradiation optimized the maximum temperature thresholds and the final water contents used for storage to ensure the stability of the dried figs during storage. As the application of gamma irradiation in the food industry is generally framed on each side by minimum value allowing the desired objective to be achieved, and a maximum value depending on the cost of treatment, and on the other hand, the product's tolerance to radiation, this study, which remains the first, suggests the use of gamma rays at a dose up to 2 kGy as a promising approach to extend the shelf life of dried figs in terms of food stability linked to water activity.

Data availability statement

The original contributions presented in the study are included in the article/supplementary material, further inquiries can be directed to the corresponding author/s.

Author contributions

LH and AI conceived and performed the project, designed, and managed the experiments. LH, AI, and RO performed the experiments and data analysis, collected data, interpreted and discussed the data, and drafted the manuscript. LH and RO contributed to the revision of manuscript. RR contributed to the data curation and visualization. MM performed irradiation experiments. All authors approved the submission of the manuscript for publication.

Acknowledgments

Special thanks to Ihssane Rhendri for her valuable support in this study.

Conflict of interest

The authors declare that the research was conducted in the absence of any commercial or financial relationships that could be construed as a potential conflict of interest.

Publisher's note

All claims expressed in this article are solely those of the authors and do not necessarily represent those of their affiliated organizations, or those of the publisher, the editors and the reviewers. Any product that may be evaluated in this article, or claim that may be made by its manufacturer, is not guaranteed or endorsed by the publisher.

References

1. Al-Muhtaseb AH, McMinn WAM, Magee TRA. Moisture sorption isotherm characteristics of food products: a review. *Food Bioprod Process*. (2002) 80:118–28. doi: 10.1205/09603080252938753

2. Farahnaky A, Ansari S, Majzoobi M. Effect of glycerol on the moisture sorption isotherms of figs. *J Food Eng*. (2009) 93:468–73. doi: 10.1016/j.jfoodeng.2009.02.014

3. Ayranci E, Ayranci G, Dogantan Z. Moisture sorption isotherms of dried apricot, fig and raisin at 20 °C and 36°C. *J Food Sci*. (1990) 55:1591–3. doi: 10.1111/j.1365-2621.1990.tb03577.x

4. Cassini AS, Marczak LDF, Noreña CPZ. Water adsorption isotherms of texturized soy protein. *J Food Eng*. (2006) 77:194–9. doi: 10.1016/j.jfoodeng.2005.05.059

5. Goula AM, Karapantsios TD, Achilias DS, Adamopoulos KG. Water sorption isotherms and glass transition temperature of spray dried tomato pulp. *J Food Eng*. (2008) 85:73–83. doi: 10.1016/j.jfoodeng.2007.07.015

6. Muzaffar K, Kumar P. Moisture sorption isotherms and storage study of spray dried tamarind pulp powder. *Powder Technol*. (2016) 291:322–7. doi: 10.1016/j.powtec.2015.12.046

7. Moussaoui H, Bahammou Y, Idlimam A, Lamharrar A, Abdenouri N. Investigation of hygroscopic equilibrium and modeling sorption isotherms of the argan products: a comparative study of leaves, pulps, and fruits. *Food Bioprod Process*. (2018) 114:12–22. doi: 10.1016/j.fbp.2018.11.002

8. Hssaini L, Hanine H, Razouk R, Ennahli S, Mekaoui A, Ejjilani A, et al. Assessment of genetic diversity in Moroccan fig (*Ficus carica* L.) collection by combining morphological and physicochemical descriptors. *Genet Resour Crop Evol*. (2020) 67:457–74. doi: 10.1007/s10722-019-00838-x

9. Hssaini L, Hernandez F, Viuda-Martos M, Charafi J, Razouk R, Houmanat K, et al. Survey of phenolic acids, flavonoids and *in vitro* antioxidant potency between fig peels and pulps: chemical and chemometric approach. *Molecules*. (2021) 26:2574. doi: 10.3390/molecules26092574

10. Meyvaci KB, Sen F, Aksoy U, Altindişli A, Emekçi M, Ferizli AG, et al. Project to phase-out methyl bromide in dried fig sector in Turkey. *Acta Horticult*. (2002) 73–81. doi: 10.17660/ActaHortic.2003.628.7

11. Aksoy U, Meyvaci BK, Sen F, Altindişli A. Impact of fumigants applied to control storage pests on fruit quality of dried figs. In: *Proceedings of the Conference of the IOBC WPRS Working Group, Integrated Protection of Stored Products*. Kuşadasi, Turkey (2003). p. 16–9.

12. Al-Bachir M. Effect of gamma irradiation on fungal load, chemical and sensory characteristics of walnuts (*Juglans regia* L.). *J Stored Prod Res*. (2004) 40:355–62. doi: 10.1016/S0022-474X(03)00030-4

13. Sen F, Meyvaci KB, Turanli F, Aksoy U. Effects of short-term controlled atmosphere treatment at elevated temperature on dried fig fruit. *J Stored Prod Res*. (2010) 46:28–33. doi: 10.1016/j.jspr.2009.07.005

14. Aksoy U, Sen F, Meyvaci KB. Effect of magnesium phosphide, an alternative to methyl bromide, on dried fig quality. *Acta Horticult*. (2008) 798:285–92. doi: 10.17660/ActaHortic.2008.798.41

15. Şen F, Meyvaci KB, Aksoy U, Tan G. Effect of sulfuryl fluoride fumigation on dried fig quality. *XXIX International Horticultural Congress on Horticulture: Sustaining Lives, Livelihoods and Landscapes (IHC2014)*. (2016) 241–4. doi: 10.17660/ActaHortic.2016.1120.36

16. Cetinkaya N, Ozyardimci B, Denli E, Ic E. Radiation processing as a post-harvest quarantine control for raisins, dried figs and dried apricots. *Radiat Phys Chem*. (2006) 75:424–31. doi: 10.1016/j.radphyschem.2005.10.009

17. Ferizli AG, Emekci M, Tütüncü S, Navarro S. The efficacy of phosphine fumigation against dried fruit pests in Turkey. *Integr Protect Stored Prod IOBC Bull*. (2004) 27:265–9.

18. Burditt AK, Hungate FP, Toba HH. Gamma irradiation: effect of dose and dose rate on development of mature codling moth larvae and adult eclosion. International Journal of Radiation Applications and Instrumentation. Part C. *Radiat Phys Chem*. (1989) 34:979–84. doi: 10.1016/1359-0197(89)90338-X

19. Mansour MY, Al-Bacheer M. Gamma irradiation as a disinfestation and quarantine treatment for faba bean seeds infested with *Bruchus dentipes* Baudi (Col., Bruchidae). *J Appl Entomol*. (1995) 119:631–6. doi: 10.1111/j.1439-0418.1995.tb01349.x

20. Azelmat K, Sayah F, Mouhib M, Ghailani N, ElGarrouj D. Effects of gamma irradiation on fourth-instar *Plodia interpunctella* (Hübner) (Lepidoptera: Pyralidae). *J Stored Prod Res*. (2005) 41:423–31. doi: 10.1016/j.jspr.2004.05.003

21. Kabak B, Dobson ADW, Var I. Strategies to prevent mycotoxin contamination of food and animal feed: a review. *Crit Rev Food Sci Nutr*. (2006) 46:593–619. doi: 10.1080/10408390500436185

22. Stefanova R, Vasilev NV, Spassov SL. Irradiation of food, current legislation framework, and detection of irradiated foods. *Food Anal Methods*. (2010) 3:225–52. doi: 10.1007/s12161-009-9118-8

23. Ahmed M. Disinfestation of stored grains, pulses, dried fruits and nuts, and other dried foods. In: Molins RA, editor. *Food Irradiation: Principles and Applications*. Dhaka University R/A, Dhaka, Bangladesh: John Wiley & Sons, Inc., Chap. 4. (2001). p. 77–112.

24. Azelmat K, ElGarrouj D, Mouhib M, Sayah F. Irradiation of "*Boufeggous*" dates: effects on chemical composition during storage. *Postharv Biol Technol*. (2006) 39:217–22. doi: 10.1016/j.postharvbio.2005.10.008

25. Hussain PR, Meena RS, Dar MA, Wani AM. Gamma irradiation of sun-dried apricots (*Prunus armeniaca* L.) for quality maintenance and quarantine purposes. *Radiat Phys Chem*. (2011) 80:817–27. doi: 10.1016/j.radphyschem.2011.02.029

26. Farkas J. Irradiation as a method for decontaminating food. *Int J Food Microbiol*. (1998) 44:189–204. doi: 10.1016/S0168-1605(98)00132-9

27. Mghazli S, Idlimam A, Mahrouz M, Lahnine L, Hidar N, Ouhammou M, et al. Comparative moisture sorption isotherms, modelling and isosteric heat of sorption of controlled and irradiated Moroccan rosemary leaves. *Indus Crops Prod*. (2016) 88:28–35. doi: 10.1016/j.indcrop.2016.02.050

28. Lahnine L, Idlimam A, Mahrouz M, Jada A, Hanine H, Mouhib M, et al. Adsorption measurements and modeling of thyme treated with gamma irradiation and thermal–biochemical treatment. *Indus Crops Prod*. (2016) 88:36–43. doi: 10.1016/j.indcrop.2016.02.049

29. Moussaoui H, Idlimam A, Lamharrar A, Kouhila M, Bahammou Y, Mouhib M, et al. The determination of moisture sorption isotherms and the isosteric heat of sorption for irradiated and non-irradiated durum wheat. *Moroccan J Chem*. (2020) 8:866–78. doi: 10.48317/IMIST.PRSM/morjchem-v8i4.19362

30. AOAC. *Official Methods of Analysis*. 18th ed. Gaithersburg, MD: Association of Official Analytical Chemists (2006).

31. UNECE STANDARD DDP-14. *The commercial quality standards developed by the United Nations Economic Commission for Europe (UNECE) concerning the marketing and commercial quality control of dried figs*. United Nations. New York and Geneva (Eds.) (2016).

32. Gal S. Recent advances in techniques for the determination of sorption isotherms. In: Duckworth RB, editor. *Water relations of Foods*. London: Academic (1975). p. 139–55. doi: 10.1016/B978-0-12-223150-6.50013-4

33. Gal S. The need for, and practical applications of sorption data. In: Jowitt R, Escher F, Hallström B, Mefert H, Spiess W, Vos G, editors. *Physical Properties of Foods—2*. London: Elsevier Applied Science (1987). p. 13–25.

34. Wolf W, Spiess WEL, Jung G. Properties of water in foods. *Standarization of Isotherm Measurements (Cost-Project 90 and 90 Bis)*. (1985) 1:661–79. doi: 10.1007/978-94-009-5103-7_40

35. Ouaabou R, Ennahli S, Di Lorenzo C, Hanine H, Bajoub A, Lahlali R, et al. Hygroscopic properties of sweet cherry powder: thermodynamic properties and microstructural changes. *J Food Qual*. (2021) 2021. doi: 10.1155/2021/3925572

36. Bizot H, Multon JL. Méthode de référence pour la mesure de l'activité de l'eau dans les produits alimentaires. *Ann Technol Agricole*. (1978) 27:441–9.

37. Bizot H, Riou N, Multon JL. Guide pratique pour la détermination des isothermes et de l'activité de l'eau. *Sci Aliments Numéro Hors-Série*. (1987).

38. Hssaini L, Ouaabou R, Charafi J, Idlimam A, Lamharrar A, Razouk R, et al. Hygroscopic proprieties of fig (*Ficus carica* L.): mathematical modelling of moisture sorption isotherms and isosteric heat kinetics. *South Afr J Bot*. (2020): 265–274.

39. Peleg M. Assessment of a semi-empirical four parameter general model for sigmoid moisture sorption isotherms. *J Food Process Eng*. (1993) 16:21–37. doi: 10.1111/j.1745-4530.1993.tb00160.x

40. Popovski D, Mitrevski V. Some new four parameter models for moisture sorption isotherms. *Electron J Environ Agric Food Chem*. (2004) 3:698–701.

41. Van Den Berg C, Bruin S. Water activity and its estimation in food systems. In Rockland LB, Stewart GF, editors. *Water Activity: Influences on Food Quality*. New York, NY: Academic Press (1981). p. 147–77. doi: 10.1016/B978-0-12-591350-8.50007-3

42. Bell LN, Labuza TP. Influence of the low-moisture state on pH and its implication for reaction kinetics. *J Food Eng*. (1994) 22:291–312. doi: 10.1016/0260-8774(94)90036-1

43. Foster KD, Bronlund JE, Paterson AHJ. The prediction of moisture sorption isotherms for dairy powders. *Int Dairy J*. (2005) 15:411–8. doi: 10.1016/j.idairyj.2004.08.003

44. Chowdhury MMI, Huda MD, Hossain MA, Hassan MS. Moisture sorption isotherms for mungbean (*Vigna radiata* L). *J Food Eng*. (2006) 74:462–7. doi: 10.1016/j.jfoodeng.2005.03.036

45. Jamali A, Kouhila M, Mohamed LA, Idlimam A, Lamharrar A. Moisture adsorption–desorption isotherms of *Citrus reticulata* leaves at three temperatures. *J Food Eng*. (2006) 77:71–8. doi: 10.1016/j.jfoodeng.2005.06.045

46. Iglesias HA, Chirife C. *Handbook of Food Isotherms: Water Sorption Parameters for Food and Food Components*, New York, NY: Academic Press (1982).

47. Cheftel JC, Cheftel H. *Introduction à la biochimie et à la technologie des aliments*. Paris: Technique et Documentation. Lavoisier (1977). p. 271–80.

48. Bahammou Y, Moussaoui H, Lamsayeh H, Tagnamas Z, Kouhila M, Ouaabou R, et al. Water sorption isotherms and drying characteristics of rupturewort (*Herniaria hirsuta*) during a convective solar drying for a better conservation. *Solar Energy*. (2020) 201:916–26. doi: 10.1016/j.solener.2020.03.071

49. Hidar N, Ouhammou M, Idlimam A, Jaouad A, Bouchdoug M, Lamharrar A, et al. Investigation of water adsorption and thermodynamic properties of stevia powder. *J Food Measur Characteriz*. (2018):2615–25. doi: 10.1007/s11694-018-9879-0

50. Tolaba MP, Peltzer M, Enriquez N, Lucia Pollio M. Grain sorption equilibria of quinoa grains. *J Food Eng*. (2004) 61:365–71. doi: 10.1016/S0260-8774(03)00143-2

51. Kaur D, Wani AA, Sogi DS, Shivhare US. Sorption isotherms and drying characteristics of tomato peel isolated from tomato pomace. *Drying Technol*. (2006) 24:1515–20. doi: 10.1080/07373930600961371

52. Leffer J, Grunwald E. *Rates and Equilibria of Organic Reactions*. New York, NY: Wiley (1963).

53. Brunauer S, Deming LS, Deming WE, Teller E. On a Theory of the van der Waals Adsorption of Gases. *J Am Chem Soc*. (1940) 62:1723–32. doi: 10.1021/ja01864a025

54. Figura LO, Teixeira AA. Food physics. In: *Physical Properties-Measurements and Applications: Rheological Properties*. New York, NY: Springer (2007).

55. Singh B, Datta PS. Effect of low dose gamma irradiation on plant and grain nutrition of wheat. *Radiat Phys Chem*. (2010) 79:819–25. doi: 10.1016/j.radphyschem.2010.03.011

56. Ansari S, Farahnaky A, Majzoobi M, Badii F. Modeling the effect of glucose syrup on the moisture sorption isotherm of figs. *Food Biophys*. (2011) 6:377–89. doi: 10.1007/s11483-011-9213-4

57. Bell LN, Labuza TP. *Practical Aspects of Moisture Sorption Isotherm Measurement and Use*. 2nd ed. Eagan, MN: AACC Eagan Press (2000).

58. Benjelloun M, Miyah Y, Evrendilek GA, Zerrouq F, Lairini S. Recent advances in adsorption kinetic models: their application to dye types. *Arabian J Chem*. (2021) 14:103031. doi: 10.1016/j.arabjc.2021.103031

59. Labuza TP. Sorption phenomena in foods. *Food Technol II*. (1968) 22:263–72.

60. Taitano LZ, Singh RP, Lee JH, Kong F. thermodynamic analysis of moisture adsorption isotherms of raw and blanched almonds. *J Food Process Eng*. (2011) 35:840–50. doi: 10.1111/j.1745-4530.2010.00632.x

61. Calzetta Resio AN, Tolaba MP, Suarez C. Some physical and thermal characteristics of amaranth starch. Algunas propiedades fisicas y térmicas del almidón de amaranto. *Food Sci Technol Int*. (2000) 6:371–8. doi: 10.1177/108201320000600503

62. Esnault MA, Legue F, Chenal C. Ionizing radiation: advances in plant response. *Environ Exp Bot*. (2010) 68:231–7. doi: 10.1016/j.envexpbot.2010.01.007

63. Sparrow AH, Binnington JP, Pond V. Bibliography on the effects of ionizing radiations on plants 1896–1955. *Brookhaven Nat Lab*. (1958) 504:222.

64. Gunckel JE, Sparrow AH. Ionizing radiations: biochemical, physiological and morphological aspects of their effects of plants. *Encyclop Plant Physiol*. (1961) 16:555–611.

65. Jan S, Parween T, Siddiqi TO, Mahmooduzzafar. Effect of gamma radiation on morphological, biochemical, and physiological aspects of plants and plant products. *Environ Rev*. (2012) 20:17–39. doi: 10.1139/a11-021

66. Fernandes A, Pereira C, Antonio AL, Ferreira ICFR. Chapter 11: food irradiation chemistry. In: Ferreira ICFR, Antonio AL, Verde SC, editors. *Food Irradiation Technologies: Concepts, Applications and Outcomes*. London, UK: The Royal Society of Chemistry (2018). p. 210–36. doi: 10.1039/9781788010252-00210

67. Farkas J. Physical methods of food preservation. In: Doyle MP, Beuchat LR, Monteville TJ,editors. *Food Microbiology: Fundamentals and Frontiers*. Washington, DC: American Society for Microbiology (1997). p. 497–519.

68. Tunç S, Duman O. Thermodynamic properties and moisture adsorption isotherms of cottonseed protein isolate and different forms of cottonseed samples. *J Food Eng*. (2007) 81:133–43. doi: 10.1016/j.jfoodeng.2006.10.015

69. Moreira R, Chenlo F, Torres MD, Vallejo N. Thermodynamic analysis of experimental sorption isotherms of loquat and quince fruits. *J Food Eng*. (2008) 88:514–21. doi: 10.1016/j.jfoodeng.2008.03.011

70. Moraes MA, Rosa GS, Pinto LAA. Moisture sorption isotherms and thermodynamic properties of apple Fuji and garlic. *Int J Food Sci Technol*. (2008) 43:1824–31. doi: 10.1111/j.1365-2621.2008.01716.x

71. Kovács E, Keresztes Á. Effect of gamma and UV-B/C radiation on plant cells. *Micron*. (2002) 33:199–210. doi: 10.1016/S0968-4328(01)00012-9

72. Wi SG, Chung BY, Kim J-S, Kim J-H, Baek M-H, Lee J-W, et al. Effects of gamma irradiation on morphological changes and biological responses in plants. *Micron*. (2007) 38:553–64. doi: 10.1016/j.micron.2006.11.002

73. Keresztes Á, Kovács E. Ultrastructural effects of ionizing radiation on plant cells. *Scann Microsc*. (1990) 5:28.

74. Madamba PS, Driscoll RH, Buckle KA. Enthalpy-entropy compensation models for sorption and browning of garlic. *J Food Eng*. (1996) 28:109–19. doi: 10.1016/0260-8774(94)00072-7

75. Alpizar-Reyes E, Carrillo-Navas H, Romero-Romero R, Varela-Guerrero V, Alvarez-Ramírez J, Pérez-Alonso C. Thermodynamic sorption properties and glass transition temperature of tamarind seed mucilage (*Tamarindus indica* L.). *Food Bioprod Process*. (2017) 101:166–76. doi: 10.1016/j.fbp.2016.11.006

76. Simal S, Femenia A, Castell-Palou Á, Rosselló C. Water desorption thermodynamic properties of pineapple. *J Food Eng*. (2007) 80:1293–301. doi: 10.1016/j.jfoodeng.2006.10.001

77. Dunitz JD. Win some, lose some: enthalpy-entropy compensation in weak intermolecular interactions. *Chem Biol*. (1995) 2:709–12. doi: 10.1016/1074-5521(95)90097-7

78. Liu L, Guo QX. Isokinetic relationship, isoequilibrium relationship, and enthalpy–entropy compensation. *Chem Rev*. (2001) 101:673–96. doi: 10.1021/cr990416z

79. Lai V. Kinetic compensation effect in depolymerisation of food polysaccharides. *Food Chem*. (2000) 68:319–25. doi: 10.1016/S0308-8146(99)00198-3

80. McMinn WAM, Al-Muhtaseb AH, Magee TRA. Enthalpy–entropy compensation in sorption phenomena of starch materials. *Food Res Int*. (2005) 38:505–10. doi: 10.1016/j.foodres.2004.11.004

81. Beristain CI, Garcia HS, Azuara E. Enthalpy-Entropy compensation in food vapor adsorption. *J Food Eng*. (1996) 30:405–15. doi: 10.1016/S0260-8774(96)00011-8

82. Sarnavi HJ, Precoppe M, García-Triñanes P, Chapuis A, Tran T, Bradley MS, et al. Determining the heat of desorption for cassava products based on data measured by an automated gravimetric moisture sorption system. *J Sci Food Agric*. (2022). doi: 10.1002/jsfa.12153

83. Fan K, Chen L, Wei X, He J, Yan F. Moisture adsorption isotherms and thermodynamic properties of A uricularia auricula. *J Food Process Preserv*. (2015) 39:1534–41. doi: 10.1111/jfpp.12379

frontiers | Frontiers in Nutrition

TYPE Original Research
PUBLISHED 18 October 2022
DOI 10.3389/fnut.2022.1042868

OPEN ACCESS

EDITED BY
John-Lewis Zinia Zaukuu,
Kwame Nkrumah University of Science and Technology, Ghana

REVIEWED BY
Zsanett Bodor,
Semmelweis University, Hungary
David Tjandra Nugraha,
KU Leuven, Belgium

*CORRESPONDENCE
Yong Hao
haonm@163.com

SPECIALTY SECTION
This article was submitted to Nutrition and Food Science Technology, a section of the journal Frontiers in Nutrition

RECEIVED 13 September 2022
ACCEPTED 03 October 2022
PUBLISHED 18 October 2022

CITATION
Hao Y, Li X, Zhang C and Lei Z (2022) Research on construction method and validity mechanism of robust analysis model in snow peach quality detection based on visible-near infrared spectroscopy. *Front. Nutr.* 9:1042868. doi: 10.3389/fnut.2022.1042868

Research on construction method and validity mechanism of robust analysis model in snow peach quality detection based on visible-near infrared spectroscopy

Yong Hao[1,2]*, Xiyan Li[1], Chengxiang Zhang[1] and Zuxiang Lei[3]

[1]School of Mechatronics and Vehicle Engineering, East China Jiaotong University, Nanchang, China, [2]Key Laboratory of Conveyance Equipment of the Ministry of Education, East China Jiaotong University, Nanchang, China, [3]School of Civil Engineering and Architecture, East China Jiaotong University, Nanchang, China

Visible-near infrared (Vis-NIR) spectra analysis method is widely used in the quality grading of bulk fruits with its rapid, non-destructive, diverse detection modes and flexible modular integration scheme. However, during the online grading of fruits, the random mechanized way of dropping fruit onto the conveyor belt method and the open detection environment led to more spectral abnormal samples, which affect the accuracy of the detection. In this paper, the soluble solids content (SSC) of snow peach is quantitatively analyzed by static and online detection methods. Several spectral preprocessing methods including Norris-Williams Smoothing (NWS), Savitzky-Golay Smoothing (SGS), Continuous Wavelet Derivative (CWD), Multivariate Scattering Correction (MSC), and Variable Sorting for Normalization (VSN) are adopted to eliminate spectral rotation and translation errors and improve the signal-to-noise ratio. Monte Carlo Uninformative Variable Elimination (MCUVE) method is used for the selection of optimal characteristic modeling variables. Partial Least Squares Regression (PLSR) is used to model and analyze the preprocessed spectra and the spectral variables optimized by MCUVE, and the effectiveness of the method is evaluated. Sparse Partial Least Squares Regression (SPLSR) and Sparse Partial Robust M Regression (SPRMR) are used for the construction of robust models. The results showed that the SGS preprocessing method can effectively improve the analysis accuracy of static and online models. The MCUVE method can realize the extraction of stable characteristic variables. The SPRMR model based on SGS preprocessing method and the effective variables has the optimal analysis results. The analysis accuracy of snow peach static model is slightly better than that of online analytical model. Through the test results of the PLSR, SPLSR and SPRMR models by the artificially adding noise test method, it can be seen that the SPRMR method eliminates the influence of abnormal samples on the model during the modeling process, which can effectively improve the anti-noise ability and detection reliability.

KEYWORDS

robust model, Sparse Partial Robust M Regression, visible-near infrared reflectance spectroscopy, soluble solids content, Lijiang snow peach

Introduction

Lijiang snow peach is an excellent variety of winter peaches cultivated by Lijiang's unique natural environment, with an average single fruit of about 500 g. With a regular shape, large fruit and bright color, each peach is rich in nutrients (1). Proper consumption of snow peach can play a role in tonifying qi and moistening lungs, and can prevent cardiovascular diseases as well. As a relatively high-end new fruit in China, snow peach is deeply loved by consumers. In recent years, with the gradual enhancement of health awareness, consumers have higher requirements for the taste and internal quality of snow peach. As a result, fruit producers and retailers must strictly control the quality of fruit. The internal SSC of snow peach characterizes its sweetness. The higher the sweetness, the better the taste. However, there is no correlation between sweetness and appearance quality. Although the fruit industry is the third largest planting industry in China, its share of international trade has been low. The main reason is that the post-harvest processing ability of the fruit is low. Therefore, it is important to explore a non-destructive, green and rapid detection method. The agricultural standard NYT 2026–2011 (Evaluation Standard for Excellent Crop Germplasm Resources Peach) stipulates that Soluble Solids Content (SSC) is one of the important indicators to identify whether the peach is an excellent germplasm resource (2). The commercial processing of peach after picking mainly includes the external quality detection of fruit shape index and surface defects based on machine vision and the internal quality grading based on SSC. Due to the regular shapes of snow peach, the detection of SSC has become an important basis for fruit suppliers to judge their quality grades. However, the conventional measurement method of fruit SSC requires the process of sampling, crushing, juicing and filtering, and then the filtrate is detected by digital refractometer. This destructive sampling detection method is not suitable for the commercialization of large-scale fruits.

Visible-near infrared (Vis-NIR) spectroscopy is widely used in the detection of fruit components and defects with its rapid, nondestructive, and flexible integrated detection device. Jiang et al. (3) studied the online detection of SSC in navel orange by using Vis-NIR technology. The results showed that the variable selection method combined with Partial Least Squares Regression (PLSR) can obtain a better analytical model, with Correlation Coefficient of Prediction (R_P) and Root Mean Squared Error of Prediction (RMSEP) of 0.824 and 0.670, respectively. Liu et al. (4) used dynamic online detection equipment to collect spectral information to compare the changes of peach SSC under two storage conditions, and obtained R_P of 0.819 and 0.828 for the peach SSC models under room temperature and refrigerated conditions, respectively. Yang et al. (5) combined the Vis-NIR spectroscopy to establish an analytical model for predicting tomato SSC. The results showed that the PLSR model with 22 key wavelengths selected by Competitive Adaptive Weighted Sampling (CARS) had better model performance than the full-wavelength model. Kim et al. (6) discussed the prediction of melon SSC based on different analytical models. The results showed that the prediction accuracy of different modeling methods was quite different, and the best method was PLSR combined with Artificial Neural Networks (ANN). Hao et al. (7) explored the influence of three kinds of navel orange placement postures on the modeling results. The results showed that the spectral information of measured samples under different postures was different, and the placement position affected the prediction accuracy of the model. Because the randomness of sample placement affects the repeatability of spectrum, more spectral abnormal samples are generated, resulting in large prediction error of online model.

In recent years, the construction of the robust regression model has been widely used in many fields. Lu et al. (8) applied Robust Partial Least Squares Regression (RPLSR) and Partial Robust M Regression (PRMR) to determine the content of each component in rapeseed. The results showed that compared with traditional quantitative methods, robust regression could reduce the influence of outliers on the model accuracy and obtain reliable prediction results. Yao et al. (9) utilized Vis-NIR combined with Sparse Partial Least Squares Regression (SPLSR) to construct an industrial analytical model of sawdust biomass. The results showed that SPLSR could ignore the interference of singular values and improve the interpretability of the model. Robust Regression (Rob-Reg) method proposed by Hao et al. (10) could effectively overcome the over-fitting problem, establish a reliable and stable analytical model, and obtain stable prediction results. The above research results show that the robust regression method has the advantages of preventing over-fitting and reducing the influence of outliers or strong influence values on the stability of the model, which can improve the prediction accuracy of the model to a certain extent.

When static and online detection of Lijiang snow peach SSC is carried out by Vis-NIR, the static collection mode of manually placed samples can ensure the repeatability of spectral collection areas and spectra; While during the online detection, the random loading method with a mechanized conveyor belt leads to inconsistent spectral acquisition area and more abnormal spectral samples, thus affecting the accuracy of detection. In this paper, different spectral preprocessing and MCUVE methods are used to enhance and optimize the characteristic variable information of fruit SSC. The robust grading model of snow peach quality is constructed by combining SPLSR and Sparse Partial Robust M Regression (SPRMR), so as to improve the anti-interference and analysis accuracy of the model.

Materials and methods

Sample preparation

The samples in this experiment were called Yunnan Lijiang snow peach, which was collected from an orchard and transported to the laboratory under refrigeration. The samples were stored at a constant temperature of 20°C, and the experiments were carried out after standing for 24 h. In order to prevent the stains attached to the surface of the snow peach after harvesting from affecting the accuracy of the spectrum acquisition, it is necessary to clean the snow peach before the experiment. In the experiment, the reflection spectra of 400 samples were collected for static and online detection modes respectively. The Atago digital refractometer (SSC detection, Saitama, Japan) was used to conduct five SSC tests on the filtrate after filtering the whole fruit juice after denucleating, and the average value was used as the final SSC of the samples. The sample set was divided by means of the average distribution of SSC contents combined with the spectral-spatial distribution. Select representative samples for modeling from the aspects of SSC content and spectral distribution, so as to ensure that the modeling samples cover the test samples. The calibration set and the prediction set are divided according to the ratio of 2:1. Finally, 267 calibration samples were used for modeling, and 133 prediction samples for model evaluation. The statistical information of the experimental samples is shown in Table 1.

Acquisition of Vis-NIR spectra

Vis-NIR spectra of snow peach were acquired by Ocean Optic Marine Optical QE65000 spectrometer (Optical inspection, Florida, USA), with a wavelength range of 346–1,130 nm and a resolution of ca. 1 nm. Therefore, each spectrum contains 1,044 wavelength variables. The light source adopted two 100-watt halogen tungsten lamps (OSRAM), which were arranged at an angle of 45 degrees along the transmission direction of the conveyor belt. The schematic diagram of spectral acquisition device is shown in Figure 1, which consists of a spectrometer, a light source, a conveyor belt, an optical fiber and a computer. Both static and online detection experiments were completed on this device, and the conveyor belt stopped during the static collection, and the fruit cup was located directly above the center of two light sources. During the dynamic acquisition, the speed of the conveyor belt was 6 peaches per second. The difference between static detection and online detection is that the static method can control the position of the fruit to obtain more stable spectral information by manually placing the fruit. While the online detection adopts the method of mechanized random fruit loading, and the position of the fruit reaching the detection point is random, thus the obtained spectral information contains more interference.

Preprocessing of Vis-NIR spectra

In order to eliminate the background and noise existing in the original spectrum and the interference caused by the instruments and placement methods in the acquisition process, it is necessary to preprocess the original spectrum. Data smoothing, derivative and scattering correction are used to preprocess the static and dynamic online spectra (11). The purpose of the smoothing algorithm is to improve the signal-to-noise ratio of the research samples and eliminate spectral noise. The derivative algorithm is mainly to eliminate the influence of the spectral instrument on the signal. The scattering correction is used to eliminate scattering effects caused by particles of different sizes. Among them, Norris-Williams Smoothing (NWS) (7) and Savitzky-Golay Smoothing (SGS) (12) are used for smoothing; the derivative adopts Continuous Wavelet Derivative (CWD) (13) method; Multivariate Scatter Correction (MSC) (14) and Variable Sorting for Normalization (VSN) (15) methods are used for scattering correction.

MCUVE variable optimization method

The purpose of variable selection is to optimize the model, save calculation time and make the model more explanatory (16). Each Vis-NIR spectrum of peach samples contains 1,044 wavelength points, with many uninformed variables and high-dimensional overlap. In order to eliminate redundant and uninformed variables, this paper adopts MCUVE variable selection method to select effective wavelength.

The idea of MCUVE method is basically consistent with that of Uninformative Variable Elimination (UVE). The difference is that MCUVE uses Monte Carlo (MC) sampling instead of adding random noises to UVE, which combines MC process with UVE, makes full use of the intrinsic correlation between samples, evaluates the contribution of wavelength variables in high-dimensional spectral data, sorts the stability of each wavelength according to the contribution value of each wavelength, and finally establishes a series of the PLSR models. At last, the upper and lower thresholds are determined by the Root Mean Squared Error of Cross Validation (RMSECV) of the optimal PLS model. The variables outside the threshold are retained and those within the threshold are discarded.

Calibration model

Partial least squares regression

Partial Least Squares Regression (PLSR) (17) is a widely used regression technique for Vis-NIR spectral data analysis. This method combines the advantages of principal component regression, multiple linear regression and canonical correlation analysis, and can be applied to an effective regression method

TABLE 1 Statistical information of the experimental samples.

Detection mode	Sample set	N	R_{SSC} (°Brix)	Mean	Standard deviation
Static	Calibration set	267	10.1–15.1	12.859	0.966
	Prediction set	133	10.1–15.0	12.844	0.952
Online	Calibration set	267	10.1–15.1	12.872	0.943
	Prediction set	133	10.1–15.1	12.863	0.935

N represents the number of samples; R_{SSC} indicates the range of SSC.

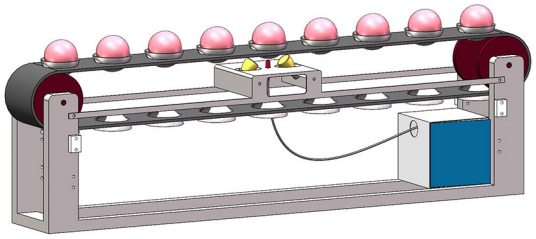

FIGURE 1
Schematic diagram of spectral acquisition device.

for processing high-dimensional data. Its core idea is to project high-dimensional data into the hidden space, obtain the RMSECV value by the leave-one-out method or the MC cross-validation method, and obtain the best factor number combined with F-test and establish the model.

Robust regression method

The SPLSR method is realized by NIPALS algorithm, which is a linear combination of original variables through a set of weighted vectors, belonging to the sparse version of PLS (18). The algorithm generates sparse solutions by keeping the subsequence structure of the direction vector in the restricted X space of the selected variables (19). The SPLSR algorithm is a method that integrates dimensionality reduction and variable selection (18). In general, methods with inherent variable selection properties have smaller prediction errors than methods lacking the inherent variable selection properties. Compared with the classical PLSR algorithm, the SPLSR algorithm can reduce the interference of irrelevant information, improve the accuracy of the quantitative analysis of the model, and enhance the explanatory ability of the model (9).

Based on PRMR algorithm, SPRMR algorithm introduces sparse factors. SPRMR estimator can be regarded as a sparse version of PRMR estimator, and it can also be used as a method of SPLSR estimator. SPRMR is the first method to combine dimension reduction with regression, which can generate partial least squares estimation, sparse and robust to feature vectors and responses. The advantage of SPRMR lies in that the algorithm can not only automatically identify vertical outliers and leverage points (vertical outliers are outliers in the response; lever points are outliers in the predictor), but also automatically reduce the dimension of high-dimensional data. The specific algorithm of PRMR is shown in Reference (19), and SPRMR is shown in Reference (20).

Model evaluation

Correlation Coefficient of Cross Validation (R_{CV}) and RMSECV are used as evaluation indexes of preprocessing methods and variable selection, and the R_{CV}, R_P, RMSECV, RMSEP, Residual Predictive Deviation (RPD) and The Ratio of Error Range (RER) are used as evaluation indexes of regression models. The closer R_{CV} and R_P are to 1 and RMSEP and RMSECV are to 0, indicating that the better the model is. Among them, the smaller the error between R_{CV} and R_P, RMSECV and RMSEP is, the better the model is, and the smaller the difference is, the more stable the model is. The values of RPD and RER indicate the model quality. The larger the value is, the better the model is. Nicolaï et al. (21) defined that RPD value of 1.5–2 means the model can make rough quantitative prediction; 2–2.5 means the model has reliable prediction performance; >3 means the model has excellent prediction performance; Badaró et al. (22) defined that RER value >10 means the model can achieve excellent prediction accuracy.

The formulas of R_{CV}, R_P, RMSEC, RMSEP, RPD and RER are as follows:

$$R_{CV}, R_P = \sqrt{1 - \left[\sum_{i=1}^{n} (y_i - y_{pi})^2\right] \Big/ \left[\sum_{i=1}^{n} (y_i - y_m)^2\right]} \tag{1}$$

$$RMSECV, RMSEP = \sqrt{\frac{1}{n}\sum_{i=1}^{n} (y_i - y_{pi})^2} \tag{2}$$

$$RPD = \frac{SD}{RMSEP} = \sqrt{\frac{1}{n-1}\sum_{i=1}^{n} (y_i - y_m)^2} \Big/ \sqrt{\frac{1}{n}\sum_{i=1}^{n} (y_i - y_{pi})^2} \tag{3}$$

$$RER = P_r / RMSEP \tag{4}$$

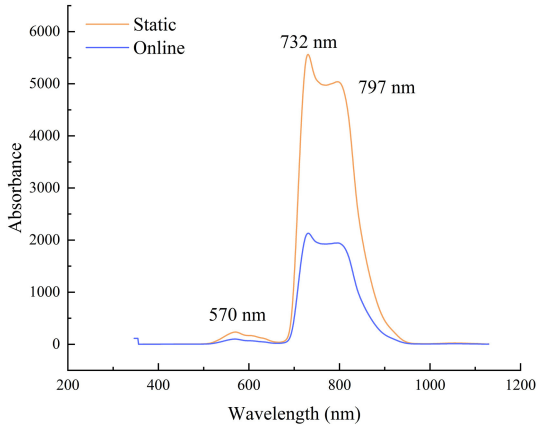

FIGURE 2
Average Vis-NIR spectra of snow peach samples with static and online detection.

wherein, y_i and y_{pi} represent SSC values of the calibration set and the prediction set respectively; y_m represents the average value of actual measured SSC in the calibration set and prediction set; n represents the number of samples in the calibration set or prediction set; SD represents the standard deviation of prediction set; P_r represents the SSC range of the prediction set.

Results and discussion

Vis-NIR analysis of snow peach samples with static and online detection

In order to explore the overall difference between static and online detection spectra, the Vis-NIR average reflectance spectra of 400 snow peacher samples were used for illustration (Figure 2). It can be seen from the figure that the spectral curves obtained under different detection modes are basically similar. The difference is that the static spectra have higher response intensity than the online spectra, and spectra have obvious absorption peaks around 570, 732, and 797 nm. The reason for the existence of peaks is related to the stretching and contraction of hydrogen-containing groups (O–H, C–H or N–H) in the internal components of snow peach (23). The two absorption peaks observed around 732 and 797 nm may be related to the stretching of the third overtone of C–H functional group and the second and the third overtones of O–H functional group respectively (24). The absorption peak at 570 nm is mainly related to colors and shapes of the peach (25).

Spectral preprocessing and characteristic analysis

Optimization of spectral preprocessing methods

In order to further improve the quality of the modeling spectra, five different preprocessing methods are used to eliminate the drift, scattering and noises of original spectra. PLSR is used to model and analyze the preprocessed spectra, and the effectiveness of the method is evaluated. The evaluation indicators are LV_S, R_{CV} and RMSECV. After sample spectra are preprocessed by different preprocessing methods, the modeling results of snow peach SSC models are shown in Table 2.

It can be seen from Table 2 that the LVS, R_{CV} and RMSECV of the original static spectral modeling are 18, 0.831 and 0.540, respectively; the LVS, R_{CV} and RMSECV of the original dynamic spectral modeling are 19, 0.820 and 0.543, respectively. By comparison, it can be seen that, except for the improvement of R_{CV} and the decrease of RMSECV after SGS preprocessing, the data processing results of other preprocessing methods are worse than the results of direct modeling of the original spectrum. In terms of the number of factors involved in modeling, the LVS of SGS in both modes increases by one, indicating that the modeling complexity has increased. However, the modeling accuracy of SGS is much higher than that of the original spectrum, so this effect is ignored. Compared with the original spectra, the R_{CV} of the model is increased by 0.160 and RMSECV is reduced by 0.413° Brix after the SGS pretreatment method is used for the static detection data. The R_{CV} is increased by 0.171 and RMSECV is reduced by 0.418° Brix after the SGS pretreatment method is used for online detection data.

Robust variable selection based on MCUVE method

In order to further improve the model accuracy, simplify the model and improve its interpretability, MCUVE method is used for wavelength selection based on SGS preprocessing. After the optimization, the wavelengths of static and online detection are reduced from 1,044 in a full spectrum to 250 and 450 respectively. The variable distribution optimized by MCUVE variable selection method for the two detection methods is shown in Figure 3. It can be seen from the figure that the selected modeling variables for static and online detection are mainly concentrated in three regions of 347–694, 716–820 and 827–1,129 nm. The selected variables in the spectral range of 347–694 nm are related to the absorption of carotenoids in snow peach (26); the selected variables in the spectral range of 716–820 nm are mainly related to the absorption of chlorophyll in snow peach (27); the selected variables in the spectral range of 827–1,129 nm are mainly related to the absorption of water in snow peach (28). It can be seen from Figure 3 that the regions of the variables selected by the MCUVE method for static

TABLE 2 The modeling results of snow peach SSC models with different spectral preprocessing methods.

Preprocessing methods	Static			Online		
	LVs	R_{CV}	RMSECV	LVs	R_{CV}	RMSECV
Raw	18	0.831	0.540	19	0.820	0.543
NWS	18	0.824	0.550	19	0.810	0.556
SGS	19	0.991	0.127	20	0.991	0.125
CWD	18	0.820	0.555	19	0.811	0.554
MSC	18	0.827	0.545	18	0.811	0.556
VSN	15	0.822	0.554	18	0.806	0.566

NWS selects 15-point smoothing; in static mode, the polynomial order of SGS is set to 3, and the number of smoothing points is set to 17; in online mode, the polynomial order of SGS is set to 3, and the number of smoothing points is set to 15; the decomposition scale of CWD is set to 60.

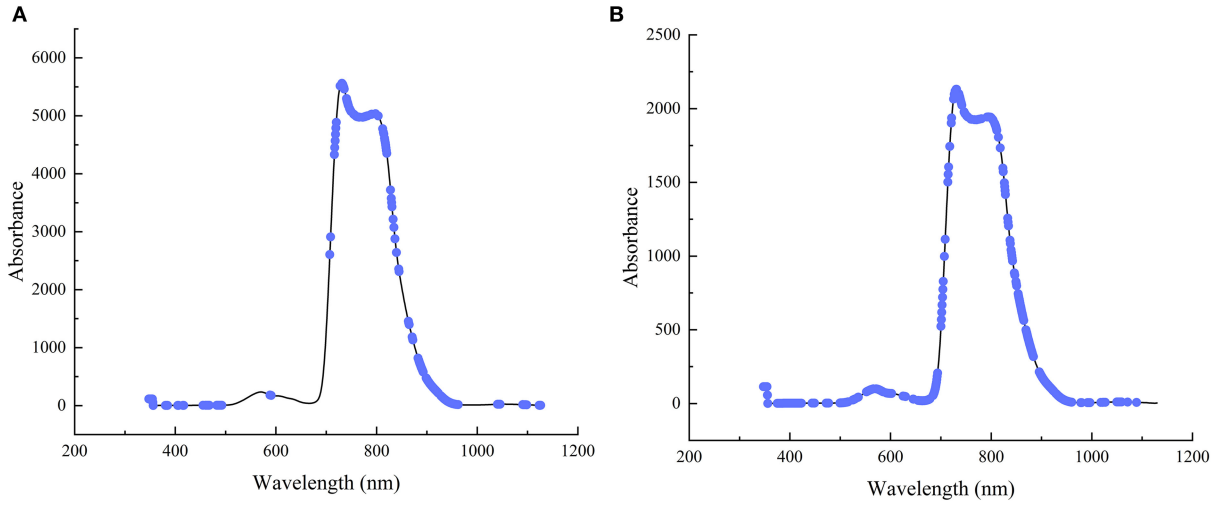

FIGURE 3
(A) Variable optimization results with MCUVE for static detection; **(B)** Variable optimization results with MCUVE for online detection.

and online detection are basically the same, indicating that the variable selection is reasonable.

Construction of SSC robust model for snow peach

Robust model construction and analysis based on SPLSR and SPRMR methods

Combined with SGS preprocessing algorithm and MCUVE variable selection algorithm, the robust models of SPLSR and SPRMR for the SSC of snow peach are established respectively. Table 3 shows the modeling results of snow peach SSC calibration set and prediction set based on different modeling methods. It can be seen from the table that the difference between R_{CV} and R_P, RMSECV and RMSEP of the SPRMR model is smaller than that of the SPLSR model, indicating that the SPRMR model is more stable than the SPLSR model and its prediction results are more reliable. The RPD values of SPRMR and SPLSR in static detection are 5.926 and 5.498 respectively, which are >3, indicating that both models have excellent prediction performance in static detection mode. The RPD values of SPRMR and SPLSR in online detection are 3.848 and 3.744 respectively, indicating that both the SPRMR model and the SPLSR model have excellent prediction performance in online detection mode. In addition, the RER values of two robust regression models under different detection modes are all >10, and the RER value of static detection is higher than that of online detection.

Reliability analysis of robust regression method with different background noise interference

In order to test the robustness of the model, N random data in the calibration set samples and prediction set samples were selected from this experiment, and white gaussian noise (WGN)

10.3389/fnut.2022.1042868

TABLE 3 Quantitative analysis results of snow peach SSC with PLSR, SPLSR and SPRMR modeling methods.

Models	Static							Online						
	Calibration set			Prediction set				Calibration set			Prediction set			
	LVs	R_{CV}	RMSECV	R_P	RMSEP	RPD	RER	LVs	R_{CV}	RMSECV	R_P	RMSEP	RPD	RER
PLSR	18	0.992	0.124	0.983	0.182	5.263	26.981	19	0.991	0.128	0.966	0.247	3.800	20.245
SPLSR	18	0.991	0.131	0.984	0.174	5.498	28.191	19	0.993	0.109	0.965	0.251	3.744	19.944
SPRMR	19	0.994	0.106	0.987	0.161	5.926	30.388	19	0.993	0.111	0.967	0.244	3.848	20.500

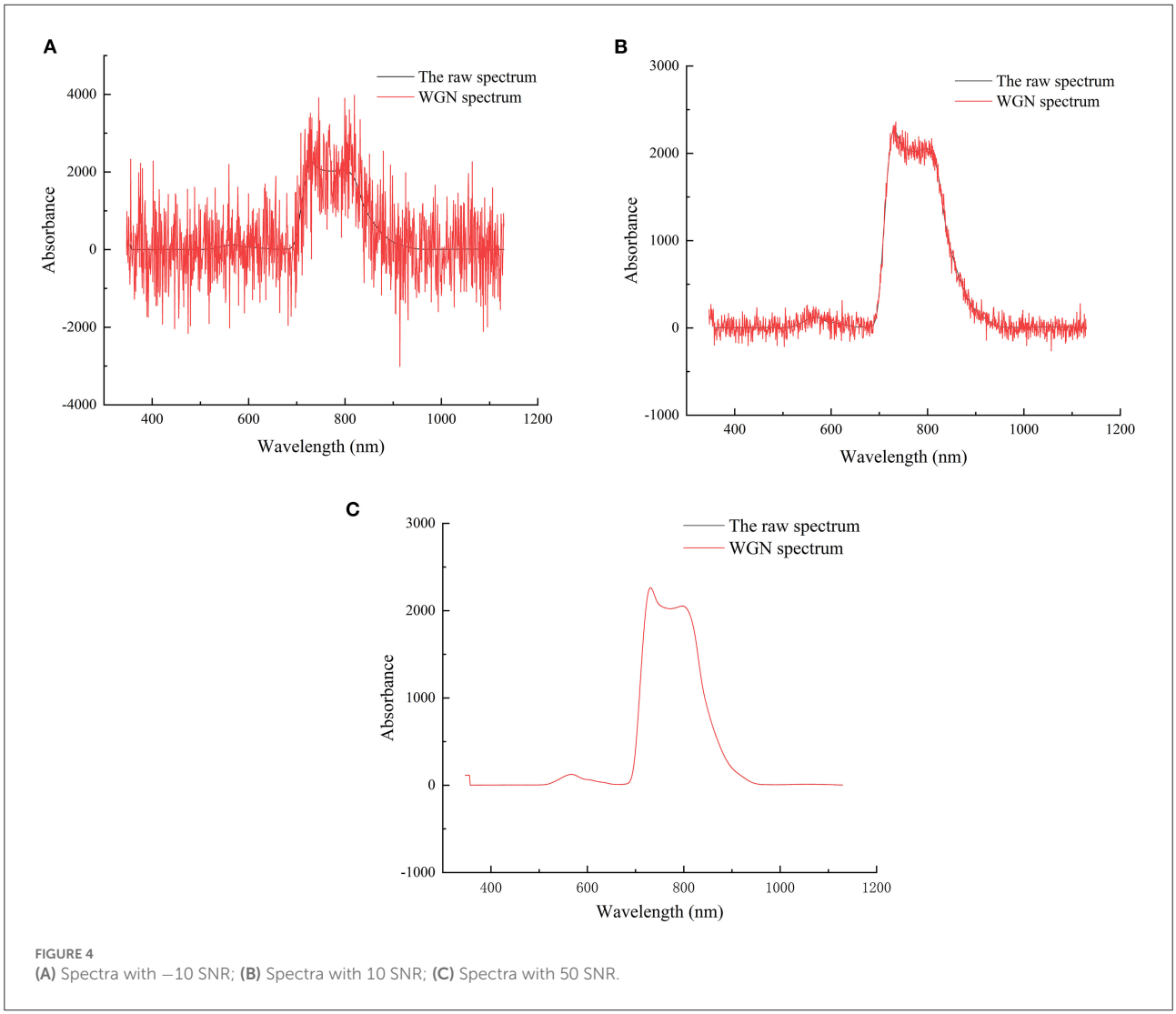

FIGURE 4
(A) Spectra with −10 SNR; **(B)** Spectra with 10 SNR; **(C)** Spectra with 50 SNR.

was added to observe the recognition accuracy of the PLSR, SPLSR and SPRMR models on noise and abnormal samples. In the experiment, the intensity of the added WGN is adjusted by changing the signal-to-noise ratio (SNR). N is set as 10, i.e., 10 samples are randomly drawn from both datasets and added with noise. Figure 4 shows three spectra with SNR of −10, 10, 50 in static detection mode.

Generally, the larger the SNR is, the smaller the mixed noise is, so the model accuracy should gradually increase with the increase of SNR. The variation trend of R_P for different models with noise intensity is shown in Figure 5. It can be seen from Figure 5 that with the addition of different noises, the accuracy of SPLSR and SPRMR models is less affected; while the accuracy of PLSR model decreases greatly and shows instability.

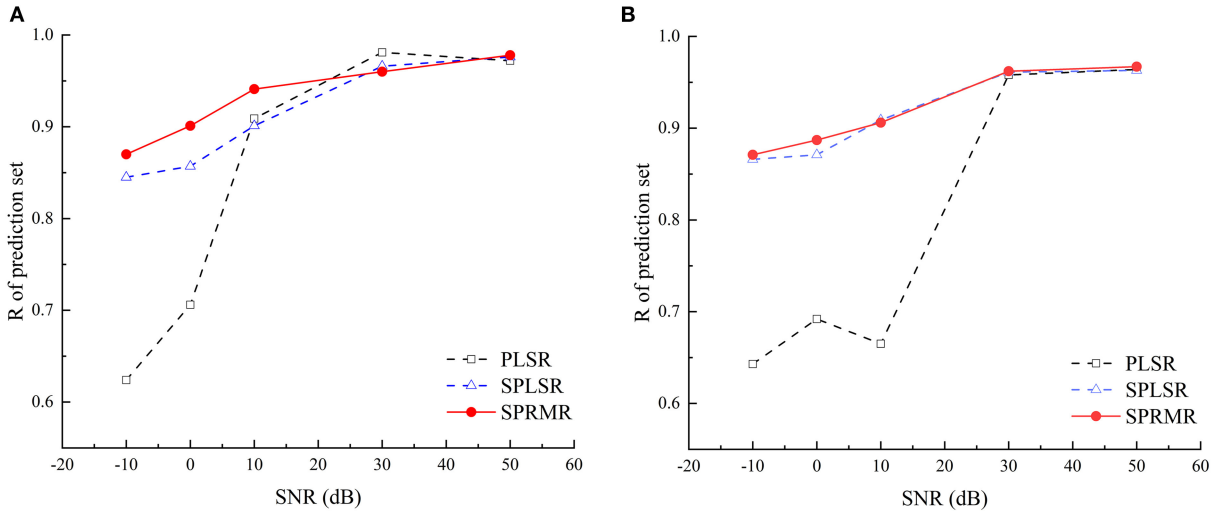

FIGURE 5
The influence trends of WGN with different SNR on calibration correlation coefficient of three models. **(A)** The static detection; **(B)** The online detection.

TABLE 4 The RMSEP of the prediction set including 10 noise samples with SNR of 10.

Models	RMSEP of static detection			RMSEP of online detection		
	Noise	Non-noise	Whole	Noise	Non-noise	Whole
PLSR	1.148	0.738	0.776	0.806	0.722	0.729
SPLSR	0.551	0.556	0.556	0.659	0.452	0.470
SPRMR	2.241	0.271	0.667	2.065	0.366	0.666

By observing the trend of the curve, it can be seen that the predictive ability of the SPRMR model is slightly higher than that of the SPLSR model. Even if the noise level reaches −10, the SPRMR model still has a good prediction performance and outperforms other models.

In order to verify the ability of the SPRMR model to automatically identify abnormal samples, the RMSEP of the data with noise, the data with non-noise and the whole data were calculated in the case of adding noise, respectively. The anti-interference ability of the SPRMR model is illustrated by observing the errors of the prediction set composed of two parts of data. Table 4 shows the RMSEP of the prediction set including 10 noise samples with SNR of 10. It can be seen from Table 4 that the prediction error of the SPRMR model for normal samples with non-noise is small, and the SSC of the samples can be more accurately predicted. However, the RMSEP of the data with noise exceeds 2° Brix, the deviation is larger. It shows that the noise data added in the training set can be accurately identified during the modeling of SPRMR. The model regards the samples with noise as abnormal samples, and assigns a smaller weight during modeling. So, for the 10 data with noise added in the prediction set, there is a larger prediction bias.

For another robust regression model, SPLSR, it can be observed from Table 4 that there is little difference between the RMSEP results of the data with noise and the data with non-noise. This is because the SPLSR model does not have the ability to identify outliers, and the abnormal samples are regarded as normal samples during the modeling process and participate in the modeling. In addition, the model has inherent variable selection property, which can automatically discard the variables that have a greater impact on the modeling results during modeling, and optimize the model to a certain extent. Therefore, the RMSEP of the data with noise and the data with non-noise are basically similar.

In conclusion, robust regression models are less affected by noise, and have the advantages of preventing over-fitting and reducing the influence of outliers or strong influence values on the stability of the model. In addition, the SPRMR model can identify outliers and has strong anti-interference ability.

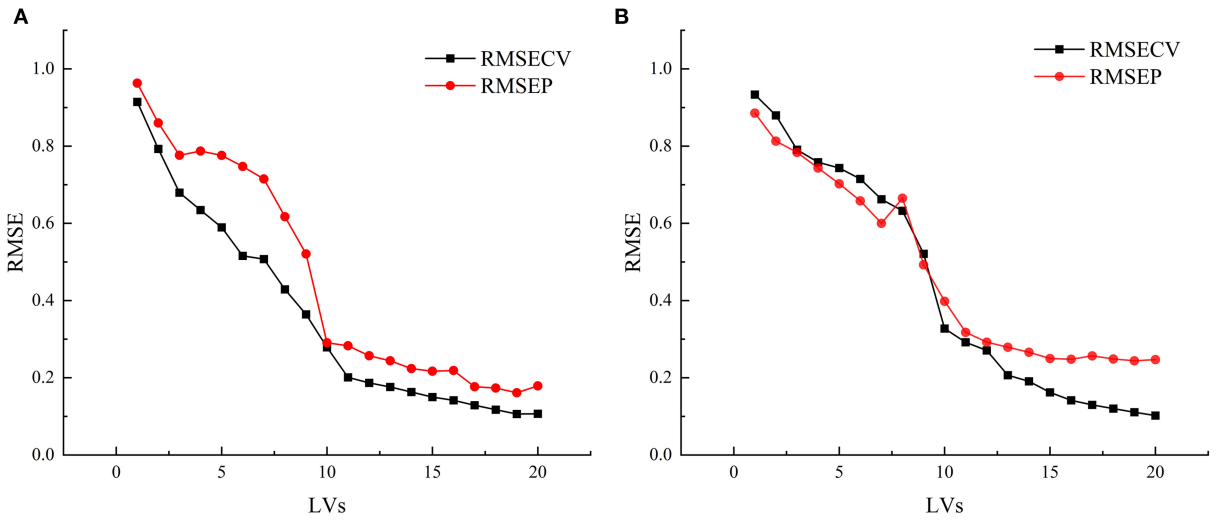

FIGURE 6
(A) Factor graph of SPRMR model for static detection; **(B)** Factor graph of SPRMR model for online detection.

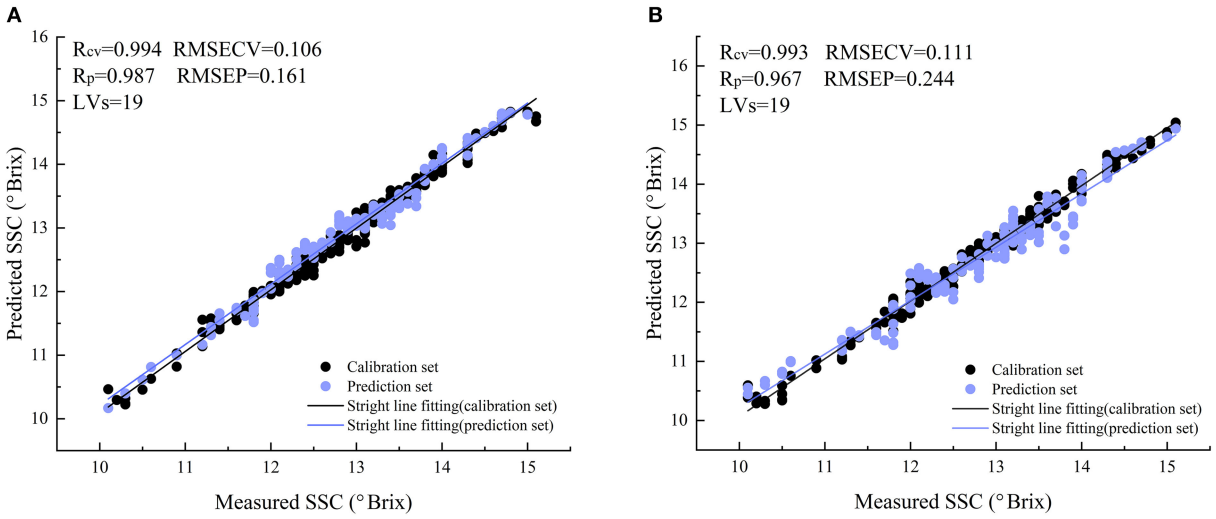

FIGURE 7
The correlation diagrams between the measured values of SSC and the predicted values of the models. **(A)** The static detection of snow peach; **(B)** The online detection of snow peach.

Analysis of SSC optimal robust model for snow peach

A suitable robust regression model is established to achieve a better prediction of snow peach SSC in static and online detection. Through values of R_P, RMSEP, RPD and RER, the PLSR, SPLSR and SPRMR models are comprehensively compared. It can be seen from Table 3 that the analytical model with the best prediction of snow peach SSC content is SPRMR for both static and online detection. Since the experimental samples are collected from the same orchard and the interference and noise contained in the sample information are small, the superior performance of the SPRMR model has not been fully highlighted. However, it can be seen from the noise experiment in the previous section that the SPRMR model is still superior to the PLSR and SPLSR models in the presence of strong noises, showing strong anti-interference ability. Therefore, the optimal model for snow peach SSC prediction is the SPRMR model combined with SGS and MCUVE.

Figure 6 shows the factor diagram of the variation of RMSECV and RMSEP with the principal component fraction

of the SPRMR model. The number of factors in both static and online models is 19. It can be seen from the figure that the variation trends of RMSECV and RMSEP are basically similar, indicating that the model fitting is reasonable. Figure 7 shows the correlation between the measured values and predicted values of snow peach SSC. It can be seen from the figure that for the static detection model, when the factor number is 19, the R_{CV} and R_P of the model are 0.994 and 0.987 respectively, and RMSECV and RMSEP are 0.106 and 0.161 respectively. For the online model, when the factor number is 19, the R_{CV} and R_P are 0.993 and 0.967 respectively, and RMSECV and RMSEP are 0.111 and 0.244 respectively. The analysis shows that the correlation coefficient (R) and Root Mean Square Error (RMSE) under two detection modes are similar, indicating that the over-fitting risk of the model is small. In general, the SPRMR model has strong anti-noise ability, which can realize the reliable analysis of snow peach SSC.

Conclusion

The Vis-NIR spectroscopy combined with PLSR, SPLSR and SPRMR methods is used for rapid analysis of SSC in snow peach. NWS, SGS, CWD, MSC and VSN preprocessing methods and MCUVE variable selection method are used to enhance and optimize the information of snow peach characteristic variables. The results show that the SGS preprocessing method can effectively improve the analysis accuracy of static and online models. The MCUVE method realizes the extraction of stable characteristic variables; the accuracy of static detection is slightly better than that of online detection. The SPRMR method has strong robustness and anti-interference ability. Therefore, the SPRMR model constructed by combining Vis-NIR spectroscopy combined with SGS preprocessing method and MCUVE variable selection method can realize the prediction of SSC in snow peach.

In view of the current research on single system of static detection or online detection, this experiment makes a comparative analysis of the two detection methods. The application of a robust model in fruit SSC has been discussed, which provides ideas for the future application of robust models combined with Vis-NIR spectroscopy in fruit quality detection. The shortcomings of this experiment are as follows: (1) Although 400 experimental samples are collected in batches from different planting areas of the same orchard, the time interval is so short that sample spectra do not contain information about different planting environments; (2) In the Vis-NIR spectrum acquisition, the peaches are not fully mature and their skin is hard (if analyzed after maturity, it is easy to bump in the grading process). In this case, the SSC detection value is small, and the distribution of SSC value affects the subsequent modeling accuracy.

Data availability statement

The raw data supporting the conclusions of this article will be made available by the authors, without undue reservation.

Author contributions

YH: conceptualization, investigation, supervision, and writing—original draft and review and editing. XL: methodology, formal analysis, software, and writing—original draft and editing. CZ: formal analysis and writing—original draft and review. ZL: supervision, conceptualization, and writing—review and editing. All authors contributed to the article and approved the submitted version.

Funding

This study was funded by the National Natural Science Foundation of China (grant number 31960497), Jiangxi Provincial Natural Science Foundation of China (grant number 20212BAB204009), and Jiangxi Provincial Natural Science Foundation of China (grant number 20202ACB211002).

Conflict of interest

The authors declare that the research was conducted in the absence of any commercial or financial relationships that could be construed as a potential conflict of interest.

Publisher's note

References

1. Long XZ. Research on fertilization technology of Lijiang snow peach. *Bull Agric Sci Technol.* (2021) 2021:198–200. Available online at: https://kns.cnki.net/kcms/detail/detail.aspx?FileName=XBPG201716011&DbName=CJFQ2017

2. NY/T 2026-2011. *Evaluating Standards for Elite and Rare Germplasm Resources-Peach* (*Prunus persica* L.). Industry Standard – Agriculture. (2011).

3. Jiang SQ, Sun T. Online detection of soluble solid content in navel orange based on visible/near infrared spectroscopy and variable selection. *Food Mach.* (2020) 36:89–93. doi: 10.13652/j.issn.1003-5788.2020.02.016

4. Liu YD, Zhang Y, Jiang XG, Liu HC. Detection of the quality of juicy peach during storage by visible/near infrared spectroscopy. *Vib Spectrosc.* (2020) 111:103152. doi: 10.1016/j.vibspec.2020.103152

5. Yang Y, Zhao CJ, Huang WQ, Tian X, Fan SX, Wang QY, et al. Optimization and compensation of models on tomato soluble solids content assessment with online Vis/NIRS diffuse transmission system. *Infrared Phys Techn.* (2022) 121:104050. doi: 10.1016/j.infrared.2022.104050

6. Kim SY, Hong SJ, Kim E, Lee CH, Kim G. Neural network based prediction of soluble solids concentrationin oriental melon using VIS/NIR spectroscopy. *Appl Eng Agric.* (2021) 37:653–63. doi: 10.13031/aea.14332

7. Hao Y, Wang QM, Zhang SM. Online accurate detection of soluble solids content in navel orange assisted by automatic orientation correction device. *Infrared Phys Technol.* (2021) 118:103871. doi: 10.1016/j.infrared.2021.103871

8. Lu YZ, Du CW Yu CB, Zhou JM. Quantitative analysis of rapeseeds using infrared photoacoustic spectroscopy combined with robust regression. *J Instrum Anal.* (2013) 32:1096–100. doi: 10.3969/j.issn.1004-4957.2013.09.012

9. Yao Y, Wang CY, Liu HJ, Tang JB, Cai JH, Wang JJ. Biomass compositional analysis using sparse partial least squares regression and near infrared spectrum technique. *Spectrosc Spect Anal.* (2015) 35:1864–9. doi: 10.3964/j.issn.1000-0593(2015)07-1864-06

10. Hao Y, Lu YH Li XY. Study on robust model construction method of multi-batch fruit online sorting by near-infrared spectroscopy. *Spectrochim Acta A.* (2022) 280:121478. doi: 10.1016/j.saa.2022.121478

11. Zhang JY, Zhu HT. A survey of spectral preprocessing methods. *West Leather.* (2017) 39:14. Available online at: https://kns.cnki.net/kcms/detail/detail.aspx?FileName=KJTX202111058&DbName=CJFQ2021

12. Hernández-Sánchez N. Gómez-del-Campo M. From NIR spectra to singular wavelengths for the estimation of the oil and water contents in olive fruits. *Grasas y Aceites.* (2018) 69:e278. doi: 10.3989/gya.0457181

13. Hao Y, Du JJ, Zhang SM, Wang QM. Research on construction of visible-near infrared spectroscopy analysis model for soluble solid content in different colors of jujube. *Spectrosc Spect Anal.* (2021) 41:3385–91. doi: 10.3964/j.issn.1000-0593(2021)11-3385-07

14. Hao Y, Wu WH, Shang QY, Geng P. Analysis model of oleic and linoleic acids in camellia oil *via* near-infrared spectroscopy. *Acta Opt Sin.* (2019) 39:381–6. doi: 10.3788/AOS201939.0930004

15. Mishra P, Polder G, Gowen A, Rutledge DN, Roger J-M. Utilising variable sorting for normalisation to correct illumination effects in close-range spectral images of potato plants. *Biosyst Eng.* (2020) 197:318–23. doi: 10.1016/j.biosystemseng.2020.07.010

16. Lao CC, Chen JY, Zhang ZT, Chen YW, Ma Y, Chen HR, et al. Predicting the contents of soil salt and major water-soluble ions with fractional-order derivative spectral indices and variable selection. *Comput Electron Agr.* (2021) 182:106031. doi: 10.1016/j.compag.2021.106031

17. Zhang DY, Yang Y, Chen G, Tian X, Wang ZL, Fan SX, et al. Nondestructive evaluation of soluble solids content in tomato with different stage by using Vis/NIR technology and multivariate algorithms. *Spectrochim Acta A.* (2021) 248:119139. doi: 10.1016/j.saa.2020.119139

18. Chun H, Keleş S. Sparse partial least squares regression for simultaneous dimension reduction and variable selection. *J R Stat Soc B.* (2010) 72:3–25. doi: 10.1111/j.1467-9868.2009.00723.x

19. Serneels S, Croux C, Filzmoser P, Van Espen PJ. Partial robust M-regression. *Chemometr Intell Lab.* (2005) 79:55–64. doi: 10.1016/j.chemolab.2005.04.007

20. Hoffmann I, Serneels S, Filzmoser P, Croux C. Sparse partial robust M regression. *Chemometr Intell Lab.* (2015) 149:50–9. doi: 10.1016/j.chemolab.2015.09.019

21. Nicolaï BM, Beullens K, Bobelyn E, Peirs A, Saeys W. Theron, KI, et al. Nondestructive measurement of fruit and vegetable quality by means of NIR spectroscopy: a review. *Postharvest Biol Technol.* (2007) 46:99–118. doi: 10.1016/j.postharvbio.2007.06.024

22. Badaró AT, Garcia-Martin JF. López-Barrera MdC, Barbin DF, Alvarez-Mateos P. Determination of pectin content in orange peels by near infrared hyperspectral imaging. *Food Chem.* (2020) 323:126861. doi: 10.1016/j.foodchem.2020.126861

23. Zhang J, Hu Y, Zhou LX Li BY. Progress of chemometric algorithms in near-infrared spectroscopic analysis. *J Instrum Anal.* (2020) 39:1196–203. doi: 10.3969/j.issn.1004-4957.2020.10.003

24. Zou XB, Zhao JW, Povey MJW, Holmes M, Mao HP. Variables selection methods in near-infrared spectroscopy. *Anal Chim Acta.* (2010) 667:14–32. doi: 10.1016/j.aca.2010.03.048

25. Shao YN, Bao YD, He Y. Visible/near-infrared spectra for linear and nonlinear calibrations: a case to predict soluble solids contents and pH value in peach. *Food Bioprocess Tech.* (2011) 4:1376–83. doi: 10.1007/s11947-009-0227-6

26. Qin JW, Lu RF. Measurement of the optical properties of fruits and vegetables using spatially resolved hyperspectral diffuse reflectance imaging technique. *Postharvest Biol Tec.* (2008) 49:355–65. doi: 10.1016/j.postharvbio.2008.03.010

27. Ziosi V, Noferini M, Fiori G, Tadiello A, Trainotti L, Casadoro G, et al. A new index based on vis spectroscopy to characterize the progression of ripening in peach fruit. *Postharvest Biol Technol.* (2008) 49:319–29. doi: 10.1016/j.postharvbio.2008.01.017

28. Uwadaira Y, Sekiyama Y, Ikehata A. An examination of the principle of non-destructive flesh firmness measurement of peach fruit by using VIS-NIR spectroscopy. *Heliyon.* (2018) 4:e00531. doi: 10.1016/j.heliyon.2018.e00531

frontiers | Frontiers in Nutrition

TYPE Original Research
PUBLISHED 19 October 2022
DOI 10.3389/fnut.2022.993737

OPEN ACCESS

EDITED BY
John-Lewis Zinia Zaukuu,
Kwame Nkrumah University of Science and Technology, Ghana

REVIEWED BY
Guantao Xuan,
Shandong Agricultural University, China
Sicong Liu,
Tongji University, China

*CORRESPONDENCE
Long Xue
ultimata@163.com

SPECIALTY SECTION
This article was submitted to Nutrition and Food Science Technology, a section of the journal Frontiers in Nutrition

RECEIVED 14 July 2022
ACCEPTED 28 September 2022
PUBLISHED 19 October 2022

CITATION
Li J, He L, Liu M, Chen J and Xue L (2022) Hyperspectral dimension reduction and navel orange surface disease defect classification using independent component analysis-genetic algorithm. *Front. Nutr.* 9:993737. doi: 10.3389/fnut.2022.993737

Hyperspectral dimension reduction and navel orange surface disease defect classification using independent component analysis-genetic algorithm

Jing Li[1], Liang He[1], Muhua Liu[1], Jinyin Chen[2] and Long Xue[1,3]*

[1]Jiangxi Key Laboratory of Modern Agricultural Equipment, College of Engineering, Jiangxi Agricultural University, Nanchang, China, [2]Collaborative Innovation Center of Postharvest Key Technology and Quality Safety of Fruits and Vegetables in Jiangxi Province, Nanchang, China, [3]Key Laboratory of Optics-Electrics Application of Biomaterials of Jiangxi Province, Jiangxi Agricultural University, Nanchang, China

Canker is a common disease of navel oranges that is visible before harvest, and penicilliosis is a common disease occurring after harvest and storage. In this research, the typical fruit surface, canker spots, penicillium spore, and hypha of navel oranges were, respectively, identified by hyperspectral imaging. First, the light intensity on the edge of samples in hyperspectral images was improved by spherical correction. Then, independent component images and weight coefficients were obtained using independent component analysis. This approach, combined with use of a genetic algorithm, was used to select six characteristic wavelengths. The method achieved dimension reduction of hyperspectral data, and the testing time was reduced from 46.21 to 1.26 s for a self-developed online detection system. Finally, a deep learning neural network model was established, and the four kinds of surface pixels were identified accurately.

KEYWORDS

canker, penicilliosis, navel orange, hyperspectral image, ICA-GA

Introduction

Navel orange is an important fruit crop grown in Jiangxi Province, China and many other agricultural areas in subtropical regions. The fruit is generally round, oblate, or elliptic in shape and usually orange-yellow or orange-red in color (1). The calyx of the fruit has a few immature pericardial groups, which form the characteristic navel, and

the core is solid or semi-solid. In the process of transportation and packaging of navel oranges after harvest, a spore from a single navel orange can cause an entire batch to start sporing within a short time (2). Therefore, the post-harvest sorting of navel orange is conducive to improving their value and increasing the preservation period, and technology to accomplish this objective is urgently needed for fruit production (3).

In present-day fruit sorting operations, machine vision technology is mainly used to assess fruit appearance quality, including fruit shape and visible defects, for example, brown spots, spores, granulation, edema, etc. However, for some defects, such as decay caused by fungi, machine vision methods seem ineffective. The main reason is that the skin color of a decayed area can be close to that of the normal skin areas, so it is hard to distinguished using images from a color camera. However, the skin damage is related to the characteristics of the fruit skin that can be detected by near infrared spectroscopy (NIRS). Moreover, NIRS can also be used for non-destructive testing of the internal components of fruits, such as soluble solids (4), acidity, and other traits (5, 6). Although NIRS technology can reflect the internal quality of fruit, only a small part of the fruit surface can be collected, and the fruit appearance quality cannot be perfectly determined.

Hyperspectral image technology combines the advantages of spectrum- and image-based approaches (7). It not only can achieve fruit appearance image inspection, but can also collect the surface spectra which can be used to detect the invisible defect (8, 9). The hyperspectral image is a three-dimensional image. Through the selection of characteristic wavelengths of hyperspectral images, simultaneous external and internal fruit quality testing can be realized; this is a major development trend in the field of fruit detection (10). Hyperspectral image technology can be used to detect meat quality (11), orange spores, cucumber frostbite (12), guava maturity (13), strawberry ripeness (14), Moisture of Okra (15), and many other food defects (16–18). However, hyperspectral images contain large amounts of wavelength information, thus requiring a long time to collect information; accordingly, its online detection applications are limited. Therefore, the study of hyperspectral data dimension reduction technology has become the key to improving the speed of online detection. Current dimension reduction methods mainly include genetic algorithm (19), principal component analysis (20, 21), independent component analysis (22), and some deep learning (23) methods. However, most approaches have only been applied to hyperspectral test platforms, and online detection has not yet been realized.

In this study, the hyperspectral images of navel orange samples were dynamically collected using a self-designed online detection system. The spectra ranged from 975.18 to 2,196.2 nm. The method employed combined independent component analysis (ICA) with genetic algorithm (GA) to select the characteristic spectra. The dimensions of the hyperspectral images were reduced, and then the cankered and spored fruit were separated. This study had the following specific objectives: (1) spectral preprocessing of the collected hyperspectral images; (2) use of an ICA method to obtain independent component images and weight coefficients; (3) combining these data with GA after characteristic selection of wavelengths to achieve dimensionality reduction of hyperspectral data; (4) establishment of a deep neural network method of classified of navel orange surface defects and subsequent automated classification of fruits with a normal versus defective surface. Six characteristic wavelengths were selected by ICA-GA, and the surface defect detection model of navel orange was established based on LSTM. Finally, the online detection of navel orange was achieved.

Materials and methods

Experimental materials

The navel orange samples used in this experiment were collected in November 2019 from Ganzhou City, Jiangxi Province, China. After harvest, the navel oranges were first cleaned in the laboratory. Thirty normal navel orange samples without defects (group 1) and thirty navel oranges with canker defects on their surfaces (group 2) were selected. Then, the hyperspectral image of the samples in categories 1 and 2 were acquired. Meantime, one navel orange inoculated with penicilliosis was stored with some normal navel oranges in the laboratory. After 30 days, 30 infected navel orange were selected as samples with penicilliosis on their surfaces (group 3), and the hyperspectral image data of them were also acquired. Images of samples from each category are shown in **Figures 1A–C**, respectively.

In order to distinguish navel oranges with surface defects online, it is necessary to identify the above defects on surfaces of navel orange samples. In this study, navel orange surfaces were mainly divided into four categories: normal navel orange surface without defects, cankered surface, penicillium spore surface, and hypha surface. **Figure 1A** shows a navel orange without defects on its surface, and the category is defined as Surface. Since normal navel oranges have a large surface range, only rectangular areas A and B were selected. **Figure 1B** shows the surface of a navel orange with cankers, as indicated by the arrow in area C. This type of sample is referred to as Canker. **Figure 1C** is the image of a penicilliosis navel orange sample. Areas D and E were, respectively, the surface of penicillium spores and penicillium hypha, which are referred to as Spore and Hypha, respectively.

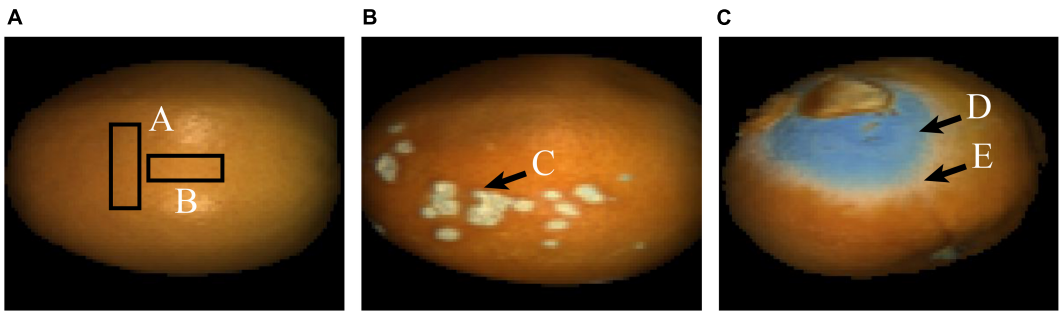

FIGURE 1
False-color images of the typical navel orange. **(A)** Navel orange sample with an intact surface; **(B)** navel orange sample with canker; **(C)** navel orange sample with penicilliosis.

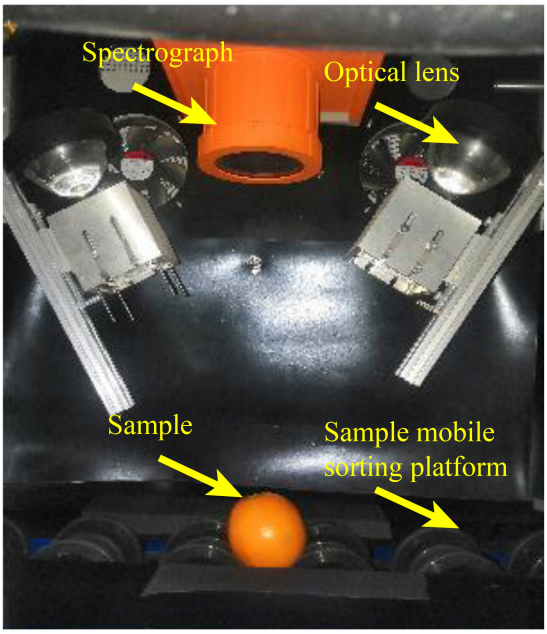

FIGURE 2
Hyperspectral imaging sorting system.

Hyperspectral imaging sorting system

The hyperspectral image system mainly includes a hyperspectral camera (SWIR-CL-400-N25E, SPECIM, Finland), two 150-Watt halogen lamps, two focusing lenses, and a mobile sorting platform setup, as show in Figure 2. Before collecting hyperspectral images, the lamp was turned on for about 15 min, and the white and black calibration images of the hyperspectral camera were captured. The white calibration image was acquired from a 99.9% reflectance white board (Spectralon SRT-99-100, Labsphere Inc., North Sutton, NH, USA) 30 cm below the camera. The black calibration image was acquired when the lens was completely shielded.

The hyperspectral images of samples were corrected using Equation (1):

$$I = \frac{I_{data} - I_{black}}{I_{white} - I_{black}} \quad (1)$$

Here, I_{data} represents the acquired hyperspectral image, I_{black} represents the black calibration image, I_{white} represents the white calibration image, and I represents the corrected image. The exposure time and the frame rate of the hyperspectral camera were 1.8 ms and 120 f/s, respectively.

Spectral preprocessing

The average spectrum of rectangular areas A (in Figure 1) corrected by the black and white calibration images is shown in Figure 3. It can be seen that there is considerable noise at both ends of the spectrum, at ranges of 946.43–975.18 nm and 2,196.2–2,256.82 nm, respectively. Therefore, in the subsequent processing, these two parts of spectra were eliminated, and the spectral range within 975.18–2,196.2 nm between the two black rectangular boxes in Figure 3 was used. The red asterisk in Figure 3 represents the three wave peaks of the surface spectral curve of navel oranges, which are respectively, 1,078.31, 1,266.07, and 1,655.72 nm. The hyperspectral images corresponding to these three bands were selected to produce false color images of navel oranges, like the one shown in Figure 1.

As navel oranges are spherical fruits, the reflected light on the upper surface of the navel oranges collected by the hyperspectral camera is the strongest. In contrast, the reflected light at the edges of the navel oranges is very weak. In order to improve the reflected light intensity on the surface of the spherical fruits and increase the light intensity at the edges, the hyperspectral images of each spherical fruit were corrected (24). This is achieved through the following correction process: (1) the binary-value image of the sample is built using a 1,078.31 nm wavelength; (2) the center of gravity of the binarization region is found, and the image is then segmented into 16 equal parts; (3)

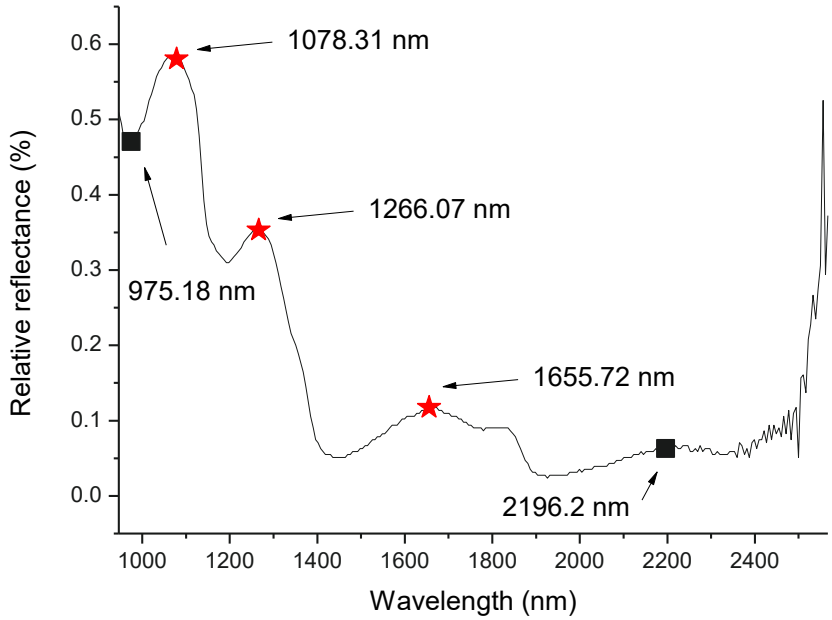

FIGURE 3
Reflection spectrum of a normal navel orange surface.

TABLE 1 Spectra number of each category.

Category	Spectra number	Selected spectra number	Spectra number of training dataset	Spectra number of validation dataset	Spectra number of test dataset
Spore	1,954	1,300	1,065	123	112
Hypha	1,374	1,300	1,044	135	121
Canker	3,302	1,300	1,016	161	123
Surface	3,775	1,300	1,035	121	144
Total	10,405	5,200	4,160	540	500

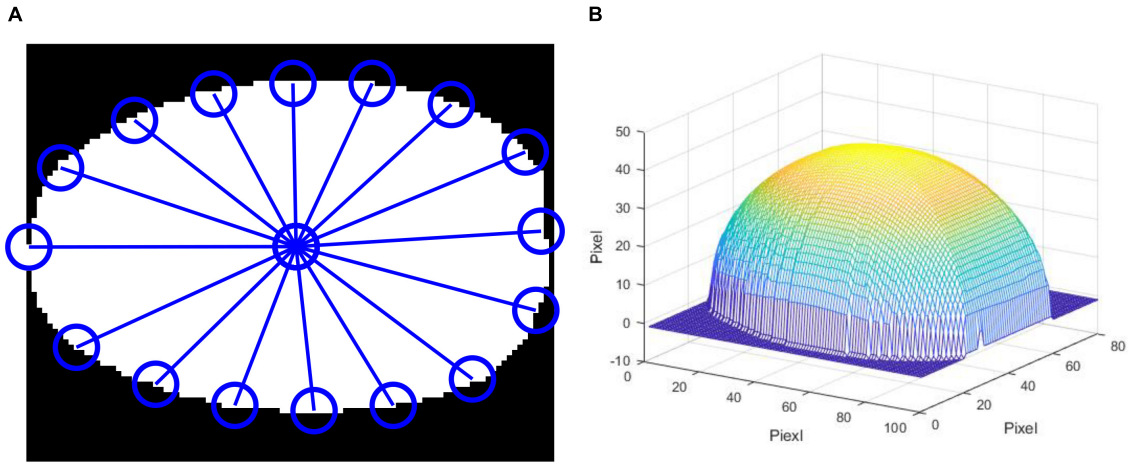

FIGURE 4
Correction of the spherical fruit. **(A)** segmentation of the mask image, **(B)** 3D reconstruction of spherical fruit.

FIGURE 5
False-color images after spherical correction. **(A)** Navel orange sample with an intact surface; **(B)** navel orange sample with cankers; **(C)** navel orange sample with penicilliosis.

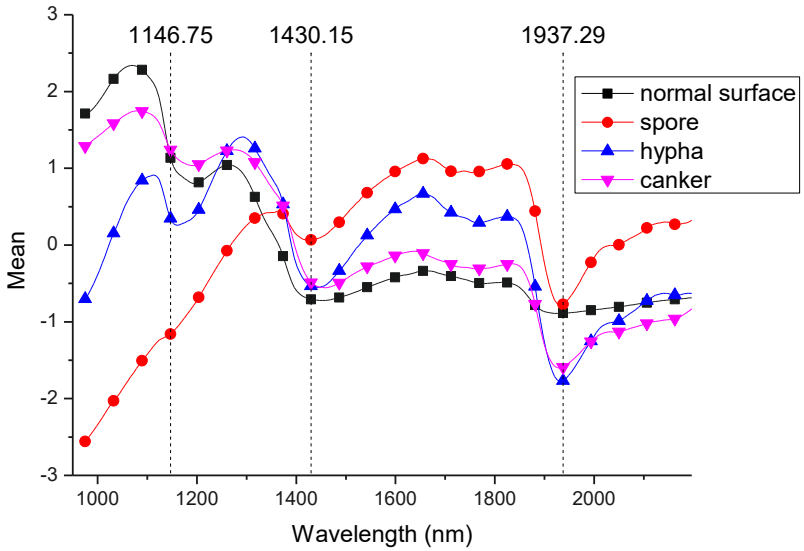

FIGURE 6
Spectral curves of the four categories of surface after spherical correction and standard normal variable (SNV) transformation.

the height of the sample based on the distance from the center of gravity to points in each of the 16 equal parts is calculated; (4) the height of each pixel in the segmented binary image according to four quadrants is calculated, and the reflected light intensity is then corrected. Then, standard normal variate (SNV) transformation is used to eliminate baseline drift.

Establishment of deep neural network model

Deep neural networks are widely used in deep learning and image recognition (25–27). In this study, a long short-term memory (LSTM) deep neural network was applied to 217 spectra in the range of 975.18–1,146.75 nm to establish a classification model. Before establishing a LSTM deep neural network, training and validation datasets for training model should be provided. From Figure 3, it can be seen the reflection is the strongest at a wavelength of 1,078.31 nm. Based on the 1,078.31 nm hyperspectral images, the tool "Image Labeler" in MATLAB (MathWorks Ltd., Natick, MA, USA) was used to select the most representative pixels on the surface of navel oranges from the prediction dataset. For this dataset, 15 penicilliosis navel oranges, six rotten navel oranges, 30 cankered navel oranges, and 16 normal navel oranges were selected. After sample selection, the image "label" and file "gTruth" were generated for each navel orange. The image "label" contains the features selected from each navel orange. The file "gTruth" contains the file storage location of the corresponding file and the storage location and classification name of the corresponding image "label."

Thus, 10,405 data points were obtained for training. As shown in Table 1, 1,300 data points for each category were randomly selected as the modeling data, thus obtaining a total of

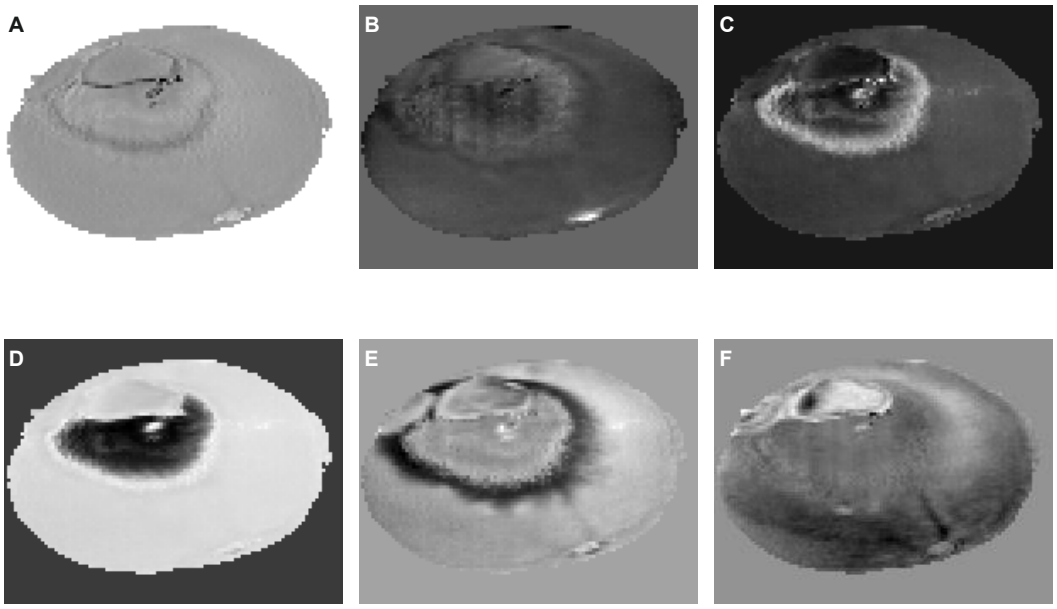

FIGURE 7
Six independent component images by independent component analysis. **(A)** ICA01, **(B)** ICA02, **(C)** ICA03, **(D)** ICA04, **(E)** ICA05, **(F)** ICA06.

5,200 modeling data points. These data were randomly divided into a training dataset, validation dataset, and test dataset according to the approximate ratio of 0.8:0.1:0.1.

The LSTM model is mainly composed of five layers: (1) sequenceInputLayer, (2) bilstmLayer, (3) fullyConnectedLayer, (4) softmaxLayer, and (5) classificationLayer. The second layer has 200 hidden layer nodes, and the fifth layer has four output categories. The numbers of hidden layer nodes are selected by comparing the results using 50, 100, 150, 200, and 250 hidden layer nodes. The LSTM cell with a Forget Gate can be mathematically expressed as follows:

$$f_t = \sigma\left(W_{fh}h_{t-1} + W_{fx}x_t + b_f\right),$$

$$i_t = \sigma\left(W_{ih}h_{t-1} + W_{ix}x_t + b_i\right),$$

$$\tilde{c}_t = \tanh\left(W_{\tilde{c}h}h_{t-1} + W_{\tilde{c}x}x_t + b_{\tilde{c}}\right),$$

$$c_t = f_t \cdot c_{t-1} + i_t \cdot \tilde{c}_t,$$

$$o_t = \sigma\left(W_{oh}h_{t-1} + W_{ox}x_t + b_o\right),$$

$$h_t = o_t \cdot \tanh\left(c_t\right) \quad (2)$$

Where $_{f_t}$ is the forget gate, and the value of $_{f_t}$ can decide what information will be thrown away from the cell state. Where $_{c_t}$ denotes the cell state of LSTM. $_{W_i}$, $_{W_{\tilde{c}}}$, and $_{W_o}$ are the weights.

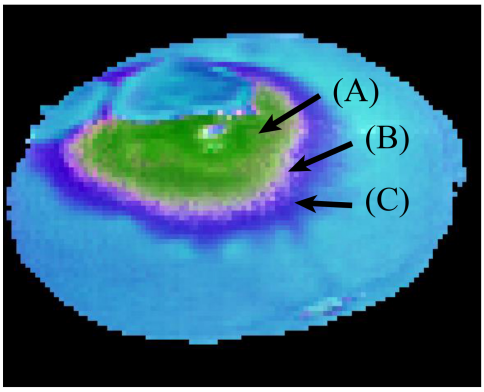

FIGURE 8
Pseudo-color image of a penicilliosis navel orange sample.

Selection of characteristic wavelengths

The data collected by the hyperspectral imaging system are usually very large. Therefore, a method of model establishment that uses a small number of characteristic wavelengths cannot only reduce the time spent in modeling, but also effectively avoid the problem of information similarity between adjacent wavelengths while reducing the over-fitting of the model. Therefore, using characteristic wavelengths to establish prediction models can reduce data calculation and meet the efficiency requirements of online detection.

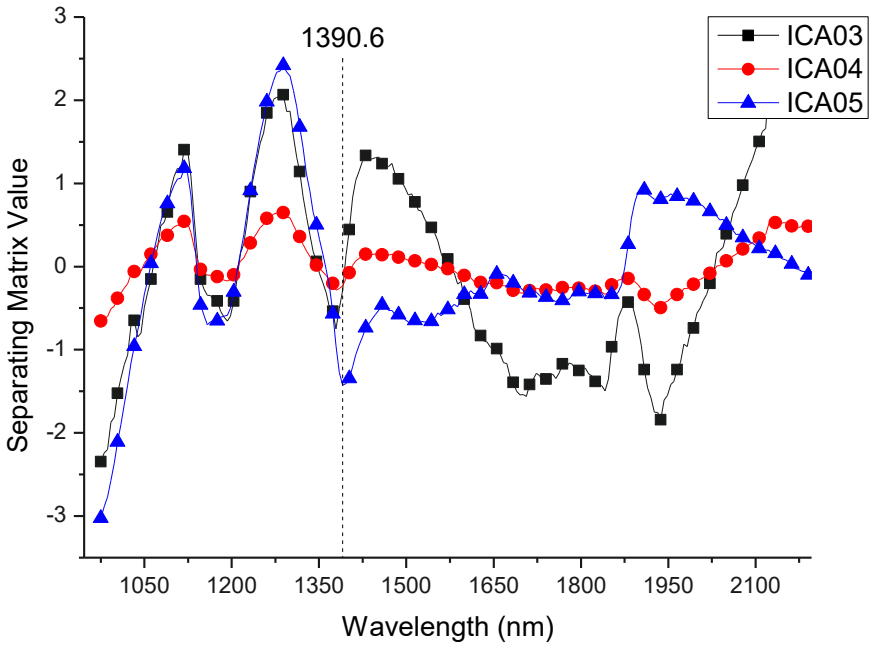

FIGURE 9
Separating matrix of ICA03, ICA04, ICA05.

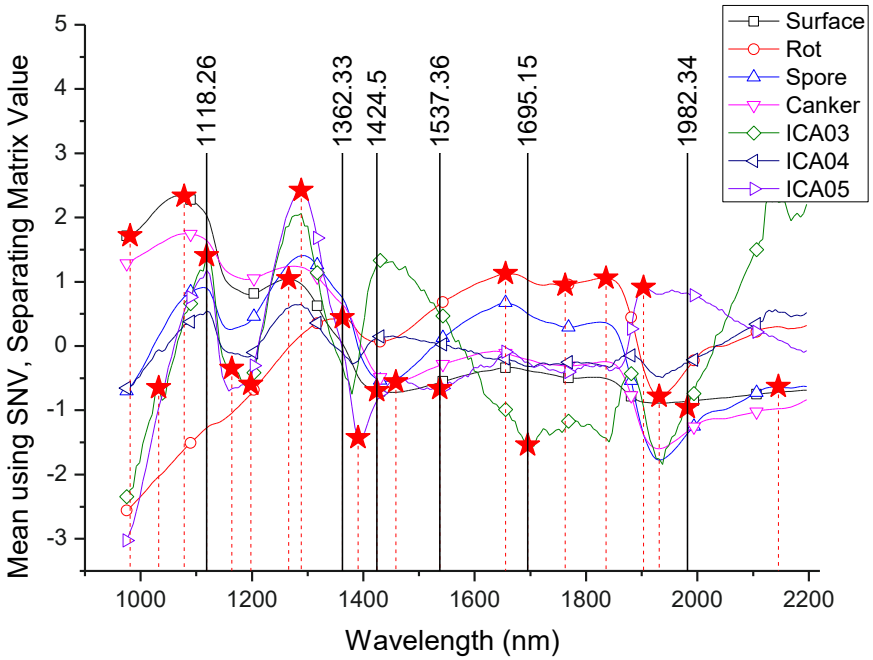

FIGURE 10
Selection of characteristic wavelengths.

The extraction methods of characteristic wavelengths include principal component analysis (PCA) and independent principal component analysis (ICA). ICA has a superior applicability to solve the problem of blind source separation in spectral analysis (28). Accordingly, this study adopted the ICA method to extract characteristic spectra. The main steps are as follows. First, the binarization extraction of the hyperspectral image is conducted to obtain a mask, which is used to

TABLE 2 List of 21 characteristic wavelengths.

Number of wavelengths	Characteristic wavelengths (nm)
21	980.930, 1,032.55, 1,078.31, *1,118.26*, 1,163.83, 1,197.95, 1,266.07, 1,288.74, *1,362.33*, 1,390.60, *1,424.50*, 1,458.38, *1,537.36*, 1,655.72, *1,695.15*, 1,762.73, 1,835.94, 1,903.51, 1,931.66, *1,982.34*, 2,145.61

Italic values are the result of wavelength selection.

separate the background and the fruit area. According to the position of fruit pixels in the mask, the hyperspectral image is subjected to two-dimensional decomposition, thus obtaining a two-dimensional array. The array included the spectra of the fruit surface, but not the background part in the mask. Then, the first six independent components and the corresponding weight coefficients were obtained by ICA analysis of spectral data. Finally, six independent components were reconstructed according to the positions of the mask pixel points, and the values of independent components. Then the characteristic wavelengths can be selected by the ICA analysis based on the corresponding weight coefficients.

Genetic algorithm

For online detection, the number of characteristic wavelengths should be reduced as much as possible. Therefore, on the basis of the selected wavelengths using ICA analysis, a genetic algorithm (GA) was applied to select characteristic wavelengths once more (29, 30). A genetic algorithm is a kind of efficient global search optimization algorithm that can find the optimal solution within a large solution space, and its global search ability can greatly improve search efficiency while avoiding local minimal solutions. In this paper, the main genetic algorithm program was written using the software MATLAB. The characteristic wavelengths were selected by GA based on the accuracy of the test dataset as the fitness function. The following main parameters were used for the genetic algorithm: six characteristic wavelengths were selected without repetition each time. That is, the number of individuals was six, the population contained six individuals, the maximum genetic algebra was 30, and the generation gap was 0.9.

Results and discussion

Spherical fruit correction

The segmented and reconstructed navel orange 3D image is shown in Figure 4.

For the corrected hyperspectral images, the 1,078.31, 1,266.07, and 1,655.72 nm wavelength images were extracted and fused into false-color images, as shown in Figure 5. Compared with Figure 1, the light intensity of the edge was significantly improved.

After spherical correction, the hyperspectral images of navel oranges were decomposed into two dimensions, and the spectra were preprocessed using standard normal variate (SNV) transformation to eliminate baseline drift. Corrected characteristic spectra of normal Surface, Canker, Spore, and Hypha samples are shown in Figure 6. In the wavelength range of 975.18–1,146.75 nm, the spectral value of Surface is the highest, while the spectral value of Spore is the lowest. In the wavelength range of 1,146.75–1,430.15 nm, the spectral curves of Canker, Spore, and Hypha show some differences. At the wavelength of 1,430.15 nm and 1,937.29 nm, the spectral values of Surface and Hypha were the lowest. The four types of spectra all had a double-peak structure, and at 1,430.15 nm, there was a significant trough. At 1,937.29–2,196.26 nm, the spectral curves of Canker, Spore, and Hypha samples all increased, while the Surface spectral curve was relatively stable.

Model using full bands

The LSTM01 model was obtained by using the whole spectra, which included 217 bands. After training, the accuracy of the training, validation, and test dataset were 91.80, 90.56, and 92.81%, respectively. The modeling time was about 3,265.691 s, and the average test time for each orange was about 46.21 s.

Characteristic wavelengths using independent component analysis

Six independent component images were obtained, as shown in Figure 7. ICA01–ICA06 represent the first through sixth independent component images, respectively. Figure 7 shows the ICA result of a navel orange sample with penicilliosis. It can be seen that ICA03, ICA04, and ICA05 are sensitive to penicilliosis navel orange images. ICA03 and ICA05 are sensitive to penicillium hypha images, and ICA04 is sensitive to penicillium spore category images.

Figure 8 is a pseudo-color image of a penicilliosis navel orange sample synthesized by ICA03, ICA04, and ICA05. The figure shows that the spore region (A) and hypha region (C) are relatively obvious, and the region (B) between regions (A) and (C) is the transitional region between spores and hyphae. On this basis, the characteristic wavelength can be selected through the weight coefficients of the wavelength variates of the three independent components.

Figure 9 shows the separating matrix values of the wavelengths for independent components ICA03, ICA04, and

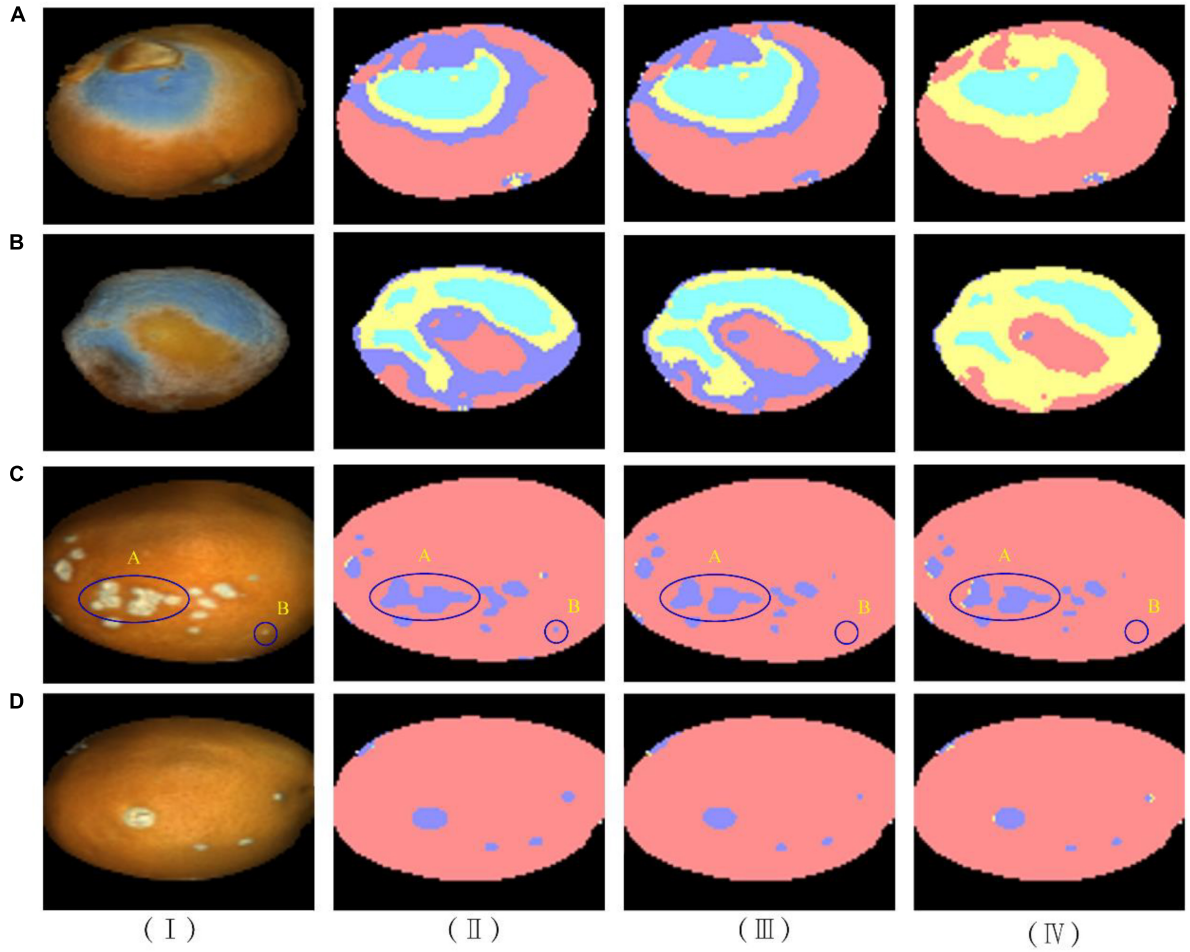

FIGURE 11
Result of the three LSTM models for four typical samples. (I) Sample hyperspectral images and corresponding images for models (II) LSTM01, (III) LSTM02, (IV) LSTM03.

ICA05. It can be seen that ICA03 and ICA05 have similar curve trends in the range of 975.18–1,390.6 nm. The curves both contain two wave peaks. In the range of 1,390.6–2,196.26 nm, the three independent component curves showed obvious differences. According to the curve trend of the independent component, the characteristic wavelengths were selected based on the peaks and troughs of the curves. In the selection process, in order to contain as much information about the classified features as possible, the selection of feature wavelengths also included the peaks and troughs of the spectral curves of the four categories in Figure 6. Thus, a total of 21 characteristic wavelengths were selected, which are marked with asterisks in Figure 10 and Table 2.

The LSTM02 model was obtained by training the LSTM model with 21 characteristic wavelengths. The accuracies of the training dataset, validation dataset, and test dataset were 94.87, 94.07, and 95.01%, respectively. The modeling time was about 328.4015 s, and the average test time for each orange was about 3.71 s. Compared with the LSTM01 model trained with full spectra, it can be seen that the accuracy has been improved, the modeling time has been reduced by about 10 times, and the number of wavelengths used has been reduced from 217 to 21.

Characteristic wavelengths using genetic algorithm

Based on the 21 characteristic wavelengths selected by ICA, GA was used for further dimension reduction, and the six characteristic wavelengths are 1,118.26, 1,362.33, 1,424.50, 1,537.36, 1,695.15, and 1,982.34 nm. In Table 2, the values specified in italic font are the six characteristic wavelengths. Then, the LSTM03 model was established with six characteristic wavelengths. The accuracies of the modeling set, prediction set, and verification set were 94.03, 93.148, and 93.41%. The modeling time was about 105.223 s, and the average test time

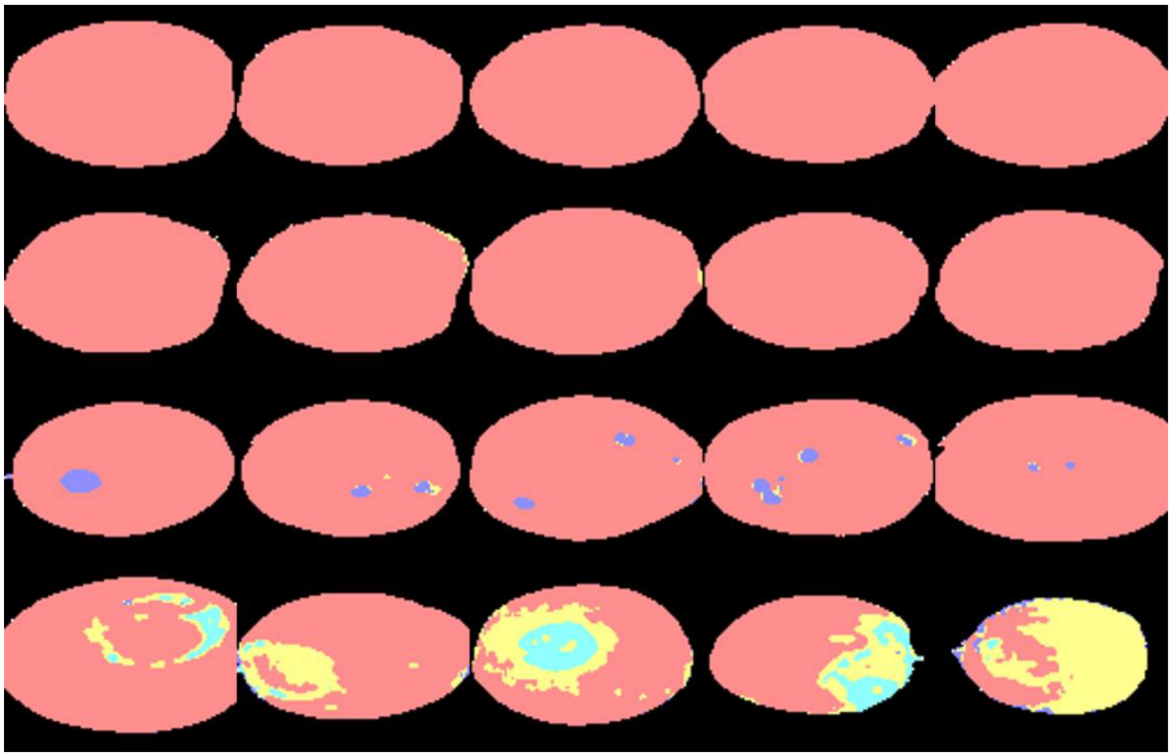

FIGURE 12
Discrimination results of 20 navel orange samples.

for each orange was about 1.26 s. It can be seen that through the selection of wavelengths by GA, the number of wavelengths is reduced from 21 to 6, and the time required for modeling is also reduced by about three-fold compared with the LSTM02 model.

Prediction results

The prediction results show that the prediction accuracy of LSTM01, LSTM02, and LSTM03 models were 92.81, 95.01, and 93.41%, respectively. Although the prediction accuracy of LSTM03 model was slightly lower than that of LSTM02, the prediction time of LSTM03 model for each navel orange was the shortest, only 1.26 s, the prediction time of LSTM02 was 3.7 s, and the prediction time of LSTM01 is the longest, 46.21 s. Thus, in order to ensure the accuracy and efficiency at the same time, the LSTM03 model was better than LSTM02, which is conducive to the online monitoring of fruits by accurately predicting the location of penicillium spore defects.

Figure 11 shows the classification results of four navel oranges in the application of the three LSTM models. In the column (I), (A) and (B) are pseudo-color images of penicilliosis navel oranges, while (C) and (D) are pseudo-color images of navel oranges with canker. The proportions and positions of penicillium disease and canker on the navel orange surface differ. In the column (II), the prediction results of the LSTM01 model are shown. It can be seen that part of the hypha area was misjudged as canker in (A) and (B), but the location of penicillium disease was fairly accurate. The predictions for (C) and (D) were relatively accurate. A smaller canker part was detected in circular region B. However, two canker regions were connected in elliptic region A. In the column (III), the prediction results of the LSTM02 model are shown; (A) and (B) show that the prediction results of penicilliosis were good, but some hypha area were still misjudged as canker. The canker locations in (C) and (D) also had high recognition rates. Compared with the predicted results of the LSTM01 model, two canker parts in the elliptic region A were identified separately, while the smaller canker was not successfully identified and was instead misjudged as normal surface, as shown in circular region B. Among the results of LSTM03 in the column (IV), the prediction results showed that hypha areas in (A) and (B) are accurately identified. The discriminant results of canker in (C) and (D) are similar to that of the LSTM02 model, and the overall area of the discriminant result is slightly smaller than that of the LSTM02 model.

Figure 12 shows the classification results for 20 navel oranges using the LSTM03 model. The first and second rows are the discriminant results of hyperspectral data from navel orange samples collected on the first and fifth days after

picking, respectively. It can be seen that the hyperspectral image data collected on the fifth day included misjudged hyphae, especially the edge part of navel oranges. The third row is the discrimination result of hyperspectral image data with canker, which shows that this model can accurately identify the canker location and size on navel orange surfaces. The fourth row shows the discrimination results of hyperspectral image data collected after 30 days in the laboratory. This model can accurately identify penicilliosis on navel oranges.

Conclusion

Based on ICA and wavelength optimization by GA, a total of six characteristic wavelengths were selected to establish a deep learning neural network model. The model was used to classify and detect surface defects of navel oranges. The categories included penicillium spore, penicillium hypha, canker, and normal navel orange surfaces. The characteristic wavelengths were, respectively, 1,118.26, 1,362.33, 1,424.50, 1,537.36, 1,695.15, and 1,982.34 nm. Through the selection of characteristic wavelengths, the test time of the LSTM03 model for each navel orange sample was reduced from 46.21 s (with the full spectrum model) to 1.26 s. It was conductive to the hyperspectral online detection of fruit, and its prediction accuracy was also improved. It can be seen that this method can be used to detect the surface defects of navel oranges online. However, the hyperspectral images were collected in this experiment through translation movement of navel orange samples. Thus, only images from the upper surface of the navel orange were collected, while lower surface images were not. Therefore, a major research focus includes capturing and analyzing images of the entire surface of navel oranges in subsequent online detection work.

Data availability statement

The raw data supporting the conclusions of this article will be made available by the authors, without undue reservation.

Author contributions

JL: conceptualization, funding acquisition, writing – original draft review, and editing. ML: writing – original draft and visualization. LX: supervision and writing – review and editing. JC: conceptualization and funding acquisition. LH: conceptualization, investigation, software, and writing – review and editing. All authors contributed to the article and approved the submitted version.

Funding

This work was supported by Key Science and Technology Research Project in Jiangxi Province Department of Education (GJJ180169) and National Natural Science Foundation of China (31871526). This work was also partially funded by the Collaborative Innovation Center of Postharvest Key Technology and Quality Safety of Fruits and Vegetables in Jiangxi Province (JXGS-05) and supported by Jiangxi Province Science and Technology Innovation Team Building Plans (20171BCB24006).

Conflict of interest

The authors declare that the research was conducted in the absence of any commercial or financial relationships that could be construed as a potential conflict of interest.

Publisher's note

References

1. Zhang L, Ling W, Yan Z, Liang Y, Guo C, Ouyang Z, et al. Effects of storage conditions and heat treatment on the hesperidin concentration in Newhall navel orange (*Citrus sinensis* Osbeck Cv. Newhall) juice. *J Food Compos Anal.* (2020) 85:103338. doi: 10.1016/j.jfca.2019.103338

2. Gao Y, Liu Y, Kan C, Chen M, Chen J. Changes of peel color and fruit quality in navel orange fruits under different storage methods. *Sci Hortic.* (2019) 256:108522. doi: 10.1016/j.scienta.2019.05.049

3. Gao Y, Kan C, Wan C, Chen C, Chen M, Chen J. Quality and biochemical changes of navel orange fruits during storage as affected by cinnamaldehyde -chitosan coating. *Sci Hortic.* (2018) 239:80–6. doi: 10.1016/j.scienta.2018.05.012

4. Song J, Li G, Yang X, Liu X, Xie L. Rapid analysis of soluble solid content in navel orange based on visible-near infrared spectroscopy combined with a swarm intelligence optimization method. *Spectrochim Acta A Mol Biomol Spectrosc.* (2020) 228:117815. doi: 10.1016/j.saa.2019.117815

5. Borba KR, Spricigo PC, Aykas DP, Mitsuyuki MC, Colnago LA, Ferreira MD. Non-invasive quantification of vitamin C, citric acid, and sugar in 'valência' oranges using infrared spectroscopies. *J Food Sci Technol.* (2020) 58:731–8. doi: 10.1007/s13197-020-04589-x

6. Singh H, Sridhar A, Saini SS. Ultra-low-cost self-referencing multispectral detector for non-destructive measurement of fruit quality. *Food Anal Methods.* (2020) 13:1879–93. doi: 10.1007/s12161-020-01810-7

7. Feng L, Wu B, Zhu S, He Y, Zhang C. Application of visible/infrared spectroscopy and hyperspectral imaging with machine learning techniques for identifying food varieties and geographical origins. *Front Nutr.* (2021) 8:680357. doi: 10.3389/fnut.2021.680357

8. Li J, Zhang Y, Liu M, Chen J, Xue L. Rapid detection and visualization of mechanical bruises on "Nanfeng" mandarin using the hyperspectral imaging combined with ICA_LSQ method. *Food Anal Methods.* (2019) 12:1936–9751. doi: 10.1007/s12161-019-01546-z

9. Zhang C, Wu W, Zhou L, Cheng H, Ye X, He Y. Developing deep learning based regression approaches for determination of chemical compositions in dry black Goji berries (*Lycium ruthenicum* Murr.) using near-infrared hyperspectral imaging. *Food Chem.* (2020) 319:126536. doi: 10.1016/j.foodchem.2020.126536

10. Badaró AT, Garcia-Martin JF, López-Barrera MDC, Barbin DF, Alvarez-Mateos P. Determination of pectin content in orange peels by near infrared hyperspectral imaging. *Food Chem.* (2020) 323:126861. doi: 10.1016/j.foodchem.2020.126861

11. Al-Sarayreh M, Reis MM, Yan WQ, Klette R. Potential of deep learning and snapshot hyperspectral imaging for classification of species in meat. *Food Control.* (2020) 117:107332. doi: 10.1016/j.foodcont.2020.107332

12. Cen H, Lu R, Zhu Q, Mendoza F. Nondestructive detection of chilling injury in cucumber fruit using hyperspectral imaging with feature selection and supervised classification. *Postharvest Biol Technol.* (2016) 111:352–61. doi: 10.1016/j.postharvbio.2015.09.027

13. Mayorga-Martínez AA, Olvera-Trejo D, Elías-Zúñiga A, Parra-Saldívar R, Chuck-Hernández C. Non-destructive assessment of guava (*Psidium guajava* L.) maturity and firmness based on mechanical vibration response. *Food Bioprocess Technol.* (2016) 9:1471–80. doi: 10.1007/s11947-016-1736-8

14. Gao Z, Shao Y, Xuan G, Wang Y, Liu Y, Han X. Real-time hyperspectral imaging for the in-field estimation of strawberry ripeness with deep learning. *Artif Intell Agric.* (2020) 4:31–8. doi: 10.1016/j.aiia.2020.04.003

15. Xuan G, Gao C, Shao Y, Wang X, Wang Y, Wang K. Maturity determination at harvest and spatial assessment of moisture content in Okra using vis-NIR hyperspectral imaging. *Postharvest Biol Technol.* (2021) 180:111597. doi: 10.1016/j.postharvbio.2021.111597

16. Zhao J, Ouyang Q, Chen Q, Wang J. Detection of bruise on pear by hyperspectral imaging sensor with different classification algorithms. *Sensor Lett.* (2010) 8:570–6.

17. Zareef M, Chen Q, Hassan MM, Arslan M, Hashim MM, Ahmad W, et al. An overview on the applications of typical non-linear algorithms coupled with NIR spectroscopy in food analysis. *Food Eng Rev.* (2020) 12:173–90. doi: 10.1007/s12393-020-09210-7

18. Xuan G, Gao C, Shao Y. Spectral and image analysis of hyperspectral data for internal and external quality assessment of peach fruit. *Spectrochim Acta A Mol Biomol Spectrosc.* (2022) 272:121016. doi: 10.1016/j.saa.2022.121016

19. Zhang D, Xu L, Liang D, Xu C, Jin X, Weng S. fast prediction of sugar content in Dangshan pear (*Pyrus* Spp.) using hyperspectral imagery data. *Food Anal Methods.* (2018) 11:2336–45. doi: 10.1007/s12161-018-1212-3

20. Kang X, Xiang X, Li S, Benediktsson JA. Pca-based edge-preserving features for hyperspectral image classification. *IEEE Trans Geosci Remote Sens.* (2017) 55:7140–51. doi: 10.1109/TGRS.2017.2743102

21. Liu Q, Zhou D, Tu S, Xiao H, Zhang B, Sun Y, et al. Quantitative visualization of fungal contamination in peach fruit using hyperspectral imaging. *Food Anal Methods.* (2020) 13:1262–70. doi: 10.1007/s12161-020-01747-x

22. Shi J, Wang Y, Li Z, Huang X, Shen T, Zou X. Characterization of invisible symptoms caused by early phosphorus deficiency in cucumber plants using near-infrared hyperspectral imaging technology. *Spectrochim Acta A Mol Biomol Spectrosc.* (2022) 267:120540. doi: 10.1016/j.saa.2021.120540

23. Li S, Song W, Fang L, Chen Y, Ghamisi P, Benediktsson JA. Deep learning for hyperspectral image classification: an overview. *IEEE Trans Geosci Remote Sens.* (2019) 57:6690–709. doi: 10.1109/TGRS.2019.2907932

24. Gomez-Sanchis J, Molto E, Camps-Valls G, Gomez-Chova L, Aleixos N, Blasco J. Automatic correction of the effects of the light source on spherical objects. An application to the analysis of hyperspectral images of citrus fruits. *J Food Eng.* (2008) 85:191–200. doi: 10.1016/j.jfoodeng.2007.06.036

25. Agarwal M, Al-Shuwaili T, Nugaliyadde A, Wang P, Wong KW, Ren Y. Identification and diagnosis of whole body and fragments of *Trogoderma granarium* and *Trogoderma* variabile using visible near infrared hyperspectral imaging technique coupled with deep learning. *Comput Electron Agric.* (2020) 173:105438. doi: 10.1016/j.compag.2020.105438

26. Xin Z, Jun S, Yan T, Quansheng C, Xiaohong W, Yingying HA. Deep learning based regression method on hyperspectral data for rapid prediction of cadmium residue in lettuce leaves. *Chemom Intell Lab Syst.* (2020) 200:103996. doi: 10.1016/j.chemolab.2020.103996

27. Zhou X, Sun J, Tian Y, Lu B, Hang Y, Chen Q. Hyperspectral technique combined with deep learning algorithm for detection of compound heavy metals in lettuce. *Food Chem.* (2020) 321:126503. doi: 10.1016/j.foodchem.2020.126503

28. Mishra P, Cordella CBY, Rutledge DN, Barreiro P, Roger JM, Diezma B. Application of independent components analysis with the jade algorithm and NIR hyperspectral imaging for revealing food adulteration. *J Food Eng.* (2016) 168:7–15. doi: 10.1016/j.jfoodeng.2015.07.008

29. Zehtabian A, Ghassemian H. Combining genetic algorithm with Pdes for improving the performance of statistical region merging based object extraction. *J Indian Soc Remote Sens.* (2016) 44:395–407. doi: 10.1007/s12524-015-0515-8

30. Feng Y-Z, Sun D-W. Near-Infrared hyperspectral imaging in tandem with partial least squares regression and genetic algorithm for non-destructive determination and visualization of *Pseudomonas* loads in chicken fillets. *Talanta.* (2013) 109:74–83. doi: 10.1016/j.talanta.2013.01.057

frontiers | Frontiers in Nutrition

TYPE Original Research
PUBLISHED 24 October 2022
DOI 10.3389/fnut.2022.1026730

OPEN ACCESS

EDITED BY
John-Lewis Zinia Zaukuu,
Kwame Nkrumah University of Science and Technology, Ghana

REVIEWED BY
Vijander Singh,
Netaji Subhas University of Technology, India
Balkis Aouadi,
Hungarian University of Agriculture and Life Sciences, Hungary

*CORRESPONDENCE
Yong Hao
haonm@163.com

SPECIALTY SECTION
This article was submitted to Nutrition and Food Science Technology, a section of the journal Frontiers in Nutrition

RECEIVED 24 August 2022
ACCEPTED 26 September 2022
PUBLISHED 24 October 2022

CITATION
Hao Y, Zhang C, Li X and Lei Z (2022) Establishment of online deep learning model for insect-affected pests in "Yali" pears based on visible-near-infrared spectroscopy. *Front. Nutr.* 9:1026730. doi: 10.3389/fnut.2022.1026730

Establishment of online deep learning model for insect-affected pests in "Yali" pears based on visible-near-infrared spectroscopy

Yong Hao[1,2]*, Chengxiang Zhang[1], Xiyan Li[1] and Zuxiang Lei[3]

[1]School of Mechatronics and Vehicle Engineering, East China Jiaotong University, Nanchang, China, [2]Key Laboratory of Conveyance Equipment of the Ministry of Education, Nanchang, China, [3]School of Civil Engineering and Architecture, East China Jiaotong University, Nanchang, China

Insect-affected pests, as an important indicator in inspection and quarantine, must be inspected in the imports and exports of fruits like "Yali" pears (a kind of duck head-shaped pear). Therefore, the insect-affected pests in Yali pears should be previously detected in an online, real-time, and accurate manner during the commercial sorting process, thus improving the import and export trade competitiveness of Yali pears. This paper intends to establish a model of online and real-time discrimination for recessive insect-affected pests in Yali pears during commercial sorting. The visible-near-infrared (Vis-NIR) spectra of Yali samples were pretreated to reduce noise interference and improve the spectral signal-to-noise ratio (SNR). The Competitive Adaptive Reweighted Sampling (CARS) method was adopted for the selection of feature modeling variables, while Partial Least Squares Discriminant Analysis (PLS-DA), Support Vector Machine (SVM), and Convolutional Block Attention Module-Convolutional Neural Networks (CBAM-CNN) were used to establish online discriminant models. T-distributed Stochastic Neighbor Embedding (T-SNE) and Gradient-weighted Class Activation Mapping (Grad-CAM) were used for the clustering and attention distribution display of spectral features of deep learning models. The results show that the online discriminant model obtained by SGS pretreatment combined with the CBAM-CNN deep learning method exhibits the best performance, with 96.88 and 92.71% accuracy on the calibration set and validation set, respectively. The prediction time of a single pear is 0.032 s, which meets the online sorting requirements.

KEYWORDS

insect-affected pears, Vis-NIR spectroscopy, CBAM attention module, online discrimination model, deep learning model

Introduction

Yali pears (duck head-shaped pears) are rich in nutrients, tasting good, and have a huge consumer market (1). However, because of careless nursing, pear trees are subject to damages caused by insect pests such as pirivorella, grapholita molesta busck, and halyomorpha picus. These insect pests are widely distributed in temperate and subtropical regions of Asia, Europe, America, Africa, and Australia (2). In "the hometown of Yali pears," Hebei province in China, insect-affected pests in Yali pears are so rampant that the damage rate can reach more than 85% due to improper management, which seriously undermines the quality of Yali pears, resulting in shrinking sales (3). The quality classification of Yali pears mainly includes two indicators, internal quality and external quality. The external quality of Yali pears mainly adopts manual and mechanical classification. Manual classification has many shortcomings such as high labor cost, low efficiency, unclear classification standard and lack of objectivity. As the production volume increases, the traditional manual classification can no longer satisfy the production demands (4). In contrast, classification by machines has higher efficiency, and the size, surface quality and weight of Yali pears are usually analyzed with the help of sensors such as image and gravity. The internal quality of Yali pears is usually detected by non-destructive and destructive methods. The destructive methods are only suitable for limited scenarios such as sampling or initial screening. But the non-destructive methods, if combined with sophisticated mechanical structure, can realize full-coverage detection of the samples. However, the key to successful application of non-destructive methods lies in the correct analysis of sensing signals by machine learning method (5). In recent years, the international community has carried out strict regulations on the defects of exported Yali pears. According to Chinese regulations on quarantine techniques of exported Yali pears, Yali pears cannot be sampled for quarantine inspection unless they have been stored in refrigerator for at least 21 days. Each batch of pears is sampled at 2% of the total number of all boxes, and all samples are detected. Lengthy inspection and quarantine process leads to higher export costs and deterioration risks. For this reason, there is an urgent need to figure out a rapid and non-destructive mechanical sorting method for full-coverage inspection of recessive defects in Yali pears, so as to improve the export quality and qualified rate of Yali pears.

Visible-near-infrared (Vis-NIR) spectroscopy is a non-destructive detection method which has been widely used in the internal quality detection of fruits and crops (6–8). Compared with other non-destructive detection methods such as machine vision (9), X-ray (10), and magnetic resonance imaging (MRI) (11), Vis-NIR spectroscopy has higher speed, lower costs and wider application of detection. According to the literature research, there are few studies on Vis-NIR detection of recessive pests in fruits and crops. Khodabakhshian et al. (12) detected Carob moths in pomegranates, and they found that the identification rate of insect pests in the combined sample sets through PLS-DA method could reach as high as 86%. Abbaspour-Gilandeh et al. (13) detected codling moths in red apples by digital image processing and sparse coding method, and the pest identification rates in healthy apples and diseased apples reached 81 and 86%. Moscetti et al. (14) detected Tortrices and Weevil in chestnuts, and the total error of identification was reduced to 8.41% by the Genetic Algorithm - Linear Discriminant Analysis (GA-LDA) method. The above researchers have proved that it is feasible to detect recessive insect pests in fruits by using Vis-NIR spectroscopy. Be that as it may, few researches have been conducted on Vis-NIR online identification of recessive insect pests inside Yali pears.

In this paper, an online rapid non-destructive detection method for internal defects of Yali pears based on Vis-NIR has been proposed, in a bid to tackle the online rapid screening of recessive Yali pear pests in the commercial sorting process. First, different pretreatment methods are used to suppress noise and enhance information on the original spectrum to improve the signal-to-noise ratio of the spectrum, such as Savitzky-Golay Smoothing (SGS), Spectral Standardization (SS), Max-min Normalization (MMN) and Standard Normal Variate Transformation (SNV). Second, Competitive Adaptive Reweighted Sampling (CARS) was used for the optimal selection of feature variables. Last, Partial Least Squares Discriminant Analysis (PLS-DA) and Support Vector Machines (SVM) were used to establish shallow learning model of online discrimination for Yali pears, and Convolutional Block Attention Module-Convolutional Neural Networks (CBAM-CNN) was used to establish deep learning model for online discrimination of Yali pears. This paper intends to figure out a method to establish an accurate and rapid online discrimination model for recessive insect pests inside fruits, in a bid to improve the quality sorting of fresh fruits.

Samples and methods

Spectral acquisition device

The online sorting device for insect-affected Yali pears is shown in **Figure 1**. The device is composed of five parts: spectrometer, optical fiber, microcomputer, light source and conveyor belt. The spectrometer is QE6500 Pro produced by the Ocean optics INC; the detector range is 200-1100 nm; the integration time of the acquisition device is set to 80 ms; the conveyor transports six samples per second; the optical fiber probe is located below the fruit cup, 12 mm from the conveyor belt. The light source consisted of ten 100-Watt halogen tungsten lamps (Osram) positioned above the sample and arranged along the concentrating coil with an oblique angle of 45 degrees. The light sources are arranged as shown in

Figure 2, with five light sources equally spaced on each side around the central spectral acquisition station.

Prior to spectral acquisition, the parameters of the spectrometer must be calibrated. First, the light sources were turned on for 30 min to ensure the thermal stability of light sources and detector. Second, a PTFE ball with a diameter of about 70 mm was used to calibrate each fruit cup, so as to maintain the consistency of measurement background. In the fruit cup, the pear samples were placed in a way that the connection direction between the pear stalk (C) and the pear pedicel (D) was always perpendicular to the running direction of the conveyor belt.

The working process of the Vis-NIR online sorting device for Yali pears is shown as follows. The Yali pear samples are placed according to Figure 2. In other words, the connection direction between the pear stalk (C) and the pear pedicel (D) was always perpendicular to the running direction of the conveyor belt. When the sample reaches the spectral acquisition position, the light source penetrates the inside of the pear and then reaches the optical detector. The whole spectral acquisition process is completed in the light shield, which effectively reduces the disturbances of external stray light to spectral signals.

Preparation of Yali pear samples and discrimination of insect pests

Samples for experiment are Yali pears produced in Hebei province, with a total number of 960. These samples were transported in refrigerated vehicles to laboratory, and then were stored at a constant temperature of 20° for 21 days. Prior to experiment, the stains and moisture on the surface of Yali pear samples were removed. After collecting the samples of the Vis-NIR spectrum, the artificial incision identification method was used to identify the internal pests of the pear. When cutting Yali pears, the first cutting was conducted along the A–B connection direction, and the second cutting was conducted along the C–D connection direction, as shown in Figure 2. Observing carefully whether there were indicators of insect decay inside the pear and insect holes on the surface. Evaluated whether it was insect-affected pears or not and decided by three experts with years of experience in planting and sales of Yali pears. Some of the insect-affected Yali pear samples are shown in Figure 3 (The area indicated by the red circle).

Classification of sample sets

A total of 960 Yali pear samples were divided at a ratio of 4:1 into calibration set and validation set using SPXY algorithm. SPXY algorithm is developed on the basis of KS algorithm, and its principle is to ensure the difference and representativeness of samples by calculating the distance between the spectral feature values of different samples. SPXY can effectively cover the multi-dimensional vector space to avoid the over-fitting or poor prediction effect of the prediction model caused by too small or identical differences between samples, so as to improve the stability and accuracy of the model (15). The information of sample sets is shown in Table 1, the calibration set includes 768 samples (468 healthy pears and 300 insect-affected pears); the validation set includes 192 samples (124 healthy pears and 68 insect-affected pears).

Methods of spectral pretreatment and feature variable selection

As shown in Figure 1, the online detection device is an open system and the Yali pear itself is not an ellipsoid with a regular shape. Therefore, in the process of spectral signal acquisition, it is often disturbed by stray light, noises, baseline drift and so on, thus affecting the final quantitative and qualitative analysis results. For this reason, it is necessary to pretreat original spectra and optimally select feature variables before modeling, so as to eliminate or reduce the interference of invalid information to pear spectra (16). Taking into account the surface morphology of pear samples and the structure of spectral acquisition device, SGS smoothing was used to eliminate the random noises in spectral signals and improve the SNR of samples (17). Spectral Standard (SS) was adopted to reduce the scale difference in spectral signals (18). Max-min Normalization (MMN) was adopted to eliminate the baseline drift and irrelevant noise signals with interference in spectral signals (19). The scattering effect caused by uneven particle distribution and different particle size in the spectral signal was eliminated through the Standard Normal Variate (SNV) transformation (20).

For the feature variable selection method, CARS method is one of the most commonly used methods in the selection of fruit spectral variables, which combines Monte Carlo sampling and PLS model regression coefficients (21). Compared with other variable selection methods like Principle Component Analysis (PCA), Uninformative Variable Elimination (UVE), and Successive Projections Algorithm (SPA), the CARS method is more convenient and the feature variables selected by the CARS are more representative, which can effectively reduce the high collinearity between wavebands caused by the number of spectral wavelength points greater than the number of samples. In this way, the prediction accuracy and speed of model can be improved (22).

Establishment of discrimination model for insect-affected Yali pears

Shallow learning method

Partial Least Squares Discriminant Analysis (PLS-DA) is a multivariate statistical method under supervision, which integrates the basic functions of PCA, canonical correlation

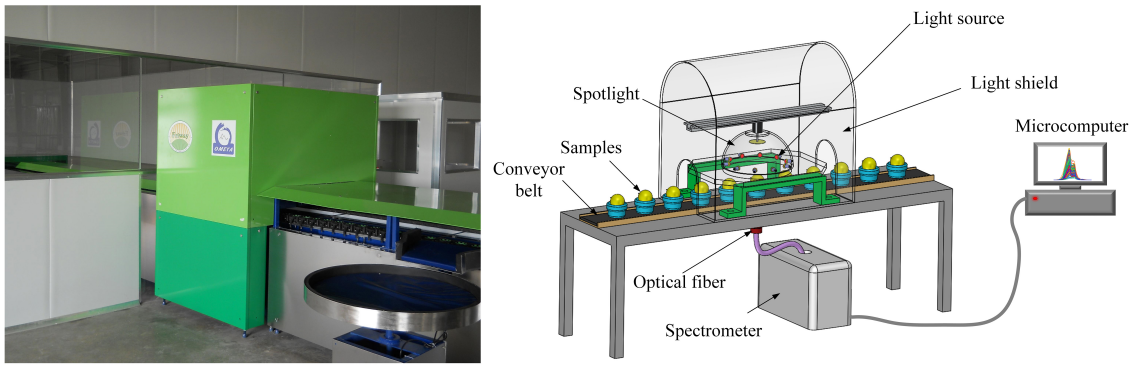

FIGURE 1
Schematic diagram of the Vis-NIR online sorting device for Yali pears.

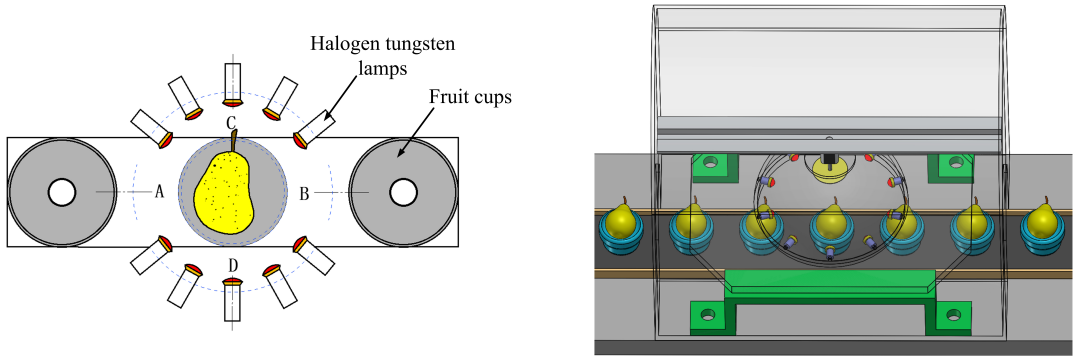

FIGURE 2
Schematic diagram of light source (halogen tungsten lamps) layout.

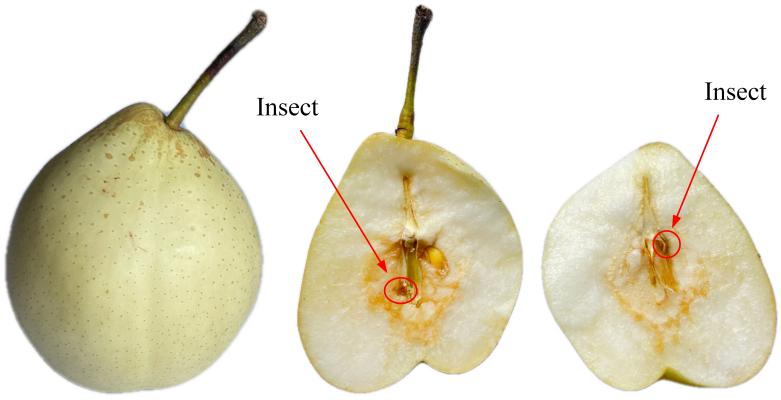

FIGURE 3
Insect-affected Yali pear samples.

analysis and multiple regression analysis, and can compress data and extract feature information (23). The principle of PLS-DA is to separately train the features of samples processed by different methods, so as to generate the calibration set and test its confidence. This method can group the required observation variables in advance, and conduct statistical analysis on the data according to the nature of the grouping, so as to learn the key variables that affect the grouping (24). PLS-DA is usually used for classification and discrimination. When the difference between groups is small and the sample

TABLE 1 Sample set information.

Sample set	Healthy pears	Insect-affected pears	Total number	Proportion/%
Calibration set	468	300	768	80%
Validation set	124	68	192	20%

size of each group varies significantly, this method can effectively distinguish the observed variables between groups, and its linear classification feature is widely used in Vis-NIR qualitative analysis.

Support Vector Machine (SVM) is an algorithm based on small-sample statistics theory, which finds out the optimal classification hyperplane by maximizing the geometric interval between the classification hyperplane and the data (25), and determines the constraint parameters of the model through the geometric interval. SVM method can map complex nonlinear problems to high-dimensional space and transform them into linear problems through kernel functions. The model algorithm can quickly train and learn to find the complex functional relationship between input and output. SVM is widely applied in classification of nonlinear, high-dimension, and small-size data samples. The optimization goal of SVM method is listed as follows.

$$\min \frac{1}{2}\|\omega\|^2 + c\sum_{i=1}^{n}\xi_i, \qquad \xi_i \geq 0 \tag{1}$$

$$s.t = \begin{cases} y_i\left(\omega x_i + b\right) \geq 1 - \xi_i \\ c \geq 0 \end{cases}, \qquad i = 1, 2, 3 \ldots n \tag{2}$$

In Formula (1), n represents the number of calibration samples. In Formula (2), x_i is the support vector of calibration sample; y_i is the category of corresponding sample, whose value range is [−1, 1]. ω is the normal vector of hyperplane; b is offset vector. c is penalty factor. ξ_i is slack variable.

As two representative shallow learning methods, PLS-DA and SVM are both widely employed in Vis-NIR qualitative analysis. Both methods have their own characteristics of spectral data processing, PLS-DA is suitable for processing linear problems while SVM for nonlinear problems, but these two methods can neither select feature variables. When the data amount is large or the difference between spectral data is small, PLS-DA and SVM show poor classification performance and heavily rely on spectral data. Under such circumstances, a combination of spectral pretreatment methods and feature selection methods is necessary to obtain desirable classification effect.

Deep learning method

Convolutional Neural Network (CNN) is one of the widely studied deep learning algorithms with characteristics of local connection, weight sharing and down-sampling (26). The traditional CNN model is mainly composed of convolution layer, pooling layer and full connection layer. The convolutional layer extracts the features of the local sensing domain through the convolution kernel and non-linear transformation, and uses the activation function to filter the extracted features, thus effectively extracting the features of the input image while avoiding the problem of insufficient linear computing ability. Pooling layer, also known as sampling layer, down sampling the feature map according to rules, and reduces the dimension of the feature quantity after convolution in order to lessen the number of parameters and computation inside CNN and inhibit the network over-fitting at the same time. As the output layer, the full connection layer can not only connect the neurons of the upper and lower layers, but also output the weight score of each category through the activation function to obtain the final classification results. The traditional CNN model pays little attention to the extracted key features, so part of the noise information is retained and part of the key features are lost during feature transmission, which has a great influence on the model results (27). In view of the shortcomings of the traditional CNN model, the paper exerts more attention on the key features in the spectrum by using attention mechanism, so as to improve its ability of capturing key feature information and thus improve the recognition rate of the model for insect-affected Yali pears.

The structure of CBAM module is shown in **Figure 4**. Convolutional Block Attention Module-Convolutional Neural Networks (CBAM-CNN) adds the CBAM attention module to the original CNN model which makes the original CNN network have characteristic attention and improves the classification accuracy of the model. The CBAM module is an integrated module combining the Chanel Attention Module and the Spatial Attention Module, which can adaptively focus on the regions with obvious changes of feature points in the spectral matrix (28). Compared with a single attention module, the CBAM module can adaptively focus on "where are the important features" in the space relations and "which features are more important" in the channel relations, so that spectral features after a series of convolution can get more attention in CBAM module, and the corresponding weight information can be obtained in the full connection layer, so as to optimize the classification results.

Research procedures

For the collected spectral data, this paper has realized the identification of insect-affected pears in three steps. The flowchart of the research method is shown in **Figure 5**. The first step, the necessary spectral pretreatment is a key step to reduce spectral noise. This step in this paper is realized by the SGS, SS,

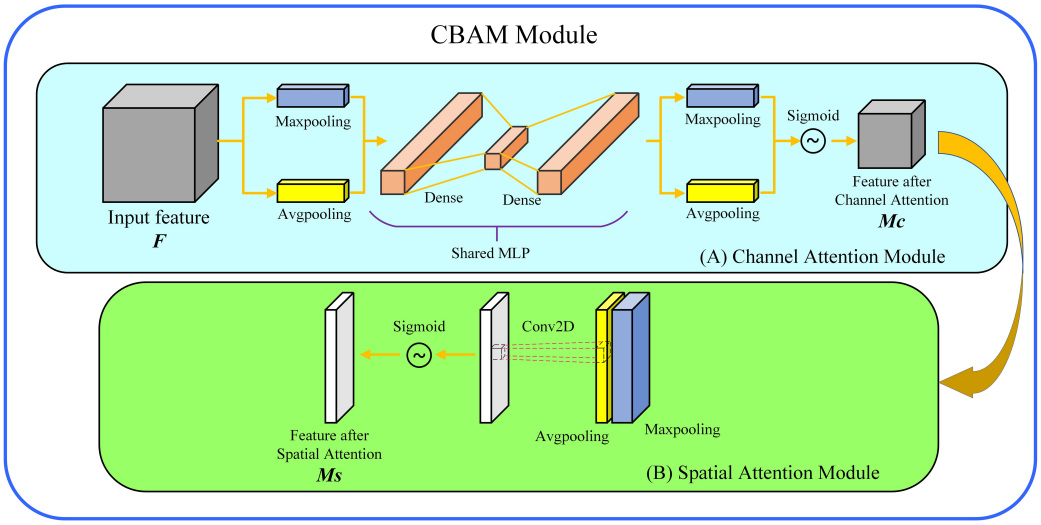

FIGURE 4
Convolutional block attention module (CBAM): **(A)** Channel attention module, **(B)** spatial attention module.

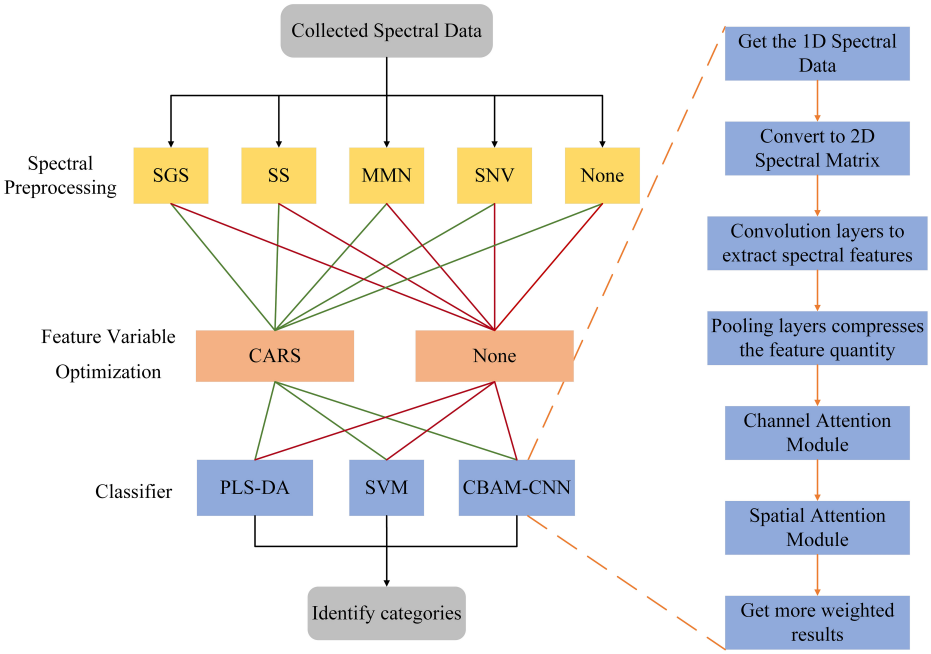

FIGURE 5
Research method flowchart.

MMN, and SNV methods. The second step, the optimization of feature variables is also an important step to improve the recognition rate. It has selected out more representative spectral bands in the entire spectrum. This step in this paper has been achieved by using the CARS method. In the third step, the choice of classifier also affect the recognition results. Three different classifiers are selected in this paper, including PLS-DA, SVM shallow learning models and CBAM-CNN deep learning model. For the CBAM-CNN deep learning model, its structural parameters are relatively complex than those of the shallow learning model. The CBAM-CNN model mainly consists of three parts, spectral data reading and conversion, feature extraction from convolution pooling and CBAM modules, and output model recognition results. Through three steps, the final Yali pear recognition category is obtained, and the optimal Yali pear recognition model is found.

Evaluation indexes of models

In this paper, classification accuracy (Accuracy), classification accuracy of healthy pears (RH) and classification accuracy of insect-affected pears (RB) were used to comprehensively evaluate the prediction accuracy of the model. When the accuracy, RH, and RB values are closer to 100%, the classification performance is better. The evaluation indexes can be calculated according to the following Formulas (3–4).

$$Accuracy = \left(1 - \frac{H_e + B_e}{H + B}\right) \times 100\% \quad (3)$$

$$RH = \left(1 - \frac{H_e}{H}\right) \times 100\% \quad (4)$$

$$RB = \left(1 - \frac{B_e}{B}\right) \times 100\% \quad (5)$$

Where, H is the total number of healthy pears; B is the total number of insect-affected pears; H_e is the number of healthy pears misclassified as insect-affected pears; B_e is the number of insect-affected pears misclassified as healthy pears.

Results and analysis

Visible-near-infrared spectral analysis of healthy pears and insect-affected pears

The Vis-NIR spectra of Yali pears are shown in Figure 6A, in which each curve represents an individual Yali pears sample. It can be seen that the spectra of healthy pears and insect-affected pears are highly similar, and it is difficult to distinguish the spectral curves of the two categories. Five spectra were randomly selected from each category of sample spectra (as shown in Figure 6B). From the randomly selected 10 spectra of Yali pears, it can be seen that the spectra of healthy pears and insect-affected pears present obvious absorption peaks at the range of 691–798 nm, which is due to the information of color and pigment analysis (such as chlorophyll) of Yali pears in the spectral range of 400–750 nm, and the information of macro components (such as water and carbohydrate) of Yali pears in the spectral range of 750–2500 nm (29). From the spectral curves of healthy Yali pears and insect-affected pears, it can be seen that there is a phenomenon of spectral mixing between the two, and the clear threshold segmentation line cannot be found. Therefore, it is difficult to distinguish from the spectral figure whether Yali pears are damaged by insect-affected or not.

The spatial distribution of two kinds of pear samples in calibration set is analyzed by T-distributed Stochastic Neighbor Embedding (T-SNE) method. The T-SNE method is a nonlinear data-driven tool for dimension-reduction and visualization, which shows better performance in data visualization compared with other tools (30). The feature visualization of T-SNE method is shown in Figure 7. It can be seen from the figure that the spectral spatial distribution of healthy pears and insect-affected pears are intertwined, indicating that the T-SNE method cannot visually distinguish the spatial distribution of healthy pear samples and insect-affected pear samples. Hence, it is necessary to further explore the effectiveness of supervised pattern recognition in the identification of insect-affected Yali pears.

In view of the large amount of spectral data of Yali pears and the redundancy and overlap of spectral information, the CARS algorithm is used to select feature variables to reduce the high collinearity between spectral variables. Through each adaptive weighted sampling, the variables with larger absolute weight of regression coefficients in PLS model are retained as new subsets and the variables with smaller weight are removed.

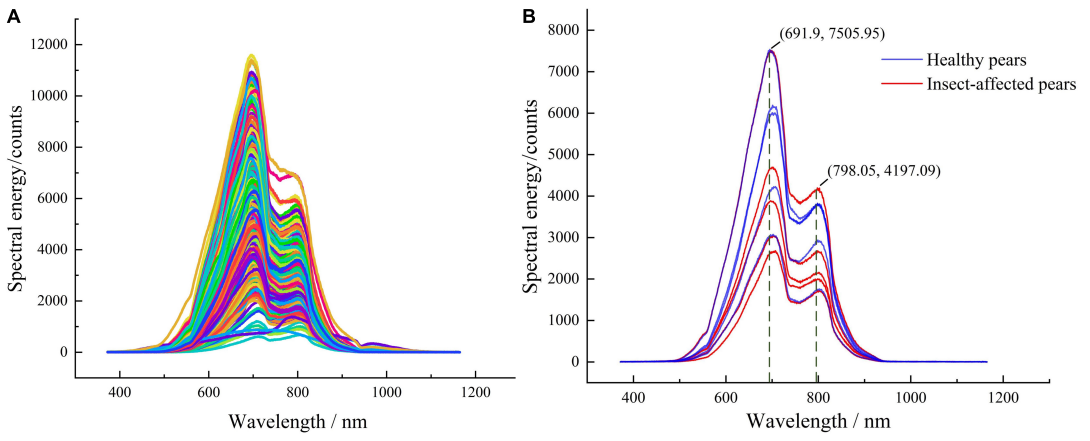

FIGURE 6
Vis-NIR spectra of healthy pears and insect-affected pears **(A)** original Vis-NIR spectra, **(B)** spectra of some samples.

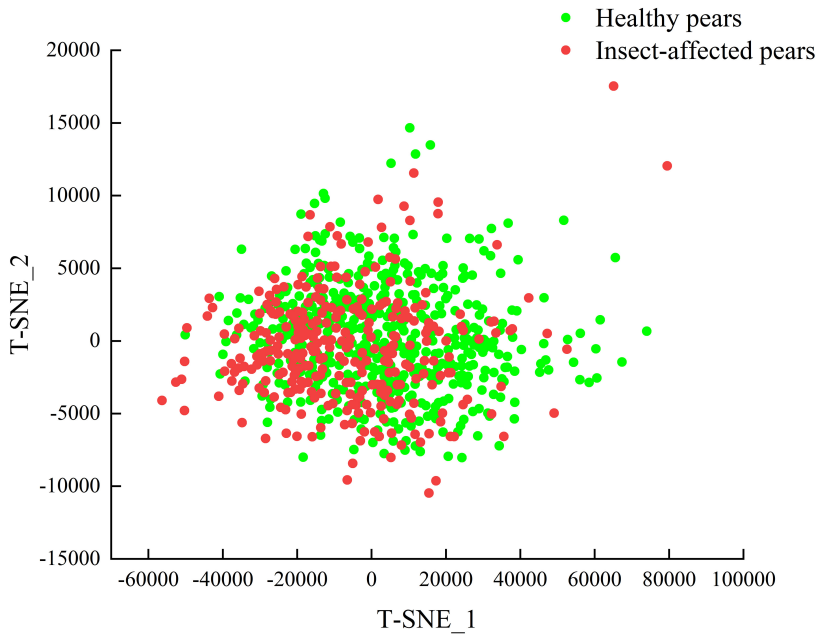

FIGURE 7
Feature visualization of healthy pears and insect-affected pears.

In the algorithm implementation of the CARS method, the range of Monte Carlo randomness is 20–50, the sampling step is 1, and the sampling ratio is between 0.2 and 0.8. When the sampling times are 27 and the sampling rate is 0.8, the RMSECV is the minimum value of 0.33. After CARS screening, a total of 70 wavelength variables were selected, and the combination of wavelength variables selected at this time has the best effect. The distribution of feature spectral variables of Yali pears selected by CARS method is shown in **Figure 8**. It can be observed that wavelength points are mainly concentrated at the range of 450–550, 740–800, and 810–980 nm, which contain the main spectral information of Yali pears.

Analysis on partial least squares discriminant analysis discrimination model of insect-affected Yali pears

The selection of the number of principal factors is the key to establish the model of Yali pears using the PLS-DA method. The leave-one-out cross validation is used to determine the optimal main factor number of the model, and the Accuracy and RMSECV of calibration set generated in the PLS model are calculated. The number of factors corresponding to the minimum RMSECV is selected as the optimal number of factors. The calibration results of different pretreatment methods and CARS modeling variable optimization methods combined with PLS-DA model are shown in **Table 2**.

It can be seen from **Table 2** that before the CARS method feature variables are optimized, SS pretreatment method shows better classification results in the calibration set, with an accuracy of 86.46%. However, the classification results obtained by MMN and SNV pretreatment methods are not as good as the original spectral classification results, indicating that these two pretreatment methods are not suitable for the original spectral data. After the optimization of the CARS method feature variables, the number of features become less and the high collinearity among spectral bands is reduced, so the classification results of original data and processed spectra by pretreatment methods are both improved. The SS pretreatment method still shows good classification results in calibration set, with the accuracy of 87.37% and the number of selected principal factors of 15. In conclusion, the modeling effect of PLS-DA is better after being pretreated by the SS-CARS method.

Analysis on support vector machine discrimination model of insect-affected Yali pears

The Grid Search (GS) is used to optimize the kernel function, c and g of the SVM model to achieve the optimal classification result. The calibration results of different pretreatment methods and the CARS method feature variable optimization methods combined with SVM model are shown in **Table 3**.

It can be seen from **Table 3** that before the optimization of the CARS method feature variables, the SNV pretreatment method shows good classification results in the calibration set, with an accuracy of 87.89%. The SGS, MMN, and SS

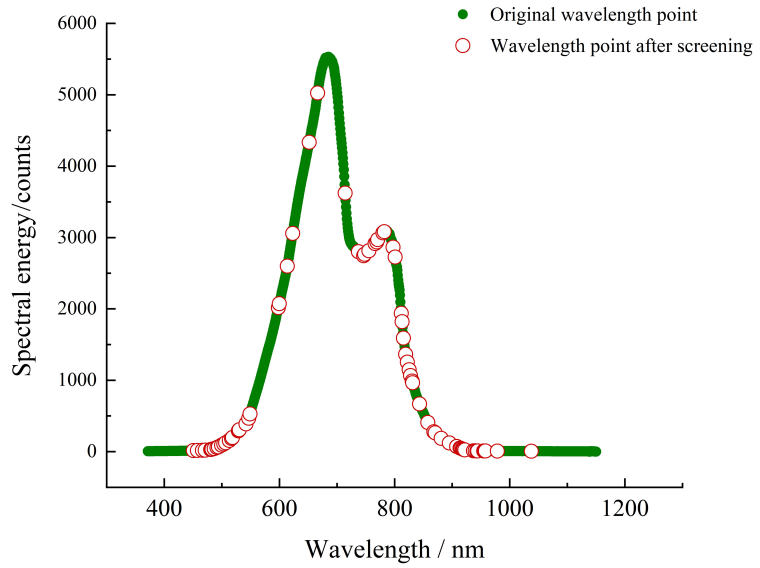

FIGURE 8
Distribution of feature spectral variables for Yali pears selected by CARS method.

TABLE 2 Calibration results of PLS-DA models based on different pretreatment methods and modeling variables.

Modeling variables	Pretreatment	Accuracy/%	RH/%	RB/%
All variables	None	80.73	88.98	66.89
	SGS	84.89	88.68	79.00
	MMN	76.43	85.47	62.33
	SS	**86.46**	**89.32**	**82.00**
	SNV	71.88	82.05	56.00
Selected variables	None	82.81	86.567	76.92
	SGS	85.42	88.46	80.67
	MMN	80.08	84.61	73.00
	SS	**87.37**	**90.39**	**82.67**
	SNV	73.18	82.27	59.00

pretreatment methods have improved the original spectral method, and the accuracy rate increases from 75% to more than 80%. After the optimization of the CARS method characteristic variables, the SS and SNV pretreatment methods show good classification results, with an accuracy of over 90%. The SNV pretreatment method presents the best classification results, with an accuracy of 92.06%, in this case, the selected kernel function is RBF, c is 50, and g is 3. In conclusion, the modeling effect of the SVM is better after the SNV-CARS pretreatment method.

Analysis on convolutional block attention module-convolutional neural networks discrimination model of insect-affected Yali pears

Since the input data type of the CBAM-CNN model is two-dimensional image data while the original spectral data is one-dimensional data, so before the CBAM-CNN modeling process, it is necessary to transform one-dimensional data into two-dimensional image matrix and input the model in the form of image matrix. In the process of two-dimensional image matrix transformation, it is necessary to intercept the fixed length vector from front to back, stack the intercepted vector according to the line, and stack all the vectors in turn to form a two-dimensional image matrix. In this paper, 1,024 waveband points in the whole waveband are selected, and a row vector is formed by 32 waveband points in each row to evenly separate the whole waveband. Finally, the formed row vectors are stacked to create a 32 × 32 two-dimensional spectral matrix, and the visualization of the two-dimensional spectral matrix is shown in Figure 9.

The structure of CBAM-CNN model is shown in Figure 10. In the construction of online Yali pear model through CBAM-CNN, convolutional layer, batch normalization (BN) layer, maxpooling layer, flattening layer and full connection layer are used. First, the network first carries out two-dimensional

spectral matrix conversion, spectral pretreatment and feature variable optimization of spectral data. Second, the optimized two-dimensional spectral matrix is input into the model. The model first extracts the characteristics from the spectral matrix through the convolution layer, and then adds the maxpooling layer after each convolution layer to remove redundant information by down-sampling. Third, the convergence rate of the model training is accelerated by BN layer to prevent gradient explosion; the flattening layer compresses the output features from the pooling layer to compress the two-dimensional feature data into one-dimensional features. Last, the category with the largest weight score is output by *Sigmoid* activation function as the final model classification results.

In the network structure of the CBAM-CNN model, the BN layer is added to solve the problem of gradient disappearance and accelerate the convergence speed of the network, which has a certain regularization effect. Since there has some over-fitting of the network during training, L2 regularization term is added to limit weight information, and the Dropout layer is added to randomly shut down 20% of the neurons. In the setting of hyperparameters, *Relu* activation function and Adam optimizer are used to automatically reduce the learning rate. The initial learning rate is 0.001. The loss value doesn't decrease every two times during training, the learning rate decays to 0.1 times of the previous time, with 50 batches and 300 epochs in total. The calibration results of different pretreatment methods and CARS feature variable optimization methods combined with CBAM-CNN model are shown in Table 4.

It can be seen from Table 4 that the SGS pretreatment method shows the best classification result in the calibration set without the optimization of CARS feature variables, with an accuracy of 96.88%. The MMN, SS, and SNV pretreatment methods all present better accuracy than the original spectral method. After the optimization of CARS feature variables, the MMN pretreatment method shows good classification results, with an accuracy of 87.76%; but the overall classification results are poorer than those before the selection of CARS feature variables. The reason behind worse classification results is that

TABLE 3 Calibration results of SVM models based on different pretreatment methods and modeling variables.

Modeling variables	Pretreatment	Accuracy/%	RH/%	RB/%
All variables	None	75.00	75.601	73.568
	SGS	80.59	83.72	75.59
	MMN	83.59	84.76	81.52
	SS	84.51	84.42	84.67
	SNV	**87.89**	**86.69**	**90.27**
Selected variables	None	80.33	83.37	75.43
	SGS	81.38	83.51	77.74
	MMN	87.24	87.63	82.82
	SS	90.88	92.16	88.85
	SNV	**92.06**	**90.95**	**94.10**

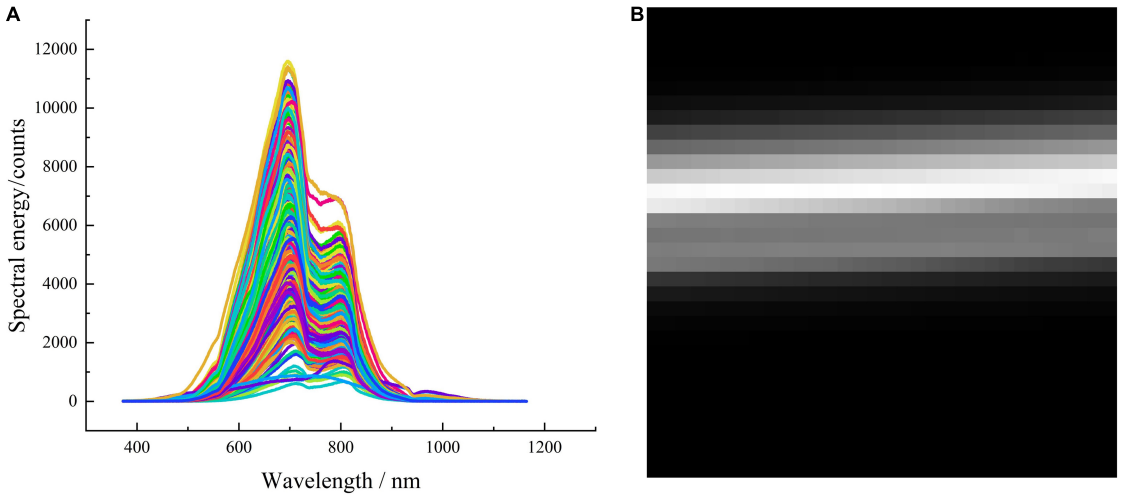

FIGURE 9
Original spectra of Yali pears and the transformed two-dimensional spectral image **(A)** original spectra, **(B)** two-dimensional spectral image.

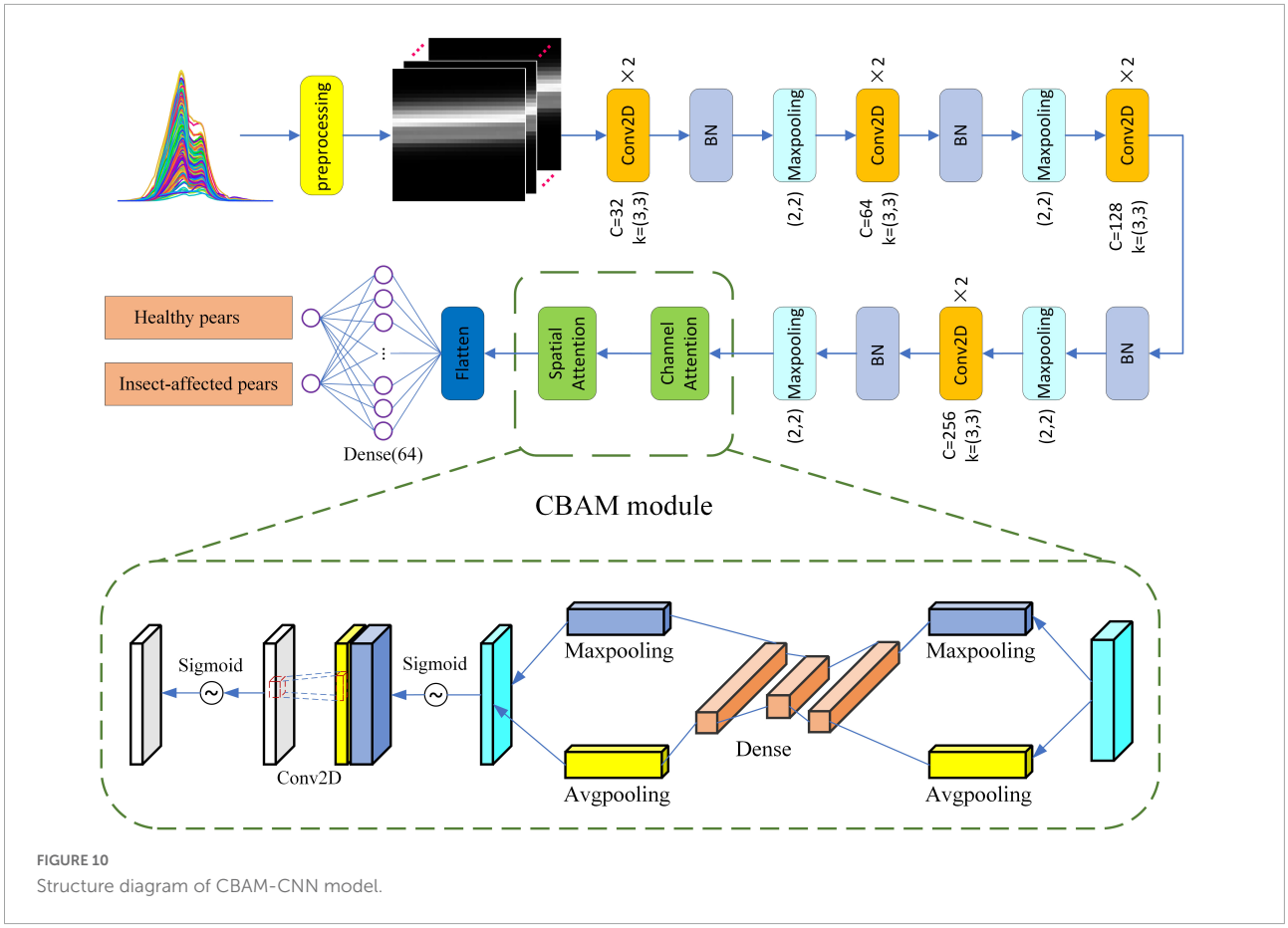

FIGURE 10
Structure diagram of CBAM-CNN model.

TABLE 4 Calibration results of CBAM-CNN models based on different pretreatment methods and modeling variables.

Modeling variables	Pretreatment	Accuracy/%	RH/%	RB/%
All variables	None	85.42	86.35	83.95
	SGS	**96.88**	**97.44**	**96.00**
	MMN	88.41	95.18	77.32
	SS	94.53	95.65	92.63
	SNV	90.62	92.97	87.68
Selected variables	None	86.85	89.73	82.13
	SGS	80.21	83.93	74.24
	MMN	**87.76**	**90.39**	**83.39**
	SS	83.33	93.97	65.51
	SNV	75.39	77.99	71.13

although the nonlinear problem between spectral data reduced after feature variables are selected by the CARS method, the number of spectral data features also reduced, leading to the insufficient feature quantity that can be learned by the deep learning model.

The validity of CBAM module is verified by constructing CNN model. During the construction of CNN model, the network structure, hyperparameters and the optimization scheme of spectral data of CNN model are consistent with those of the CBAM-CNN model. The test verifies that for the CNN model pretreated by SGS method, the calibration accuracy, RH and RB reach 95.18, 96.15, and 93.67%, respectively. Compared with the CBAM-CNN model, the accuracy decreases from 96.88 to 95.18%, indicating that the CBAM-CNN model has more attention to key feature points in spectral data than CNN model, thus improving the classification effect of the model on the insect-affected pears.

Analysis on optimal model and discrimination mechanism of insect-affected Yali pears

The optimal results of PLS-DA model, SVM model and CBAM-CNN model are selected to analyze the specific classification of Yali pears in the validation set for each model, as shown in Table 5.

It can be seen that there is a small amount of imbalance in the spectral data of calibration set, resulting in more or less classification bias in the classification of each model, that is, the classification accuracy of the healthy pears (RH) is higher than that of the insect-affected pears (RB).

As classified by the PLS-DA model, the accuracy of validation set, RH, and RB are 90.63, 94.36, and 83.82%, respectively. A total of 18 Yali pears are misclassified, demonstrating that the classification results are average. The PLS is sensitive to the difference between groups, but the difference between spectral data groups of Yali pears in this experiment is large, thus leading to the misclassification. As classified by the SVM model, the accuracy of validation set, RH, and RB are 81.25, 92.74, and 60.29%, respectively. A total of 36 Yali pears are misclassified, demonstrating that the classification results are poor. Although the spectral data is pretreated, there is still overlapping of data points aliasing, which cannot be separated by a suitable hyperplane; besides, c and g obtained by the GS method are not the optimal parameters.

As classified by the CBAM-CNN model, the accuracy of validation set, RH, and RB are 92.71, 95.97, and 86.76%, respectively. A total of 14 Yali pears are misclassified, demonstrating that the classification results are the best. Due to the increase of attention module in the network, more attention is paid to the spectral characteristics in the spatial dimension and channel, thereby reducing the impact of unbalanced data. The misclassification of 14 pears results from the similarity of two types of original spectral data, and the difference between them fails to be amplified after the pretreatment by SGS. But in general, the CBAM-CNN model only pretreated by SGS shows better performance than other models.

The validation set accuracy of the traditional shallow PLS-DA learning model is 90.63%, and the prediction time of a single pear is 0.018 s, which is relatively short. The validation set accuracy of CBAM-CNN deep learning model is 92.71%, and the prediction time of a single pear is 0.032 s, which takes relatively long computation time. In the actual online sorting, the detection time of a single pear is mainly calculated by the integration time of the spectrometer and the prediction time of the sample spectrum of the model. In this case, the integration time is about 0.08 s and the prediction time is 0.032 s, so the total prediction time of a single pear is 0.112 s. In the production line, a single fruit cup conveyed six pears per second, and the average transmission time of a single fruit cup is 0.167 s. The verification results show that the total predicted time of a single pear is less than the transmission time of a fruit cup, and the time difference meets the requirements of online analysis.

Interpretation of convolutional block attention module-convolutional neural networks deep learning model

In this paper, the T-SNE method is adopted to visualize the output features of CBAM-CNN model, so as to analyze the data clustering of Yali pear samples by the model. The Gradient-weighted Class Activation Mapping (Grad-CAM) is used to visualize the attention area of CBAM module, in a bid to locate the attention distribution in the spectral features.

The visualization of output features by T-SNE is shown in Figure 11. It can be observed that compared with the visualization of original spectral data features in Figure 7, the CBAM-CNN model has obvious classification effect for the two types of spectral data, as there is only a small amount of overlapping in the contact area rather than in the concentration area of the two types.

The Grad-CAM method is used to generate class activation mappings for localizing the portion of spectral features displayed in the attention module. The feature heatmap is

TABLE 5 Classification results of the validation set samples by PLS-DA, SVM, and CBAM-CNN models.

Model	Pretreatment	Sample status	n	n_c	n_w	Accuracy (%)	RH (%)	RB (%)	Prediction time(s)
PLS-DA	SS-CARS	Healthy	124	117	7	90.63	94.36	83.82	0.018
		Insect-affected	68	57	11				
SVM	SNV-CARS	Healthy	124	115	9	81.25	92.74	60.29	0.025
		Insect-affected	68	41	27				
CBAM-CNN	**SGS**	Healthy	124	119	5	**92.71**	**95.97**	**86.76**	**0.032**
		Insect-affected	68	59	9				

[a] n: Number of samples in the validation set.
[b] n_c: Correct classification.
[c] n_w: Wrong classification.

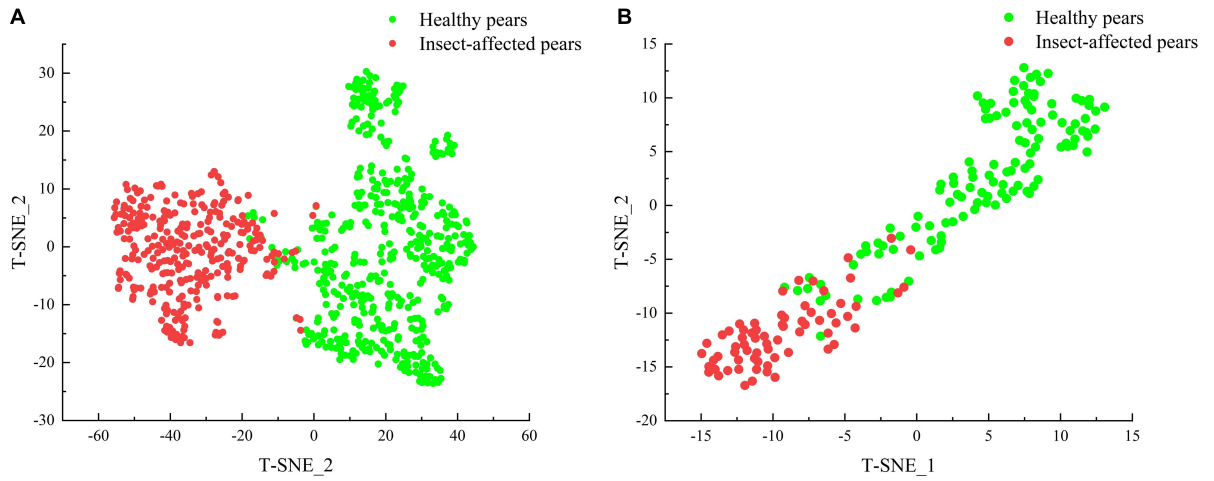

FIGURE 11
Visualization of output features by T-SNE: **(A)** Calibration set features distribution, **(B)** validation set features distribution.

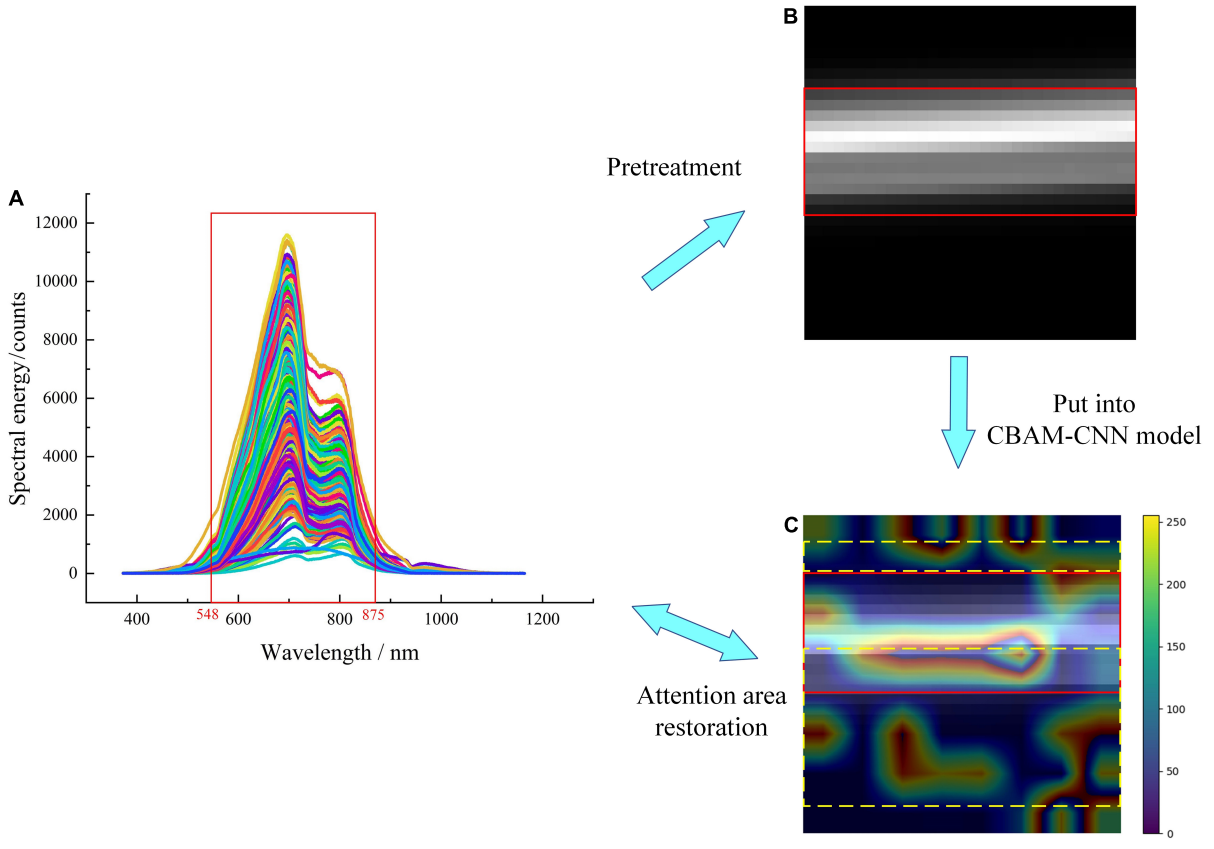

FIGURE 12
Visualization of Grad-CAM attention area: **(A)** Original spectra, **(B)** original spectral matrix image, **(C)** attention area spectral image.

superimposed with the original image, which further shows the localization of some regions in the image by the network, and more intuitively explains the learning ability of the network (31). The color bar in the figure indicates the grading weight; as the color changes gradually from blue to red, and the corresponding weight value also increases. The larger the weight

value, the stronger the ability of the model to learn features. The visualization of the attention area of Grad-CAM is shown in Figure 12. The highlight part in Figure 12B corresponds to the waveband at 548–875 nm in Figure 12A, which contains the entire wave peak of the spectrum region and is more representative.

The localization of the attention area of spectral matrix image by CBAM module is shown in Figure 12C. It can be seen that the attention modules can effectively pay attention to the wavebands corresponding to wave peaks tending to rise or fall in Figure 12A of the original spectral image (solid red line-box area), and the wavebands at 450–550, 740–800, and 810–980 nm optimally selected by CARS (yellow dotted line-box area). Besides, the highlight part and the optimally selected wavebands are given more red bands with high weight values, and targeted learning has been carried out.

Through the visualization analysis of the optimal model and feature, it can be seen that the classification of the deep learning model after spectral pretreatment on Yali pear pests is better than that of the shallow learning model after pretreatment and CARS feature variables optimization. The deep learning model itself can automatically extract features and learn, and use activate functions, attention mechanism and pooling layer, thus realizing the dual role of feature extraction and feature variable selection of spectral data. Therefore, the CBAM-CNN deep learning model shows better performance in discriminating insect-affected Yali pears than the PLS-DA and SVM shallow learning models.

Conclusion

This paper proposes a non-destructive, rapid and online method to detect internal defects of Yali pears based on Vis-NIR, in order to rapidly find out the recessive insect-affected Yali pears during commercial sorting. Different pretreatment methods have been adopted in combination with CARS feature variables optimization to establish the PLS-DA and SVM shallow learning models and the CBAM-CNN deep learning model for online discrimination. The T-SNE and Grad-CAM are used to cluster the output characteristics of the model and visualize the attention area. The experimental results show that the recognition accuracy of PLS-DA and SVM shallow learning online discriminant model improved and is improved to more than 80% after spectral pretreatment and CARS feature variables optimization. The online discriminant model established based on spectra pretreated by SGS combined with CBAM-CNN deep learning method shows the best performance, the accuracy of calibration set and validation set is 96.88 and 92.71%, respectively, and the prediction time of single Yali pear is 0.032 s. Compared with shallow learning method, the deep learning method makes full use of the its autonomous feature extraction and learning ability, thus simplifying the modeling process and obtaining good feature clustering and attention areas of the models. The Vis-NIR model proposed in this paper meets the requirements of accuracy and time for online detection; Hence, it can be applied to detect insect-affected Yali pears during commercial sorting in the coming future.

Data availability statement

The raw data supporting the conclusions of this article will be made available by the authors, without undue reservation.

Author contributions

YH: theoretical methods, funding acquisition, manuscript writing, and writing—review and editing. CZ: experiments, software, method implementation, and writing and editing. XL: experimentation, supervision, and writing—review and editing. ZL: funding acquisition and writing—review. All authors contributed to this article and approved the submitted version.

Funding

This study was funded by the National Natural Science Foundation of China (grant number 31960497), Jiangxi Provincial Natural Science Foundation of China (grant numbers 20212BAB204009 and 20202ACB211002), Primary Research & Development Plan of Jiangxi Province of China (grant number 20212BBE53016), and Intelligent Detection and Management System of Axle Workshop (grant number SF/QH-TZ05-2021-281).

Conflict of interest

The authors declare that the research was conducted in the absence of any commercial or financial relationships that could be construed as a potential conflict of interest.

Publisher's note

References

1. Guan YT, Li WX, Wen SM, Chang SM. Research progress on functional ingredients and food development of ya pear. *Farm Prod Proc.* (2021) 6:59–62. doi: 10.16693/j.cnki.1671-9646(X).2021.03.050

2. Sarker S, Woo YH, Lim UT. Developmental stages of peach, plum, and apple fruit influence development and fecundity of *Grapholita molesta* (Lepidoptera: Tortricidae). *Sci Rep-UK.* (2021) 11:2105. doi: 10.1038/s41598-021-81651-4

3. Han XF, Meng JM, Wei YQ, Gao TJ, Jin YW. Causes and comprehensive control measures of the severe occurrence of pear carnivora in the southern fruit area of Hebei. *Fruit Grower' Friend.* (2010) 9:30–2.

4. Mohamed A, El Masry G, Radwan SAA, Elgamal R. Development of a real-time machine vision prototype to detect external defects in some agricultural products. *J Soil Sci Agric Eng.* (2021) 12:317–25. doi: 10.21608/jssae.2021.178987

5. Khodabakhshian R, Emadi B. Application of Vis/SNIR hyperspectral imaging in ripeness classification of pear. *Int J Food Prop.* (2017) 20:S3149–63. doi: 10.1080/10942912.2017.1354022

6. Pan T, Li J, Fu C, Chang N, Chen J. Visible and near-infrared spectroscopy combined with bayes classifier based on wavelength model optimization applied to wine multibrand identification. *Front Nutr.* (2022) 9:796463. doi: 10.3389/fnut.2022.796463

7. Feng L, Wu B, Zhu S, He Y, Zhang C. Application of visible/infrared spectroscopy and hyperspectral imaging with machine learning techniques for identifying food varieties and geographical origins. *Front Nutr.* (2021) 8:680357. doi: 10.3389/fnut.2021.680357

8. Yang X, Zhu L, Huang X, Zhang Q, Li S, Chen Q, et al. Determination of the soluble solids content in korla fragrant pears based on visible and near-infrared spectroscopy combined with model analysis and variable selection. *Front Plant Sci.* (2022) 13:960926. doi: 10.3389/fpls.2022.938162

9. Barnes M, Duckett T, Cielniak G, Stroud G, Harper G. Visual detection of blemishes in potatoes using minimalist boosted classifiers. *J Food Eng.* (2010) 98:339–46. doi: 10.1016/j.jfoodeng.2010.01.010

10. Haff RP, Toyofuku N. X-ray detection of defects and contaminants in the food industry. *Sens Instrument Food Qual Safety.* (2008) 2:262–73. doi: 10.1007/s11694-008-9059-8

11. Zhang L, McCarthy MJ. Assessment of pomegranate postharvest quality using nuclear magnetic resonance. *Postharvest Biol Tec.* (2013) 77:59–66. doi: 10.1016/j.postharvbio.2012.11.006

12. Khodabakhshian R, Emadi B, Khojastehpour M, Golzarian MR. Carob moth, *Ectomyelois ceratoniae*, detection in pomegranate using visible/near infrared spectroscopy. *Comput Electron Agric.* (2016) 129:9–14. doi: 10.1016/j.compag.2016.09.006

13. Abbaspour-Gilandeh Y, Aghabara A, Davari M, Maja JM. Feasibility of using computer vision and artificial intelligence techniques in detection of some apple pests and diseases. *Appl Sci Basel.* (2022) 12:960. doi: 10.3390/app12020906

14. Moscetti R, Haff RP, Saranwong S, Monarca D, Cecchini M, Massantini R. Nondestructive detection of insect infested chestnuts based on NIR spectroscopy. *Postharvest Biol Tec.* (2014) 87:88–94. doi: 10.1016/j.postharvbio.2013.08.010

15. Tian H, Zhang LN, Li M, Wang Y, Sheng DG, Liu J, et al. Weighted SPXY method for calibration set selection for composition analysis based on near-infrared spectroscopy. *Infrared Phys Tech.* (2018) 95:88–92. doi: 10.1016/j.infrared.2018.10.030

16. Diwu PY, Bian XH, Wang ZF, Liu W. Study on the selection of spectral preprocessing methods. *Spectrosc Spect Anal.* (2019) 39:2800–6. doi: 10.3964/j.issn.1000-0593(2019)09-2800-07

17. Peng X, Shi T, Song A, Chen Y, Gao W. Estimating soil organic carbon using VIS/NIR spectroscopy with SVMR and SPA methods. *Remote Sens Basel.* (2014) 6:2699–717. doi: 10.3390/rs6042699

18. Schoot M, Kapper C, van Kollenburg GH, Postma GJ, van Kessel G, Buydens LMC, et al. Investigating the need for preprocessing of near-infrared spectroscopic data as a function of sample size. *Chemometr Intell Lab.* (2020) 204:104105. doi: 10.1016/j.chemolab.2020.104105

19. Chu XL, Yuan HF, Lu WZ. Progress and application of spectral data pretreatment and wavelength selection methods in NIR analytical technique. *Prog Chem.* (2004) 16:528–42.

20. Fu XS, Xu L, Yu XP, Ye ZH, Cui HF. Robust and automated internal quality grading of a Chinese green tea (Longjing) by near-infrared spectroscopy and chemometrics. *J Spectrosc.* (2013) 2013:139347. doi: 10.1155/2013/139347

21. Xie CQ, Wang QN, He Y. Identification of different varieties of sesame oil using near-infrared hyperspectral imaging and chemometrics algorithms. *PLoS One.* (2014) 9:e98522. doi: 10.1371/journal.pone.0098522

22. Tang HT, Meng XT, Su XX, Ma T, Liu HJ, Bao YL, et al. Hyperspectral prediction on soil organic matter of different types using CARS algorithm. *Trans Chine Soc Agric Eng.* (2021) 37:105–13. doi: 10.11975/j.issn.1002-6819.2021.2.013

23. Tang J, Liao X, Tong H, Gao J. GC-MS combined with PLS-DA to discriminate the varieties of XinJiang lavender essential oil. *Comput Appl Chem.* (2014) 32:701–4. doi: 10.11719/com.app.chem20140613

24. Wold S, Sjostrom M, Eriksson L. PLS-regression: a basic tool of chemometrics. *Chemometr Intell Lab.* (2001) 58:109–30. doi: 10.1016/s0169-7439(01)00155-1

25. Shi Q, Zhang H. Fault diagnosis of an autonomous vehicle with an improved SVM algorithm subject to unbalanced datasets. *IEEE T Ind Electron.* (2021) 68:6248–56. doi: 10.1109/tie.2020.2994868

26. Cui CH, Fearn T. Modern practical convolutional neural networks for multivariate regression: applications to NIR calibration. *Chemometr Intell Lab.* (2018) 182:9–20. doi: 10.1016/j.chemolab.2018.07.008

27. Zhao XY, Huang P, Shu XB. Wavelet-attention CNN for image classification. *Multimedia Syst.* (2022) 28:915–24. doi: 10.1007/s00530-022-00889-8

28. Woo S, Park J, Lee JY, Kweon IS. CBAM: convolutional block attention module. In: Ferrari V, Hebert M, Sminchisescu C, Weiss Y editors. *Computer Vision – ECCV 2018. ECCV 2018. Lecture Notes in Computer Science.* (Vol. 11211), Cham: Springer (2018). p. 3–19. doi: 10.1007/978-3-030-01234-2_1

29. Li M, Pullanagari R, Yule I, East A. Segregation of 'Hayward' kiwifruit for storage potential using Vis-NIR spectroscopy. *Postharvest Biol Tec.* (2022) 189:11189. doi: 10.1016/j.postharvbio.2022.111893

30. Van Der Maaten L, Hinton G. Visualizing data using t-SNE. *J Mach Learn Res.* (2008) 9:2579–605.

31. Selvaraju RR, Cogswell M, Das A, Vedantam R, Parikh D, Batra D. Grad-CAM: visual explanations from deep networks via gradient-based localization. *Int J Comput Vision.* (2020) 128:336–59. doi: 10.1007/s11263-019-01228-7

frontiers | Frontiers in Nutrition

TYPE Original Research
PUBLISHED 01 November 2022
DOI 10.3389/fnut.2022.983940

OPEN ACCESS

EDITED BY
John-Lewis Zinia Zaukuu,
Kwame Nkrumah University of Science and Technology, Ghana

REVIEWED BY
Maria Kapsokefalou,
Agricultural University of Athens, Greece
Antonis Vlassopoulos,
Agricultural University of Athens, Greece

*CORRESPONDENCE
Marie Tassy
marie.tassy@rd.nestle.com

SPECIALTY SECTION
This article was submitted to Nutrition and Food Science Technology, a section of the journal Frontiers in Nutrition

RECEIVED 01 July 2022
ACCEPTED 17 October 2022
PUBLISHED 01 November 2022

CITATION
Tassy M, Rytz A, Drewnowski A, Lecat A, Jacquier EF and Charles VR (2022) Monitoring improvements in the nutritional quality of new packaged foods launched between 2016 and 2020.
Front. Nutr. 9:983940.
doi: 10.3389/fnut.2022.983940

Monitoring improvements in the nutritional quality of new packaged foods launched between 2016 and 2020

Marie Tassy[1]*, Andréas Rytz[1], Adam Drewnowski[2], Alec Lecat[1], Emma F. Jacquier[1] and Véronique Rheiner Charles[1]

[1]Nestlé Research, Vers-chez-les-Blanc, Lausanne, Switzerland, [2]Department of Epidemiology, Center for Public Health Nutrition, School of Public Health, University of Washington, Seattle, WA, United States

Food and beverage companies reformulate packaged foods and to better align their products with public health policies and evolving consumer needs. The nutritional quality of packaged foodscan be tracked using nutrient profiling methods. The present study compared the nutritional quality of packaged foods launched globally between 2016 and 2018 and those launched in 2018–2020, as reported in the Mintel Global New Products Database. Nutrient profiling analyses showed that the nutrient composition of product categories shifted for almost 40% of newly launched products between 2016–2018 and 2018–2020. For example, pizzas that had been assigned to one nutritionally homogenous category in 2016–2018 separated in two nutritionally distinct subgroups in 2018–2020. The new products that were reduced in protein, saturated fat, and sodium were now nutritionally distinct from the traditional pizza offer. By 2018–2020 "best of category" products were significantly lower in sugar and sodium than before; however, no clear trend was observed for saturated fats, proteins, or fibers. The relative speed of product reformulation was category specific. This analysis of the Mintel Global New Products Database suggests that the WHO nutritional recommendations focusing on sugar and sodium reduction did have a positive impact on the composition of new packaged foods, whether through reformulation of existing products, launches of line extensions or new product development.

KEYWORDS

Mintel Global New Products Database, nutrient profiling, food supply, packaged food, monitoring

Introduction

The World Health Organization has urged food companies to lower the fat, sugar, and salt content of packaged foods (1), but it is not easy to evaluate the global impact of these recommendations on the evolution of the nutritional quality of packaged foods. This impact can be tracked using the Mintel Global New Products database, which lists, annually, more than 130,000 newly launched products in 86 countries along with their energy and nutrient content. Mintel product categories are linked to product manufacturing and marketing and are commonly used by food and beverage industries because they provide an actionable and up-to-date representation of the global food supply (2).

The present objective was to monitor the changes in the nutrient content of the global food supply, as tracked by Mintel, during two time periods: 2016–2018 and 2018–2020. The present method was based on nutrient profiling of product categories. Food manufacturers use nutrient profiling models that rank or classify foods based on their energy and nutrient content to continuously reformulate existing products and to set nutrition targets for line extensions and product innovation (3). While many nutrient profiling models are across-the-board (4), food manufacturers prefer to use nutrient profiling models that are category-specific and better correspond to product lines (5). One problem with those food category assignments that are driven by marketing or product positioning is that they can include foods that are very heterogeneous from the nutrition standpoint. Breakfast cereals or pizza can be of variable nutrient density. To overcome this problem, we have developed a new methodology (6) to disaggregate marketing categories into product subgroups or "classes" that were more nutritionally homogeneous. That procedure was used to set reformulation targets for new products that were comparable to those that in 2016-18 were judged to be "best of class" (6).

Analyses of emerging packaged foods can inform reformulation and innovation efforts by the food industry. First, monitoring nutrient composition of new product launches is one way to identify the most common reformulation targets. Such analyses can provide additional insights as to the emergence of new product categories that are distinct from the more traditional products on offer. Second, given the global nature of Mintel data, such analyses can help determine whether product reformulation is occurring globally and whether it affects multiple product categories. Third, the present study explored whether consumers were effectively informed about the observed evolutions through changes on a category specific front-of-pack labeling system.

Materials and methods

The present model relies on three algorithms to analyze the distributions of five public health sensitive nutrients—total sugars, total sodium, and saturated fat along with protein and fiber (7)—that were recently developed and discussed in detail (6). The first algorithm identified which of the five considered nutrients were relevant for each category; a nutrient was considered category-relevant if more than half of the products within this category had a declared nutrient content with a value that exceeded the "low in" or the "source of" limit. The second algorithm identified nutritionally homogeneous subcategories by analyzing the distribution modes of the category relevant nutrients. The third algorithm used a multivariate percentile approach to derive subcategory specific nutrient targets.

The Mintel Global New Products Database for the period 2016–2018, lists 416,706 packaged foods. Based on their nutrient content, products with relevant labeled information can be analyzed and portioned into 292 nutritional homogeneous subcategories. For the full 3-year period 2018–2020, the Mintel Global New Products Database lists 397,958 products that can be split into 288 nutritional subcategories. In a previous study, we used 350,994 products for 263 subcategories, but the 3 years period was truncated to 30 months instead of 36 (6).

Data for these two 3-year periods—with a 1-year overlap—were analyzed to identify both the structural changes of the categorization and the nutritional changes within categories. Since both sugars and sodium have been targeted by global reduction campaigns around the world (8), special attention was given to categories such as yogurts that significantly contribute to sugar intakes (9), as well as noodles and pizzas that are highly consumed all around the world (10) and that significantly contribute to sodium intakes (11, 12). Bread and cheese were among categories featuring large numbers of launched products.

Additional algorithms were developed to assess the evolution of both the food supply category structure and the targets within nutritionally homogenous subcategories. These algorithms are introduced through examples to make them most intuitive.

Partition-matching algorithm to assess the structural evolution of nutritional categories

When applying the model on both considered periods, it appears that Mintel categories such as "Bread and Bread Products" or "Hard Cheese and Semi-Hard Cheese" do not require any further subcategorization. Although featuring products that cover a wide range in terms of sodium and protein,

their distributions are unimodal and therefore reveal that they belong to one homogeneous nutritional category. For such cases, the structure remains stable.

Similarly, the Mintel category "Pizzas" is nutritionally homogeneous in 2016–2018 but the protein distribution appears to become bimodal in 2018–2020, indicating that two nutritionally different pizza subcategories have emerged. On the contrary, the Mintel category "Plant Based Spoonable Yogurts" moved from two sugar modes in 2016–2018 to one homogeneous category in 2018–2020. These examples are simple cases of structural evolution with only one category in either one of the two periods considered for the evolution.

For Mintel categories such as "Spoonable yogurts" and "Instant Noodles" with, respectively, two and four nutritionally homogeneous subcategories in both 2016–2018 and 2018–2020, the structural evolution can only be assessed if being able to match the two partitions of subcategories. For doing so, since the two periods were overlapping 1 year, it was possible to develop a simple partition matching algorithm. To illustrate this algorithm, the example of "Instant Noodles" is displayed (Table 1). As a first (A), the number of products launched in 2018—the year that is common to the two considered periods—is cross-tabulated across the two partitions. As a second (B), the proportional distribution of each old category (2016-18) across the new categories (2018–2020) is calculated. Finally, the algorithm matches any new category with the old category for which its prevalence was highest. In this example, New.1 is matched with Old.1, because prevalence of New.1 was 84% in Old.1 and 0% elsewhere; New.2 is matched to Old.2, because prevalence of New.2 was 35% in Old.2 and lower elsewhere; similarly New.3 is matched with Old.3 and New.4 is matched with Old.4. If the prevalence for a new category was the same in two old categories, the new category was matched with the larger of the two old categories. This method ensures that each new category is matched to a unique old category. In cases an old category is not matched with a new category, the algorithm is simply reversed.

Weighted-average algorithm to assess the evolution of nutrient quality

For all nutritionally homogenous subcategories that can be matched one to one over the two periods, the comparison of thresholds between the two periods is straightforward. It can be expressed as a relative improvement for reduction of disqualifying nutrients and increase of qualifying nutrients. Results focus on relative changes larger than 5% to account for the evolutions having highest nutritional impact. This threshold of 5% could naturally be adapted to match alternative objectives, but due to the limited number of products in certain categories, smaller changes should be considered with caution.

TABLE 1 Total of 1,476 products in Mintel category "Instant Noodles" in 2018.

	New.1	New.2	New.3	New.4	New.Sum
(A)					
Old.1	228	27	13	4	272
Old.2	0	159	0	292	451
Old.3	0	0	27	6	33
Old.4	0	0	0	720	720
Old.Sum	228	186	40	1,022	1,476
(B)					
Old.1	84	10	5	1	100
Old.2	0	35	0	65	100
Old.3	0	0	82	18	100
Old.4	0	0	0	100	100

Split into four nutritionally distinctive subcategories for both periods 2016–2018 (Old) and 2018–2020 (New) with (A) cross-tabulation of the two partitions and (B) Proportional distribution of each old category across all new categories. Underlined values represent the old category in which prevalence of new category is the highest.

For a case like pizza that matches one subcategory of 2016–2018 with two subcategories of 2018–2020, the comparison of thresholds is performed after averaging the thresholds of the two categories using a weighted average approach, with the weights given by the number of products in each of the two subcategories (Table 2).

Assessing health star rating evolution within Mintel categories

To compare the launches of 2016–2018 with those of 2018–2020 in a more direct and holistic way, the Health Star Rating (HSR) of all launched products was estimated (13). Since this estimation relies on complete labels, the estimate could only be done for less than 90% of all products considered previously.

Among other widely recognized front-of-pack labeling systems, HSR was selected because it was designed to enable an easy and standardized comparison of packaged foods. It differentiates nutritional quality within and between categories, is publicly available and gives a holistic view of the nutritional quality of the product. It is based on a scoring algorithm that deducts points for disqualifying nutrients (overall energy, sodium, total sugar, and saturated fat) and adds points for qualifying nutrients and ingredients (protein, fiber, and fruit and vegetables). These scores are converted to a "Health Star Rating" between 1/2 to 5 stars. This rating scale featuring 10 levels allows to discriminate products more than other systems that rely on less levels. HSR has therefore been chosen to increase the chances to observe changes, but any other front-of-pack labeling system could have been used.

TABLE 2 Total of 4,025 products in Mintel category "Pizzas" for the period 2018-20, with nutritional thresholds for the two nutritionally homogenous subcategories and their weighted average (e.g., Mean Sodium threshold = 592 mg/100 g = (572*2,831 + 640*1,194)/4,025), and comparison with the thresholds of the 3928 pizzas of 2016–18.

	N	Sfa (g/100 g)	Sodium (mg/100 g)	Protein (g/100 g)
Pizzas 2018–2020 (1)	2,831	4.6	572	8.0
Pizzas 2018–2020 (2)	1,194	6.2	640	11.6
Pizzas 2018–2020 (weight. Av.)	4,025	5.1	592	9.1
Pizzas 2016–2018	3928	5.0	600	8.8
Relative improvement		−2%	+1%	+3%

The average HSR ratings of each Mintel category was calculated and compared between the two periods of time.

Results

Structural evolution of nutritional categories between 2016 and 2020

The partition matching algorithm yields three cases: (1) a single subcategory in 2016-18 matching a unique one in 2018–2020, (2) two or more subcategories merging into one, and (3) a single subcategory splitting into two or more smaller ones (**Figure 1**).

As a result, 62% products launched in 2018–2020 belong to a subcategory that remained stable between 2016–2018. The structure of the global Mintel categories "Sugar and Gum Confectionery," "Juice Drinks," "Carbonated Soft Drinks," "Soup," "RTDs," and "Dairy Hot Beverages" remained completely stable.

Moreover, 22% products launched in 2018–2020 belong to a subcategory that merged two or more subcategories since 2016–2018, indicating that the competitive landscape became more homogeneous in terms of nutritional quality; this tendency is strongest, with more than 40%, for the three global Mintel categories "Chocolate Confectionery," "Meals and Meals Centers," and "Processed Fish, Meat and Egg."

Finally, 16% products launched in 2018–2020 belong to a subcategory that split from a subcategory that was larger 2 years before. This tendency is strongest, with more than 20%, for the three global Mintel categories "Bakery," "Snacks," and "Desserts and Ice-Cream."

Evolution of nutrient thresholds within subcategories between 2016 and 2020

Between 2016 and 2020, 83% of all products belong to subcategories for which the total sugars threshold did not evolve by more than 5%. It improved for 13% and was relaxed in only 4%, leading to a positive difference of 9% (**Figure 1**). This difference is + 75% in "Dairy Hot Beverages," + 51% in "Breakfast Cereals," + 46% in "RTDs," + 27% in "Bakery," + 21% in "Dairy," + 16% in "Other Beverages" and + 11% in "Sugar and Gum Confectionery." The difference is negative for "Snacks" (-14%). No evolution is observed for categories such as "Meals and Meal Centers," "Side Dishes," "Processed Fish, Meat and Egg" or "Soups" for which sugar is not a category-relevant nutrient.

For sodium, the threshold improved for 12% and was relaxed in 8%, leading to a positive difference of + 4%. This difference is + 25% in "Savory Spreads," +24% in "Breakfast Cereals," + 17% in "Bakery," + 11% in "Dairy," + 9% in "Side Dishes" and + 5% in "Sauces and Seasonings." The difference is negative for "Meals and Meal Centers" (-15%). However, 15% products being assessed vs. stricter thresholds are products with an average of more than 1300 mg/100 g, whereas the 30% of food products being assessed vs. more relaxed thresholds are products with an average of less than 430 mg/100 g.

For saturated fat, protein and fibers, no global overall trend is observed, but in some categories, interesting patterns are observed with noticeable efforts to reduce saturated fat in "Snacks" and "Processed Fish, Meat and Egg" or to increase proteins in categories such as "Breakfast Cereals," "Side Dishes," "Bakery," "Other Beverages" and "Dairy" or fibers in "Snacks."

Evolution of structure and nutrient threshold in selected categories

Results for selected categories focus on total sugars and sodium because no noticeable evolution could be observed for the other nutrients in these categories (**Figure 2**). The Mintel category "Spoonable Yogurts" featured two nutritionally homogenous subcategories both in 2016–2018 and 2018–2020: the first with higher thresholds in total sugars and saturated fat than the other. An improvement was observed for both subcategories with a decrease of the total sugar threshold of 4% for the first and of 16% for the second subcategory moving from 9.0 to 7.6 g/100 g. The two subcategories that constituted "Plant Based Spoonable Yogurts" merged into one homogenous category with a total sugar threshold that was decreased from 7.7 to 6.5 g/100 g (16% improvement).

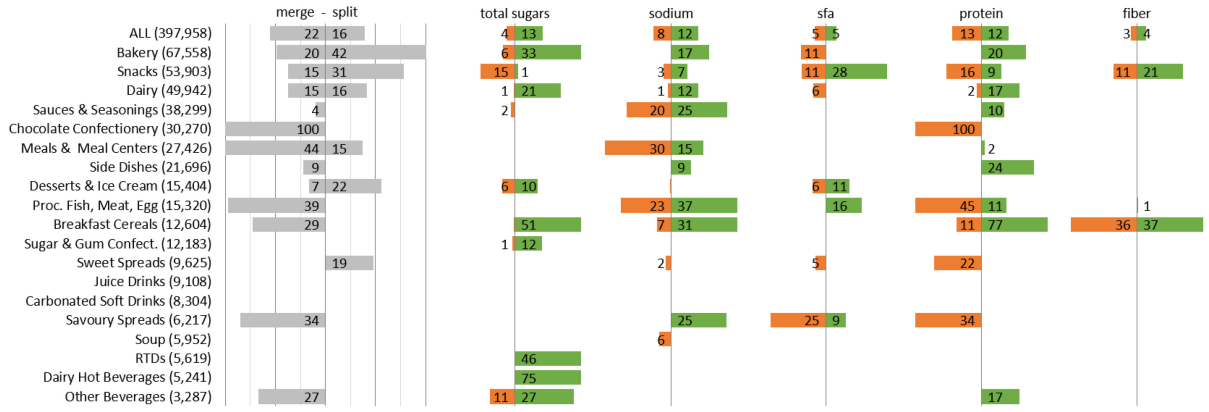

FIGURE 1

Percentage of products belonging to a nutritionally homogeneous subcategory in 2018–2020 that either merged two or more subcategories of 2016–2018 or that split from a larger category. For each nutrient, percentage of products belonging to a subcategory for which the nutrient threshold improved by at least 5% (green) or was relaxed by at least 5% (orange) between 2016–2018 and 2018–2020.

	Structure	N1	N2	sugars 1	sugars 2	sodium 1	sodium 2
Spoonable Yogurt (1)	1→1	5,596	5,319	13.6	13.0		
Spoonable Yogurt (2)	1→1	2,292	1,965	9.0	7.6		
Plant Based Spoonable Yogurts	2→1	783	1,039	7.7	6.5		
Hard Cheese & Semi-Hard Cheese	1→1	7,649	9,244			786	800
Bread & Bread Products	1→1	11,932	12,510			560	554
Pizzas	1→2	3,928	4,025			600	592
Instant Noodles (1)	1→1	842	741			395	360
Instant Noodles (2)	1→1	1,045	454			1,235	830
Instant Noodles (3)	1→1	72	110			2,000	1,628
Instant Noodles (4)	1→1	2,556	2,473			2,524	2,031

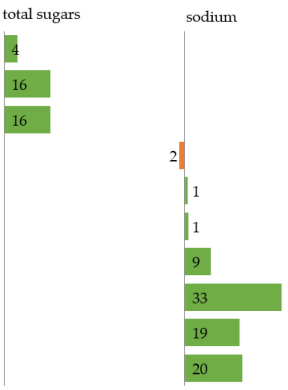

FIGURE 2

Ten selected nutritionally homogeneous subcategories, type of structural changes between 2016 and 2020, Number of products N1 for 2016–2018 and N2 for 2018–2020, sugar content (g/100 g) and sodium content (mg/100 g) and relative improvement between the two periods as bar charts.

	N1	N2	sugars 1	sugars 2	sodium 1	sodium 2	HSR 1	HSR 2
Spoonable Yogurt	7,888	7,152	1.9	1.7	<0.5	<0.5	3.75	3.85
Plant Based Spoonable Yogurts	783	1,022	1.0	0.9	<0.5	<0.5	3.40	3.40
Hard Cheese & Semi-Hard Cheese	7,649	9,057	<0.5	<0.5	7.1	7.3	3.35	3.35
Bread & Bread Products	11,932	12,240	0.6	0.6	5.0	4.9	3.30	3.30
Pizzas	3,928	3,950	<0.5	<0.5	5.1	5.0	2.85	2.85
Instant Noodles	4,515	3,719	1.0	0.7	16.9	14.5	1.50	1.50

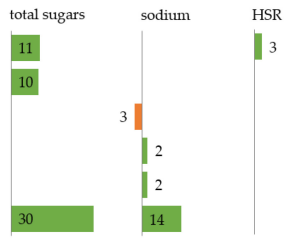

FIGURE 3

Six selected Mintel categories, Number of products N1 for 2016–2018 and N2 for 2018–2020, mean HSR points for total sugar and sodium, mean HSR, and relative improvement between the two periods as bar charts.

No significant evolution in structure or quality was observed for "Hard Cheese and Semi-Hard Cheese" and "Bread and Bread Products." The single Pizzas category of 2016–2018 split into two subcategories in 2018–2020 (Table 2). Indeed, the distribution of protein content of Pizzas category which was unimodal in 2016–2018 and ranged from 0 g/100 g to 23.1 g/100 g, became bimodal in 2018–2020 with one mode at 9.8 g/100 g and one at 12.4 g/100 g, and a split between the two

modes at 11.1 g/100 g. The two subcategories of 2018–2020 have significantly different content of protein (45%), saturated fat (35%), and sodium (12%). However, when comparing globally the "pizza" category between the two time periods, none of these nutrients changed by more than 5%.

For "Instant Noodles," the structure did not change with four nutritionally homogenous subcategories. Interestingly, for all four subcategories, the sodium threshold improved between 9% (for low sodium noodles) to 19–33% for the three other subcategories (higher sodium).

Evolution of health star rating in selected categories

Overall, HSR scores and ratings could be estimated for less than 90% of products, due to incomplete nutritional declaration. For the previously selected categories, there was no such issue since HSR could be estimated for more than 98% products. Overall, the findings on total sugar and sodium improvements derived from HSR ratings are well aligned with those derived from the threshold method (**Figure 3**).

For total sugars, mean HSR scores show that total sugars have decreased by respectively 10 and 11% for "Spoonable Yogurts" and "Plant Based Yogurts." Furthermore, this decrease was even 30% for "Instant Noodles"; this latter decrease was not identified by the threshold method, simply because total sugars is not a category-relevant nutrient.

For sodium, the only significant improvement in mean HSR scores is observed for "Instant Noodles" with a 14% decrease. This is overall aligned with the mean evolution of the thresholds but lacks the granularity that could be observed for the different "Instant Noodle" subcategories.

Finally, in terms of mean HSR rating, no significant evolution could be observed. Mean HSR rating remained stable with 3.4 stars for "Plant Based Spoonable Yogurts," 3.35 stars for "Hard Cheese and Semi-Hard Cheese," 3.30 stars for "Bread and Bread Products," 2.85 stars for "Pizzas" and 1.50 for "Instant Noodles." For "Spoonable Yogurt," the 11% decrease in total sugars was sufficient to yield a 3% increase in the mean HSR rating, moving from 3.75 to 3.85 stars. At the other end, "Instant Noodles," although decreasing sodium by 14% was not yielding an increased mean HSR rating.

Discussion

The present analyses confirm the effect of WHO nutritional recommendations to reduce sugar and sodium in packaged foods. Compared to year 2016, by 2020, the "best of class" products were overall significantly lower in both sugar and sodium. By contrast, no clear trend could be observed for the reduction in saturated fats, or for any increase in protein, or fiber content of food. Those too are among the targets for product reformulation by the food industry. To our knowledge this work is the first one to monitor the changing nutrient composition of the global packaged food supply. Many other studies have either focused on specific countries (14) or single nutrients such as sugar (15) or sodium (16).

Further, product categories identified in 2016 were not the same as product categories identified in 2020. The nutrient content of foods in nutritionally homogeneous categories evolved for more than one third of the products. Each of the 292 nutritionally homogeneous categories of 2016–2018 could be matched with one of the 288 categories of 2018–2020. This matching showed that between 2016 and 2020, both the category structure and the quality within categories evolved noticeably. Thus, the profiling system previously developed to effectively guide product reformulation enables one to determine category-specific nutrient thresholds applicable at one time point, and, when combined with a partition matching algorithm, to monitor the qualitative and quantitative changes in the manufactured food supply over the years.

Monitoring new product launches can be used to track the appearance, or disappearance, of food products on offer and to assess their nutritional quality. The Pizza category that was unique and homogeneous in 2016–2018 evolved into two subcategories with distinctive nutrient profiles between 2018 and 2020. The two categories were identified through a bimodal distribution of protein, but their content of saturated fat and sodium were also significantly different. This is because meat and cheese content of pizzas simultaneously affect protein, sodium and saturated fat. The newly emerging pizza category contained less nutrients of public health concern, reflecting perhaps current trends toward improved nutrition. Since Mintel does not report the volumes or sales of new launches, how consumers reacted to the changes in products offering is not known. Further study could aim looking at evolution of packaged food supply on a longer time, to detect lasting trends in product food offering which have been accepted by consumers.

The new pizza category may have been the result of reformulation or new product entries (17). Emerging new categories were also observed for "Bakery," "Snacks," and "Desserts and Ice-Cream," suggesting that those categories were also targets for reformulation and for improving nutrient density. On the other hand, Plant Based Spoonable Yogurts were split into two categories in 2016–2018, based on sugar content. Two years later, Plant Based Spoonable Yogurts became a single category with a sugar content that was uniformly low. For confectionery and snacks, tracking shifts in category membership is especially difficult. Such products can contain multiple ingredients and can be of highly variable nutritional value, making it difficult to detect changes over time.

For the most part, product categories remained stable between 2016 and 2020. New product categories were characterized by less total sugars and less sodium. Both dairy

yogurts and their plant-based alternatives' sugar thresholds decreased by 15%, a trend observed for almost one fourth of dairy products, and sodium thresholds dropped for 12% of 2018–2020 new launches. A cut in sodium and sugars was observed mostly in categories where levels were high, respectively, more than 1350 mg/100 g and 20 g/100 g, showing that reduction efforts focus on the subcategories where it matters most, while not stopping the effort even in the more healthful subcategories. This analysis is therefore reflecting the consequences of major WHO nutritional policies of the past decade (18) and its implementation by countries (19, 20) and efforts by food manufacturers (21–24) who focused on categories were the contents were critical. The changes for unsaturated fat, protein and fiber thresholds are less obvious when looking at global new launches, however, significant changes happened at category levels. More than 25% of dairy products were assessed against stricter protein thresholds after 2 years, and more specifically soft, semi-soft and processed cheese, which may reflect the recent trends for low fat and high protein products (25) and consumers looking for help with weight management (26).

Nutrient profiling of product categories provides a more precise way to track changes in the global food supply when compared to regional front-of-pack labeling system such as HSR. Indeed, both methods showed a decrease in the sodium content of Instant Noodles, and an absence of significant variation in the nutritional quality of pizzas after 2 years. Yet there was no improvements in HSR ratings. Moreover, the HSR analysis did not catch the reduction of sugar threshold of low sugar Spoonable Yogurts. The analysis herein demonstrates an alternative approach to detect nutritional changes in packaged food, which HSR might miss. This type of analysis may be useful for future application to demonstrate, comprehensively, the nutritional evolution of the food supply.

Conclusion

The present analysis of the Mintel Global New Product Database shows that the nutrient content of packaged foods significantly improved over a 5-year period (2016–2020). As trajectories of change were category specific, targets for reformulation should be periodically revisited to promote a continuous improvement of the global packaged food supply. Further analyses could apply this methodology to other product nutrient composition databases and could include volumes and sales data to assess, more accurately, the impact of WHO recommendations and consumer trends on global consumption.

Data availability statement

The data analyzed in this study is subject to the following licenses/restrictions: Data was obtained from 2020 Mintel Group Ltd. Requests to access these datasets should be directed to https://www.mintel.com/global-new-products-database.

Author contributions

MT, AR, and VC: conceptualization, formal analysis, methodology, and writing—original draft. AD, EJ, and AL: supervision and writing—review and editing. All authors have read and agreed to the published version of the manuscript.

Conflict of interest

This study was sponsored by Nestlé. MT, AR, VC, EJ, and AL were employed by Nestlé at the time of the study and AD was a member of the Nestlé Scientific Advisory Board. AD was the developer of the Nutrient Rich Food (NRF) index, a nutrient profiling model, and has received grants, contracts, and honoraria from entities, both public and private, with an interest in nutrient density of foods, complex meals, and the total diet.

Publisher's note

References

1. WHO. *Tackling NCDs: 'Best Buys' and Other Recommended Interventions for the Prevention and Control of Non-Communicable Diseases*. Geneva: WHO (2017).

2. MINTEL. *MINTEL Global New Product Database*. (2020). Available online at: https://www.mintel.com/global-new-products-database (accessed Dec 31, 2018).

3. WHO. *Nutrient Profiling: Report of a WHO/IASO Technical Meeting, London, United Kingdom 4-6 October 2010*. Geneva: World Health Organization (2011).

4. Drewnowski A, Amanquah D, Gavin-Smith B. Perspective: how to develop nutrient profiling models intended for global use: a manual. *Adv Nutr*. (2021) 12:609–20. doi: 10.1093/advances/nmab018

5. Scarborough P, Rayner M, Stockley L. Developing nutrient profile models: a systematic approach. *Public Health Nutr*. (2007) 10:330–6. doi: 10.1017/S1368980007223870

6. Leroy F, Rytz A, Drewnowski A, Tassy M, Orengo A, Charles VR, et al. A new method to monitor the nutritional quality of packaged foods in the global food supply in order to provide feasible targets for reformulation. *Nutrients.* (2021) 13:576. doi: 10.3390/nu13020576

7. WHO. *WHO Diet, Nutrition and the Prevention of Chronic Diseases: Report of a Joint FAO/WHO Expert Consultation, in WHO Technical Report Series 916*. Geneva: WHO (2003). p. 53–4.

8. World Action on Salt, Sugar and Health. *Reformulation*. (2021). Available online at: https://www.worldactiononsalt.com/worldaction/reformulation/ (accessed October 21, 2022).

9. Azaïs-Braesco V, Sluik D, Maillot M, Kok F, Moreno LA. A review of total & added sugar intakes and dietary sources in Europe. *Nutr J.* (2017) 16:6. doi: 10.1186/s12937-016-0225-2

10. WINA. *Demand Rankings*. (2021). Available online at: https://instantnoodles.org/en/noodles/demand/table/ (accessed April 8, 2022).

11. Farrand C, Charlton K, Crino M, Santos J, Rodriguez-Fernandez R, Ni Mhurchu C, et al. Know your noodles! Assessing variations in sodium content of instant noodles across countries. *Nutrients.* (2017) 9:612. doi: 10.3390/nu9060612

12. McGuire S, Rhodes DG, Adler ME, Clemens JC, LaComb RP, Moshfegh AJ. Consumption of pizza: what we eat in America, NHANES 2007-2010. Food surveys research group dietary data brief no. 11. February 2014. *Adv Nutr.* (2014) 5:456. doi: 10.3945/an.114.006171

13. Commonwealth of Australia. *Health Star Rating System*. (2014). Available online at: http://www.healthstarrating.gov.au/internet/healthstarrating/publishing.nsf/Content/Home (accessed Aug 31, 2020).

14. Bandy LK, Hollowell S, Harrington R, Scarborough P, Jebb S, Rayner M. Assessing the healthiness of UK food companies' product portfolios using food sales and nutrient composition data. *PLoS One.* (2021) 16:e0254833. doi: 10.1371/journal.pone.0254833

15. Bandy LK, Scarborough P, Harrington RA, Rayner M, Jebb SA. The sugar content of foods in the UK by category and company: a repeated cross-sectional study, 2015-2018. *PLoS Med.* (2021) 18:e1003647. doi: 10.1371/journal.pmed.1003647

16. Santos JA, Sparks E, Thout SR, McKenzie B, Trieu K, Hoek A, et al. The science of salt: a global review on changes in sodium levels in foods. *J Clin Hypertens.* (2019) 21:1043–56. doi: 10.1111/jch.13628

17. Apostol S. *A Year of Innovation in Pizza and Pies, 2020*. London: Mintel Group Ltd (2020).

18. WHO. *Global Action Plan for the Prevention and Control of NCDs 2013-2020*. Geneva: WHO (2013).

19. Public Health England. *Salt Targets 2020: Second Progress Report A Report on the Food Industry's Progress Towards Meeting the 2017 Salt Targets*. London: Public Health England (2017).

20. Public Health England. *Sugar Reduction: Achieving the 20% A Technical Report Outlining Progress to Date, Guidelines for Industry, 2015 Baseline Levels in Key Foods and Next Steps*. London: Public Health England (2017).

21. Martin A. *Danone Nutrition Commitments & Added Sugar Reduction*. Paris: ACI (2018).

22. Nestlé. *Nestlé Policy on Sodium (Salt)*. Vevey: Nestlé (2017).

23. Nestlé. *Nestlé Policy on Sugars*. Vevey: Nestlé (2017).

24. Unilever. *Unilever Sustainable Living Plan 2010 to 2020*. London: Unilever (2021).

25. IFIC Foundation. *2018 Food & Health Survey*. Washington, DC: IFIC Foundation (2018).

26. IFIC Foundation. *2019 Food & Health Survey*. Washington, DC: IFIC Foundation (2019).

frontiers | Frontiers in Nutrition

TYPE Original Research
PUBLISHED 09 December 2022
DOI 10.3389/fnut.2022.1058173

OPEN ACCESS

EDITED BY
John-Lewis Zinia Zaukuu,
Kwame Nkrumah University of Science and Technology, Ghana

REVIEWED BY
Alessandra Biancolillo,
University of L'Aquila, Italy
Lei Nie,
Shandong University, China

*CORRESPONDENCE
Roumiana Tsenkova
rtsen@kobe-u.ac.jp

†These authors have contributed equally to this work and share first authorship

SPECIALTY SECTION
This article was submitted to Nutrition and Food Science Technology, a section of the journal Frontiers in Nutrition

RECEIVED 30 September 2022
ACCEPTED 21 November 2022
PUBLISHED 09 December 2022

CITATION
Muncan J, Anantawittayanon S, Furuta T, Kaneko T and Tsenkova R (2022) Aquaphotomics monitoring of strawberry fruit during cold storage – A comparison of two cooling systems.
Front. Nutr. 9:1058173.
doi: 10.3389/fnut.2022.1058173

Aquaphotomics monitoring of strawberry fruit during cold storage – A comparison of two cooling systems

Jelena Muncan[1†], Sukritta Anantawittayanon[1†], Tetsuya Furuta[2], Toshiya Kaneko[2] and Roumiana Tsenkova[1*]

[1]Aquaphotomics Research Department, Graduate School of Agricultural Science, Kobe University, Kobe, Japan, [2]Nichiei Intec Co., Ltd., Tokyo, Japan

The objective of this study was to use aquaphotomics and near-infrared (NIR) spectroscopy to follow the changes in strawberries during cold storage in the refrigerator with an electric field generator (supercooling fridge, SCF) and without it (control fridge, CF). The NIR spectra of strawberries stored in these refrigerators were collected over the course of 15 days using a portable mini spectrometer and their weight was measured daily. The spectral data in the region of the first overtone of water (1,300–1,600 nm) were analyzed using aquaphotomics multivariate analysis. The results showed a decrease in weight loss of strawberries, but the loss of weight was significantly lower in SCF, compared to the CF. The reduction of weight loss due to exposure to an electric field was comparable to the use of coatings. The aquaphotomics analysis showed that the NIR spectra adequately captured changes in the fruit over the storage period, and that it is possible to predict how long the fruit spent in storage, regardless of the storage type. During aquaphotomics analysis, 19 water absorbance bands were found to be consistently repeating and to have importance for the description of changes in strawberries during cold storage. These bands defined the water spectral pattern (WASP), multidimensional biomarker that was used for the description of the state and dynamics of water in strawberries during time spent in storage. Comparison of WASPs of strawberries in CF and SCF showed that exposure to an electric field leads to a delay in ripening by around 3 days. This was evidenced by the increased amount of structural, strongly bound water and vapor-like trapped water in the strawberries stored in SCF. This particular state of water in strawberries stored in SCF was related to the hardening of the strawberry skin and prevention of moisture loss, in agreement with the results of significantly decreased weight loss.

KEYWORDS

strawberry, cold storage, aquaphotomics, near infrared spectroscopy, water, water molecular structure, electric field (EF), monitoring

Introduction

Strawberry is a well-known fruit consumed in both fresh and processed forms, not only because of its unique taste and fragrance but also its beneficial health properties. Strawberries contain numerous nutrients, vitamins, and minerals and plenty of compounds with biological effects, such as anthocyanins, flavonoids, and phenolic acids, which are shown to have anti-oxidative, anti-inflammatory, antihypertensive, anticancer, and anti-neurodegenerative properties (1–3).

Strawberry is a non-climacteric fruit, one of the most perishable ones, with a short post-harvest life, prone to rapid spoilage, mechanical injury, softening, and infections by several pathogens (2, 4), which necessitates special care during transport and storage to maintain a stable supply throughout the year. To slow down the metabolism and reduce deterioration, immediately after harvesting and prior to transport or storage, strawberries are cooled to 0°C (5, 6), followed by continuous storage at low-temperatures (0–4°C) (7) to control fruit respiration and extend the shelf-life which is usually around 5 days (8). In addition to the prevalent techniques of controlling decay, which are based on rapid cooling after harvest and storage at low temperature, other techniques are investigated to maintain quality, such as heat treatment, smart packaging materials, edible coatings, modified storage atmosphere, irradiation, and others (5, 8–19). All the physical and chemical preservation techniques are aimed to control the available oxygen and moisture transfer, thereby decreasing the respiration and transpiration trend and reducing weight loss, shrinkage, and microbial activity (13, 20, 21).

Packaging and coating benefits are, however, dependent on consumers' behavior, and several studies showed that a large percentage of consumers (at least 50%, up to 89% in some cases) remove the coating or open the package, not recognizing that it has a function of preserving the food quality (22–24). In addition, as several studies showed, most of the current preservation strategies are money and time-consuming, while fruit still experiences changes in color or flavor (14, 25–27). The application of electromagnetic fields in cooling systems is one of the novel strategies explored with the aim to develop better storage conditions for agricultural products. Research studies have shown that electromagnetic treatment helps the biological systems activate their defensive reactions, leading to an increase in the ability to repair the physical damages and benefit preservation (28–32).

Most fruits, including strawberries, have high water content per weight. In strawberries, about 90% of their weight is water. Water is a strong absorber of light - it absorbs over the entire electromagnetic spectrum, but in the near-infrared (NIR) spectral region 700–2,500 nm, the absorbance of water, especially compared to infrared light, is much smaller, making spectroscopic characterization possible for samples with high water content (33). Near-infrared (NIR) spectroscopy (NIRS) is a widely used non-destructive method that allows the acquisition of data without damaging the samples.

The primary features of the NIR spectrum of water, or any sample with high water content, are two prominent bands, called the first overtone of water and combination band, with several smaller bands due to higher overtones and combinations (34). Owing to the employment of many chemometrics and data analysis techniques, it is now well-recognized that these broad features are composed of many specific water absorbance bands that can be assigned to specific water molecular species (conformations). This new lens to the bio-system investigation was first recognized by a young scientific discipline, aquaphotomics, established by Prof. Dr. Roumiana Tsenkova in 2005 (35). The NIR aquaphotomics takes advantage of non-destructive NIRS measurements and ground-breaking knowledge of water–light interaction for the development of the non-destructive, integrative analysis of intact biological systems (34). This concept opens a novel, dynamic, non-invasive way of biosystems monitoring.

This research aimed to utilize aquaphotomic NIRS for monitoring during cold storage and better understanding of the mechanisms for maintaining freshness, choosing the strawberry fruit as a fruit-model system. The combination of NIRS and aquaphotomics has been already used to monitor aqueous and biological systems non-invasively for various purposes, such as evaluation of fresh and processed fruits and vegetables quality (36–42), milk quality (43, 44), viral infections in plants, bacterial cultures (45, 46) and fermentation (47–49), and physiological monitoring and diagnostics in higher organisms (50–55). The second aim of the investigation was to compare the effects of different cooling technologies on the preservation of strawberries. The applications of aquaphotomics in the monitoring during storage and estimation of freshness and shelf-life have only recently been explored (41, 56). This study employed two different cooling technologies. The first cooling system was based on conventional refrigeration technology, while the second one, employed exactly the same system but with the addition of an electric field generation device. The effects of different cooling systems were explored using non-destructive measurements by near-infrared spectroscopy (NIRS) and evaluated using an innovative aquaphotomics approach, which provides information about the molecular structure of water in the strawberries and connects it with their system functionality. The aquaphotomics analysis was focused on the spectra of strawberries collected in the NIR range 1,300–1,600 nm, the first overtone of water symmetric and asymmetric stretching vibrations. To this date, this range of spectra is considered the best for the understanding of the water molecular structure in various bio-aqueous systems in relation to their observed functionality, which is well-documented in many literature sources (35, 57–60).

To the authors' knowledge, only one research study used a similar approach to monitor changes during the storage of fresh produce (41), but this study went even further with the added novelty of exploring the differences in stored fruit depending on the employed cooling technology. While there are scientific studies concerned with the exploration of how novel cooling technologies affect food during storage or extend shelf life, the studies which explain the underlying mechanisms behind the shelf-life extension are still scarce. The application of aquaphotomics and in-depth investigation of water molecular structure in fruit during storage and how it changes with the time spent in storage, described in minute details, as this work will show, is a pioneering one and might set the direction of future research in this area. Interpretation of the found differences within the framework of known functionality of different water molecular species could serve as a basis for improved refrigeration, maintaining freshness, and prolonged shelf life. This information will provide novel possibilities for the development of non-destructive food monitoring technologies and a better understanding of postharvest food preservation mechanisms.

Materials and methods

Samples and storage conditions

Strawberries (*Fragaria L.*) of the 'New Harumi' cultivar were purchased in the local supermarket in Hyogo prefecture in Japan. After the transport to laboratory, the fruits were screened for uniformity, defects, and damage, and without washing or any other treatment, randomly distributed on the paper plates, eight strawberries per plate. Each individual fruit was assigned with the number label on the paper to provide identification of each biological replicate. The samples were then stored in different cooling system environments, 24 strawberries (three plates) per each storage condition – in the commercially available refrigerator (Model no. YRC-080RM2, Nichiei Intec Co., Ltd, referred to as a "Control Fridge: CF"), and also commercially available refrigerator, which employs electric field (Super Cooling Plant, Nichiei Intec Co., Ltd., referred to as a "Super Cooling Fridge: SCF" (61). The sinusoidal waveform in the frequency range of 48–62 Hz is used to form an electric field; the field is static with a strength of 3,000 V.

The nominal working temperature of both refrigerators was set to the same value of T = 0°C with a relative humidity of 90%. The samples were stored without any cover, packaging, or coating, in order to examine only the effects of different cooling systems, simulating the typical scenario of how the majority of consumers would behave.

Weight loss monitoring

The weight of each strawberry sample was measured immediately before the spectral acquisition for each fruit each day during the period of monitoring. Weight loss rate was calculated from the weight difference compared to the first measurement, when the storage period started, for each individual strawberry, according to the following equation:

$$Weight\ loss\ rate\ (\%) = \frac{(W_f - W_s)}{W_f} \times 100, \quad (1)$$

Where W_f represents the weight of a particular sample before storage (fresh) and W_s represents the weight of the sample on the respective day of storage.

To explore the dynamic changes in weight loss, the daily weight loss was also calculated. Daily weight loss represents the weight difference between a certain day of storage compared to the weight measured on the previous day, which is plotted as a function of time and shows the dynamic weight change in the strawberries.

Near infrared spectral acquisition

Spectral acquisition was performed using a portable, hand-held MicroNIR instrument (Viavi Solutions, Santa Rosa, CA, USA) in the spectral range of 908–1,670 nm, with approximately 7 nm resolution step.

The spectra were collected from 2 positions, front and back (**Figure 1**), per sample, with three consecutive measurements, for 14 days of the storage duration. The measurements were performed at 3.00 PM every day. The spectra collected on the first day of experiment, prior to putting the strawberries in the cold storage, are labeled as "day 0;" therefore, these are the spectra of fresh strawberries. The spectra collected afterward are labeled according to the number of days spent in cold storage, such as "day 1" and "day 2" finishing with "day 14". In total, 2,160 spectra (15 days × 24 strawberries × 2 positions × 3 consecutive measurements) were collected from each storage condition group.

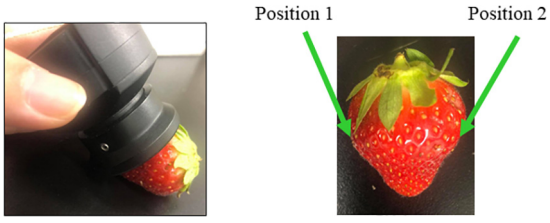

FIGURE 1
Acquisition of strawberry spectra using hand-held MicroNIR spectrometer was performed on two measurement positions.

Data analysis

Statistical analysis of weight loss

A paired samples *t*-test assuming equal variance at 95% confidence level was performed to confirm the significant difference in the %weight loss rate and daily weight loss between the two different cooling storage systems during the first 7 days of the storage. The statistical analysis was performed using Microsoft Excel (Microsoft, Redmond, WA, USA).

Multivariate analysis

Multivariate analysis of the water spectra was performed using Pirouette software v4.5 (Infometrix Inc. USA). Standard normal variate (SNV) transformation (62) was applied as a pre-processing treatment to eliminate the baseline differences among the spectra before calculating the difference spectra. In all other instances, the analysis was performed using raw spectra to introduce all available information to the model.

The difference spectra were calculated by subtracting the averaged spectrum of SNV-transformed spectra acquired on the first day of the storage [$S_{day\ (1)}$], from each of the averaged SNV-transformed spectra on subsequent days [$S_{day(n)}$] to see the spectral changes during the storage, as given by the following equation:

$$Difference\ spectra\ =\ avg\left(S_{day(n)}\right) - avg(S_{day(1)}). \quad (2)$$

Soft independent modeling of class analogies (SIMCA) analysis, a supervised classification method (63), was performed with the objective of discrimination between different days of storage [class variable – duration of storage (days)]. This algorithm employs principal components analysis of spectra for the construction of mathematical models for each sample group (class: storage day) with confidence limits. Interclass distances are calculated using between-class residuals, and variable importance is determined by comparing the average residual variance of each class to all classes and the residual variance of all classes to themselves. Variable importance, known as discriminating power, was used to find variables (wavelengths) with the highest contribution to discrimination between classes. The analysis was performed using mean-centered spectra, and the SIMCA models were developed separately for each cooling system.

Partial least squares regression (PLSR) analysis (64) was performed to explore spectral changes as the function of the storage duration (number of storage days). The models were developed separately for each different cooling system, and the water spectral data were mean-centered prior to regression modeling using the number of days of storage as a dependent variable. The analysis was applied twice to investigate changes during 4 and during 14 days of storage, according to the changing trends shown in the difference spectra. The validation was performed using stepwise exclusion of six spectra in each iteration. The accuracy of the PLSR models was evaluated by determining the coefficient of determination of calibration (R_c^2), standard error of calibration (SEC), coefficient of determination of cross validation (R_{cv}^2), and standard error of cross-validation (SECV). The optimum number of latent variables (LV) was determined based on the lowest SEC and lowest SECV, for calibration and cross-validation, respectively. The maximum number of LVs (factors) included in all models was limited to 15 in order to include as much as possible information but based on visual inspection of regression vectors for any appearance of "jaggedness" to prevent overfitting (65).

Aquagrams

Aquagrams (66, 67) were used to visualize the water spectral pattern in the strawberry flesh and how it changes along with time and depending whether the strawberries were stored in controlled or supercooling fridge. The representative water absorbance bands that were used as radial axes on aquagram, were selected from all the analysis results, following the procedure described elsewhere (67, 68) to ensure their importance and consistency. There are several ways to create aquagrams, depending on the purpose of the investigation (67). In this study, the aquagrams were calculated according to the procedure for calculating classical aquagram (67). In brief, the SNV – transformed and normalized absorbance values were averaged for each day, for SCF and CF conditions separately, and the values calculated for the first day of storage were subtracted. This calculated difference in absorbance was plotted at the found representative water absorbance bands to illustrate the changes in strawberries each day and depending on the storage conditions. The aquagram display was created in two different ways, first to allow the comparison of the storage conditions in general, and second, to provide better insight into the differences between the strawberries stored in different conditions on day-to-day basis.

Results and discussion

Weight loss of the strawberries during storage

Although the values were slightly different between individual strawberries, due to the natural variety of the biological replicates, the weight of the strawberries during storage, on average, linearly decreased with the progress of storage time irrespective of the applied cooling system. The weight was monitored for 14 days; however, here, only the results of weight change after 7 days will be presented, to allow comparison with most of the available literature sources.

There was a significant difference in the weight loss rate of strawberries stored in the control CF (mean M = 7.3%, standard deviation SD = 0.009737) and supercooling fridge SCF (mean M = 5.9%, standard deviation SD = 0.009964) [t(df) = 3.3342,

p = 0.000849; **Figure 2A**] after 7 days of storage. The weight loss during this period was shown to be fluctuating on a day-by-day basis (**Figure 2B**) but mainly followed the linear trend as the function of storage days, in agreement with many previous studies (5, 10, 69). Despite the similar pattern in weight loss from day to day, the weight loss of strawberries in SCF was each day smaller in comparison with CF.

The loss of weight in strawberries is associated with the respiration rate and evaporation of water through the fruit surface; the rapid loss of water is the major factor associated with the perishability of fruits, leading to shrinkage and deterioration (70–72). The observed conservation of weight in strawberries in SCF indicates that the exposure to the electric field might be delaying water loss, probably through prevention of the water evaporation. The weight loss of around 6% after 7 days in cold storage is comparable to the influence of coatings which form semi-permeable layer on fruit surface and act as protective barrier to reduce transpiration (7, 73, 74). For example, using chitosan coatings with different molecular weight was reported to limit the weight loss in strawberries to 5.28–5.66% after 14 days of storage at 4°C with the relative humidity of 85% (69). Gelatin coating resulted in 5.26% weight loss after 12 days of storage at 4°C and the relative humidity of 95% (10).

Super cooling fridge showed more potential to limit the water loss in the strawberry samples with a significant difference. Since water loss in strawberry is actually related to respiration and transpiration, this finding suggests that that presence of electric field in SCF influences these major cellular processes (13, 75). Controlling relative humidity in storage in combination with using electric field exposure seems to be promising direction to further limit the water loss which will be investigated in the next phase of this research.

Difference spectra and the changes in the water matrix of fruit flesh during storage

The raw absorbance spectra of strawberries collected over the course of 15 days is presented in **Figure 3A** for strawberries in CF and **Figure 3B** for SCF conditions, respectively. Prior to spectral subtraction, the spectra from both groups were corrected for baseline differences using SNV transformation.

The difference between spectra measured when the samples were just divided into two different groups and assigned to different storage conditions (day 0), and the spectra measured after the samples spent 1 day of storage (day 1) in CF and SCF, respectively, are shown in **Figure 4A**. The spectra for each group were averaged, and the difference spectra calculated by subtracting average spectrum at day 0 from average spectrum at day 1. The difference spectra reveal decreased absorbance with the minimum in 1,350–1,450 nm regions after 1 day of cold storage. The entire region corresponds to absorption of weakly hydrogen-bonded water, which encompasses proton hydrates, water hydration shells, and water vapor (56) among other water species, indicating the loss of water from fruit through transpiration, in agreement with what was observed in weight loss measurements.

The change for strawberries in SCF showed the minimum absorbance peak located at 1,385 nm (water hydration shell) (66). In comparison, the change in absorbance was less intense for strawberries stored in CF in the region 1,350–1,400 nm, but slightly more in 1,400–1,450 nm, with the minimum located at 1,404 nm (free water) (66). These results revealed different nature of changes in the water molecular structure of strawberry flesh due to the cooling in CF and SCF.

The differences in effects of CF and SCF started to decrease after the strawberries spent 4 days in storage, as can be seen from the difference spectra between the 4th and 1st day of storage of strawberries in the CF and SCF fridge given in **Figure 4B**. Interestingly, the subtracted spectra in both groups had very similar spectral patterns based mostly on the same water absorbance bands. It is important to note here that the subtracted spectra were not spectra collected prior to cold storage (day 0); therefore, the difference spectra reflect only the changes in strawberries due to the time spent in cold storage.

The value of absorbance in the region 1,350–1,450 nm stayed on the negative side, showing that the continuous loss of weakly hydrogen-bonded water is a common feature for both CF and SCF. The subtle difference between the storage conditions could be seen in the absorbance region around 1,380–1,410 nm, where absorbance bands of water hydration shells (1,380–1,388 nm), trapped water (1,396–1,403 nm) and free water molecules (1,404–1,418 nm) are located (66, 76). The decrease in absorbance of these water species, as well as the weight loss, is more pronounced for strawberries stored in CF.

The daily difference spectra during the storage of strawberries in CF and SCF when compared to day 1 are presented in **Figures 4C,D**, respectively. The difference spectra were calculated compared to day 1, to investigate how the spectra are change each day during cold storage and if there is a difference between the cooling systems. In the first 3 days, the spectra revealed increasing trend of the absorbance in 1,340–1,400 nm region, with the highest peak at 1,373 nm (proton hydrates, one of the absorbance bands of water vapor) (44, 56, 59). The absorbance in that part reached the maximum value on the 4th day of the storage, and then declined. CF and SCF provided similar results, while the maximum of the absorbance change at 1,373 nm is larger in the SCF group. The increased absorbance in this region suggests increase in the amount of gaseous phase of water within the fruit, which is characterized by highly mobile water species that can be exchanged with the environment. These water species are highly related to the water activity (56), too.

After 5th day, the absorbance in 1,340–1,420 nm of the CF group drop rapidly, while the change in SCF condition occurred

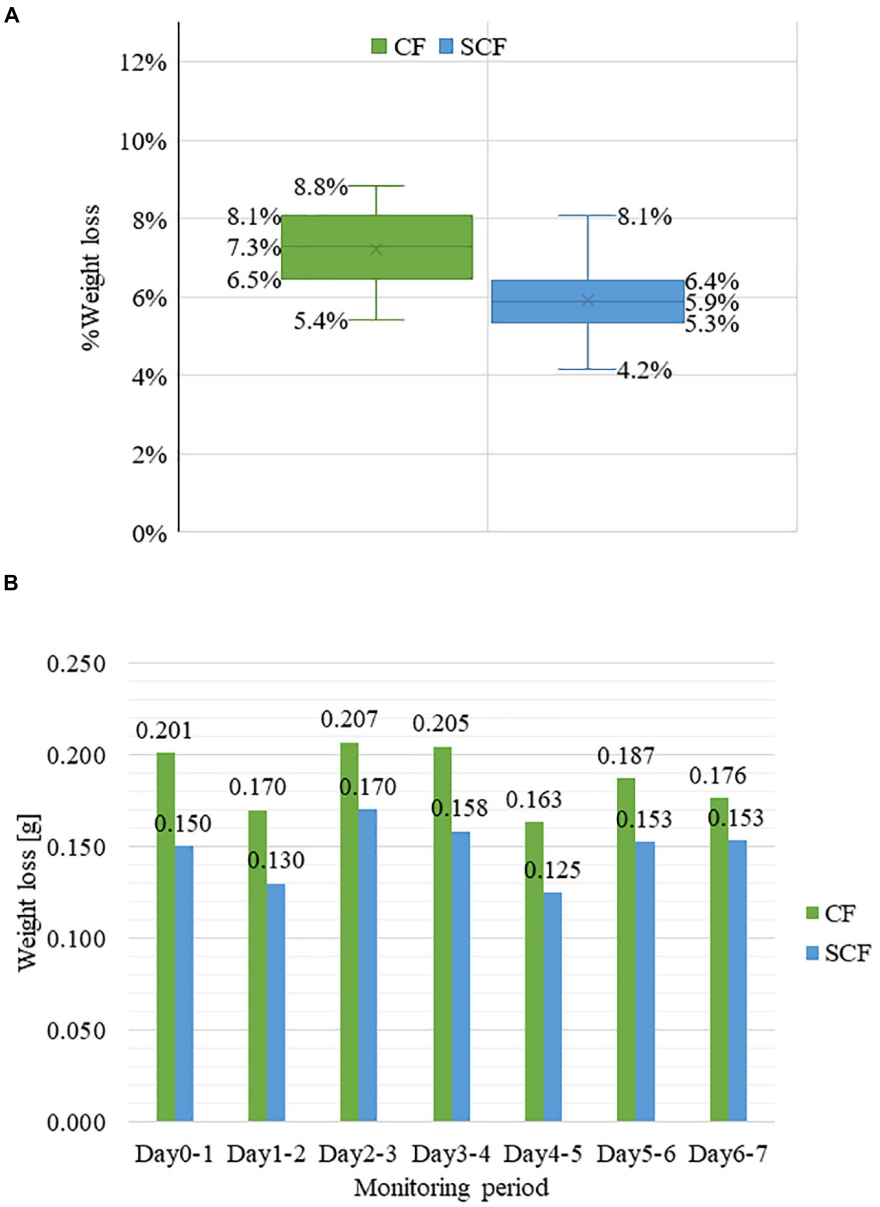

FIGURE 2
Weight loss during the storage. **(A)** % weight loss of strawberry samples in control fridge (CF) and supercooling fridge (SCF) after 7 days of storage **(B)** the daily weight change of the strawberry samples in CF and SCF conditions within 7 days.

gradually. The decreased absorbance at 1,340–1,420 nm had main negative peak located at 1,385 nm for CF, and at 1,391 nm for SCF conditions, respectively, which suggests controlled dehydration for the SCF group. The absorbance in the region 1,434–1,540 nm showed only minor changes until the 4th day of storage, then increased, with the major positive peaks located at 1,459, 1,478, 1,503, and 1,534 nm, and the main negative peaks at 1,447 and 1,490 nm. The absorbance at wavelengths above 1,534 nm was intensively decreased in the case of CF after 5 days of storage, while for SCF, the decrease was very gradual over the storage period and leveled in the last days of monitoring. Taking this into consideration, it seems that beginning from day 5, the changes in spectra of strawberries become very pronounced which is consistent with the reports that the shelf life of strawberries is around 5 days in cold storage (8).

It is interesting to point out that at two locations in the spectra there was a minimum change in absorbance throughout the storage, for both cold storage types (indicated by arrows in Figures 4C,D). The first one is located at around 1,342 nm, while the second one was located at 1,416 nm in the case of the CF, while at 1,422 nm in the case of SCF.

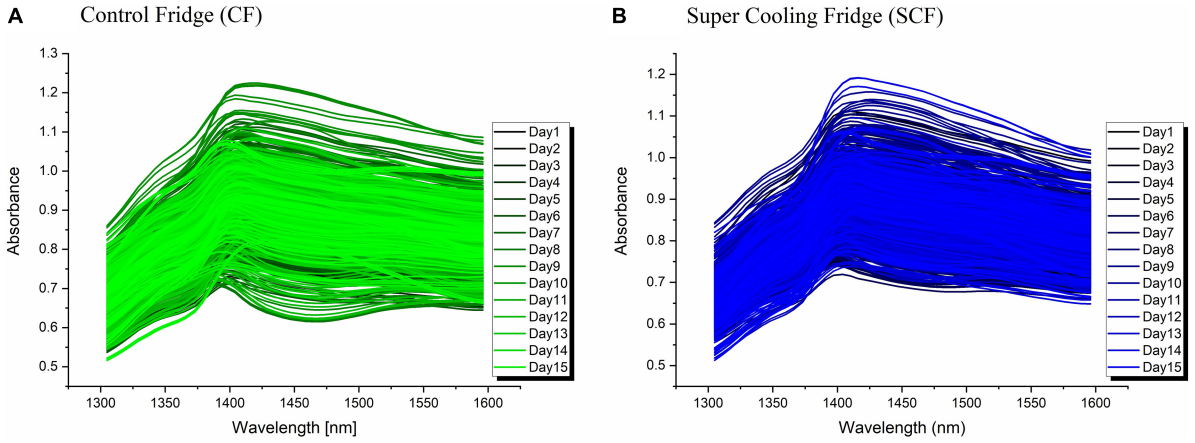

FIGURE 3
Raw absorbance spectra of strawberries in **(A)** control fridge (CF); **(B)** Super Cooling Fridge (SCF).

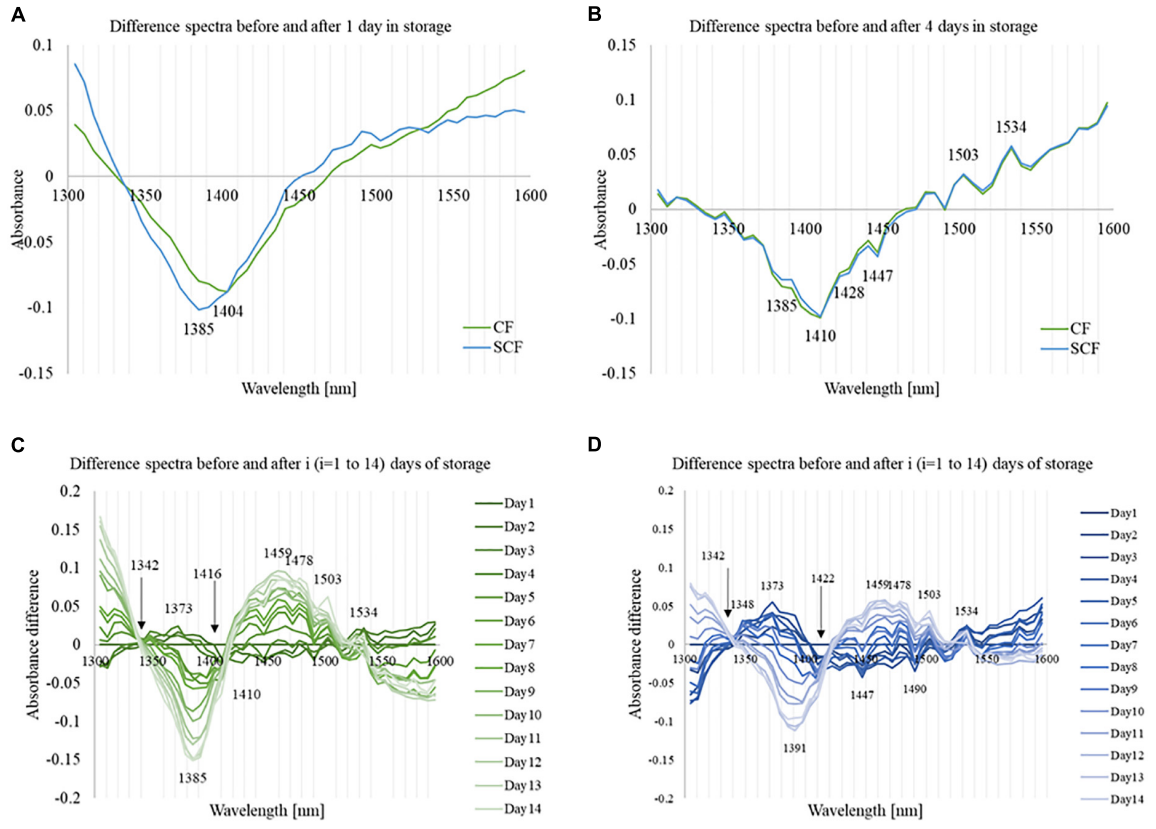

FIGURE 4
Difference spectra of the strawberry [$Day_{(i)}$ – $Day_{(1)}$] at different times during storage. **(A)** The difference spectra from day 0 to day 1 showing the impact of low-temperature storage and different cooling systems. **(B)** The difference spectra from day 0 to day 4 showing initial changes during storage and differences between the cooling systems. **(C)** The difference spectra of the strawberry [$Day_{(i)}$ – $Day_{(1)}$] during the storage in control fridge (CF). **(D)** The difference spectra of the strawberry [$Day_{(i)}$ – $Day_{(1)}$] during the storage in supercooling fridge (SCF).

All peaks that were found in the analysis so far are located within the first overtone of water symmetric and asymmetric stretching vibrations, and with the exception of 1,534 nm, all are within the ranges of, already discovered in other systems, Water Matrix Coordinates (WAMACS), absorbance bands of particular water molecular conformations (66). More detailed

assignment of these bands and interpretation from the aspect of water molecular structure will be provided later, in the 3.5 Choosing WAMACS and 3.6 "Aquagrams" section.

Soft independent modeling of class analogies analysis of the storage time classification

Soft independent modeling of class analogies analysis was performed with the objective of classifying spectra of strawberries according to the day of spectral acquisition, therefore, developing a model for prediction of how many days the strawberries were stored according to their spectra. The analysis was repeated three times, to explore the possibility of prediction for different lengths of storage time and for exploration of the most influential variables in SIMCA models. These variables, as given by discriminative power vector, can provide insight into the changes in water matrix of the fruit during storage as a function of the storage time and also as a function of different cooling system technology.

For all three SIMCA analyses, performed for the periods of 4, 8, and all 14 days, the results showed good accuracy of classification between the storage days and satisfying interclass distance.

In the case of SIMCA models developed based on the spectra from all 14 days, the classification accuracy was exceptionally high for both CF (97.87% accuracy) and SCF (99.26% accuracy) storage conditions, showing excellent possibilities of using NIR spectra for prediction of the freshness of strawberries, i.e., of predicting how many days the fruit spent in cold storage.

The values of interclass distance between storage days was larger than 1, which can be considered good, according to the reports that less than 0.8 would be a small difference (49). The discriminating powers of SIMCA models provided in **Figure 5** allow comparison of influential variables over time (since models were built for 4, 7, and 14 days) and depending on employed cooling technology - CF (**Figure 5A**) and SCF (**Figure 5B**), respectively. Discriminating power shows which absorbance bands contributed most to the successful discrimination between storage days.

The absorbance band with the highest discriminating power, representing an essential feature for all classification models, was found located at 1,528–1,534 nm for both CF and SCF conditions. In the classification model using 14 days of data, the discriminating powers of SIMCA models for CF and SCF show the common peaks at 1,311 and 1,360 nm, while 1,447 nm was more prominent in the SCF discriminating powers. SIMCA analysis results for different time periods (4, 7, and 14 days) revealed that the absorbance bands at 1,311 nm and 1,528–1,540 nm are always the variables with the highest discriminating power, describing where in spectra are the largest differences with respect to the day of the storage.

The discriminating power at 1,311 nm shows an increase along with time for SCF models but decreases for CF SIMCA models. The band located at 1,447 nm showed higher discriminating power during the first 7 days of storage for strawberries in CF, but it had highest power for 14 days of storage data when it comes to the SCF group. For CF data, the discriminating power of 1,534 nm surpassed 1,528 nm in the model using 4 days of data, but for the longer period, the discriminating power of 1,528 became higher than 1,534 nm, while in SCF 1,528 nm always had higher discriminating power than 1,534 nm regardless of the length of time.

The interesting difference between the discriminating powers between CF and SCF group is the pair of absorbance bands located at 1,360 and 1,379 nm. In the SCF group, peaks showed steady increase in discriminating power, while in the CF group, the band 1,379 nm showed an increase for 7 days, but then it dropped for 14 days model. There is also a difference in the absorbance bands featured as influential in models for CF in SCF in the area 1,484–1,510 nm. In the case of CF group, there are three different peaks located at 1,484, 1,497, and 1,509 nm, but for SCF group, there is just one broad band located at 1,503 nm.

The interesting aspect of this analysis is that despite different storage conditions, the same absorbance bands were shown as the most important for the description of how strawberries change during cold storage, and yet the analysis also captured the specifics of water molecular reorganization in fruit over time, as a function of different cooling technology.

Partial least squares regression analysis of water spectral changes during storage

According to the difference spectra results, which showed different trends of the spectral changes between the first 4 days and later storage period, the PLS regression analysis was first performed using spectral data collected during the first 4 days, and second, using all 14 days spectra [including the spectra collected before placing the strawberries in the storage (day 0)]. The dependent variable in both cases was time, expressed as "days of storage". The PLSR models were then calculated for CF and SCF data separately, and their performances were compared (**Figure 6**).

The predictions of the days of storage were successful, regardless of storage conditions with slightly less accuracy for the CF (coefficient of determination $R_{cv}^2 = 0.861$, standard error of cross-validation SECV = 2.288) compared to SCF (coefficient of determination $R_{cv}^2 = 0.875$, standard error of cross-validation SECV = 2.155 days). The PLSR results showed that the actual day of storage can be predicted with around 2 days error. The Y-fit plots that show agreement between actual and predicted day of storage show a very good linear relationship for both CF

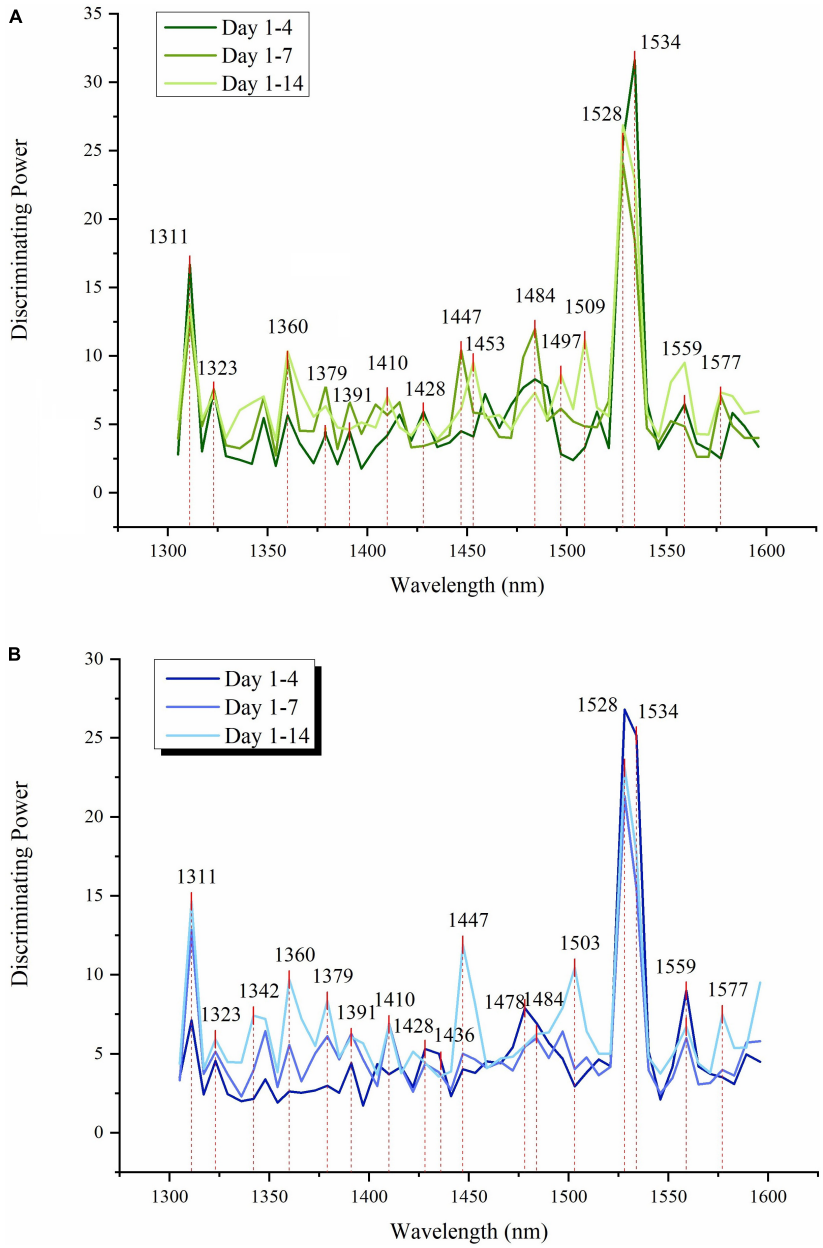

FIGURE 5
Soft independent modeling of class analogies (SIMCA) discriminating powers of absorbance bands show the importance of individual variables in NIR spectra for discrimination between the storage days of strawberries during 4, 8, and 15 days of storage **(A)** SIMCA results for CF group **(B)** SIMCA results for SCF group.

(Figure 6A) and SCF (Figure 6B) for all 14 days. The cause of error can be attributed to the differences between the individual samples which can be expected since the models were developed using raw spectral data. The adequate spectral pretreatment aimed at removal of influence of physical differences between the samples (such as surface curvature of the fruit) can probably lead to decreased error.

The results revealed that in the same time span both models for CF and SCF provided similar regression vectors as presented in Figure 6C for 4 days and Figure 6D for 14 days PLSR models. The time regression models for 14 days of storage fit linear pattern, describing the spectral change over the time with very high coefficient of determination ($R^2 > 0.85$; Figures 6A,B). This is the second analysis that confirms the ability of the NIR spectra to capture the information related to the passage of time in cold storage, and the potential for the estimation of freshness of strawberries.

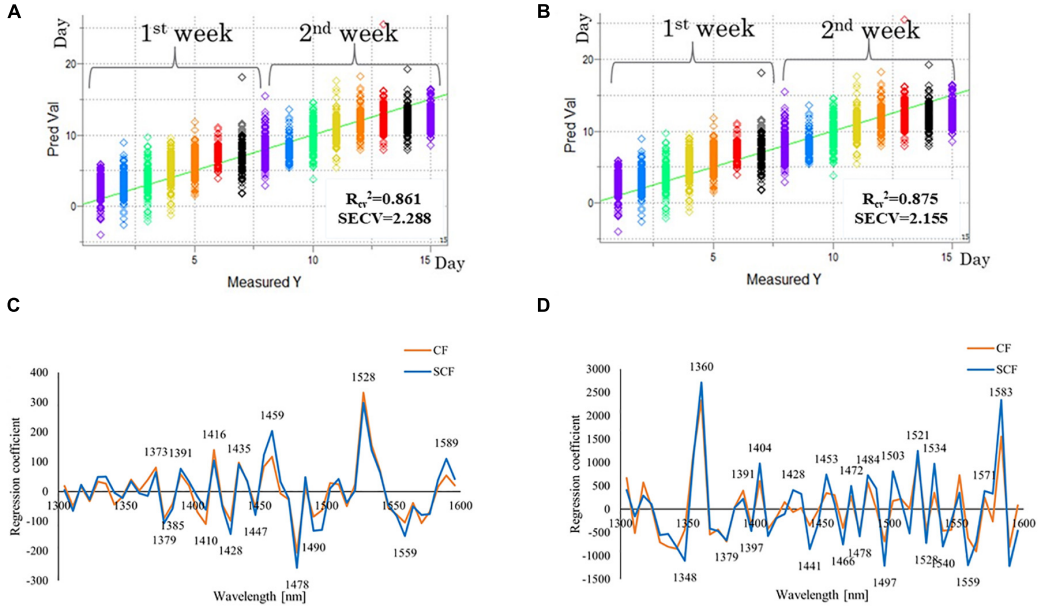

FIGURE 6
Results of partial least squares (PLS) regression modeling using time as a dependent variable (days of storage). **(A)** Y-fit plot, showing agreement between actual number of storage days and predicted number of storage days using PLS time regression model for spectra of strawberries in the control fridge (CF) condition **(B)** Y-fit plot, showing agreement between actual number of storage days and predicted number of storage days using PLS time regression model for spectra of strawberries in the supercooling fridge (SCF) condition **(C)** regression vectors of PLSR models built using spectral data of strawberry stored in CF and SCF conditions - comparison between regression vectors of models for the first 4 days of storage; **(D)** regression vectors of PLSR models built using spectral data of strawberry stored in CF and SCF conditions - comparison between regression vectors of models for the 15 days of storage.

The regression vectors shown in Figure 6C (for 4 days models) and Figure 6D (for 14 days models) can provide information which variables, i.e., absorbance bands were the most informative for modeling of storage time. As can be seen from these figures, in the first 4 days of the storage (Figure 6C), 1,528 nm appeared as a dominant peak with the highest, positive regression coefficient for both CF and SCF groups. In the model of 14 days of data (Figure 6D), 1,360 and 1,583 nm became much more prominent. There is also significant difference in the overall magnitude of regression vectors coefficients for 4 days models and 14 days models, which are almost eight times larger in the second case. There is also a difference between these models when it comes to the sign of regression vector coefficients – the peaks located at 1,373, 1,391–1,398, 1,416, and 1,528 nm were positive at first, during the 4 days period, but then become negative for the longer storage data. In comparison, the regression coefficient of 1,435 nm stayed positive in all sets, but with less weight.

The differences in regression vectors from the aspect of cooling systems are visible for the 4 days models as well as in 14 days models. The differences appear at 1,350–1,373, 1,391–1,400 nm, especially at 1,459, 1,490–1,500, and 1,559–1,583 nm for the 4 days model (Figure 6C). For the 14 days models, the differences in regression vectors appear at 1,330–1,348, 1,391, especially at 1,428 nm which shows almost no correlation with time for the CF model, and 1,441, 1,453, 1,466, 1,484, and 1,497 nm, again, very large difference at 1,503 and 1,550 nm, and finally again large difference at around 1,580 nm, where even the sign of the regression coefficients for CF and SCF is the opposite.

Taken together, this exploratory analysis of influential variables in PLS regression models show that the spectra of strawberries capture events on a molecular level in the fruit as it is stored, which seems to be common irrespective of the storage conditions. However, they also show distinct differences in effects of cooling systems, at specific absorbance bands which were already observed during previous analyses.

Choosing water matrix coordinates for aquagram display of water spectral patterns of strawberries

The analysis of spectral data of stored strawberries, despite differences in storage conditions, showed repeating and consistent absorbance bands at which the absorbance changed as a function of storage time. When all the bands from different analyses were put together (Supplementary Table 1), the importance of certain absorbance bands for description of changes in strawberries during storage, based on

TABLE 1 Water matrix coordinates (WAMACs) that carry information about the changes in strawberry during cold storage [Number of stars "*" in the column Importance represents the number of occurrences of the absorbance band as an influential variable during the whole analysis, as summarized in detail in Supplementary Table 1. Unless otherwise indicated in the table, the source of all information are references (58, 66)].

Absorbance band (nm)	Water matrix coordinates (WAMACs)	Importance	Assignment
1348	**C1** (1,336–1,348 nm)	**	Antisymmetric OH stretch of H_2O (ν3)
1360	**C2** (1,360–1,366 nm)	***	Water solvation shell OH-$(H_2O)_{1,2,4}$ Water vapor (59) and proton hydrates (44)
1373	**C3** (1,370–1,376 nm)	***	Combination of symmetric and asymmetric OH stretch of H_2O (ν1 + ν3) Water vapor (59) and proton hydrates (44)
1379 1385	**C4** (1,380–1,388 nm)	**** ****	Water solvation shell, OH–$(H_2O)_{1,4}$ and/or superoxide O_2–$(H_2O)_4$ Water vapor (59) and proton hydrates (44)
1391 and 1397	**C5** (1,396–1,403 nm)	****	Confined single water molecules (trapped water) (76) First overtone of the free OH group trapped in the hydrophobic interior (109)
1404, 1410, and 1416	**C5** (1,404–1,414 nm)	** *** *	Free water molecules
1428	**C6** (1,421–1,430 nm)	***	Water hydration band, H–OH bend hydroxide First overtone of the fundamental OH stretching vibration in water (the water molecules are condensed in one or more layers on sorption sites in the amorphous region) (81)
1435 and 1441	**C7** (1,432–1,444 nm)	* *	Non-bonded O–H stretching first overtone; overtone of the OH bending mode of H_5O_2+ water dimer
1447 and 1453	**C8** (1,448–1,454 nm)	***** *	Water solvation shell, OH–$(H_2O)_{4,5}$
1459 and 1466	**C9** (1,458–1,468 nm)	*** *	Water molecules with two hydrogen bonds
1472 and 1478	**C10** (1,472–1,482 nm)	* ****	Water molecules with three hydrogen bonds
1484, 1490, and 1497	**C11** (1,482–1,495 nm)	** ** **	Water molecules with four hydrogen bonds
1503	**Ci**	****	Strongly bound water, intermolecular hydrogen bonds (42, 110) Hydrogen bonded water molecules participating in the crystal structure (111) OH stretching vibration in Ice III (112)
1509 and 1521	**C12** (1,506–1,516 nm)	* *	Strongly bound water, symmetrical stretching fundamental vibration and doubly degenerate bending fundamental (ν1, ν2)
1528	**Cj**	****	Strongly bound water, intermolecular hydrogen bonds (113)
1534	**Ck**	*****	Hydrogen bonded hydroxyl groups (–O–$H^{\delta+}\cdots O^{\delta-}$–) (114) First over. of hydrogen bonded O-H stretching (115) Bending fundamental, $2\delta_{HOH}$ (103)
1559	**Cl**	****	Ionic bound water molecules 1st overt (99, 116) Strongly hydrogen bonded water (117) Crystalline water ice (118)

the number of their appearances as important variables in the analyses became evident.

Out of 28 absorbance bands found important for the description of changes during cold storage, 24 belong to well-known WAMACs, that is, small wavelength ranges 6–20 nm in length that corresponds to the absorbance of specific water molecular conformations (57, 58, 66) (Table 1). Additionally, four absorbance bands featured prominently in the analysis – 1,503, 1,528, 1,534, and 1,559 nm. These bands are not yet recognized as WAMACs. All four bands are located within the part of the NIR spectra where it is known that strongly hydrogen-bonded water absorbs. These four bands carried much weight in the analysis indicating the importance of their distinction and we tentatively labeled them as new WAMACs Ci, Cj, Ck, and Cl that may be of interest to monitor freshness of the agricultural products in general (Table 1).

Judging by the importance of the WAMACs, it can be observed that C4, C5, C8, and C10 and newly defined Ci, Cj, Ck, and Cl (rows highlighted in gray in Table 1) are not only important for the description of the changes during storage

but also reflect the differences in strawberries as a function of different cooling storage treatment.

Together, these WAMACs could be thought of multidimensional biomarker that can be used to describe the process of change in strawberries during storage.

Aquagrams – Water spectral patterns of strawberries during cold storage

Based on the previously found WAMACs, 19 representative water absorbance bands were selected to visualize the collective spectral change during storage of strawberries. These absorbance bands define radial axes on aquagrams on which values of difference in normalized absorbance between the respective day and the first day of storage were plotted, as presented in **Figure 7**, for cold storage in the control fridge (**Figure 7A**) and supercooling fridge (**Figure 7B**). For simplicity and practical reasons, the aquagrams are displayed for the 7 days, because of the usual shelf-life of strawberries of 5 days in cold storage.

The comparison of how water spectral pattern of strawberries change during cold storage provided stark differences depending on whether the strawberries were kept in control or supercooling fridge. First, in the area of highly active water species, which are vapor-like (57) absorbing in the region 1,348–1,385 nm, it can be observed that when strawberries are in the CF the absorbance decreases with time, while in the SCF the absorbance is increased and stays relatively stable during this 1 week. In the CF, there is particularly decrease at 1,373 and 1,385 nm on days 5–7. All these vapor-like, weakly bonded water species (water molecules in proton and ion hydration shells, water species involved with hydration of soluble charged compounds) are with high energy and very mobile (56). The observed difference suggests increased content of soluble compounds in strawberries stored in SCF, active respiration, and exchange of water in the gaseous phase with the environment and, since the bands 1,360, 1,373, and 1,385 nm are the signature bands of moisture and water activity (56), it also implies the existence of water available to participate in necessary biochemical reactions.

The differences are also present at the bands of free (1,410 nm) and quazi-free water (1,391 nm). For the case of CF, after the initial period of no changes at 1,391 nm, absorbance decreases after fifth day in storage. On the contrary, the absorbance at this band is increased for the case of SCF and declines gradually. This absorbance band is related to trapped water, either in between hydration shells of ions or in the hydrophobic interior, which implies that there is the ongoing production of some compounds in strawberries during this time, which results in their hydration and subsequently confined interior in which single water molecules get confined. This would be in agreement with increased absorbance at hydration shells bands (1,360 and 1,385 nm) signaling the increase in soluble compounds observed previously. Taken together, this implies that upon cold storage in SCF, the strawberries show more signs of active metabolism and production of soluble compounds. It is interesting to point out that the close absorbance band located at 1,398 nm, which is also attributed to trapped water, was found to be highly correlated with vitamin C content and shrinkage of fruit during hot air drying (77).

The absorbance of free water molecules (1,410 nm) is decreased immediately upon storage in both fridges; however, there is difference in the magnitude of this decrease. The decrease is much stronger, very sharp and regular in the case of SCF, while it is not regular and shows fluctuations in CF. This is most probably heavily related to the observed weight loss of strawberries and can be indicated loss of juiciness (56). It was previously observed that decrease in free water molecules is an important defense reaction in response to desiccation stress and that decrease of free water molecules might be the survival strategy in plants in the stress conditions (78). Since a decrease of free molecules is the common reaction in strawberry for both cold storage conditions, this might indeed be the case; however, the gradual and regular decrease in the case of SCF indicates organized control of water loss [also a part of survival strategy as found before (78)].

The largest differences in aquagrams could be observed in the area from 1,428 to 1,490 nm. In the SCF, the absorbance of strawberries seemed to be decreased immediately upon storage and kept that way, and only on days 6 and 7, there is increase at the bands from 1,459 to 1,484 nm. However, such decrease of absorbance was not observed for the CF, and in contrast, the absorbance shows huge increase at all these bands starting from day 4. The band at 1,428 nm, ascribed to hydration water, belongs to the WAMACS C6. In numerous studies, this band was attributed to amorphous regions in cellulose (79–84); however, in the case of strawberry, this water is associated with other polysaccharides. It seems that absorbance increase at this band is associated with drying and increased density (80, 85). There are several research studies that report bands from this particular WAMACS region, as important for the changes during processing and storage. For example, band 1,420 nm was found to be the optimal wavelength for vitamin C content prediction in apple slices during drying (77) and also had high correlation with internal quality of fruit (86, 87). Absorbance at 1,420 nm was in another study reported to be closely related to weight loss during the storage of mushrooms (88), while in another study, it was found that the absorbance at this band particularly increases as a function of storage time [similar to the change of soluble solids content (SSC)] (87). It is worth noting that, in difference spectra, there was actually a minimal change in absorbance at 1,416 nm in the case of CF and 1,422 nm in the case of SCF. While it is not clear what exactly is the difference between the bands 1,416, 1,422, and 1,428 nm, seeing that they are usually attributed to the same water molecular

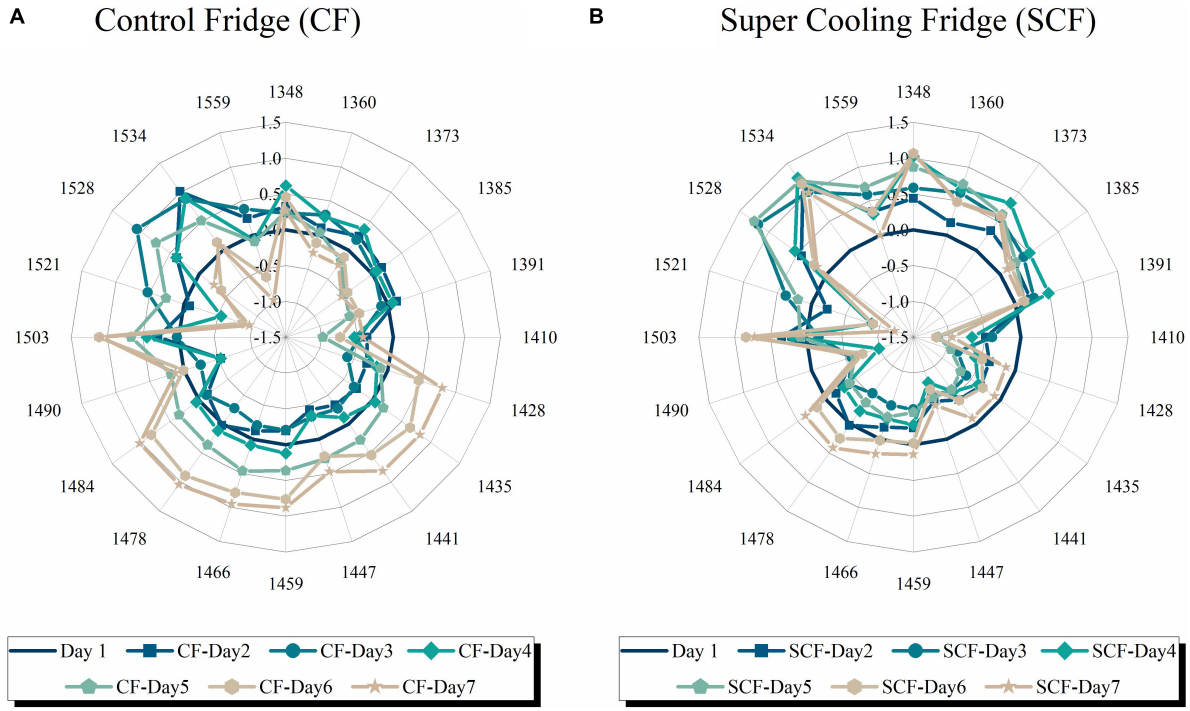

FIGURE 7
Aquagrams of strawberries showing changes in water molecular matrix of the fruit flesh during 7 days of storage in: **(A)** Control fridge (CF) and **(B)** supercooling fridge.

conformation, it is worth noting that this WAMACS region is repeatedly showing the importance of the changes during storage and internal quality of vegetable and fruits. The stark difference in behavior of absorbance at the band 1,428 nm, depending on whether strawberries were stored in CF and SCF seems to further indicate the importance of this band for preservation in cold storage, most probably because it is related to the state of turgor and cytoplasm in the cells, its shrinkage and pulling away from the cell walls. That may explain why the bands from this WAMACS region were so often found related to internal quality, damage, and vitamin C production, seeing that production of vitamin C is the part of the protection against damage. The behavior of absorbance at this band in the case of CF seems to be in agreement with the typical changes during storage; however, the opposite behavior in the case of SCF seems to indicate the presence of electric field slows down this process.

The absorbance bands from 1,435 to 1,490 nm can be related to the water molecular species interacting with biomolecules (1,435 nm), water species participating in hydration (1,459 nm) and water molecules bonding to each other, i.e., creating clusters with 1–4 hydrogen bonds. In the research about the texture of apples, it was found that water spectral pattern characterized by the low absorbance in the region 1,344–1,382 nm and high at 1,410–1,492 nm corresponds to the firm, juicy, and crispy sensory profile (36). The difference in these two particular absorbance regions, in the case of strawberries, might indicate that the presence of electric field actually slows down the process of post-harvest ripening of strawberries in the cold storage.

Next, common for both refrigeration conditions, there is a sharp decrease in absorbance at 1,492 nm, water absorbance band of water molecules with four hydrogen bonds, one of the two bands, the other one being 1,410 nm, free water molecules, related to the influence of temperature (89). For pure water, if the temperature increases the absorbance at the band 1,492 nm will decrease, while at 1,410 nm increase, because the temperature causes breaking of the hydrogen bonds in tetrahedral structure creating more free molecules. It is, therefore, interesting that in strawberry after the fruit was placed in the cold storage there was a decrease in absorbance at this particular band. This might indicate that there is an innate mechanism in the fruit which fights the creation of this type of hydrogen-bonded water. However, it seems that with the progress of time, this mechanism fails in the case of the CF, where increase in absorbance can be observed after day 4, which suggests creation of seeds of ice crystals that may become the source of damage. From this aspect, the presence of electric field in the SCF seems to act protectively.

The behavior of absorbance at band 1,503 nm is common for both storage conditions; there is a sharp, strong increase in absorbance immediately upon the storage. There are many reports about this particular band in characterization of minerals and attributed to vibrational mode of hydrous defects

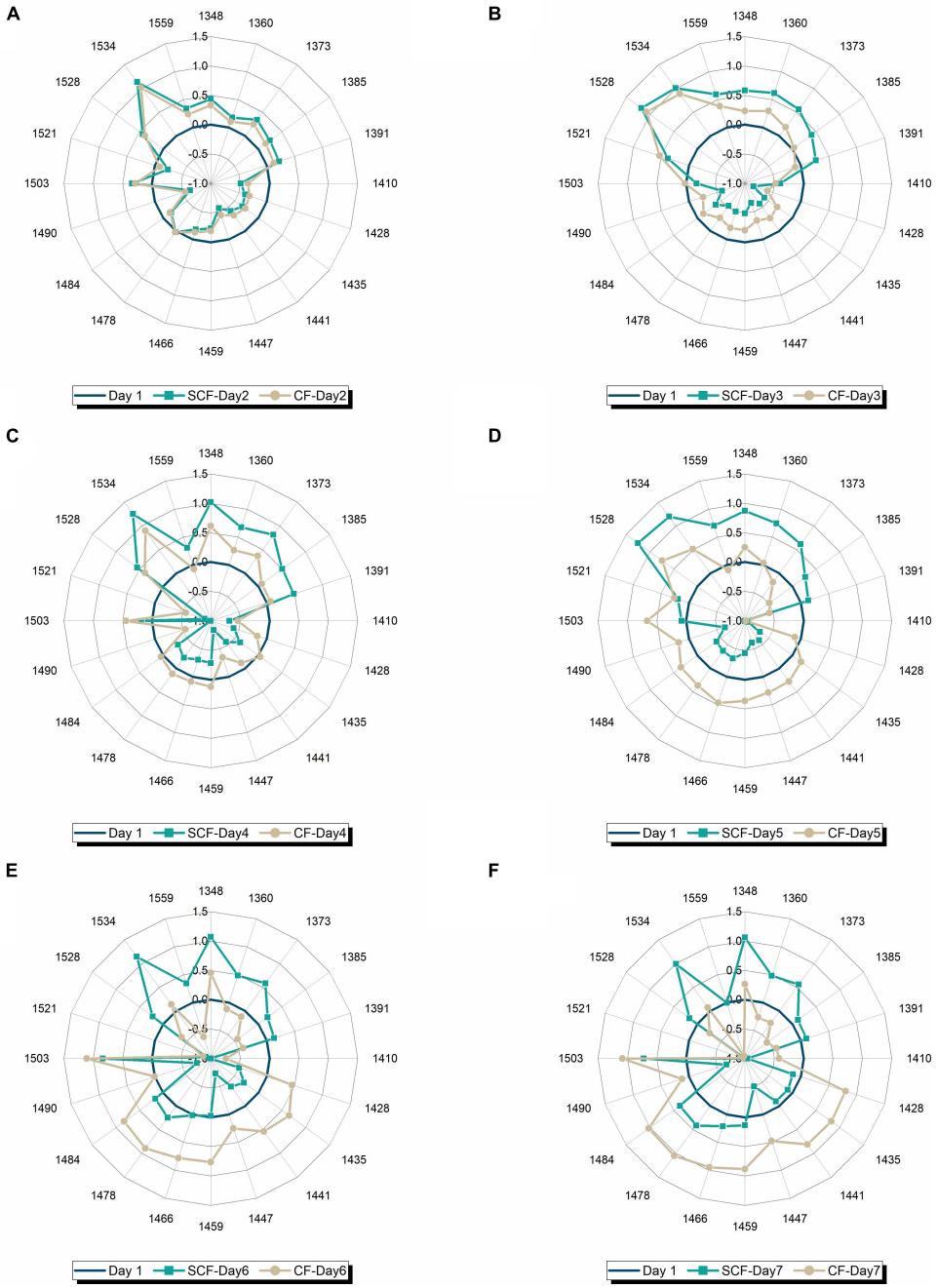

FIGURE 8
Comparison of water spectral patterns of strawberries stored in control (CF) and supercooling fridge (SCF) on day-to-day basis: **(A)** After 1 day of storage, **(B)** after 2 days of storage, **(C)** after 3 days of storage, **(D)** after 4 days of storage, **(E)** after 5 days of storage, and **(F)** after 1 week of cold storage.

in the crystal structure (90–96). In analogy to these reports, the absorbance at this band can be considered as indicator of shallow, superficial, surface damage, and small openings in the structure of materials that enhance exposure to the environment. If this is correct interpretation that would mean some surface damage on the strawberry skin appeared in both storage conditions, leaving the fruit vulnerable. The region beyond 1,503 nm, encompassing bands from 1,521 to 1,559 nm includes absorbance bands of water species that are tightly bound to the structural elements of the fruit tissue, including crystalline and polymer-bound water (97–100) and represent the water that cannot be lost to processes such as drying or squeezing (101); this water is lost only if the structural elements associated with it are lost. The difference between the

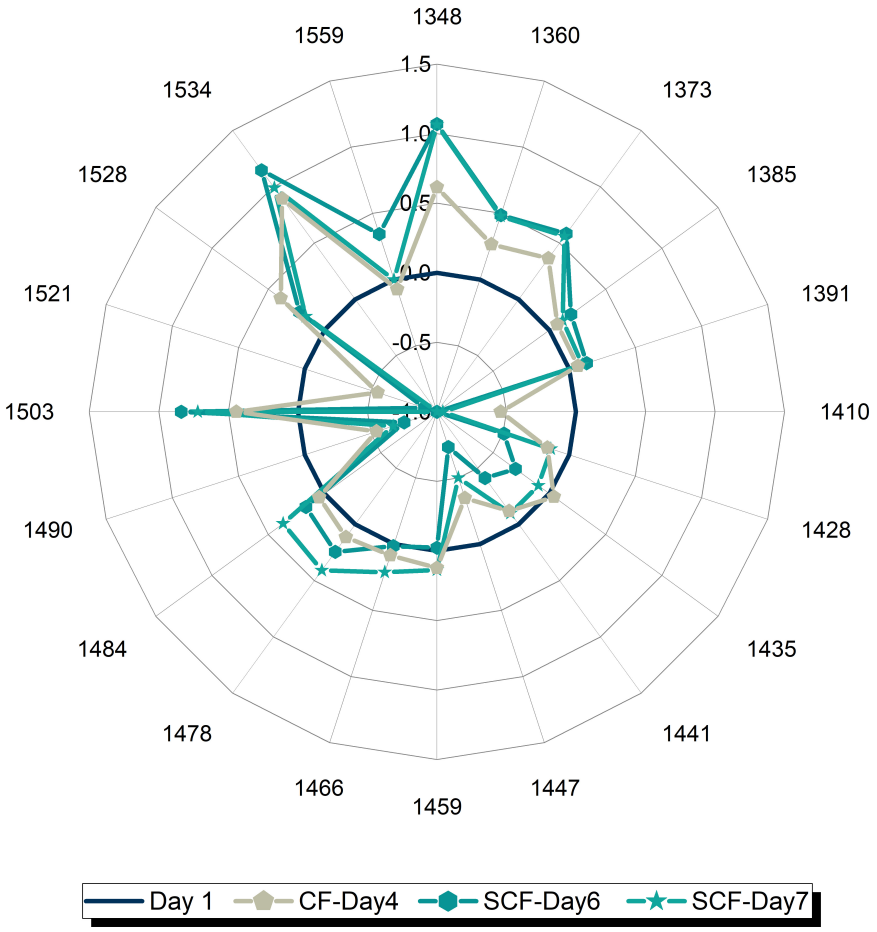

FIGURE 9
Comparison of water spectral patterns of strawberries in the control fridge (CF) on day 4 and strawberries in supercooling fridge (SCF) on days 6 and 7 shows that the presence of electric field delays the ripening in cold storage.

water species absorbing at particular bands is in the level of complexity of the structure they are engaged in, and in the strength of the bonds, which is increased with the increase in wavelength. Having this in mind, it seems that in both cold storage conditions, the strawberries suffered some level of tissue damage, seeing a sharp decrease at 1,521 and 1,559 nm bands. The band at 1,534 nm was often attributed to strongly bound water (102, 103) related to water–polymers interaction [such as cellulose (104)] that appears during initial phases of drying (105), while the band at 1,559 nm is typically assigned to bond vibration of O–H stretch in crystalline cellulose (104, 106). Here, it is important to note that while other reports are attributing these bands to cellulose, they are in fact water absorbance bands, and in the case of strawberries, this strongly bound water is bound to numerous polysaccharides, typical building block of cell walls. With the progress of time in storage, the decrease in absorbance can be observed at all those bands in the case of CF, but not in the case of SCF.

The second most striking difference between the spectral patterns of strawberries in CF and SCF seems to be exactly the decrease in absorbance at the bands of strongly bound water. This seems to be connected with the increase in absorbance of the so-called bulk water, all those small clusters of hydrogen-bonded water species observed earlier in the region 1,435–1,484 nm, which happens in the case of the CF. While the strongly bound water, as the term itself clearly indicates, is strongly bound to structures in the fruit, the bulk water is water not associated to fruit, it is the "water hydrating other water molecules". The decrease in strongly bound water can be connected to softening of the fruit during ripening and increased bulk water with swelling and expansion of vacuolar volume (107). Since these changes are not present in the SCF, it suggests that ripening of strawberries is delayed by the presence of electric field.

To examine better this possibility and see better the transformation of water spectral pattern over time, a series of aquagrams was created showing comparison of water

TABLE 2 Water matrix coordinates (WAMACS) that can be used to describe the changes during post-harvest ripening of strawberries during cold storage.

Absorbance band (nm)	Roles/Functionality/Importance in certain biological processes
1348	Self-organization (44), germination (42), changes during storage (56), and viability (119)
1360	Germination (42), water activity and changes during storage (56), hardness (120), viability (119), and texture (36)
1373	One of the bands of water vapor, proton hydration/indicator of changes in sucrose content (121), viability (119), water activity and changes during storage (56), and texture (36)
1385	Hydration of ions/important for pH modeling (122), and firmness and texture (36)
1391	Drying, dehydration, expulsion of cellular water, damage, stress, infection (101, 119, 123); and indicate the amount of vitamin C content (124)
1410	Moisture content, water activity, seed viability, firmness (125, 126); and indicate the amount of vitamin C content (124)
1428	Protein hydration, protein folding (127), water activity (56, 128), damage, and defects
1435	Phase transition, carbohydrates–water interaction, hardness, and viability (56)
1441	Preservation during desiccation stress (78)
1447	Water activity, biotic and abiotic stress indicator, preservation, and damage (36, 37, 40–42, 56)
1459	Water activity, biotic and abiotic stress indicator, preservation, and damage (36, 37, 40–42, 56)
1466	Protein–water interaction (127, 129)
1478	Semi-crystalline water associated with cellulose (81) or other polymers related to mechanical properties like stiffness (81)
1484	Associated with cellulose (104, 130, 131) or other polymers indicator of preservation of tissues, damage (113)
1490	Water activity, biotic and abiotic stress indicator, preservation, and damage (36, 37, 40–42, 56)
1503	Skin disease in plants and animals (132, 133) defects in minerals (90–96, 134), and structural defects in starch (135)
1521	Structural water; water–cellulose interaction (104), water–carbohydrate interaction (136), water–fibre (starch) interaction (137), important for discrimination of fresh/thawed meat, characteristic of fresh meat (138, 139), associated with differences in level of mechanical damage (113)
1528	Structural water; water–cellulose interaction (104), water–carbohydrate interaction (136), water–fiber (starch) interaction (137), important for discrimination of fresh/thawed meat, characteristic of fresh meat (138, 139), associated with differences in level of mechanical damage (113)
1534	Structural water; water–cellulose interaction (104), indicator of drying (105), water–protein interaction, water sorption, and clustering of water sorbed molecules (103)
1559	Structural water; associated with starch or cellulose (140, 141) and other polymers (106, 142, 143), associated with sugars (142, 144–146), associated with proteins (147) or amino compounds (148), associated with membrane structure, influenced by temperature (117), related to mechanical properties (106), indicator of fermentation (149), indicative of vegetative growth stage (142), indicator of crystallinity (118, 150), indicator of preservation of tissues, damage (113)

Currently available information and the tentative functionality of corresponding water species in biological and aqueous systems.

spectral patterns of strawberries in CF and SCF, 1 day at a time (**Figures 8A–F**). From this series of plots, the first interesting observation is that the patterns after 1 day of storage (**Figure 8A**) are nearly identical, testifying to the equality of the samples at the beginning of the experimental period, while the last plot (**Figure 8F**) shows remarkably well how different storage conditions led to the completely different water spectral patterns, i.e., how spectral pattern as a multidimensional marker accurately depicted the difference in the final state of the strawberries caused by different storage conditions. The first changes can be observed on day 3 of storage (**Figure 8B**) where higher absorbance can be observed at strongly bound water bands (1,528–1,559 nm) and at vapor-like and trapped water (1,348–1,391 nm) in the case of strawberries in SCF. This increase is continued over subsequent days (**Figures 8C–F**), while the spectral pattern of strawberries in CF is primarily characterized by decrease of absorbance at strongly bound water bands, and large increase in absorbance of bulk water. But the patterns become more and more similar, for example, the pattern of strawberries in SCF fridge on day 7 (**Figure 8F**) looks very much like the pattern of strawberries in CF fridge on day 4 (**Figure 8C**). This strongly suggests the fruit is going through the similar process, but with some time delay in the case of SCF fridge. To test this assumption, one more aquagram is created (**Figure 9**), where the water spectral patterns of strawberries on days 6 and 7 in SCF are compared to the spectral pattern of strawberries in CF on day 4. The spectral patterns show strikingly similar shape, indicating that the fruit indeed goes through a similar process, which is in SCF delayed for around 3 days. The possible mechanism of how this happens might be explained by the influence of electric field on the surface hardening of the strawberries, which limit the water diffusion and thus evaporation, as research findings reported to be the case in electric field treated apples post-harvest (108). This would be very consistent with the observed increased absorbance of strongly bound water and conserved vapor-like water within strawberries in SCF.

The important finding in this study also is that the water spectral pattern as a multidimensional biomarker captures perfectly the process of ripening and shows that it can

be described only by using water absorbance bands. The consistently found importance of these particular bands was confirmed through several analyses and they can be considered as WAMACS or water matrix coordinates that define the space of variables describing the changes of postharvest ripening that can probably be used for other biological systems as well. Numerous research works have already found these bands related to certain functionalities in other bio-aqueous systems, and this information is summarized in Table 2.

Conclusion

This study aimed at investigating the spectral changes during the storage of strawberry in order to confirm the potential of aquaphotomics NIRS for monitoring during cold storage. Further, the same technology was applied to assess the influence of the storage environments with a particular objective to find and explain the differences in applied cooling systems [without (CF) and with the electric field exposure (SCF)] on the stored fruit. The water matrix transformation during the post-harvest degradation of strawberry as well as the influence of electric field could be observed using the NIR spectra of strawberries in the 1,300–1,600 nm region.

Over the course of several analyses, the same water absorbance bands were found to be important for the description of the changes in fruit during storage. The main outcomes of the analyses were that it was possible to detect spectral changes over storage and predict the time spent in storage. The consistently repeating water absorbance bands were used to define water spectral patterns as biomarkers of the state of the strawberries in cold storage and allowed comparison of strawberries stored in different conditions. This comparison showed that the presence of electric field in supercooling fridge slows down the ripening processing, delaying it for about 3 days. The possible mechanism behind can be explained by the influence of electric field on skin hardening, which then acts as a natural coating and slows down evaporation. This agreed with the lower water loss percentage recorded for strawberries in the supercooling fridge.

Using this technique of spectral monitoring, the ripening process can be observed in a non-destructive way. This provides the potential of aquaphotomics using NIR for the post-harvest monitoring, and quality evaluation of strawberry and other agricultural products at different storage conditions.

Data availability statement

The raw data supporting the conclusions of this article will be made available by the authors, without undue reservation.

Author contributions

TF, TK, and RT: conceptualization and resources. RT, SA, and JM: methodology and investigation. SA: software. SA, TF, and RT: validation. SA and JM: formal analysis, writing—original draft preparation, and visualization. SA and RT: data curation. JM: writing—review and editing. RT: supervision and project administration. RT and TK: funding acquisition. All authors read and agreed to the published version of the manuscript.

Acknowledgments

SA gratefully acknowledges the financial support provided by the government scholarships from the Office of the Civil Service Commission (OCSC), Thailand. We gratefully acknowledge the help of Nichiei Intec Co., Ltd., Japan for providing the refrigerators used for cold storage.

Conflict of interest

The cooling systems examined in this study are produced by the Nichiei Intec Co., Ltd., a company where TF and TK were employed. All opinions presented in this manuscript belong to the authors alone, and not to any institution to which they are or were affiliated.

The remaining authors declare that the research was conducted in the absence of any commercial or financial relationships that could be construed as a potential conflict of interest.

Publisher's note

Supplementary material

The Supplementary Material for this article can be found online at: https://www.frontiersin.org/articles/10.3389/fnut.2022.1058173/full#supplementary-material

References

1. Seeram N, Adams L, Zhang Y, Lee R, Sand D, Scheuller H, et al. Blackberry, black raspberry, blueberry, cranberry, red raspberry, and strawberry extracts inhibit growth and stimulate apoptosis of human cancer cells in vitro. *J Agric Food Chem.* (2006) 54:9329–39. doi: 10.1021/jf061750g

2. Yang F, Li H, Li F, Xin Z, Zhao L, Zheng Y, et al. Effect of nano-packing on preservation quality of fresh strawberry (fragaria ananassa duch. cv fengxiang) during storage at 4 °c. *J Food Sci.* (2010) 75:C236–40. doi: 10.1111/j.1750-3841.2010.01520.x

3. Basu A, Nguyen A, Betts N, Lyons T. Strawberry as a functional food: an evidence-based review. *Crit Rev Food Sci Nutr.* (2014) 54:790–806. doi: 10.1080/10408398.2011.608174

4. Vu K, Hollingsworth R, Leroux E, Salmieri S, Lacroix M. Development of edible bioactive coating based on modified chitosan for increasing the shelf life of strawberries. *Food Res Int.* (2011) 44:198–203. doi: 10.1016/j.foodres.2010.10.037

5. Hernández-Muñoz P, Almenar E, Ocio M, Gavara R. Effect of calcium dips and chitosan coatings on postharvest life of strawberries (Fragaria x ananassa). *Postharvest Biol Technol.* (2006) 39:247–53. doi: 10.1016/j.postharvbio.2005.11.006

6. Crisosto C, Garner D, Doyle J, Day K. Relationship between fruit respiration, bruising susceptibility, and temperature in sweet cherries. *HortScience.* (1993) 28:132–5. doi: 10.21273/HORTSCI.28.2.132

7. Tahir H, Xiaobo Z, Jiyong S, Mahunu G, Zhai X, Mariod A. Quality and postharvest-shelf life of cold-stored strawberry fruit as affected by gum arabic (*Acacia senegal*) edible coating. *J Food Biochem.* (2018) 42:e12527. doi: 10.1111/jfbc.12527

8. Han C, Zhao Y, Leonard S, Traber M. Edible coatings to improve storability and enhance nutritional value of fresh and frozen strawberries (Fragaria x ananassa) and raspberries (Rubus ideaus). *Postharvest Biol Technol.* (2004) 33:67–78. doi: 10.1016/j.postharvbio.2004.01.008

9. BaoGang W, WenSheng L, JunJun Y, Lei S, XiaoYuan F, YuRu H, et al. Effect of pre-cooling on qualities of strawberry during logistics. *J Fruit Sci.* (2013) 30:878–83.

10. Barrazueta-Rojas S, Falconí J, Ojeda M, Oleas-López J, Mendoza-Zurita G. Pysicochemical properties and application of edible coatings in strawberry Fragaria × ananassa) preservation. *Rev Fac Nac Agron Medellin.* (2018) 71:8631–41. doi: 10.15446/rfnam.v71n3.73548

11. Pan J, Vicente A, Martínez G, Chaves A, Civello P. Combined use of UV-C irradiation and heat treatment to improve postharvest life of strawberry fruit. *J Sci Food Agric.* (2004) 84:1831–8. doi: 10.1002/jsfa.1894

12. Petriccione M, Mastrobuoni F, Pasquariello M, Zampella L, Nobis E, Capriolo G, et al. Effect of chitosan coating on the postharvest quality and antioxidant enzyme system response of strawberry fruit during cold storage. *Foods.* (2015) 4:501–23. doi: 10.3390/foods4040501

13. Barikloo H, Ahmadi E. Effect of nanocomposite-based packaging and chitosan coating on the physical, chemical, and mechanical traits of strawberry during storage. *J Food Meas Charact.* (2018) 12:1795–817. doi: 10.1007/s11694-018-9795-3

14. Wang Y, Li R, Lu R, Xu J, Hu K, Liu Y. Preparation of Chitosan/Corn Starch/Cinnamaldehyde Films for Strawberry Preservation. *Foods.* (2019) 8:423. doi: 10.3390/foods8090423

15. Lal Basediya A, Samuel D, Beera V. Evaporative cooling system for storage of fruits and vegetables - A review. *J Food Sci Technol.* (2013) 50:429–42. doi: 10.1007/s13197-011-0311-6

16. Pérez A, Olías R, Olías J, Sanz C. Strawberry quality as a function of the "high pressure fast cooling" design. *Food Chem.* (1998) 62:161–8. doi: 10.1016/S0308-8146(97)00211-2

17. Nunes M, Brecht J, Sargent S, Morais A. Effects of delays to cooling and wrapping on strawberry quality (cv. Sweet Charlie). *Food Control.* (1995) 6:323–8. doi: 10.1016/0956-7135(95)00024-0

18. Ouattara B, Sabato S, Lacroix M. Use of gamma-irradiation technology in combination with edible coating to produce shelf-stable foods. *Radiat Phys Chem.* (2002) 63:305–10. doi: 10.1016/S0969-806X(01)00517-5

19. Harker F, Elgar H, Watkins C, Jackson P, Hallett I. Physical and mechanical changes in strawberry fruit after high carbon dioxide treatments. *Postharvest Biol Technol.* (2000) 19:139–46. doi: 10.1016/S0925-5214(00)00090-9

20. Lazaridou A, Biliaderis C. Thermophysical properties of chitosan, chitosan-starch and chitosan-pullulan films near the glass transition. *Carbohydr Polym.* (2002) 48:179–90. doi: 10.1016/S0144-8617(01)00261-2

21. Jayakumar R, Nwe N, Tokura S, Tamura H. Sulfated chitin and chitosan as novel biomaterials. *Int J Biol Macromol.* (2007) 40:175–81. doi: 10.1016/j.ijbiomac.2006.06.021

22. Plumb A, Downing P, Parry A. *Consumer attitudes to food waste and food packaging*. Barbury,: Wrap (2013). p. 75.

23. Céline M, Valérie G, Karine G, Sandrine C, Nathalie G, Stéphane G, et al. Consumer behaviour in the prediction of postharvest losses reduction for fresh strawberries packed in modified atmosphere packaging. *Postharvest Biol Technol.* (2020) 163:111119. doi: 10.1016/j.postharvbio.2020.111119

24. Yokokawa N, Kikuchi-Uehara E, Sugiyama H, Hirao M. Framework for analyzing the effects of packaging on food loss reduction by considering consumer behavior. *J Clean Prod.* (2018) 174:26–34. doi: 10.1016/j.jclepro.2017.10.242

25. Holcroft D, Kader A. Carbon dioxide–induced changes in color and anthocyanin synthesis of stored strawberry fruit. *HortScience.* (1999) 34:1244–8.

26. Pelayo C, Ebeler S, Kader A. Postharvest life and flavor quality of three strawberry cultivars kept at 5°C in air or air+20 kPa CO2. *Postharvest Biol Technol.* (2003) 27:171–83. doi: 10.1016/S0925-5214(02)00059-5

27. Klopotek Y, Otto K, Böhm V. Processing strawberries to different products alters contents of vitamin C, total phenolics, total anthocyanins, and antioxidant capacity. *J Agric Food Chem.* (2005) 53:5640–6. doi: 10.1021/jf047947v

28. Ivanovich K, Evgenyevich S, Vasilyevich G, Nikolaevna D, Igorevich V. Features of usage of electromagnetic field of extremely low frequency for the storage of agricultural products. *J Electromagn Anal Appl.* (2013) 05:236–41. doi: 10.4236/jemaa.2013.55038

29. Aslanova M, Dydykin A, Fedulova LV, Derevitskaya O. An effect of the electromagnetic treatment on oxidative stability and microbiological safety of meat semi-prepared products. *Theory Pract meat Process.* (2017) 2:39–48. doi: 10.21323/2414-438X-2017-2-3-39-48

30. Ahmed J, Ramaswamy H. Applications of magnetic field in food preservation. In: Rahman M editor. *Handbook of food preservation*. Boca Raton: CRC Press (2020). p. 873–84. doi: 10.1201/9780429091483-55

31. Guo L, Azam S, Guo Y, Liu D, Ma H. Germicidal efficacy of the pulsed magnetic field against pathogens and spoilage microorganisms in food processing: an overview. *Food Control.* (2022) 136:108496. doi: 10.1016/J.FOODCONT.2021.108496

32. Kang T, You Y, Jun S. Supercooling preservation technology in food and biological samples: a review focused on electric and magnetic field applications. *Food Sci Biotechnol.* (2020) 29:303–21. doi: 10.1007/S10068-020-00750-6/FIGURES/6

33. Workman J. *Handbook of organic compounds: NIR, IR, Raman, and UV spectra featuring polymers and surfaces*. San Diego, CA: Academic Press (2001). p. 503.

34. Tsenkova R. Introduction aquaphotomics: dynamic spectroscopy of aqueous and biological systems describes peculiarities of water. *J Near Infrared Spectrosc.* (2009) 17:303–14.

35. Tsenkova R. Aquaphotomics: dynamic spectroscopy of aqueous and biological systems describes peculiarities of water. *J Near Infrared Spectrosc.* (2009) 17:303–13.

36. Vanoli M, Lovati F, Grassi M, Buccheri M, Zanella A, Cattaneo MP, et al. Water spectral pattern as a marker for studying apple sensory texture. *Adv Hortic Sci.* (2018) 32:343–51. doi: 10.13128/ahs-22380

37. Cattaneo T, Cutini M, Cammerata A, Stellari A, Marinoni L, Bisaglia C, et al. Near infrared spectroscopic and aquaphotomic evaluation of the efficiency of solar dehydration processes in pineapple slices. *J Near Infrared Spectrosc.* (2021) 29:352–8.

38. Kaur H. *Investigating aquaphotomics for fruit quality assessment*. Hamilton: The University of Waikato (2020). p. 227.

39. Kaur H, Künnemeyer R, McGlone A. Investigating aquaphotomics for temperature-independent prediction of soluble solids content of pure apple juice. *J Near Infrared Spectrosc.* (2020) 28:103–12. doi: 10.1177/0967033519898891

40. Cattaneo T, Vanoli M, Grassi M, Rizzolo A, Barzaghi S. The aquaphotomics approach as a tool for studying the influence of food coating materials on cheese and winter melon samples. *J Near Infrared Spectrosc.* (2016) 24:381–90. doi: 10.1255/jnirs.1238

41. Marinoni L, Buccheri M, Bianchi G, Cattaneo T. Aquaphotomic, E-nose and electrolyte leakage to monitor quality changes during the storage of ready-to-eat rocket. *Molecules.* (2022) 27:2252. doi: 10.3390/molecules27072252

42. Nugraha D, Zaukuu J, Bósquez J, Bodor Z, Vitalis F, Kovacs Z. Near-infrared spectroscopy and aquaphotomics for monitoring mung bean (*Vigna radiata*) sprout growth and validation of ascorbic acid content. *Sensors.* (2021) 21:611. doi: 10.3390/S21020611

43. Tsenkova R, Muncan J. *Aquaphotomics for bio-diagnostics in dairy - applications of near-infrared spectroscopy*. Singapore: Springer (2021).

44. Muncan J, Kovacs Z, Pollner B, Ikuta K, Ohtani Y, Terada F, et al. Near infrared aquaphotomics study on common dietary fatty acids in cow's liquid, thawed milk. *Food Control.* (2020) 122:107805. doi: 10.1016/j.foodcont.2020.107805

45. Slavchev A, Kovacs Z, Koshiba H, Bazar G, Pollner B, Krastanov A, et al. Monitoring of water spectral patterns of lactobacilli as a tool for rapid selection of probiotic candidates. *J Near Infrared Spectrosc.* (2017) 25:423–31.

46. Slavchev A, Kovacs Z, Koshiba H, Nagai A, Bázár G, Krastanov A, et al. Monitoring of water spectral pattern reveals differences in probiotics growth when used for rapid bacteria selection. *PLoS One.* (2015) 10:e0130698. doi: 10.1371/journal.pone.0130698

47. Muncan J, Tei K, Tsenkova R. Real-time monitoring of yogurt fermentation process by aquaphotomics near-infrared spectroscopy. *Sensors.* (2021) 21:177. doi: 10.3390/s21010177

48. Morita H, Hasunuma T, Vassileva M, Kondo A, Tsenkova R. A new screening method for recombinant Saccharomyces cerevisiae strains based on their xylose fermentation ability measured by near infrared spectroscopy. *Anal Methods.* (2014) 6:6628–34. doi: 10.1039/c4ay00785a

49. Morita H, Hasunuma T, Vassileva M, Tsenkova R, Kondo A. Near infrared spectroscopy as high-throughput technology for screening of xylose-fermenting recombinant Saccharomyces cerevisiae strains. *Anal Chem.* (2011) 83:4023–9. doi: 10.1021/ac103128p

50. Kinoshita K, Miyazaki M, Morita H, Vassileva M, Tang C, Li D, et al. Spectral pattern of urinary water as a biomarker of estrus in the giant panda. *Sci Rep.* (2012) 2:856. doi: 10.1038/srep00856

51. Kinoshita K, Morita H, Miyazaki M, Hama N, Kanemitsu H, Kawakami H, et al. Near infrared spectroscopy of urine proves useful for estimating ovulation in giant panda (*Ailuropoda melanoleuca*). *Anal Methods.* (2010) 2:1671–5. doi: 10.1039/c0ay00333f

52. Santos-Rivera M, Woolums A, Thoresen M, Meyer F, Vance C. Bovine respiratory syncytial virus (BRSV) infection detected in exhaled breath condensate of dairy calves by near-infrared aquaphotomics. *Molecules.* (2022) 27:549. doi: 10.3390/MOLECULES27020549

53. Santos-Rivera M, Woolums A, Thoresen M, Blair E, Jefferson V, Meyer F, et al. Profiling Mannheimia haemolytica infection in dairy calves using near infrared spectroscopy (NIRS) and multivariate analysis (MVA). *Sci Rep.* (2021) 11:1392. doi: 10.1038/s41598-021-81032-x

54. Cui X, Yu X, Cai W, Shao X. Water as a probe for serum–based diagnosis by temperature– dependent near–infrared spectroscopy. *Talanta.* (2019) 204:359–66. doi: 10.1016/j.talanta.2019.06.026

55. Li Y, Guo L, Li L, Yang C, Guang P, Huang F, et al. Early diagnosis of type 2 diabetes based on near-infrared spectroscopy combined with machine learning and aquaphotomics. *Front Chem.* (2020) 8:580489. doi: 10.3389/fchem.2020.580489

56. Malegori C, Muncan J, Mustorgi E, Tsenkova R, Oliveri P. Analysing the water spectral pattern by near-infrared spectroscopy and chemometrics as a dynamic multidimensional biomarker in preservation: rice germ storage monitoring. *Spectrochim Acta A Mol Biomol Spectrosc.* (2022) 265:120396. doi: 10.1016/J.SAA.2021.120396

57. van de Kraats E, Munćan J, Tsenkova R. Aquaphotomics – origin, concept, applications and future perspectives. *Substantia.* (2019) 3:13–28. doi: 10.13128/substantia-702

58. Muncan J, Tsenkova R. Aquaphotomics—from innovative knowledge to integrative platform in science and technology. *Molecules.* (2019) 24:2742. doi: 10.3390/molecules24152742

59. Tsenkova R, Kovacs Z, Kubota Y. Aquaphotomics: near infrared spectroscopy and water states in biological systems. In: DiSalvo E editor. *Membrane hydration*. Cham: Springer (2015). p. 189–211. doi: 10.1007/978-3-319-19060-0_8

60. Muncan J, Aouadi B, Tsenkova R. New perspectives in plant and plant-based food quality determination: aquaphotomics. In: Goyal M, Kovacs Z, Nath A, Suleria H editors. *Plant-based bioactives, functional foods, beverages and medicines: processing, analysis and health benefit*. New Jersey, NJ: Apple Academic Press (2023).

61. Nichiei Intec Co. Ltd. 日栄インテックの鮮度保持システム - *Nichi intec preservation system*. (2018). Available online at: https://www.nichieiintec.jp/scs/ (accessed September 13, 2022).

62. Dhanoa M, Barnes R, Lister S. Standard normal variate transformation and de-trending of near-infrared diffuse reflectance spectra. *Appl Spectrosc.* (1989) 43:772–7.

63. Wold S, Sjostrom M. *SIMCA: a method for analyzing chemical data in terms of similarity and analogy*. Washington, DC: American Chemical Society (1977). p. 243–82. doi: 10.1021/bk-1977-0052.ch012

64. Martens H, Martens M. *Multivariate analysis of quality?: an introduction*. New York, NY: Wiley (2001). p. 445.

65. Gowen A, Downey G, Esquerre C, O'Donnell C. Preventing over-fitting in PLS calibration models of near-infrared (NIR) spectroscopy data using regression coefficients. *J Chemom.* (2011) 25:375–81. doi: 10.1002/cem.1349

66. Tsenkova R. Aquaphotomics: water in the biological and aqueous world scrutinised with invisible light. *Spectrosc Eur.* (2010) 22:6–10.

67. Tsenkova R, Munćan J, Pollner B, Kovacs Z. Essentials of aquaphotomics and its chemometrics approaches. *Front Chem.* (2018) 6:363. doi: 10.3389/fchem.2018.00363

68. Kovacs Z, Muncan J, Veleva P, Oshima M, Shigeoka S, Tsenkova R. Aquaphotomics for monitoring of groundwater using short-wavelength near-infrared spectroscopy. *Spectrochim Acta Part A Mol Biomol Spectrosc.* (2022) 279:121378. doi: 10.1016/J.SAA.2022.121378

69. Jiang Y, Yu L, Hu Y, Zhu Z, Zhuang C, Zhao Y, et al. The preservation performance of chitosan coating with different molecular weight on strawberry using electrostatic spraying technique. *Int J Biol Macromol.* (2020) 151:278–85. doi: 10.1016/j.ijbiomac.2020.02.169

70. Aharoni Y, Barkai-Golan R. Pre-harvest fungicide sprays and polyvinyl wraps to control Botrytis rot and prolong the post- harvest storage life of strawberries. *J Hortic Sci.* (1987) 62:177–81. doi: 10.1080/14620316.1987.11515767

71. Dhital R, Mora N, Watson D, Kohli P, Choudhary R. Efficacy of limonene nano coatings on post-harvest shelf life of strawberries. *LWT.* (2018) 97:124–34. doi: 10.1016/J.LWT.2018.06.038

72. Shehata S, Abdeldaym E, Ali M, Mohamed R, Bob R, Abdelgawad K. Effect of some citrus essential oils on post-harvest shelf life and physicochemical quality of strawberries during cold storage. *Agron.* (2020) 10:1466. doi: 10.3390/AGRONOMY10101466

73. Bahmani R, Razavi F, Mortazavi S, Gohari G, Juárez-Maldonado A. Evaluation of proline-coated chitosan nanoparticles on decay control and quality preservation of strawberry fruit (cv. Camarosa) during cold storage. *Horticulture.* (2022) 8:648. doi: 10.3390/HORTICULTURAE8070648

74. Hernández-Carrillo J, Orta-Zavalza E, González-Rodríguez S, Montoya-Torres C, Sepúlveda-Ahumada D, Ortiz-Rivera Y. Evaluation of the effectivity of reuterin in pectin edible coatings to extend the shelf-life of strawberries during cold storage. *Food Packag Shelf Life.* (2021) 30:100760. doi: 10.1016/J.FPSL.2021.100760

75. Tanada-Palmu P, Grosso C. Effect of edible wheat gluten-based films and coatings on refrigerated strawberry (Fragaria ananassa) quality. *Postharvest Biol Technol.* (2005) 36:199–208. doi: 10.1016/j.postharvbio.2004.12.003

76. Kojić D, Tsenkova R, Tomobe K, Yasuoka K, Yasui M. Water confined in the local field of ions. *ChemPhysChem.* (2014) 15:4077–86. doi: 10.1002/cphc.201402381

77. Arefi A, Sturm B, von Gersdorff G, Nasirahmadi A, Hensel O. Vis-NIR hyperspectral imaging along with Gaussian process regression to monitor quality attributes of apple slices during drying. *LWT.* (2021) 152:112297.

78. Kuroki S, Tsenkova R, Moyankova D, Muncan J, Morita H, Atanassova S, et al. Water molecular structure underpins extreme desiccation tolerance of the resurrection plant Haberlea rhodopensis. *Sci Rep.* (2019) 9:3049. doi: 10.1038/s41598-019-39443-4

79. Fujimoto T, Kobori H, Tsuchikawa S. Prediction of wood density independently of moisture conditions using near infrared spectroscopy. *J Near Infrared Spectrosc.* (2012) 20:353–9. doi: 10.1255/jnirs.994

80. Tsuchikawa S, Hirashima Y, Sasaki Y, Ando K. Near-infrared spectroscopic study of the physical and mechanical properties of wood with meso- and micro-scale anatomical observation. *Appl Spectrosc.* (2005) 59:86–93. doi: 10.1366/0003702052940413

81. Fujimoto T, Yamamoto H, Tsuchikawa S. Estimation of wood stiffness and strength properties of hybrid larch by near-infrared spectroscopy. *Appl Spectrosc.* (2007) 61:882–8. doi: 10.1366/000370207781540150

82. Rambo M, Ferreira M. Determination of cellulose crystallinity of banana residues using near infrared spectroscopy and multivariate analysis. *J Braz Chem Soc.* (2015) 26:1491–9. doi: 10.5935/0103-5053.20150118

83. Tsuchikawa S, Murata A, Kohara M, Mitsui K. Spectroscopic monitoring of biomass modification by light-irradiation and heat treatment. *J Near Infrared Spectrosc.* (2003) 11:401–5. doi: 10.1255/jnirs.391

84. Wu Y, Tsuchikawa S, Hayashi K. Application of near infrared spectroscopy to assessments of colour change in plantation-grown Eucalyptus grandis wood subjected to heat and steaming treatments. *J Near Infrared Spectrosc.* (2005) 13:371–6. doi: 10.1255/jnirs.568

85. Williams P. Influence of water on prediction of composition and quality factors: the aquaphotomics of low moisture agricultural materials. *J Near Infrared Spectrosc.* (2009) 17:315–28. doi: 10.1255/jnirs.862

86. Gao M, Guo W, Huang X, Du R, Zhu X. Effect of pressing and impacting bruises on optical properties of kiwifruit flesh. *Postharvest Biol Technol.* (2021) 172:111385. doi: 10.1016/J.POSTHARVBIO.2020.111385

87. Cheng J, Guo W, Du R, Zhou Y. Optical properties of different kiwifruit cultivars (*Actinidia deliciosa* and *Actinidia chinensis*) and their correlation with internal quality. *Infrared Phys Technol.* (2022) 123:104113. doi: 10.1016/J.INFRARED.2022.104113

88. Esquerre C, Gowen A, Tsenkova R, O'Donnell C, Downey G. Identification of water matrix coefficients in mushrooms (*Agaricus bisporus*) using robust ensemble of monte carlo uninformative variable eliminarion. *Near infrared spectroscopy: proceedings of the 14th international conference*. Bangkok: IM Publications Open (2009). p. 163–4.

89. Segtnan V, Šašić Š, Isaksson T, Ozaki Y, Šašić S, Isaksson T, et al. Studies on the structure of water using two-dimensional near-infrared correlation spectroscopy and principal component analysis. *Anal Chem.* (2001) 73:3153–61. doi: 10.1021/ac010102n

90. Frost R, Scholz R, Lõpez A. Raman and infrared spectroscopic characterization of the arsenate-bearing mineral tangdanite– and in comparison with the discredited mineral clinotyrolite. *J Raman Spectrosc.* (2015) 46:920–6. doi: 10.1002/JRS.4691

91. Rémazeilles C, Refait P. Fe(II) hydroxycarbonate Fe2(OH)2CO3 (chukanovite) as iron corrosion product: synthesis and study by fourier transform infrared spectroscopy. *Polyhedron.* (2009) 28:749–56. doi: 10.1016/J.POLY.2008.12.034

92. Litasov K, Ohtani E. Systematic study of hydrogen incorporation into fe-bearing wadsleyite and water storage capacity of the transition zone. *AIP Conf Proc.* (2008) 987:113. doi: 10.1063/1.2896954

93. Walker A, Demouchy S, Wright K. Computer modelling of the energies and vibrational properties of hydroxyl groups in α- and β-Mg2SiO4. *Eur J Mineral.* (2006) 18:529–43. doi: 10.1127/0935-1221/2006/0018-0529

94. Shi G, Stavola M, Pearton S, Thieme M, Lavrov EV, Weber J. Hydrogen local modes and shallow donors in ZnO. *Phys Rev B Condens Matter Mater Phys.* (2005) 72:195211. doi: 10.1103/PHYSREVB.72.195211/FIGURES/6/MEDIUM

95. Shi G, Saboktakin M, Stavola M, Pearton S. "Hidden hydrogen" in as-grown ZnO. *Appl Phys Lett.* (2004) 85:5601. doi: 10.1063/1.1832736

96. Jacobsen S, Demouchy S, Frost D, Ballaran T, Kung J. A systematic study of OH in hydrous wadsleyite from polarized FTIR spectroscopy and single-crystal X-ray diffraction: oxygen sites for hydrogen storage in Earth's interior. *Am Mineral.* (2005) 90:61–70. doi: 10.2138/AM.2005.1624

97. Seyer J, Luner P, Kemper M. Application of diffuse reflectance near-infrared spectroscopy for determination of crystallinity. *J Pharm Sci.* (2000) 89:1305–16. doi: 10.1002/1520-6017(200010)89:103.0.CO;2-Q

98. Sagawa N, Shikata T. Hydration behavior of poly(ethylene oxide)s in aqueous solution as studied by near-infrared spectroscopic techniques. *J Phys Chem B.* (2013) 117:10883–8. doi: 10.1021/jp405794t

99. Awatani T, Midorikawa H, Kojima N, Ye J, Marcott C. Morphology of water transport channels and hydrophobic clusters in Nafion from high spatial resolution AFM-IR spectroscopy and imaging. *Electrochem Commun.* (2013) 30:5–8. doi: 10.1016/j.elecom.2013.01.021

100. Bázár G, Kovacs Z, Tanaka M, Furukawa A, Nagai A, Osawa M, et al. Water revealed as molecular mirror when measuring low concentrations of sugar with near infrared light. *Anal Chim Acta.* (2015) 896:52–62. doi: 10.1016/J.ACA.2015.09.014

101. Gowen A. Water and food quality. *Contemp Mater.* (2012) 1:31–7. doi: 10.7251/123

102. Dopfer O, Roth D, Maier J. Microsolvation of the water cation in neon: infrared spectra and potential energy surface of the H2O+-Ne open-shell ionic complex. *J Chem Phys.* (2001) 114:7081–93. doi: 10.1063/1.1359770

103. Musto P, Galizia M, Pannico M, Scherillo G, Mensitieri G. Time-resolved Fourier transform infrared spectroscopy, gravimetry, and thermodynamic modeling for a molecular level description of water sorption in poly(ε-caprolactone). *J Phys Chem B.* (2014) 118:7414–29. doi: 10.1021/JP502270H/SUPPL_FILE/JP502270H_SI_001.PDF

104. Schwanninger M, Rodrigues J, Fackler KA. Review of band assignments in near infrared spectra of wood and wood components. *J Near Infrared Spectrosc.* (2011) 19:287–308. doi: 10.1255/jnirs.955

105. Kakuda H, Okada T, Hasegawa T. Temperature-induced molecular structural changes of linear poly(ethylene imine) in water studied by mid-infrared and near-infrared spectroscopies. *J Phys Chem B.* (2009) 113:13910–6. doi: 10.1021/JP9048204

106. Via B, Jiang W. Nonlinear multivariate modeling of strand mechanical properties with near-infrared spectroscopy. *For Chron.* (2013) 89:621–30. doi: 10.5558/TFC2013-113

107. Knee M, Sargent J, Osborne D. Cell wall metabolism in developing strawberry fruits. *J Exp Bot.* (1977) 28:377–93.

108. Atungulu G, Nishiyama Y, Koide S. Electrode configuration and polarity effects on physicochemical properties of electric field treated apples post harvest. *Biosyst Eng.* (2004) 87:313–23. doi: 10.1016/J.BIOSYSTEMSENG.2003.11.011

109. Zhang L, Noda I, Czarnik-Matusewicz B, Wu Y. Multivariate estimation between mid and near-infrared spectra of hexafluoroisopropanol-water mixtures. *Anal Sci.* (2007) 23:901–5. doi: 10.2116/analsci.23.901

110. Solcaniova E, Kovac S. Hydrogen bonding in phenols. IV. Intramolecular OH. n Hydrogen bonds of some alkyl derivatives. *Chem Zvesti.* (1969) 691:687–91.

111. Frost R, Dickfos M, Čejka J. Raman spectroscopic study of the uranyl carbonate mineral zellerite. *J Raman Spectrosc.* (2008) 39:582–6. doi: 10.1002/JRS.1879

112. Bertie J, Whalley E. Infrared spectra of ices II, III, and V in the range 4000 to 350 cm -1. *J Chem Phys.* (1964) 40:1646–59. doi: 10.1063/1.1725374

113. Osborne B. Near infrared spectroscopic studies of starch and water in some processed cereal foods. *J Near Infrared Spectrosc.* (1996) 4:195–200. doi: 10.1255/jnirs.90

114. Som T, Karmakar B. Structure and properties of low-phonon antimony glasses and nano glass-ceramics in K2O–B2O3–Sb2O3 system. *J Non Cryst Solids.* (2010) 356:987–99. doi: 10.1016/J.JNONCRYSOL.2010.01.026

115. Cai C, Tao Y, Wang B, Wen M, Yang H, Cheng Y. Investigating the adsorption process of isoamyl alcohol vapor onto silica gel with near-infrared process analytical technology. *Spectrosc Lett.* (2014) 48:190–7. doi: 10.1080/00387010.2013.872668

116. Frost R, Erickson K, Čejka J, Reddy BJ. A Raman spectroscopic study of the uranyl sulphate mineral johannite. *Spectrochim Acta A Mol Biomol Spectrosc.* (2005) 61:2702–7. doi: 10.1016/J.SAA.2004.10.013

117. Wenz J. Influence of steroids on hydrogen bonds in membranes assessed by near infrared spectroscopy. *Biochim Biophys Acta Biomembr.* (2021) 1863:183553. doi: 10.1016/j.bbamem.2021.183553

118. Mastrapa R, Moore M, Hudson R, Ferrante R, Brown R, Mastrapa R, et al. Proton irradiation of crystalline water ice: timescales for amorphization in the kuiper belt. *DPS.* (2005) 37:56.10.

119. Kandpal L, Lohumi S, Kim M, Kang J, Cho B. Near-infrared hyperspectral imaging system coupled with multivariate methods to predict viability and vigor in muskmelon seeds. *Sensors Actuators B Chem.* (2016) 229:534–44. doi: 10.1016/j.snb.2016.02.015

120. Hong B, Rubenthaler G, Allan R. Wheat pentosans. II. Estimating kernel hardness and pentosans in water extracts by near-infrared reflectance. *Cereal Chem.* (1989) 66:374–7.

121. Omar A, Atan H, Matjafri M. Peak response identification through near-infrared spectroscopy analysis on aqueous sucrose, glucose, and fructose solution. *Spectrosc Lett.* (2012) 45:190–201. doi: 10.1080/00387010.2011.604065

122. Omar A, Matjafri M. Near infrared spectral linearisation in quantifying soluble solids content of intact carambola. *Sensors.* (2013) 13:4876–83. doi: 10.3390/s130404876

123. Gowen A, Tsenkova R, Esquerre C, Downey G, O'Donnell C. Use of near infrared hyperspectral imaging to identify water matrix co-ordinates in mushrooms (*Agaricus bisporus*) subjected to mechanical vibration. *J Near Infrared Spectrosc.* (2009) 17:363–71. doi: 10.1255/jnirs.860

124. Sun X, Dong X, Cai L, Hao Y, Ouyang A, Liu Y. Visible-NIR spectroscopy and least square support vector machines regression for determination of vitamin c of mandarin fruit. *Sens Lett.* (2012) 10:506–10. doi: 10.1166/sl.2012.1891

125. Lu R. Multispectral imaging for predicting firmness and soluble solids content of apple fruit. *Postharvest Biol Technol.* (2004) 31:147–57. doi: 10.1016/j.postharvbio.2003.08.006

126. Lu R. Prediction of apple fruit firmness by near-infrared multispectral scattering. *J Texture Stud.* (2004) 35:263–76. doi: 10.1111/j.1745-4603.2004.tb00837.x

127. Chatani E, Tsuchisaka Y, Masuda Y, Tsenkova R. Water molecular system dynamics associated with amyloidogenic nucleation as revealed by real time near infrared spectroscopy and aquaphotomics. *PLoS One.* (2014) 9:e101997. doi: 10.1371/journal.pone.0101997

128. Heiman A, Licht S. Fundamental baseline variations in aqueous near-infrared analysis. *Anal Chim Acta.* (1999) 394:135–47. doi: 10.1016/S0003-2670(99)00312-8

129. Tsenkova R, Iordanova I, Toyoda K, Brown D. Prion protein fate governed by metal binding. *Biochem Biophys Res Commun.* (2004) 325:1005–12. doi: 10.1016/j.bbrc.2004.10.135

130. Pu Y, Ragauskas A, Lucia L, Naithani V, Jameel H. Near-infrared spectroscopy and chemometric analysis for determining oxygen delignification yield. *J Wood Chem Technol.* (2008) 28:122–36. doi: 10.1080/02773810802125008

131. Awais M, Altgen M, Mäkelä M, Altgen D, Rautkari L. Hyperspectral near-infrared image assessment of surface-acetylated solid wood. *ACS Appl Bio Mater.* (2020) 3:5223–32. doi: 10.1021/ACSABM.0C00626/ASSET/IMAGES/LARGE/MT0C00626_0005.JPEG

132. Freitas E, Brito A, de Oliveira S, de Oliveira E. Early diagnosis of cassava frog skin disease in powdered tissue samples using near-infrared spectroscopy. *Eur J Plant Pathol.* (2020) 156:547–58. doi: 10.1007/S10658-019-01904-X/FIGURES/4

133. Dacal-Nieto A, Formella A, Carrión P, Vazquez-Fernandez E, Fernández-Delgado M. Common scab detection on potatoes using an infrared hyperspectral imaging system. In: Maino G, Foresti G editors. *Image analysis and processing – ICIAP 2011. Lecture notes in computer science*. Berlin: Springer (2011). p. 303–12. doi: 10.1007/978-3-642-24088-1_32

134. Herklotz F, Chaplygin I, Lavrov EV, Neiman A, Reeves R, Allen M. Bistability of a hydrogen defect with a vibrational mode at 3326cm-1 in ZnO. *Phys Rev B.* (2019) 99:115203. doi: 10.1103/PHYSREVB.99.115203/FIGURES/7/MEDIUM

135. Wang W, Jin X, Zhu Y, Zhu C, Yang J, Wang H, et al. Effect of vapor-phase glutaraldehyde crosslinking on electrospun starch fibers. *Carbohydr Polym.* (2016) 140:356–61. doi: 10.1016/J.CARBPOL.2015.12.061

136. Yang X, Guang P, Xu G, Zhu S, Chen Z, Huang F. Manuka honey adulteration detection based on near-infrared spectroscopy combined with aquaphotomics. *LWT.* (2020) 132:109837. doi: 10.1016/j.lwt.2020.109837

137. Badaró A, Morimitsu F, Ferreira A, Clerici M, Fernandes Barbin D. Identification of fiber added to semolina by near infrared (NIR) spectral techniques. *Food Chem.* (2019) 289:195–203. doi: 10.1016/J.FOODCHEM.2019.03.057

138. Sannia M, Serva L, Balzan S, Segato S, Novelli E, Fasolato L. Application of near-infrared spectroscopy for frozen-thawed characterization of cuttlefish (*Sepia officinalis*). *J Food Sci Technol.* (2019) 56:4437–47. doi: 10.1007/s13197-019-03957-6

139. Andueza D, Picard F, Hocquette J, Listrat A. Prediction of the intramuscular connective tissue components of fresh and freeze-dried samples by near infrared spectroscopy. *Meat Sci.* (2021) 179:108537. doi: 10.1016/J.MEATSCI.2021.108537

140. Fengel D. Influence of water on the OH valency range in deconvoluted FTIR spectra of cellulose. *Holzforschung.* (1993) 47:103–8. doi: 10.1515/HFSG.1993.47.2.103/MACHINEREADABLECITATION/RIS

141. Paladini G, Venuti V, Crupi V, Majolino D, Fiorati A, Punta C. 2D correlation spectroscopy (2DCoS) analysis of temperature-dependent FTIR-ATR spectra in branched polyethyleneimine/TEMPO-oxidized cellulose nano-fiber xerogels. *Polymers.* (2021) 13:528. doi: 10.3390/POLYM13040528

142. Hassanzadeh A, Murphy S, Pethybridge S, van Aardt J. Growth stage classification and harvest scheduling of snap bean using hyperspectral sensing: a greenhouse study. *Remote Sens.* (2020) 12:3809. doi: 10.3390/RS12223809

143. Devasahayam S, Bandyopadhyay S, Hill D. Study of victorian brown coal dewatering by super absorbent polymers using attenuated total reflection fourier transform infrared spectroscopy. *Miner Process Extr Metall Rev.* (2016) 37:220–6. doi: 10.1080/08827508.2016.1168417

144. Liu J, Liu R, Xu K. Accuracy of noninvasive glucose sensing based on near-infrared spectroscopy. *Appl Spectrosc.* (2015) 69:1313–8. doi: 10.1366/14-07728

145. Saiga N, Hamada C, Ikeda J. Near infrared spectroscopy assessment of the glucose solution processed by ultrasonic cavitation. *Ultrasonics.* (2006) 44:e101–4. doi: 10.1016/J.ULTRAS.2006.06.029

146. Wiercigroch E, Szafraniec E, Czamara K, Pacia M, Majzner K, Kochan K, et al. Raman and infrared spectroscopy of carbohydrates: a review. *Spectrochim Acta A Mol Biomol Spectrosc.* (2017) 185:317–35. doi: 10.1016/J.SAA.2017.05.045

147. Li H, Lv X, Wang J, Li J, Yang H, Qin Y. Quantitative determination of soybean meal content in compound feeds: comparison of near-infrared spectroscopy and real-time PCR. *Anal Bioanal Chem.* (2007) 389:2313–22. doi: 10.1007/S00216-007-1624-1/FIGURES/6

148. Unger R, Braun U, Fankhänel J, Daum B, Arash B, Rolfes R. Molecular modelling of epoxy resin crosslinking experimentally validated by near-infrared spectroscopy. *Comput Mater Sci.* (2019) 161:223–35. doi: 10.1016/J.COMMATSCI.2019.01.054

149. Chen S, Wang C, Tsai C, Yang I, Luo S, Chuang Y. Fermentation quality evaluation of tea by estimating total catechins and theanine using near-infrared spectroscopy. *Vib Spectrosc.* (2021) 115:103278. doi: 10.1016/J.VIBSPEC.2021.103278

150. Hu Y, Macfhionnghaile P, Caron V, Tajber L, Healy A, Erxleben A, et al. Formation, physical stability, and quantification of process-induced disorder in cryomilled samples of a model polymorphic drug. *J Pharm Sci.* (2013) 102:93–103. doi: 10.1002/JPS.23338

frontiers | Frontiers in Nutrition

TYPE Review
PUBLISHED 06 January 2023
DOI 10.3389/fnut.2022.1082671

OPEN ACCESS

EDITED BY
John-Lewis Zinia Zaukuu,
Kwame Nkrumah University of Science and Technology, Ghana

REVIEWED BY
Michael Arthur,
Teagasc Food Research Centre, Ireland
Damian Laryea,
King Mongkut's Institute of Technology Ladkrabang, Thailand

*CORRESPONDENCE
Haiyan Chen
haiyanchen_cc@yeah.net

SPECIALTY SECTION
This article was submitted to Nutrition and Food Science Technology, a section of the journal Frontiers in Nutrition

RECEIVED 28 October 2022
ACCEPTED 13 December 2022
PUBLISHED 06 January 2023

CITATION
Zhao F, Li R, Liu Y and Chen H (2023) Perspectives on lecithin from egg yolk: Extraction, physicochemical properties, modification, and applications. *Front. Nutr.* 9:1082671. doi: 10.3389/fnut.2022.1082671

Perspectives on lecithin from egg yolk: Extraction, physicochemical properties, modification, and applications

Feng Zhao[1], Rongji Li[1], Yun Liu[2] and Haiyan Chen[3,4]*

[1]College of Food Science and Engineering, Jilin Agriculture University, Changchun, Jilin, China, [2]College of Life Sciences, Beijing University of Chemical Technology, Beijing, China, [3]College of Food Science and Engineering, Changchun Sci-Tech University, Changchun, Jilin, China, [4]College of Pharmacy, Changchun University of Chinese Medicine, Changchun, Jilin, China

Egg yolk lecithin has physiological activities as an antioxidant, antibacterial, anti-inflammatory, and neurologic, cardiovascular, and cerebrovascular protectant. There are several methods for extracting egg yolk lecithin, including solvent extraction and supercritical extraction. However, changes in extraction methods and functional activity of egg yolk lecithin are a matter of debate. In this review we summarized the molecular structure, extraction method, and functional activity of egg yolk lecithin to provide a good reference for the development of egg yolk lecithin products in the future.

KEYWORDS

egg yolk lecithin, biological modification, metabolism emulsion, review, food nutrient

1. Introduction

Phospholipids refer to phosphorus-containing lipids that were first separated from egg yolk by Gobley in 1844 and named lecithin in Greek (1). The components of egg yolk lecithin include phosphatidylcholine (PC), phosphatidylethanolamine (PE), and lysophosphatidyl choline (2). Phosphatidylcholine (PC) is the main component of lecithin, the content of which is ~73.0%. The content of lecithin in egg yolk is three times higher than the content of lecithin in soybean. It has been shown that the content of lecithin in egg yolk and duck egg yolk is large, accounting for ~10% of total lecithin (3). Phospholipids are one of the basic components of cell membranes.

The membrane acts as a protective barrier for the cell, a channel for the exchange of environmental substances inside and outside the cell. The membrane is the site where many enzyme systems carry out biochemical reactions, which are the basis of living substances. Phospholipids participate in cell metabolism and have unique structures and properties, ensuring the normal functioning of cells (4). Phospholipids are also an important part of brain cells and nerve tissues, accounting for 30% of the weight of the brain, and are very important for the transmission of neuronal information within the brain (5).

Egg yolks and some oil crop seeds (soybeans and rapeseeds) contain the most abundant amount of lecithin. Due to the high cost of preparing lecithin from egg yolks, soybeans are the main source of lecithin. Compared with plant-derived phospholipids, egg yolk phospholipids have a more balanced and unique phospholipid composition (Table 1) (6) and contain specific fatty acids that are not found in plant-derived phospholipids (Table 2) (7). Lecithin derived from egg yolk is a component of the granular part of egg yolk, which accounts for ∼70% of all phospholipids in egg yolk (8). Egg yolk lecithin delays aging, protects the stomach and liver, supports the utilization of fat-soluble vitamins, improves the efficiency of blood circulation, and has good physiologic and pharmaceutical functions (9). Egg yolk lecithin is also a basic component of special medicinal emulsions and has the potential to become a new generation of drugs. At present, egg yolk lecithin has been used to improve memory in schizophrenia, childhood autism, and Alzheimer's disease, and as an anti-oxidant during organ transplantation (10).

TABLE 1 Phospholipid composition of egg yolk.

Component	Content %	Component	Content %
Phosphocholine	73.0	Hemolyso phosphorylcholine	5.8
Phosphoethanolamine	15.0	Hemolytic phosphoethanolamine	2.1
Phosphoacylserine	0.9	Sphingomyelin	2.5
Phosphatidylinositol	0.6	Other phospholipids	0.1

TABLE 2 Fatty acid component and content of yolk phospholipid.

Component	Content%	Component	Content%
Myristic acid (C14:0)	0.23	Oleic acid (C18:1)	57.80
Pentadecanoic acid (C15:0)	0.10	Linoleic acid (C18:2)	7.45
Palmitic acid (C16:0)	19.44	Linolenic acid (C18:3)	1.67
Palmitic acid (C16:1)	1.09	Arachidonic acid (C20:4)	0.83
Heptadecanoic acid (C17:0)	0.33	Docosahexaenoic acid (C22:6)	2.62
Stearic acid (C18:0)	7.72	Other	0.72

2. Method for extracting egg yolk lecithin

2.1. Organic solvent extraction

Solvent extraction is a method to separate and extract lecithin by using the difference in the selectivity of the solvent to the components of phospholipids. Solvent extraction is also the earliest method used for phospholipid extraction (11). There are two methods (single and mixed organic solvent extraction methods). During single organic solvent extraction, ethanol is used to extract lecithin from fresh egg yolk and the extraction rate can be 93.38% under suitable process conditions (12). The mixed organic solvent extraction method uses the characteristics of lecithin that is soluble in ethanol, but insoluble in acetone to extract lecithin from eggs. The organic solvent extraction method is characterized as a simple operation and low requirements for conditions, but the organic solvent extraction method takes too long, the purity is not high, and there may be residual organic solvents (Figure 1).

During the actual operation process, to improve the extraction efficiency some new auxiliary technologies have been developed to facilitate the extraction. For example, the effect of the electric pulse generated by the high-voltage pulse electric field on lecithin is assisted by the organic solvent method, and the extraction rate of egg yolk lecithin is increased by 10.2% compared with the traditional method (13). The high-voltage pulsed electric field-assisted method has the advantages of safety, speed, efficiency, and less damage to nutrients. Using ultrasonic- or microwave-assisted separation (14), ultrasonic-assisted separation can accelerate the rupture of the cell wall, and make the extracted substance and the extraction solvent more accessible.

2.2. Super- and sub-critical extraction

Supercritical extraction is a new type of separation technology that separates substances by changing the temperature and pressure according to the difference in the properties of substances in the supercritical state. Supercritical carbon dioxide extraction technology can extract lecithin with higher purity (95–98%) from egg yolk powder (15). Because phospholipids are insoluble in supercritical CO_2, it is necessary to add an entrainer to grade phospholipids (Figure 2) (16).

Subcritical extraction refers to a fluid extraction technology that uses a thermodynamic state at the edge of a supercritical state and is above the critical pressure and below the critical temperature. Compared with the supercritical fluid method, the subcritical fluid method has milder conditions and less stringent requirements for high-pressure equipment. And on the other hand, the subcritical fluid method can better retain the natural active ingredients in the extracted product with a lower cost.

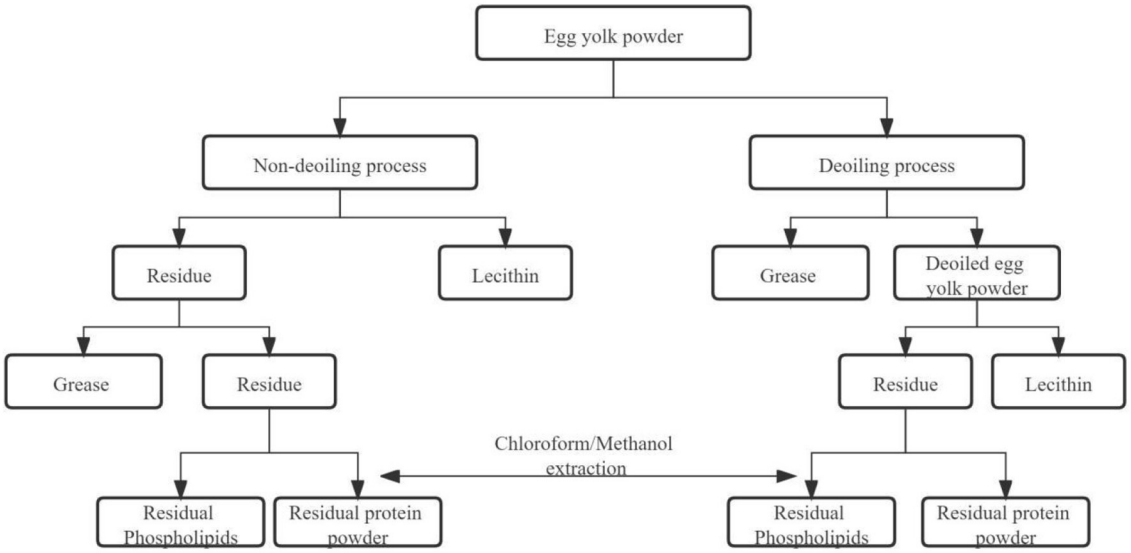

FIGURE 1
Process of leclithin by drying egg yolk powder as a raw solvent.

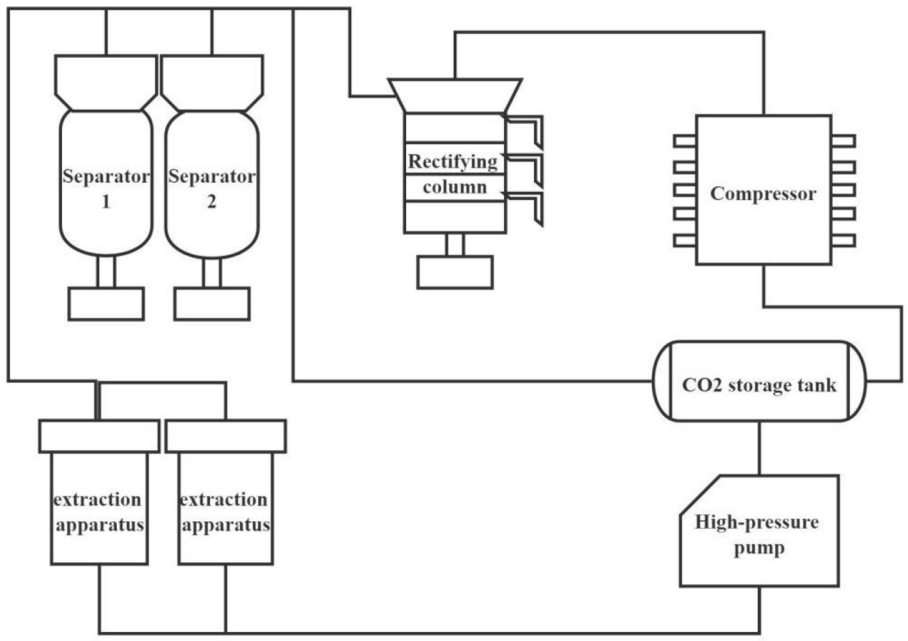

FIGURE 2
Supercritical extraction equipment.

2.3. Enzymatic hydrolysis extraction method

The enzymatic hydrolysis method uses proteases to break large molecular proteins into small molecular peptides, speed up the separation of lecithin and protein, shorten the extraction process of lecithin, thus improve the extraction efficiency of egg yolk lecithin. The volume fraction of ethanol is 95% and the volume fraction of protease is 0.06%. The extraction efficiency of lecithin is higher when performed for 2 h at 35°C (17). The

enzymatic hydrolysis method has a mild operating environment and can obtain relatively high-quality proteins and lipids. To further improve the extraction efficiency, ultrasonic-assisted enzymatic extraction can be used (18).

2.4. Column lamination method

Column chromatography uses an adsorbent as a stationary phase. When the solute in the mobile phase passes through the stationary phase, the solute achieves the purpose of separation due to different adsorption and resolution capabilities. Currently, silica gel and alumina ion exchange resin are commonly used as stationary phases in column chromatography. Moreover, the main method for producing high-purity egg yolk lecithin is column chromatography but column chromatography requires an adsorption-desorption process, the processing volume is small, and the solvent consumption is large. To avoid the residual toxicity of the solvent, the less toxic ethanol is generally used as the mobile phase (19).

2.5. Other extraction methods

In addition to the above-described methods, several more common methods of extracting lecithin exist, such as the cryo-precipitation (14) and membrane separation methods (20). Among them extraction methods, membrane technology is a relatively new technology for separating substance mixtures. Natural or synthetic membranes are used to provide driving force in external energy or chemical potential differences (pressure difference, concentration difference, and potential difference). Under such conditions, the raw material side components selectively permeate the membrane to achieve the technical method of sample separation, classification, enrichment, and purification. Hollow fiber ultrafiltration membranes and organic polymer membranes have been reported for phospholipid separation (21).

3. Basic properties of egg yolk lecithin

3.1. Physical and chemical properties of egg yolk lecithin

High-purity egg yolk lecithin products are white, waxy solids. When lecithin is in a liquid form, it is light yellow and slippery with a peculiar smell. Egg yolk lecithin contains an abundance of unsaturated fatty acids, most of lecithin products appear slightly darker than they are supposed to, due to the unsaturated fats being oxidized. In the production of lecithin, the dosage forms are in different forms due to the concentration. The concentration of liquid is ∼60%, and the concentration of granules and powder can reach more than 95%.

Egg yolk lecithin is a natural phospholipid mixture extracted and refined from egg yolk, and is an amphiphilic molecule. According to different types of backbone alcohols, egg yolk lecithins are mainly divided into two categories: based on glycerol (glycerophospholipids) and on sphingosine (sphingomyelin). Each 100 g of egg yolk contains 9.44 g of phospholipids, 1,011 mg of cholesterol, 0.83 mg of lutein, 0.42 mg of zeaxanthin, 0.53 mg of canthaxanthin, and 0.11 mg of β-carotene (22). The volume of egg yolk is 30–32% of a whole egg. The whole egg contains fat (30%), protein (15%), moisture (50%), and other chemicals. Gazolu-Rusanova et al. (23) used SDS-PAGE to isolate the type and composition of egg yolk protein. After freezing and centrifugation, the yolk was divided into two parts: supernatant; and sediment. The structure of the supernatant part is mainly in the form of aggregates, and the precipitation part is mainly spherical. The supernatant accounts for 77–81% of the dry matter weight of the egg yolk, and the sediment accounts for 19–23%. The supernatant contains 85% low-density lipoprotein (LDL) and 15% egg yolk protein (livetins).

The precipitate contains 70% high-density lipoprotein (HDL), 16% high phosphoprotein (phosvitin), and 12% low-density lipoprotein (LDL) (24). The structural features of glycerol lecithin are as follows: hydroxyl groups on glycerol sn-1 and sn-2 are esterified by saturated or unsaturated fatty acids; the hydroxyl groups on sn-3 are esterified by phosphoric acid; and the phosphoric acid is connected to the base according to the main types of glycerol lecithin, including PC, phosphatidylethanolamine (PE), phosphatidylinositol (PI), phosphatidylserine (PS), and phospholipids, phosphatidic acid (PA), and phosphatidylglycerol (PG).

In addition to the above six types of glycerol lecithin, the fatty acyl group at the sn-1 position of glycerol in the glycerophospholipid molecule is replaced by a long-chain alcohol to form a vinyl ether, which is referred to as plasmalogen. The phosphoryl group in the glycerophospholipid molecule is replaced by a phosphate group, which is referred to as a phosphate ester. Using phospholipase and specific lipase to hydrolyze glycerol lecithin produces lysophosphatidylcholine. Gazolu-Rusanova et al. (23) showed that the lysophosphatidylcholine oil/water interface and liquid membrane properties have a very important role. Sphingomyelin is composed of sphingosine, a fatty acid, phosphoric acid, and nitrogenous bases. The fatty acyl and cerol amino groups are connected by an amide bond, and the sphingosine that is formed is also referred to as ceramide. The primary alcohol group of cerol is connected to phosphatidylcholine or phosphatidylethanolamine by a phosphate bond. The fatty acids found in sphingomyelin include palmitic acid, stearic acid, tar oleic acid, and cerene acid.

3.2. Physiological function of egg yolk lecithin

3.2.1. Strengthening nerve conduction

Brain nerve cells contain a large amount of lecithin. The content of lecithin accounts for approximately one-fifth of brain nerve cell mass. Lecithin in brain cells is transformed to release choline, which combines with acetyl-CoA to produce acetylcholine. Acetylcholine is an important chemical transmitter for information transmission between various nervous systems; so lecithin can increase the degree of brain cell activation, and improve memory and intelligence. Using the brain for a long time in life and work will consume a large amount of lecithin in the body, leading to a decline in brain function. Relevant studies have shown that with age, brain function gradually declines. Consuming lecithin products effectively prevents further aging of the brain and strengthens brain function. During the growth stage, children should eat foods rich in lecithin nutrients, such as eggs. Nuts and animal liver have a positive effect on brain development, learning, and memory as well.

Alzheimer's disease is a neurodegenerative disease characterized by a loss of memory and cognitive impairment. Eating egg yolk lecithin improves memory and cognitive function (25), and delays the onset of neurodegenerative disease. Specifically, the unsaturated fatty acid chain in egg yolk lecithin structure has an indirect protective role (26). Egg yolk lecithin inhibits acetylcholinesterase activity, reduces the concentration of oxidation products, and exerts a neuroprotective function (27, 28).

3.2.2. Regulation of blood lipids

In recent years, hyperlipidemia has become a common metabolic disorder, causing cardiovascular and cerebrovascular diseases (29) that negatively impact healthful living. The molecular structure of egg yolk lecithin has dual characteristics (hydrophilicity and lipophilicity). Therefore, an emulsification reaction occurs in the body, combining lipid substances with water and emulsifying the accumulated cholesterol and neutral fats in the blood vessels. Egg yolk lecithin serves as some kind of "garbage" (i.e., cholesterol and neutral fats) remover in blood vessels, making blood circulation in the blood vessels of the entire body smoother, promoting blood flow, and penetration into the body, thereby reducing the viscosity of human blood. Thus, egg yolk lecithin can effectively reduce hyperlipidemia and coronary heart disease. Epidemiologic studies have shown that hypertension is a major cause of heart-blood diseases, such as sudden death and coronary heart disease. Egg yolk lecithin lowers blood pressure (28) by inhibiting angiotensin-converting enzyme (ACE.) Skorkowska-Telichowska (30) reported that 15 mL of lecithin fed to patients with metabolic syndrome three times a day significantly improved symptoms. Moreover,

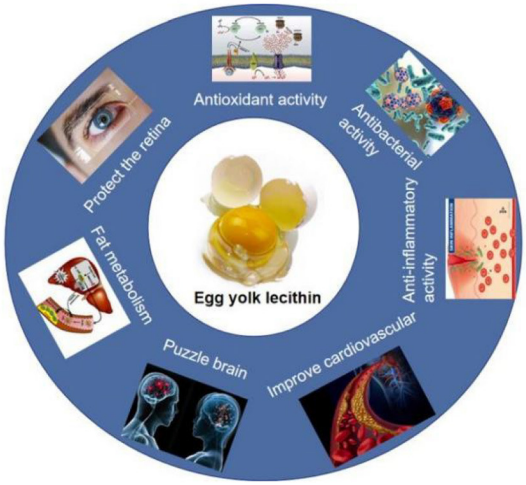

FIGURE 3
Physiologic function activity of egg yolk lecithin.

the daily intake of 1.2 mmol/L of egg yolk lecithin inhibited cholesterol absorption and transport, and prevented obesity (7, 31).

3.2.3. Repair biofilms and delay body aging

Lecithin is very important for the composition of animal somatic cells. Without lecithin, cell membranes will be damaged to varying degrees. Lecithin is an indispensable substance in cells. PC promotes the synthesis and regeneration of lipoproteins (32), repairs damaged cell membranes, increases desaturation of cell membrane fatty acids, softens and rejuvenates the cell membrane, protects mitochondria and microsomal membranes of somatic cells, and maintains cell structure. In the process of individual aging, the function of the antioxidant defense system in the body gradually weakens, and free radicals accumulate, which will cause excess free radicals to react with unsaturated fatty acids to form a peroxide and eventually deform the organelles through a series of interactions in which neurons are damaged and lecithin has the ability to scavenge free radicals (33), which improves the metabolic capacity. Lecithin can also promote skin regeneration, make the skin shiny, and prevent hair loss, which makes gray hair darker and slows the aging process.

3.2.4. Human nutritional needs

Lecithin provides 90% of the exogenous choline needed by the human body. Lecithin provides two main benefits for choline. First, unlike bound choline, free choline is degraded to methylamine by intestinal microorganisms. Second, choline is obtained by continuous methylation of

phosphatidylcholine in the liver and other fibrous tissues, and the synthesis process requires time. Therefore, when dietary choline is insufficient, the endogenous resources of lecithin can supplement body demands.

3.2.5. Egg yolk lecithin liposome

Egg yolk lecithin liposomes are drug carriers. With distinct targeting, egg yolk lecithin liposomes are an important preparation in the drug delivery system. Fatty acid composition and species of egg yolk lecithin have a great influence on liposome properties. Saturated fatty acids in the lecithin structure enhance the firmness and non-permeability of the liposome membrane. Unsaturated fatty acids in lecithin structures make liposomes have a lower phase transition, good fluidity, and low viscosity. Four types of egg yolk lecithin liposomes, which are conventional liposomes (34–36), PEG-modified liposomes (37–39), multifunctional liposomes (40–42), and ligand-targeted liposomes (43–45) currently exist. Each liposome has its own advantages and application fields. Five yolk lecithin liposomes were prepared by Kondratowicz (46), who compared the structural and mechanical properties. Both the main components of liposomes (e.g., lecithin, glycerin, and cholesterol) and the component proportions influence the structure of liposomes. Trace components, such as tocopherol and carotene, also have a great impact (see Figure 3).

4. Application of yolk lecithin

The present commercial egg yolk lecithin is mainly used in cosmetics, medications, and nutrition (47), and can be used in the preparation of liposomes (48) and fat emulsions. Liposomes are a new preparation and research focusing on drug carriers in a drug release system, and it has become one of the main directions of the manufacturing industry (49). The performance of liposomes from egg yolk, soybean, and porcine lecithin have been compared (50); the results showed that liposomes made of egg yolk lecithin had the best performance. Fat milk injection is a type of nutritional injection used in the clinical setting. Fat milk is an energy supplement outside the gastrointestinal tract. Fat milk can supplement essential fatty acids and energy for patients, and egg yolk lecithin is used as an important component emulsifier. Because lecithin is an important component of biofilms, it can also be used as a drug carrier to form complexes (51) with other drug components, which can directly transport drug components to a diseased site and improve bioavailability.

Egg yolk lecithin is widely used in the feed industry and has significant effects (52). Adding phospholipids to broiler feed improves growth, increases storage in the liver, and promotes bone growth. The different growth periods of fish and shrimp also require the addition of lecithin in feed (46). Other egg yolk lecithin can also be used as a fungicide for crops, a preservative for fruits and flowers, ink emulsifiers, and petroleum products (53).

5. Prospects of egg yolk lecithin

Lecithin is not only a high nutritional value substance, but also a highly bioactive functional component (54). For >30 years, extensive and in-depth research has been conducted on transmitters of sustained-release drugs, maintenance of function, development of functional foods, and means to improve industrial production (2). As a natural emulsifier and wetting agent, lecithin, in addition to its biological efficacy, is often used as an emulsifier for intravenous fat injection and is the main embedding material for liposomes (55). Lecithin has unique membrane permeability, and it is of high value to the packaging industry (56). At present, with the continuous improvement in the lecithin extraction and preparation process, lecithin with a high purity, low price, pure nature, and no side effects will be fully utilized and developed (57). At the same time, with the development of lecithin, a new direction for deep processing of eggs will emerge (58).

Currently, high-purity lecithin is in high demand in the international market (59). High-purity lecithin products usually refer to phospholipid products containing ∼95% PC (60). Because high-purity lecithin products are pure, have no peculiar smell, strong emulsification, and are easy to dissolve in water, they can be added and used in large quantities in the food industry and can also be made into health products and pharmaceuticals (13). The price of phospholipid products is ten times or even dozens of times higher than crude lecithin (61). Phospholipid production in China is far behind foreign countries in terms of its production scale and technical level (62). Medical oral liquid and high-purity phospholipids for injection still need to be imported in large quantities (13). With regards to deep processing of agricultural products, the production of lecithin is currently one of the key technical development areas supported by the State (63). Therefore, the prospect of developing lecithin and its deep-processed products in China is very broad.

6. Conclusions

The extraction method of lecithin in eggs is mainly based on the extraction method of soybean phospholipids, organic solvent extraction, supercritical fluid extraction, and column chromatography. With the development of technology, the enzymatic method and membrane separation method will make the extraction of lecithin from eggs more convenient, fast, efficient and environmentally-friendly. The author believes that the basic physical and chemical properties of egg yolk lecithin, the optimization of extraction methods, technological innovation, and the development of functional properties should

be studied in depth to explore differences and characteristics superior to soy lecithin to develop research methods and production suitable for egg yolk lecithin. Application technology provides theoretical basis and technical support for the future application of egg yolk lecithin in various fields.

Author contributions

Guarantor of integrity of the entire study and manuscript preparation: HC. Study concepts, study design, literature research, data analysis, and manuscript editing: FZ. Definition of intellectual content: HC and YL. Clinical studies and statistical analysis: RL. Data acquisition and manuscript review: YL. All authors contributed to the article and approved the submitted version.

Conflict of interest

The authors declare that the research was conducted in the absence of any commercial or financial relationships that could be construed as a potential conflict of interest.

Publisher's note

All claims expressed in this article are solely those of the authors and do not necessarily represent those of their affiliated organizations, or those of the publisher, the editors and the reviewers. Any product that may be evaluated in this article, or claim that may be made by its manufacturer, is not guaranteed or endorsed by the publisher.

References

1. Sinanoglou VJ, Strati IF, Miniadis-Meimaroglou S. Lipid, fatty acid and carotenoid content of edible egg yolks from avian species: a comparative study. *Food Chem.* (2011) 124:971–7. doi: 10.1016/j.foodchem.2010.07.037

2. Pokora M, Eckert E, Zambrowicz A, Bobak L, Szołtysik M, Dąbrowska A, et al. Biological and functional properties of proteolytic enzyme-modified egg protein by-products. *Food Sci Nutr.* (2013) 1:184–95. doi: 10.1002/fsn3.27

3. Li J, Wang X, Zhang T, Wang C, Huang Z, Luo X, et al. review on phospholipids and their main applications in drug delivery systems. *Asian J Pharm Sci.* (2015) 10:81–98. doi: 10.1016/j.ajps.2014.09.004

4. Singh P, Gangadharappa HV, Mruthunjaya K. Phospholipids: Unique carriers for drug delivery systems. *J Drug Deliv Sci Technol.* (2017) 39:166–79. doi: 10.1016/j.jddst.2017.03.027

5. Ali AH, Zou X, Lu J, Abed SM, Yao Y, Tao G, et al. Identification of phospholipids classes and molecular species in different types of egg yolk by using UPLC-Q-TOF-MS. *Food Chem.* (2017) 221:58–66. doi: 10.1016/j.foodchem.2016.10.043

6. Li C. *Study on the Technology of Enzymatic Extraction of Lipid Components of Fresh Egg Yolk*. Wuxi: Jiangnan University (2008). p. 56

7. Skórkowska-Telichowska K, Kosińska J, Chwojnicka M, Tuchendler D, Tabin M, Tuchendler R, et al. Positive effects of egg-derived phospholipids in patients with metabolic syndrome. *Adv Med Sci.* (2016) 61:169–74. doi: 10.1016/j.advms.2015.12.003

8. Navidghasemizad S, Temelli F, Wu J. Moisture impact on extractability of phospholipids from leftover egg yolk after enzymatic treatment using supercritical carbon dioxide. *Food Bioprod Proc.* (2015) 94:473–81. doi: 10.1016/j.fbp.2014.07.002

9. Darryl DS, Blake B, Williams I, Mullan BP, Pethick DW, Dunshea FR. Dietary lecithin supplementation can improve the quality of the *m. longissimus thoracis*. *Animals.* (2015) 5:1180–91. doi: 10.3390/ani5040405

10. Micha ÅW, Ewa D, Tomasz C. Lecithin-based wet chemical precipitation of hydroxyapatite nanoparticles. *Colloid Polym Sci.* (2015) 293:1561–8. doi: 10.1007/s00396-015-3557-0

11. Wang Q. *Isolation and Purification of Soybean Inositol Phospholipids*. Vol. 02. Wuxi: Jiangnan University (2014). p. 66.

12. Huihui Z, Luhong T. Study on a new process for preparing high-purity egg yolk lecithin for injection. *Natl Prod Res Dev.* (2014) 4:564–9.

13. Sun L, Fan W, Wu C, Zhang S, Dai J, Zhang D. Effect of substituting different concentrations of soybean lecithin and egg yolk in tris-based extender on goat semen cryopreservation. *Cryobiology*. (2020) 92:146–50. doi: 10.1016/j.cryobiol.2019.12.004

14. Huang Y. *Extraction of Egg Yolk Lecithin and Preparation of Nanoemulsion*. Beijing: Beijing University of Chemical Technology (2017).

15. Li J, Tang S, Mou X. The fraction of sphingomyelin in egg yolk lecithin Isolation and structure identification. *Guangdong Chem Ind.* (2016) 43:206–7.

16. Cao D, Qiu A, Wang X. Supercritical fluid separation of soybean phosphatidylcholine. *China Oils Fats.* (2002) 27:72–3.

17. Dhuique-Mayer C, Servent A, Messan C, Achir N, Dornier M, Mendoza Y. Bioaccessibility of biofortified sweet potato carotenoids in baby food: Impact of manufacturing process. *Front Nutr.* (2018) 5:98. doi: 10.3389/fnut.2018.00098

18. Li M. Research progress on extraction technology of lecithin. *West Leather.* (2018) 4:9.

19. Ma Y, Wang H. Extraction technology and patent analysis of lecithin. *Guangzhou Chem Ind.* (2017) 45:18–20. doi: 10.26549/met.v1i1.324

20. Xiao W, Zhang F, Li Y. Study on extraction of high purity lecithin from egg yolk by low temperature precipitation method. *Food Ind Sci Technol.* (2013) 34:256–8.

21. Yan L, Yang Z. A method for extracting lecithin from egg yolk: China. *Food Sci.* (2012) 0953:5.

22. Kim IC, Kim J-H, Lee K-H, Tak TM. Phospholipids separation (degumming) from crude vegetable oil by polyimide ultrafiltration membrane. *J Memb Sci.* (2002) 205:113–23. doi: 10.1016/S0376-7388(02)00070-4

23. Kovalcuks A, Duma M. Distribution of phospholipids, cholesterol and carotenoids in two-solvent system during egg yolk oil solvent extraction. *Int Schol Sci Res Innov.* (2016) 10:323–8.

24. Gazolu-Rusanova D, Mustan F, Vinarov Z, Tcholakova S, Denkov N, Stoyanov S, et al. Role of lysophospholipids on the interfacial and liquid film properties of enzymatically modified egg yolk solutions. *Food Hydrocoll.* (2020) 99:105319. doi: 10.1016/j.foodhyd.2019.105319

25. Anton M. Egg yolk: structures, functionalities and processes. *J Sci Food Agric.* (2013) 96:2871. doi: 10.1002/jsfa.6247

26. Zeece I. Chapter seven: food additives. In: Zeece M, editors. *Introduction to the Chemistry of Food*. New York, NY: Academic Press (2020). p. 251–311. doi: 10.1016/B978-0-12-809434-1.00007-4

27. Che H, Fu X, Zhang L, Gao X, Wen M, Du L, et al. Neuroprotective effects of n – 3 polyunsaturated fatty acid-enriched phosphatidylserine against oxidative damage in PC12 cells. *Cell Mol Neurobiol.* (2018) 741:657–68. doi: 10.1007/s10571-017-0516-y

28. Lim SY, Suzuki H. Intakes of dietary docosahexaenoic acid ethyl ester and egg phosphatidylcholine improve maze-learning ability in young and old mice. *J Nutr.* (2000) 130:1629–32. doi: 10.1093/jn/130.6.1629

29. Nowacki D, Martynowicz H, Skoczyńska A, Wojakowska A, Turczyn B, Bobak Ł, et al. Lecithin derived from ω-3 PUFA fortifed eggs decreases

blood pressure in spontaneously hypertensive rats. *Sci Rep.* (2019) 7:1–11. doi: 10.1038/s41598-017-12019-w

30. Absher JR, Madeline L, Webb SW, Rayes M. *Cerebrovascular Disease, Reference Module in Neuroscience and Biobehavioral Psychology*. Amsterdam: Elsevier (2018). doi: 10.1016/B978-0-12-809324-5.23371-3

31. Yang F, Chen G, Ma M, Qiu N, Zhu L, Li J, et al. Egg-yolk sphingomyelin and phosphatidylcholine attenuate cholesterol absorption in caco-2 cells. *Lipids.* (2018) 764:217–33. doi: 10.1002/lipd.12018

32. Saito H, Ishihara K. Antioxidant activity and active sites of phospholipids as antioxidants. *J Am Oil Chem Soc.* (1997) 74:1531–6.

33. Kundaković T, Mimica Dukić N, Kovačević N. Free radical scavenging activity of Achillea alexandri-regis extracts. *Fitoterapia.* (2005) 76:574–6. doi: 10.1016/j.fitote.2005.04.023

34. Roy AS, Das S, Samanta A. Design, formulation and evaluation of liposome containing isoniazid. *Int J Pharm.* (2018) 10:52–6. doi: 10.22159/ijap.2018v10i2.24174

35. Deng W, Chen W, Clement S, Guller A, Zhao Z, Engel A, et al. Controlled gene and drug release from a liposomal delivery platform triggered by X-ray radiation. *Nat Commun.* (2018) 9:2713. doi: 10.1038/s41467-018-05118-3

36. Gupta AS, Kshirsagar SJ, Bhalekar MR, Saldanha T. Design and development of liposomes for colon targeted drug delivery. *J Drug Target.* (2013) 12:146–60. doi: 10.3109/1061186X.2012.734311

37. Wang X, Song Y, Su Y, Tian Q, Li B, Quan J, et al. Are PEGylated liposomes better than conventional liposomes? A special case for vincristine. *Drug Deliv.* (2016) 23:1092–100. doi: 10.3109/10717544.2015.1027015

38. Osman G, Rodriguez J, Chan SY, Chisholm J, Duncan G, Kim N, et al. PEGylated enhanced cell penetrating peptide nanoparticles for lung gene therapy. *J Control Release.* (2018) 285:35–45. doi: 10.1016/j.jconrel.2018.07.001

39. Biswas S, Dodwadkar NS, Deshpande PP, Torchilin VP. Liposomes loaded with paclitaxel and modified with novel triphenylphosphonium-PEG-PE conjugate possess low toxicity, target mitochondria and demonstrate enhanced antitumor effects *in vitro* and *in vivo*. *J Control Release.* (2012) 159:393–402. doi: 10.1016/j.jconrel.2012.01.009

40. Guan J, Shen Q, Zhang Z, Jiang Z, Yang Y, Lou M, et al. Enhanced immunocompatibility of ligand-targeted liposomes by attenuating natural IgM absorption. *Nat Commun.* (2018) 9:2982. doi: 10.1038/s41467-018-05384-1

41. Fathi S, Oyelere AK. Liposomal drug delivery systems for targeted cancer therapy: Is active targeting the best choice? *Fut Med Chem.* (2016) 8:2091–112. doi: 10.4155/fmc-2016-0135

42. Eloy J O, Petrilli R, Trevizan L N F, Chorilli M. Immunoliposomes: a review on functionalization strategies and targets for drug delivery. *Colloids Surf B Biointerf.* (2017) 159:454–67. doi: 10.1016/j.colsurfb.2017.07.085

43. Wei X, Zhan C, Shen Q, Fu W, Xie C, Gao J, et al. AD-peptide ligand of nicotine acetylcholine receptors for brain-targeted drug delivery. *Angew Chem Int.* (2015) 54:3023–7. doi: 10.1002/anie.201411226

44. Bobo D, Robinson KJ, Islam J, Thurecht KJ, Corrie SR. Nanoparticle-based medicines: a review of FDA-approved materials and clinical trials to date. *Pharm Res.* (2016) 33:2373–87. doi: 10.1007/s11095-016-1958-5

45. Le NT, Cao VD, Nguyen TN, Le TT, Tran TT, Hoang Thi TT. Soy lecithin-derived liposomal delivery systems: surface modification and current applications. *Int J Mol Sci.* (2019) 20:4706–33. doi: 10.3390/ijms20194706

46. Gao B, Hu X, Xue H, Li R, Liu H, Han T, et al. The changes of umami substances and influencing factors in preserved egg yolk: pH, endogenous protease, and proteinaceous substance. *Front Nutr.* (2022) 9:998448. doi: 10.3389/fnut.2022.998448

47. Laurence M, Shahidi F, Varelis P. *Encyclopedia of Food Chemistry*. New York, NY: Academic Press (2018). p. 583–625.

48. Leiva CL, Gallardo MJ, Casanova N, Terzolo H, Chacana P. IgY-technology (egg yolk antibodies) in human medicine: a review of patents and clinical trials. *Int Immunopharmacol.* (2020) 81:106269. doi: 10.1016/j.intimp.2020.106269

49. Bondia-Martinez E, Lopez-Sabater MC, Castellote-Bargallo AI, Rodriguez-Palmero M, Gonzalez-Corbella MJ, Rivero-Urgell M, et al. Fatty acid composition of plasma and erythrocytes in term infants fed human milk and formulae with and without docosahexaenoic and arachidonic acids from egg yolk lecithin. *Early Hum Dev.* (1998) 53(Supplement 1):S109–S119.

50. List GR. Soybean lecithin: food, industrial uses, and other applications. In: Ahmad MU, Xu X, editors. *Polar Lipids*. Amsterdam: Elsevier (2015). p. 1–33. doi: 10.1016/B978-1-63067-044-3.50005-4

51. Savić V, Todosijević M, Ilić T, Lukić M, Mitsou E, Papadimitriou V, et al. Tacrolimus loaded biocompatible lecithin-based microemulsions with improved skin penetration: Structure characterization and *in vitro/in vivo* performances. *Int J Pharm.* (2017) 529:491–505. doi: 10.1016/j.ijpharm.2017.07.036

52. Peñaranda-López AL, Brito-de la Fuente E, Torrestiana-Sánchez B. Fractionation of hydrolysates from concentrated lecithin free egg yolk protein dispersions by ultrafiltration. *Food Bioprod Process.* (2020) 123:0960–3085. doi: 10.1016/j.fbp.2020.07.001

53. Nguyen VV, Ponchunchoovong S, Kupittayanant S, Kupittayanant P. Effects of egg yolk and soybean lecithin on sperm quality determined by computer-assisted sperm analysis and confocal laser scanning microscope in chilled canine sperm. *Vet Med Sci.* (2019) 5:345–60. doi: 10.1002/vms3.158

54. Akashi TE, Matsumoto KA, Takamatsu Y, Hashimoto RI, Takaoka TA, Ohno A, et al. case of a patient with bile secretion disorder for whom an egg yolk lecithin-containing liquid diet was used for enteral nutrition. *Nihon Ronen Igakkai zasshi Jpn J Geriat.* (2018) 55:411–6. doi: 10.3143/geriatrics.55.411

55. Kim MR, Shim JY, Park KH, Imm BY, Oh S, Imm JY. Optimization of the enzymatic modification of egg yolk by phospholipase A2 to improve its functionality for mayonnaise production. *LWT Food Sci Technol.* (2009) 42:250–5. doi: 10.1016/j.lwt.2008.05.014

56. Miguel-Jimenez S, Del Alamo MM, Álvarez-Rodríguez M, Hidalgo CO, Peña AI, Muiño R, et al. *In vitro* assessment of egg yolk-, soya bean lecithin-and liposome-based extenders for cryopreservation of dairy bull semen. *Anim Reprod Sci.* (2020) 215:106315. doi: 10.1016/j.anireprosci.2020.106315

57. Nadri T, Towhidi A, Zeinoaldini S, Martínez-Pastor F, Mousavi M, Noei R, et al. Lecithin nanoparticles enhance the cryosurvival of caprine sperm. *Theriogenology.* (2019) 133:38–44. doi: 10.1016/j.theriogenology.2019.04.024

58. Liu Y, Guo S, Zhang Z. Study on making technology of egg yolk powder. *Grain Oil Process Food Mach.* (2003) 12:30–33.

59. Daimer K, Kulozik U. Impact of a treatment with phospholipase A2 on the physicochemical properties of hen egg yolk. *J Agric Food Chem.* (2008) 56:4172–80. doi: 10.1021/jf703641e

60. Sun J, Zhang W, Zhang M, Liang Z, Du J. Optimization of extraction process of lecithin from duck egg yellow. *J Food Saf Qual Inspect.* (2019) 10–21:7311–5.

61. Treede I, Braun A, Sparla R, KM, Giese T, Turner JR, et al. Anti-inflammatory effects of phosphatidylcholine. *J Biol Chem.* (2007) 282:27155–64. doi: 10.1074/jbc.M704408200

62. Boselli E, Caboni MF. Supercritical carbon dioxide extraction of phospholipids from dried egg yolk without organic modifier. *J Supercrit Fluids.* (2000) 19:45–50. doi: 10.1016/S0896-8446(00)00073-5

63. Smith MC, Crist RM, Clogston JD, McNeil SE. Zeta potential: a case study of cationic, anionic, and neutral liposomes. *Anal Bioanal Chem.* (2017) 409:5779–87. doi: 10.1007/s00216-017-0527-z

frontiers | Frontiers in Nutrition

TYPE Original Research
PUBLISHED 09 February 2023
DOI 10.3389/fnut.2022.1011553

OPEN ACCESS

EDITED BY
John-Lewis Zinia Zaukuu,
Kwame Nkrumah University of Science and Technology, Ghana

REVIEWED BY
Ioana Stanciu,
University of Bucharest, Romania
Jan Skočilas,
Czech Technical University in Prague, Czechia

*CORRESPONDENCE
Adrienn Varga-Tóth
✉ toth.adrienn@uni-mate.hu

SPECIALTY SECTION
This article was submitted to Nutrition and Food Science Technology, a section of the journal Frontiers in Nutrition

RECEIVED 04 August 2022
ACCEPTED 30 August 2022
PUBLISHED 09 February 2023

CITATION
Varga-Tóth A, Németh C, Dalmadi I, Csurka T, Csorba R, Elayan M, Enkhbold M, Hidas K and Friedrich LF (2023) Investigation of the effects of bovine collagen peptides and mixed berries on rheological properties and biological activity of egg white-based beverage *via* central composite design. *Front. Nutr.* 9:1011553. doi: 10.3389/fnut.2022.1011553

Investigation of the effects of bovine collagen peptides and mixed berries on rheological properties and biological activity of egg white-based beverage *via* central composite design

Adrienn Varga-Tóth[1]*, Csaba Németh[2], István Dalmadi[1], Tamás Csurka[1], Renáta Csorba[1], Majd Elayan[1], Munkhnasan Enkhbold[1], Karina Hidas[1] and László Ferenc Friedrich[1]

[1]Department of Livestocks Products and Food Preservation Technology, Institute of Food Science and Technology, Hungarian University of Agriculture and Life Sciences, Budapest, Hungary, [2]Capriovus Ltd., Szigetcsép, Hungary

Modern consumer expectations have become highly diversified: they want more opportunities to meet diverse family needs (diversity of family members in age, gender, physical activity, etc. ,) and individual health goals with a huge variety of sensorial preferences. Our research is aimed to develop a protein-dense, highly bioactive, lactose- and whey protein-free beverage applying a central composite rotational design (CCRD) with 2 factors. For this purpose, an egg white-based beverage was flavored with mixed berries (factor A) and enriched with bovine collagen peptides (factor B). After suitable sample preparation, the rheological properties were investigated by an Anton Paar MCR 92 rheometer (with CC 27 system, and flow behavior was analyzed with a Herschel-Bulkley (H-B) model). The antioxidant capacity of samples was investigated by Ferric Reducing Antioxidant Power (FRAP) method, the total anthocyanin content was estimated based on a spectrophotometric method, and the total phenolic content was determined by the Folin Ciocalteu method. Our results are figured on response surfaces demonstrating that both factors and their interactions show a positive correlation with the examined parameters. Based on the CCRD, all investigated parameters are significantly influenced by at least one aspect and can be adequately estimated for further product development.

KEYWORDS

egg white, dairy replacement, functional food, central composite design - response surface methodology, bioactive compounds, bovine collagen peptides, berries and fruits, rheological properties

1. Introduction

The demand for functional foods was already raised about a half-century ago when the first health and nutrition concerns were established. However, real definitions and first needs for regulation have been formulated since the 1980s when the first regulation was introduced in Japan (1). Finally, in 2006, the European Parliament and Council introduced their first regulation on nutritional and health claims [Reg. (EU) n. 1924/2006] (2). But despite this, due to the exploding demand for specific functional foods and food ingredients, there is still a continuously existing need for further definitions and regulations (3). As support for understanding our work, two widely accepted definitions are introduced in the following. As comprehensively formulated

by Gur et al. (4), functional foods are natural or processed foods that contain biologically active compounds; that, in defined, effective, and non-toxic amounts, provide a clinically proven and documented health benefit utilizing specific biomarkers for the prevention, management, or treatment of chronic disease or its symptoms. According to a short definition by Santini et al. (5), functional foods are nutritional products that provide health and medical benefits, including the prevention and treatment of disease. In these aspects, the addition of antioxidant compounds such as anthocyanins, phenolic and polyphenolic compounds, or bioactive peptides may achieve a functional effect on foods. Regarding studies in the field of consumer acceptance (6), the term "functional food" has already reached the recognition of food consumers and has been becoming increasingly prominent in advertising campaigns which might be a successful tool for product introduction.

Fruits such as berries should be an important part of a healthy diet due to their content of bioactive compounds. The most consumed berries, such as blackberry, blueberry, cranberry, raspberry, and strawberry, are important sources of bioactive compounds and are consumed worldwide as fresh or processed products (7). An increasing interest is shown in literature and clinical experiments for the role of berries and their components in the modulation of oxidative stress (8), cardio-vascular symptoms (9), inflammation, and lipid metabolism (10, 11).

Antioxidants are an extremely heterogeneous 'class' of compounds differing in chemical structures (i.e., hydrophilic, hydrophobic), distribution in nature (i.e., some are specific to vegetable species, others are generally present in food raw materials), and range of concentrations both in foods and in the human body (from nanograms to milligrams). Some classes of antioxidants, such as some vitamins, carotenoids, and polyphenols, merit specific attention not only because they are well represented in our diet but also because they are differently absorbed and metabolized and may exert diverse functions with significant impact on our health (12). They may have different actions, effectiveness against oxidative stress, and specificity (e.g., scavenging of superoxide, hydroxyl or peroxyl radicals, quenching of singlet oxygen or ferryl species, etc.) and biological action apart from the antioxidant one (e.g., modulation of functions such as detoxification, immune response, inflammation) (13).

Anthocyanins—a group of naturally occurring flavonoid heterosides in the plant kingdom—are well-known as natural colorant compounds from fruits and vegetables responsible for the red, purple, or blue color and are used as natural additives in many food products, providing a reddish, blueish color depending on the pH-value of the food product. Depending on their chemical structure, anthocyanins are generally considered heat and storage-sensitive compounds (14). For example, the major anthocyanins in strawberry are mono-glycosidi (e.g., pelargonidin-3-glycoside and pelargonidin-3-rutinoside) that undergo structural changes during storage which may lead to a deceleration (15). However, anthocyanins stability might be improved by the addition of peptides and polysaccharides (16).

Phenolic compounds such as polyphenols are reported as health-supporting natural compounds usually of plant origin. Flavonoids and non-flavonoids are the two major classes of phenolic compounds common to berries. Blueberries score extraordinarily well in rankings among polyphenol-rich berry fruits (17). Flavonoids (40%) and phenolic acids (59%) are the dominant phenolic compound fractions in them, their concentration may reach 3 mg/g during ripening (18).

Only a little scientific evidence is available on the effect of processing on polyphenol bioavailability. Some data are present in the literature on the effect of cooking on the stability and retention of some polyphenols (17), however, investigations on the absorption response are limited.

The addition of different protein sources may lead to a higher functionality of foods as well. For example, bovine collagen peptides are reported as functional compounds for skin protective and renewal effects e.g., in the healing of pressure ulcers (19). Dermal collagen is associated with skin and joint elasticity (20) which shows a close relation to collagen type I RNA expression and fibroblast growth after oral collagen peptide (CP) treatments (21).

The effect of concentration on the apparent viscosity of hydrocolloids is generally described by either an exponential or a power relationship (22, 23). Despite the huge availability as a waste by-product from meat livestock industries and a great interest in nutrition, only a few reports describe the potential use and characterization of collagen peptides, especially bovine collagen peptides (24), Currently about 28 types of collagen of different structure, amino acid composition, and biological role are reported (25). A collagen molecule consists of three left-handed helical polypeptide chains, rolled into a right-handed triple helix (c.a. 300 kDa). But the common feature of all collagens is a repeating Gly-X-Y amino-acid sequence (26, 27), where X and Y can be any amino acid, however, proline (Pro) and hydroxyproline (Pro-OH) residues are reported as the most often encountered (28). Collagen contains both polar [e.g., aspartic acid (Asp), glutamic acid (Glu), arginine (Arg), lysine (Lys)], and apolar [e.g., proline (Pro), serine (Ser), glycine (Gly)] amino acids (29). However, the native collagen helixes are rolled in a way to expose the hydrophilic segments to the solution, they might have amphiphilic character. The latter can be unleashed by denaturation and/or hydrolysis of the triple helix, using chemical or enzymatic reactions (30, 31).

Low-molecular-weight collagen peptides from fish skin have been presented as high immunomodulatory and antioxidant activity and better absorbable compounds than whole molecule collagens (32). Collagen peptide as a hydrolysate of collagen has been reported to have various beneficial effects, e.g., protecting skin aging, promoting better wound healing (33, 34), increasing muscle strength (35), reducing obesity (36), maintaining blood pressure (37), preventing atherosclerosis (38) and modifying lipid metabolism (39). Despite the health promotion of collagen peptides, a balanced and moderated—considering age, gender, physical and health state—daily protein and amino acid intake is still recommended to avoid overconsumption and related harmful effects (40). Despite a huge number of publications reporting the health benefits and bioactivity of collagen peptides, there is a lack of publications investigating the impacts of collagen peptides on techno-functional attributes. Global market for collagen peptides estimated at 564.4 million US$ in the year 2020, is projected to increase to 822.9 million US$ by 2027, growing at a CAGR of 5.5% over the investigated 7 years (41).

A further opportunity for functional food development is to exchange or reform or inhibit some compounds such as lactose or whey proteins. However, dairy products are considered highly nutritious food products, and increasing the absorption of several micronutrients (e.g., calcium and magnesium) their consumption is recommended on a daily basis. Some consumers have to replace them by consuming lactose-free and/or dairy-replacement products (42). Lactose intolerance and whey protein allergy have become today hot topics in the field of food and nutrition. In the last 10,000 years, the

use of domesticated ruminants as a source of milk and dairy products has expanded until today when the dairy industry has become one of the largest sectors in the modern food industry, including the spread at the present time to countries such as China and Japan (43). About 70% of the adult world population is lactose-intolerant, due to low levels of intestinal lactase, (lactase-phlorizin hydrolase (LPH), a β-d-galactosidase). This may be due to the loss of intestinal lactase in adulthood, a condition transmitted by an autosomal recessive gene, which differs in humans according to race. According to the cultural-historical hypothesis, the mutation that allows the metabolization of lactose appeared about 10,000 years ago in the inhabitants of Northern Europe where mammalian milk continued in the diet after weaning, and lactase-persistent populations were genetically selected in some areas. Many intolerant individuals can tolerate low levels of lactose in their daily diet. Many products are marketed nowadays as alternatives to dairy products for lactose-intolerant individuals. However, the rules for low-lactose foods are currently not harmonized in the European Union (44). Bovine milk proteins are described as potential allergens affecting about 1–3% of adults and 3–5% of children under of the age 1 year worldwide (45). Cow's milk contains ∼30–35 g/L of proteins and the class of lactoserum proteins (whey) represents 20% of total protein. β-lactoglobulin is the most immunogenic and abundant from whey proteins (c.a. 50%) (46).

Milk and dairy replacements (analogs) are produced usually from plant-driven raw materials worldwide satisfying the increasing demand for casein- and whey-protein-free products, although these products have generally poor nutritional quality (47). Although milk and dairy replacements are considered functional foods because they might have additional positive effects on human digestion. An excellent opportunity is to produce egg white-based dairy and milk replacement products. Avian eggs and egg white have been reported as natural functional foods (48). E.g., certain egg white-derived peptides can play a role in controlling the development of hypertension by exerting Vaso relaxing effects (due to ovokinin) (49). Hen egg white lysozyme-derived peptides showed moderate inhibitory activities against calmodulin-dependent phosphodiesterase (CaMPDE) and free-radical scavenging properties. Egg lysozyme hydrolysates have the potential as functional foods and nutraceuticals (50, 51).

The aim of this study is the development and investigation of a beverage containing highly bioactive proteins-containing beverage providing a huge concentration of bioactive compounds such as antioxidants and polyphenols. For this purpose, a central composite rotatable design (CCRD) was applied for investigating the effects of concentrations of bovine collagen peptides and mixed berries' concentration on the rheological properties and bioactive compounds of an egg white-based dairy replacement product.

2. Materials and methods

2.1. Materials and sample preparation

2.1.1. Materials used for sample preparation

The egg white-based milk replacement "ToTu beverage" produced by Capriovus (Szigetcsép, Hungary) was used as the main ingredient in our samples. According to the producer, this milk replacement is made due to acidic and enzymatic reactions from liquid egg white (52). The product contains carbohydrates and fats only in traces. But at the same time, it is a great source of easy-digestible peptides and proteins (53), so its consumption may be recommended for people replacing bovine milk and dairy, dealing with diabetes or insulin resistance (54).

In every sample, erythritol (distributed by Bulkshop, Budapest, Hungary) was used as a low-calorie sugar-alcohol sweetener in a range of 15 % m/m. Regarding the literature, erythritol is concerned as a popular and highly accepted sugar alcohol sweetener (55). Furthermore from pilot experiments, it has been concluded that its sweet taste is similar to white sugar in plate and flavored ToTu beverages.

The frozen mixed berries (distributed by Lidl Budapest, Hungary; containing strawberries, raspberries, blueberries, and red currants) were used after thawing (from −18 to 10°C at room temperature) and homogenized in an electric shaker (PHILIPS HR3655/00 smoothie maker) for 2 min. The berries were used as a smoothie, or pulp containing flesh and skin, because antioxidant and phenolic compounds are reported to be present in high concentration in the skin of blueberries and red currant (56). Mixed berries were used in different concentrations (between 1.89 and 23.11 g /100 g) in samples according to the CCRD, as shown in Table 2.

The bovine collagen peptides were used because of their high popularity among collagen peptides (41) and their great bioactivity (51). They were purchased from and distributed by GAL SynergyTech Zrt. (Budapest, Hungary) and were added in different concentrations (between 3.52 and 0 g/100 g) to each sample regarding the CCRD presented in Table 2.

2.1.2. Sample preparation

ToTu beverage, erythritol, mixed berries, and bovine collagen peptides were mixed in the adequate ratios given in CCRD and described above. After measurements of the ingredients, the samples were homogenized in an electric shaker (PHILIPS HR3655/00 smoothie maker) for 2 min. Directly after homogenization, the samples were bottled in 250 mL PET bottles and closed.

The heat treatment was carried out in a laboratory water bath at 65°C for 3 h. Both parameters were selected due to the recommendations of the ToTu beverage's producer. Following heat treatment, samples were immediately cooled to 10°C in melting ice. The measurements were carried out 24 h after the heat treatment.

2.2. Methods

2.2.1. Determination of rheological properties

The samples after heat treatment and cooling period showed smoothie-like or yogurt beverage-like consistency depending on the mixed berries' concentration, so their rheological properties were analyzed by Anton Paar MCR 92 rheometer (Anton Paar, France) in rotational mode equipped with a concentric cylinder (CC27) similar to Hidas et al. (57). Anton Paar RheoCompass software (v 1.21.852) was used to control the measurements. The temperature of the rheological experiment was kept constant at 15°C. Shear stress was measured in increasing and decreasing shear rate intervals between 10 and 1,000 s^{-1} for 31 measurement points in each interval with a period of 3 s.

The Herschel-Bulkley model (see equation below) was used to analyze the flow curves (shear rate-shear stress diagrams)

data of decreasing shear rate interval were analyzed using Excel solver (58–60)

$$\tau = \tau_0 + K\gamma^n \quad (1)$$

- τ—shear stress (Pa);
- τ_0–yield stress (Pa);
- γ–shear rate (s^{-1});
- K—consistency coefficient (Pa s^n);
- n—flow behavior index (dimensionless).

This model was used to describe the rheological properties of the samples. All determination coefficient values (R^2) of the fitted models were higher than 0.98.

2.2.2. Determination of total anthocyanin concentration (TA)

In this method, the anthocyanin content of egg white-based beverage samples was measured by the pH differential method presented by Lee et al. (61) and Taghavi et al. (62). One mL of the egg white-based beverage samples was mixed thoroughly with 19 mL buffer pH 1.0 (0.025 M potassium chloride) and 1 mL of the egg white-based beverage samples was mixed thoroughly with 19 mL buffer pH 4.5 (0.4 M sodium acetate buffer). Both sample-buffer solutions were incubated for 20 min at room temperature and centrifuged at room temperature, for 15 min, at 1,0000 rpm (Hettich MIKRO 120, Andreas Hettich GmbH. Tuttlingen, Germany). The supernatant was then removed, and the absorbance was read at 520 and 700 nm (Hitachi U-2900 spectrophotometer). The following equation was used for the calculation of the anthocyanin concentration.

$$TA = A{*}VM \quad (2)$$

- A: (A520 nm–A700 nm) pH 1.0 – (A520 nm–A700 nm) pH 4.5;
- V: volume of extract (mL);
- M: mass of the egg white-based beverage sample (g).

2.2.3. Determination of total antioxidant capacity

The total antioxidant capacity was obtained by FRAP (Ferric Reducing Antioxidant Power) method described by Moure et al. (63). The method reported by Carletti et al. (64) was slightly modified for the measurement of FRAP of the egg white-based beverage samples.

The FRAP reagent was freshly prepared as a mixture of acetate buffer (300 mM, pH = 3.6), TPTZ (10 mM), and ferric chloride (20 mM) at a 10:1:1 (v/v/v) ratio, respectively. Then, 3 mL of the FRAP reagent and 100 µL of the sample were mixed and incubated at 30°C for 30 min in a water bath avoiding light. The absorbance was determined at 593 nm using a Hitachi U-2900 spectrophotometer. Calibration was carried out using ascorbic acid solutions between 0.01 and 0.1-mM concentrations. The results were expressed as g ascorbic acid equivalent/l egg white-based beverage.

2.2.4. Determination of total polyphenols content (TPC)

The total polyphenolic content (TPC) was determined using the colorimetric Folin–Ciocalteu method (65) by spectrophotometric analysis (spectrophotometer Hitachi U-2900). The measurement was carried out similarly to Musilova et al. (66). The absorbance of blue solutions was measured in cuvettes of 1 cm width at a wavelength of 765 nm. The calibration was carried out with gallic acid solutions in a concentration range between 0.01 and 1.5 g/L. The content of total polyphenols in the sample was expressed as the content of gallic acid in g/l of the sample.

2.2.5. Experimental design: Central composite rotational design (CCRD)

For the experiment, a central composite rotational design (CCRD) with two variables was performed for design and data evaluation as described by Box and Draper (67). The two variables were the concentration of mixed berries (factor A) and the bovine collagen peptide concentration (factor B). The factor levels are demonstrated in Table 1. The concentrations of mixed berries and bovine collagen peptides used for every sample are presented in Table 2.

For approximation, we used the response surface obtained based on the secondary polynomial model. The measurements were carried out in a random order, and the data were analyzed by specific software (The Unscrambler 10.0.0 Camo-software, Norway). The general form of the polynomial model used in our study is described by the following equation:

$$\mathbf{Y} = \beta_0 + \beta_1\mathbf{X_1} + \beta_2\mathbf{X_2} + \beta_{11}{*}\mathbf{X_1^2} + \beta_{22}\mathbf{X_2^2} + \beta_{12}\mathbf{X_1X_2}, \quad (3)$$

- Y = independent variable;
- β_1, β_2, β_{11}, β_{22}, β_{12} = regression coefficients;
- X_1 = a mixed berries concentration, % m/m;
- X_2 = bovine collagen peptides concentration, % m/m.

Three replicates of the center point were selected (12.5 g/100 g mixed berries and 1.75 g/100 g bovine collagen peptides' concentration) based on a pilot experiment considering the sensorial attributes of enriched and flavored egg white-based beverage. The independent variables (a: mixed berries and B: bovine collagen peptides) were varied between 1.89 and 23.11 and 0.0 and 3.52/100 g, respectively, and dependent variables of τ_0, n K, TA, FRAP, and TPC were measured.

3. Results and discussion

3.1. Changes in rheological properties

Figure 1 shows the flow curves (shear stress vs. shear rate), which presents the downward curves of all examined samples. The upwards curves are not shown in this study because it would make the figure crowded. The samples behave as non-Newtonian fluids, namely the pseudoplastic type. According to Holdsworth (68), most fluid foods exhibit pseudoplastic behavior, where the shear stress and the apparent viscosity decrease with increasing deformation rate (22).

However, they may vary highly in rheological behavior due to their complex structure and composition (concentration and ripening stage of fruit ingredients, etc.). Shear stress values of almost all samples show some outlier values between 10 and 100 1/s shear rates, which may be explained on the one hand by

TABLE 1 The trial design and factor levels in encoded values applied in the central composite rotational design (CCRD) (*is a theoretically calculated value, 0/100 g bovine collagen peptides were added).

Variable	Encoded factor	−1.4142	−1	0	1	1.4142
mixed berries concentration, g/100 g	X1	1.89	5.00	12.50	20.00	23.11
bovine collagen peptides concentration, g/100 g	X2	−0.02*	0.50	1.75	3.00	3.52

TABLE 2 The calculated concentrations of mixed berries and bovine collagen peptides according to the central composite rotational design (CCRD) (*is a theoretically calculated value, 0/100 g bovine collagen peptides were added).

CCRD	test nr.	Mixed berries concentration, g/100 g (A)	Bovine collagen peptides concentration, g/100 g (B)
*L:A-a	1	1.89	1.75
*H:A-a	2	23.11	1.75
*L:B-a	3	12.50	−0.02*
∗H:B-a	4	12.50	3.52
Cube001a	5	5.00	0.50
Cube002a	6	20.00	0.50
Cube003a	7	5.00	3.00
Cube004a	8	20.00	3.00
Cent-a	9	12.50	1.75
Cent-b	10	12.50	1.75
Cent-c	11	12.50	1.75

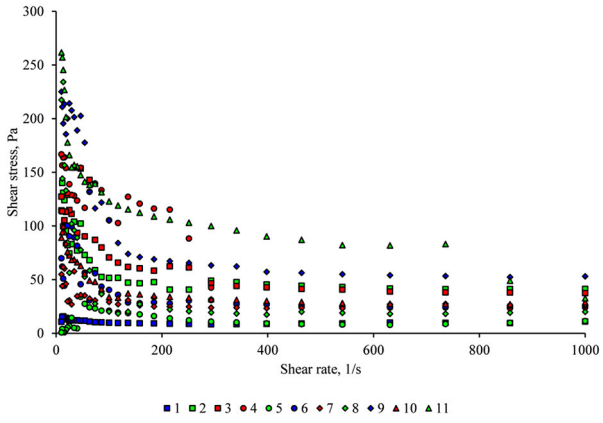

FIGURE 1
The flow curves (shear stress vs. shear rate) of egg white-based beverages with different mixed berries and bovine collagen peptide concentrations (samples are coded by test numbers).

the inaccurate measurement at low shear stress values, on the other hand by the slight foaming of samples observed during the rheological investigation.

τ_0 values calculated by the Herschel-Bulkley model varied between 0.12 and 37.38 Pa (Table 3). The lowest τ_0 value was calculated for the sample containing the lowest mixed berry concentration (1.89/100 g, sample 1), and its flow curve shows the lowest shear stress values in the entire investigated interval. The highest τ_0 value (37.38) was calculated for sample 11. On the flow curves, the highest shear stress values are observed for the core points of CCRD (samples 9, 10, and 11) containing 12.5 g/100 g mixed berries and 1.75 g/100 bovine collagen peptides. It might suggest that the mixed berries' concentration (factor A) has a positive and the bovine collagen peptides' concentration has a negative correlation with τ_0 values. Thus, in CCRD, a positive β-coefficient of factor A and a negative β-coefficient for B are calculated. However, the CCRD model is not significant ($p = 0.529$). It means that τ_0 values can't be estimated for the examined beverage samples.

The highest flow behavior index, n was calculated for sample 1, containing the lowest mixed berries concentration. If $n > 1$, the flow behavior is considered dilatant or shear thickening. Accordingly, sample 1 should have a dilatant behavior ($n = 1.14$), as long as, all other samples could be described as pseudoplastic fluids (calculated n values between 0.55 and 0.75, Table 4). But dilatancy is considered as the behavior showing an increase in viscosity with increasing shear rate. But investigating (Figure 1) it is clear, that every sample has a decreasing shear stress in the function of shear rate. It means that they have pseudoplastic behavior. In our samples, it is recognized that pseudoplasticity represents an irreversible structural breakdown and the decrease in viscosity occurs as a result of molecular alignment that takes place within such a substance (69).

The mixed berries concentration had a significant effect on n values ($p = 0.0363$). Although it showed a negative correlation with both factors, but a positive correlation with their interaction. Despite this, the CCRD model was not significant ($p = 0.179$). Similar flow behavior index values and a negative correlation of fruit concentration flow behavior index were found by Wang et al. (70) in strawberry-flavored goat milk beverages. In aspects of τ_0 and n the applied CCRD statistical model fails in the prediction of the rheological behavior of the beverages. Thus, it can be seen that increasing mixed berries and bovine collagen peptide concentrations have practical effects on rheological properties and have to be considered for further product and technology development.

The calculated values of the Herschel-Bulkley model are presented in Table 3.

In the investigation of rheological parameters, only the consistency coefficient (or consistency indices) is described by a statistically significant CCRD model ($p = 0.0007$). The measured K values are summarized in Table 4: their values ranged from 0.01 to 16.34 Pas^n. The measured K values may imply that the higher mixed berries concentration and/or higher bovine collagen peptides' concentration was used, the higher K values are calculated. This suspension is proven by the β-values shown in Table 4. The

TABLE 3 Experiment design [central composite rotational design (CCRD)] and factor levels with actual values, and measured results of Herschel-Bulkley model and bioactive compounds (*is a theoretically calculated value, 0/100 g bovine collagen peptides were added).

Test nr.	Mixed berries concentration, g/100 g (A)	Bovine collagen peptides concentration, g/100 g (B)	τ_0, Pa	k, Pa s^n	n, -	R^2	Total anthocyanin concentration, mg/L	FRAP-value, g/L	Total polyphenol content, g/L
1	1.89	1.75	0.12 ± 0.05	0.01 ± 0.004	1.14 ± 0.21	0.99	3.42	0.63	0.05
2	23.11	1.75	21.43 ± 1.31	11.97 ± 0.92	0.60 ± 0.09	0.98	141.97	1.19	1.03
3	12.50	−0.02*	36.48 ± 2.47	7.36 ± 0.58	0.65 ± 0.04	0.99	60.27	0.84	0.69
4	12.50	3.52	11.47 ± 1.16	14.60 ± 1.25	0.65 ± 0.05	0.98	58.97	0.94	0.70
5	5.00	0.50	2.86 ± 0.72	2.06 ± 0.05	0.75 ± 0.06	0.98	6.11	0.73	0.07
6	20.00	0.50	17.54 ± 0.95	6.11 ± 0.24	0.61 ± 0.06	0.99	101.63	1.07	0.85
7	5.00	3.00	3.29 ± 0.12	7.10 ± 0.48	0.64 ± 0.05	0.98	5.03	0.77	0.06
8	20.00	3.00	15.28 ± 1.61	16.34 ± 1.27	0.55 ± 0.04	0.98	98.74	1.04	0.87
9	12.50	1.75	7.96 ± 0.91	15.55 ± 2.01	0.67 ± 0.06	0.99	59.20	1.09	0.71
10	12.50	1.75	7.45 ± 0.84	11.90 ± 0.92	0.67 ± 0.05	0.98	58.90	0.98	0.69
11	12.50	1.75	37.38 ± 2.56	7.58 ± 0.55	0.55 ± 0.03	0.98	60.87	1.00	0.71

TABLE 4 The regression coefficients of the quadratic polynomial model for response analysis with encoded units.

Constant	17.598	0.5299	0.63	0.1787	11.68	0.0007*	59.66	0.0001*	1.023	0*	0.71	0.0001*
A	0.947	0.1831	−1.66E-02	0.0363*	0.50	0.0113*	6.42	0*	2.31E-02	0.0003*	4.97E-02	0.0002*
B	−3.719	0.3584	−1.67E−02	0.6555	2.552	0.0214*	−0.58	0.8185	1.44E-02	0.3835	2.93E-03	0.9242
AxB	−0.536	0.9219	8.78E-03	0.8667	1.04	0.385	−0.36	0.9192	−1.31E-02	0.5677	5.78E-03	0.8946
AxA	−4.256	0.3757	7.04E-02	0.1536	−2.39	0.0481*	2.56	0.4117	−4.45E-02	0.0562	−9.61E-02	0.0401*
BxB	1.025	0.8242	−1.69E-02	0.7034	−0.39	0.6846	−2.67	0.3933	−5.32E-02	0.0315*	−3.58E-02	0.3518

A: Mixed berries concentration, g/100 g; B: Bovine collagen peptides concentration, g/100 g; * significant effect ($p < 0.05$).

10.3389/fnut.2022.1011553

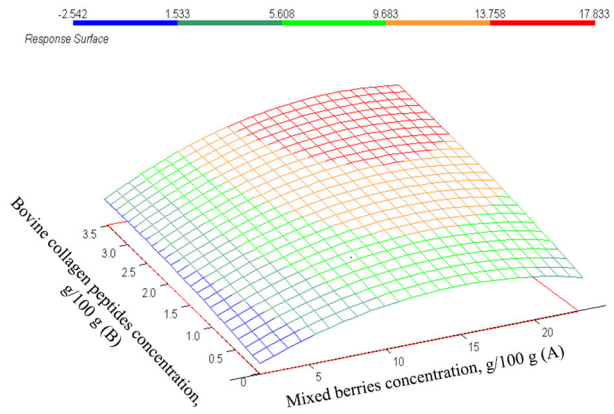

FIGURE 2
The estimated values of K in function of mixed berries concentration (A) and bovine collagen peptides concentration (B).

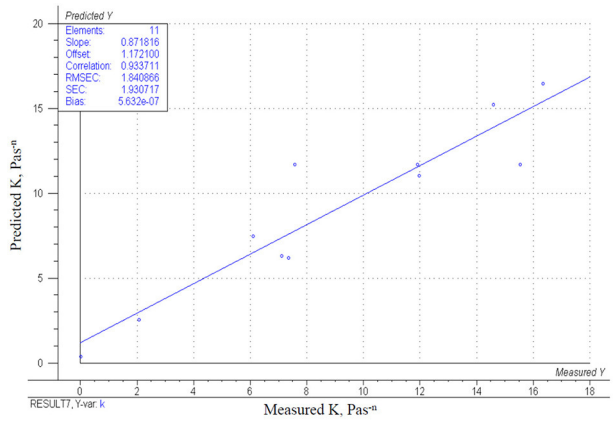

FIGURE 3
Correlation of the obtained model and the measured results for the change in K.

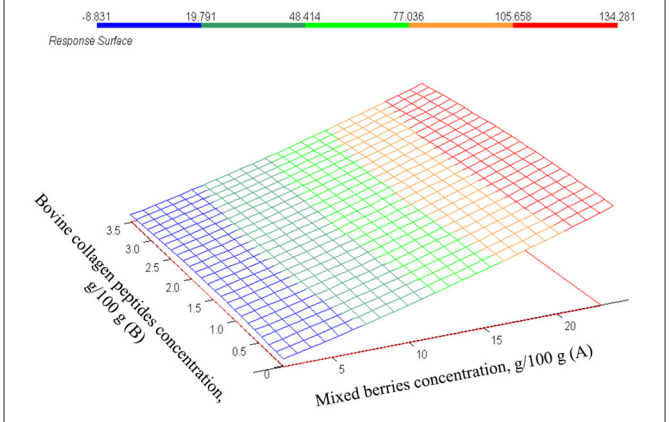

FIGURE 4
The estimated values of total anthocyanin concentration. mg/L in function of mixed berries concentration (A) and bovine collagen peptides concentration (B).

interaction of both parameters gives a positive β-coefficient. The effects of parameters are demonstrated in Figure 2. The higher consistency coefficient (K) was estimated if higher concentrations of mixed berries or bovine collagen peptides were used. It means that the increase of one or both factors results in a thickener, more contentious beverage. The correlation of the model with the measuring points ($r^2 = 0.87$) is shown in Figure 3.

Similar results were reported by Penna et al. (71) analyzing the rheological parameters of commercial lactic beverages obtained by the Herschel–Bulkley model. The authors explained their findings by inter- and intramolecular changes in their samples, which may be the reason in our experiment as well.

However, our samples were less consistent than some milk-based beverages reported by Dogaru et al. (72), the difference may be based on the different sweetener types and fruit concentrations used. In practice, the increase of both factors indicated a thicker consistency and more deviation from Newtonian flow behavior, providing a low-fat yogurt beverage with similar flow behavior (73) that could be accepted by consumers as a dairy beverage replacement.

3.2. Total anthocyanin concentration

The measured total anthocyanin concentration (TA) of samples is summarized in Table 3. which shows a proportional tendency between 3.42 and 141.97 mg/L in the function of mixed berries concentration. The higher the concentration of mixed berries concentration added, the darker and more reddish-blueish coloration was observed in the samples. This phenomenon seems to be in correlation with TA concentration. For example, the dark blue coloration of blueberries is a result of the high level of anthocyanin concentration (56, 74).

Regarding the CCRD model ($p = 0.0001$) the total anthocyanin concentration is significantly influenced only by mixed berries concentration ($p = 0.000$) as presented in Table 4. However, the bovine collagen peptides' concentration has a positive correlation, and the interaction of factors has a negative effect on the total anthocyanin concentration, it is not statistically significant. The estimated effects are represented in the response surface shown in Figure 4. The increasing values of total anthocyanin concentration are clearly visualized as the effect of increasing mixed berries concentration The correlation between the estimated model and measured values is demonstrated in Figure 5 ($r^2 = 0.98$).

The same order of magnitudes TA were reported in fresh, frozen, and frozen-dried strawberries using a similar method to Taghavi et al. (62). It seems that anthocyanin and phenolic compounds stay stable during cold storage of fruit yogurts due to the bounds between proteins and phenolic compounds (75), the intermolecular actions between bovine collagen, egg white proteins, and anthocyanins haven't been deeply analyzed yet. Although, it can be suggested that collagen peptides can interact with anthocyanin and phenolic compounds (26, 27, 32) and in practice, it may play a key role in the development of long-term stabilized color of egg white-based fruit flavored beverages. From the rheological investigation, it may be concluded that in our samples, intermolecular reactions took place which may help stabilize their color during longer storage as well.

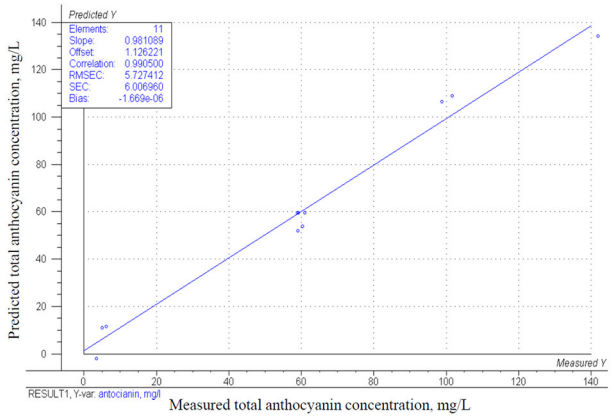

FIGURE 5
Correlation of the obtained model and the measured results for the change in total anthocyanin concentration mg/L.

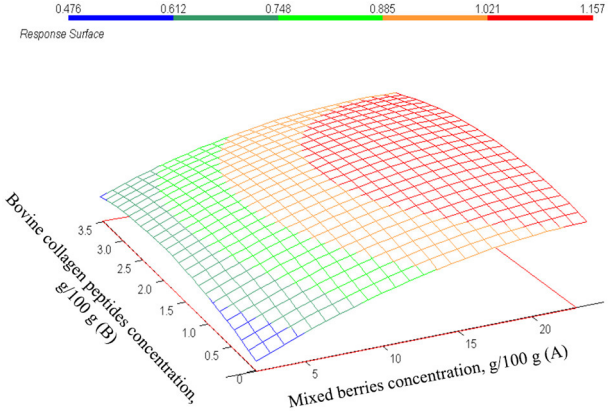

FIGURE 6
The estimated values of FRAP g/L in function of mixed berries concentration (A) and bovine collagen peptides concentration (B).

3.3. Total antioxidant capacity

Table 3 presents the measured values of total antioxidant capacity expressed in g/l ascorbic acid equivalent FRAP values. The measured antioxidant capacities (0.63 1.9 g/l) meet the range of published values found in berries (74) and reported in fruit-flavored yogurts (76). Antioxidant concentrations of fresh blueberries and strawberries were reported at 1,107.14 and 199.49 mg/kg, respectively by Mustafa et al. (77) using an HPLC-MS/MS method. However, the method used in our study is different, the magnitude of measured FRAP values are showing a similar antioxidant concentration.

The data of the fitted CCRD model are summarized in Table 4: the model is significant ($p = 0.000$). Similar to the total anthocyanin concentration, mixed berries concentration has a significant effect on the FRAP values ($p = 0.0003$) and its correlation is positive to the measured values. However, collagen peptides have antioxidant activity (49, 51), and show a positive correlation (β-coefficient = 1.44E-02) in our model, their effect is not statistically significant ($p = 0.383$). The estimated values of total antioxidant capacity are shown in Figure 6 as a function of the bovine collagen peptides and mixed berries concentrations. If the goal is to achieve the highest total antioxidant capacity in egg white-based berry flavored beverages, a wide range of bovine collagen peptides' concentration (between 0.5 and 3.2/100 g) and a higher mixed berries concentration (between 28 and 23/100 g) are recommended. Figure 7 represents the correlation ($r^2 = 0.95$) of measured and estimated FRAP values.

A preservation technology applied for extending shelf-life is required for all food products. In the case of milk and egg products, heat treatments are commonly applied. The heat treatment seems to increase antioxidant capacity and bioavailability of bioactive compounds (53, 66), so in this context, the heat treatment applied in our experiment may improve the bioactivity of the egg white-based beverages.

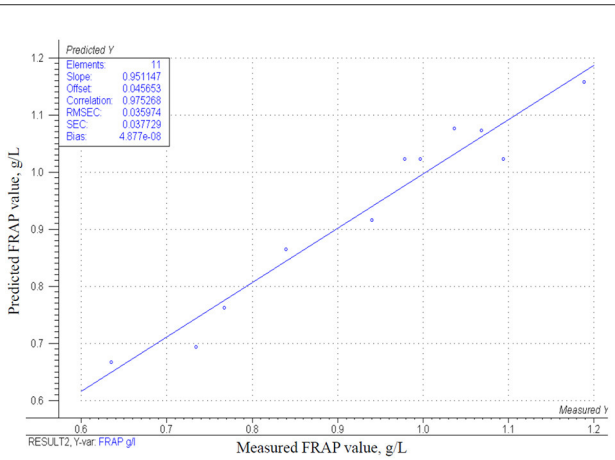

FIGURE 7
Correlation of the obtained model and the measured results for the change in FRAP g/L.

3.4. Total polyphenols content

The measured total polyphenol concentrations (TPC) presented in Table 3 vary greatly between 0.05 and 1.03 g/L. A positive correlation between mixed berries concentration and TPC might be assumed from measured values. This finding is supported by the results of the estimated CCRD model ($p = 0.0001$) described in Table 4. Regarding the regression coefficients and p-values, the mixed berries concentration has a significant effect ($p = 0.0002$) on TPC and the correlation of both factors are positive (β-coefficient = 4.97E-02; β-coefficient = 2.93E-03, respectively) as well as their interaction correlates positively (β-coefficient = 5.78E-03), although factor B and the interaction of both factors are not significant ($p = 0.924$ and $p = 0.895$, respectively). This is shown in Figure 8. The estimated values and measured values are demonstrated in Figure 9 ($r^2 = 0.96$).

Blueberry is considered a berry fruit rich in phenolic compounds, ascorbic acid, and other antioxidants (78) as discussed above. TPC values were reported in a range of 77–82 mg/100 g for blueberries grown in the Black Sea Region of Turkey (74) and 305.38 ± 5.09 mg/100 g for blueberries from the subtropical areas of Brazil (79). In fresh and frozen raspberries a total phenolic concentration of 185.57 mg GAE/100 g and 1,476.62 mg GAE /100 g were reported, respectively (80). These levels correspond to yogurt beverages enriched with different berries (76) and with our

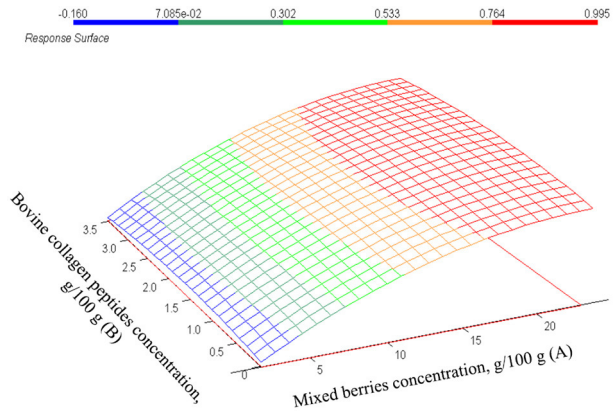

FIGURE 8
The estimated values of total polyphenol content. g/L in function of mixed berries concentration (A) and bovine collagen peptides concentration (B).

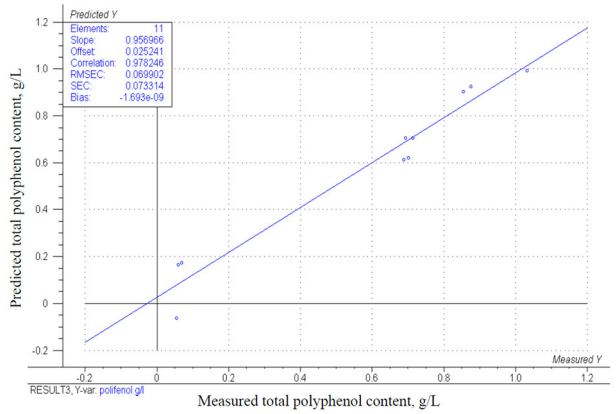

FIGURE 9
Correlation of the obtained model and the measured results for the change in total polyphenol content g/L.

measured results (taking into consideration the used concentrations of mixed berries). However, in most studies investigating the effects of thermal treatments on the antioxidant capacity and total phenolic content, the results are contradictory (81). It seems that some antioxidants and phenolic compounds' concentration increase above 70°C (82). This temperature range for heat treatment is considered to have inactivating and decreasing effects on food spoilage microbiota.

4. Conclusions

Modern food consumers, who exclude dairy from their diet or want to make their nutrition more varied, can be successfully encouraged by foods providing high bioactivity and great amino acid composition. To fulfill these requirements, in our study, an egg white-based berry-flavored and collagen peptide-enriched dairy replacement was investigated. For this purpose, a central composite rotational design (CCRD) was used with two factors (mixed berries concentration and bovine collagen peptides' concentration, 1.89–23.11/100 g and 0.00 and 3.52/100 g, respectively). The effects of both factors were examined on modeled rheological parameters (τ_0, K, and n) and bioactive composition (total anthocyanin concentration, antioxidant capacity, and total polyphenolic content) by using response surface methodology.

Berries are used as a well-known source of bioactive compounds and are popular because of their sensorial attributes. They showed positive correlations and significant effects on the examined parameters. Thus, their use in higher concentrations in egg white-based beverages could provide a high quantity of bioactive compounds for consumers. Nevertheless, their sensorial characteristics (color, flavor, and taste formation) effects are popular among consumers, regardless of gender and age. For further investigations and product development, mixed berries concentrations of 12.5/100 g and 23.11/100 g (or even higher) are recommended to increase the concentration of bioactive compounds and to achieve superior sensorial attributes.

Despite this, bovine collagen peptides, which are rich in highly bioactive and digestible amino acids, had lower effects on the investigated parameters, despite this, according to the literature, their addition may have a positive effect on the retardation and expression of bioactive compounds Their use in dairy replacement products such as yogurt beverage replacements, might be a useful tool for providing higher bioactivity, and higher protein concentration, and a better amino acid composition.

The product development based on the central composite rotatable design presented and investigated in our study obtained potential opportunities to replace traditional dairy beverages with an egg white-based option. Egg white and egg white-based products could be considered cheap and environmentally friendly raw materials for further dairy analogs development, providing a higher functionality through their amino acid composition.

Data availability statement

The raw data supporting the conclusions of this article will be made available by the authors, without undue reservation.

Author contributions

AV-T contributed to the conception. AV-T and ID designed the analysis. ID carried out the statistical analysis. AV-T and RC collected data and performed the analysis. AV-T and TC wrote the first draft of the manuscript, and CN and KH contributed to manuscript revision, read, and approved the submitted version. MEl and MEn created Tables and Figures and supervised the manuscript in nutritional aspects. LF revised the draft and supervised the entire work procedure. All authors contributed to the article and approved the submitted version.

Funding

This work was supported by the ÚNKP-21-4 New National Excellence Program of the Ministry for Innovation and Technology from the source of the National Research, Development, and Innovation Fund.

Acknowledgments

We owe a great thanks to the colleagues of the Dept. of Livestock Products and Food Preservation Technology, MATE, and Capriovus Ltd. for providing their help for the experiment introduced in this study.

Conflict of interest

CN was employed by Capriovus Ltd.

The remaining authors declare that the research was conducted in the absence of any commercial or financial relationships that could be construed as a potential conflict of interest.

Publisher's note

All claims expressed in this article are solely those of the authors and do not necessarily represent those of their affiliated organizations, or those of the publisher, the editors and the reviewers. Any product that may be evaluated in this article, or claim that may be made by its manufacturer, is not guaranteed or endorsed by the publisher.

References

1. Arai S, Morinaga Y, Yoshikava T, Ichiishi E, Kiso Y, Yamazaki M, et al. Recent trends in functional food science and the industry in Japan. *Biosci Biotechnol Biochem.* (2002) 66:2017–29. doi: 10.1271/bbb.66.2017

2. Regulation (EC) No 1924/2006 of the European Parliament and of the Council of 20 December 2006 on nutrition and health claims made on foods. (2006). Available online at: http://data.europa.eu/eli/reg/2006/1924/oj/eng (accessed July 31, 2022).

3. Vergari F, Tibuzzi A, Basile G. "An Overview of the Functional Food Market: From Marketing Issues and Commercial Players to Future Demand from Life in Space.," In: Giardi MT, Rea G, Berra B, editors. *Bio-Farms for Nutraceuticals: Functional Food and Safety Control by Biosensors*. Advances in Experimental Medicine and Biology. Boston, MA: Springer US (2010). p. 308–321 doi: 10.1007/978-1-4419-7347-4_23

4. Gur J, Mawuntu M, Martirosyan D. FFC's advancement of functional food definition. *Funct Foods Health Dis.* (2018) 8:385. doi: 10.31989/ffhd.v8i7.531

5. Santini A, Cammarata SM, Capone G, Ianaro A, Tenore GC, Pani L, et al. Nutraceuticals: opening the debate for a regulatory framework. *Br J Clin Pharmacol.* (2018) 84:659–72. doi: 10.1111/bcp.13496

6. Toydemir G, Gultekin Subasi B, Hall RD, Beekwilder J, Boyacioglu D, Capanoglu E. Effect of food processing on antioxidants, their bioavailability and potential relevance to human health. *Food Chem X.* (2022) 14:100334. doi: 10.1016/j.fochx.2022.100334

7. Jimenez-Garcia SN, Guevara-Gonzalez RG, Miranda-Lopez R, Feregrino-Perez AA, Torres-Pacheco I, Vazquez-Cruz MA. Functional properties and quality characteristics of bioactive compounds in berries: Biochemistry, biotechnology, and genomics. *Food Res Int.* (2013) 54:1195–207. doi: 10.1016/j.foodres.2012.11.004

8. Del Bo' C, Martini D, Porrini M, Klimis-Zacas D, Riso P. Berries and oxidative stress markers: an overview of human intervention studies. *Food Funct.* (2015) 6:2890–2917. doi: 10.1039/C5FO00657K

9. Blanch N, Clifton PM, Keogh JB. A systematic review of vascular and endothelial function: effects of fruit, vegetable and potassium intake. *Nutr Metab Cardiovasc Dis NMCD.* (2015) 25:253–66. doi: 10.1016/j.numecd.2014.10.001

10. Vendrame S, Klimis-Zacas D. Anti-inflammatory effect of anthocyanins *via* modulation of nuclear factor-κB and mitogen-activated protein kinase signaling cascades. *Nutr Rev.* (2015) 73:348–58. doi: 10.1093/nutrit/nuu066

11. Vendrame S. Del Bo' C, Ciappellano S, Riso P, Klimis-Zacas D. Berry fruit consumption and metabolic syndrome. *Antioxidants.* (2016) 5:34. doi: 10.3390/antiox5040034

12. Benzie IFF, Choi S-W. Antioxidants in food: content, measurement, significance, action, cautions, caveats, and research needs. *Adv Food Nutr Res.* (2014) 71:1–53. doi: 10.1016/B978-0-12-800270-4.00001-8

13. Porrini M, Riso P. Factors influencing the bioavailability of antioxidants in foods: a critical appraisal. *Nutr Metab Cardiovasc Dis.* (2008) 18:647–50. doi: 10.1016/j.numecd.2008.08.004

14. de Aguiar Cipriano P, Ekici L, Barnes RC, Gomes C, Talcott ST. Pre-heating and polyphenol oxidase inhibition impact on extraction of purple sweet potato anthocyanins. *Food Chem.* (2015) 180:227–34. doi: 10.1016/j.foodchem.2015.02.020

15. Aamer RA, Amin WA, Attia RS. Enhancement of color stability in strawberry nectar during storage. *Ann Agric Sci.* (2021) 66:121–30. doi: 10.1016/j.aoas.2021.08.003

16. Fernandes A, Brás NF, Mateus N, de Freitas V. Understanding the molecular mechanism of anthocyanin binding to pectin. *Langmuir.* (2014) 30:8516–27. doi: 10.1021/la501879w

17. Eichholz I, Huyskens-Keil S, Rohn S. "Chapter 21—Blueberry Phenolic Compounds: Fruit Maturation, Ripening and Post-Harvest Effects.," In: Preedy V, editor. *Processing and Impact on Active Components in Food*. San Diego: Academic Press (2015). p. 173–180 doi: 10.1016/B978-0-12-404699-3.00021-4

18. Törrönen R, Häkkinen S, Kärenlampi S, Mykkänen H. Flavonoids and phenolic acids in selected berries. *Cancer Lett.* (1997) 114:191–2. doi: 10.1016/S0304-3835(97)04660-0

19. Yamanaka H, Okada S, Sanada H, A. multicenter, randomized, controlled study of the use of nutritional supplements containing collagen peptides to facilitate the healing of pressure ulcers. *J Nutr Intermed Metab.* (2017) 8:51–9. doi: 10.1016/j.jnim.2017.05.001

20. Varani J, Warner RL, Gharacee-Kermani M, Phan SH, Kang S, Chung JH, et al. Vitamin A antagonizes decreased cell growth and elevated collagen-degrading matrix metalloproteinases and stimulates collagen accumulation in naturally aged human skin1 | Elsevier enhanced reader. *J Invest Dermatol.* (2000) 114:480–6. doi: 10.1046/j.1523-1747.2000.00902.x

21. Marini A, Grether-Beck S, Jaenicke T, Weber M, Burki C, Formann P, et al. Pycnogenol® Effects on skin elasticity and hydration coincide with increased gene expressions of collagen type i and hyaluronic acid synthase in women. *Skin Pharmacol Physiol.* (2012) 25:86–92. doi: 10.1159/000335261

22. Rao MA. Rheology of liquid foods—a review1. *J Texture Stud.* (1977) 8:135–68. doi: 10.1111/j.1745-4603.1977.tb01173.x

23. Speers RA, Tung MA. Concentration and temperature dependence of flow behavior of xanthan gum dispersions. *J Food Sci.* (1986) 51:96–8. doi: 10.1111/j.1365-2621.1986.tb10844.x

24. Kezwoń A, Chromińska I, Fraczyk T, Wojciechowski K. Effect of enzymatic hydrolysis on surface activity and surface rheology of type I collagen. *Colloids Surf B Biointerfaces.* (2016) 137:60–9. doi: 10.1016/j.colsurfb.2015.05.017

25. Kadler KE, Baldock C, Bella J, Boot-Handford RP. Collagens at a glance. *J Cell Sci.* (2007) 120:1955–8. doi: 10.1242/jcs.03453

26. Kasotakis E, Mitraki A. Designed self-assembling peptides as templates for the synthesis of metal nanoparticles. *Methods Mol Biol Clifton NJ.* (2013) 996:195–202. doi: 10.1007/978-1-62703-354-1_11

27. Yang Y, Dicko C, Bain CD, Gong Z, Jacobs RMJ, Shao Z, et al. Behavior of silk protein at the air–water interface. *Soft Matter.* (2012) 8:9705–12. doi: 10.1039/c2sm26054a

28. Punitha V, Raman SS, Parthasarathi R, Subramanian V, Rao JR, Nair BU, et al. Molecular dynamics investigations on the effect of D amino acid substitution in a triple-helix structure and the stability of collagen. *J Phys Chem B.* (2009) 113:8983–92. doi: 10.1021/jp808690m

29. Li C, Tian H, Duan L, Tian Z, Li G. Characterization of acylated pepsin-solubilized collagen with better surface activity. *Int J Biol Macromol.* (2013) 57:92–8. doi: 10.1016/j.ijbiomac.2013.02.021

30. Cabra V, Arreguin R, Vazquez-Duhalt R, Farres A. Effect of alkaline deamidation on the structure, surface hydrophobicity, and emulsifying properties of the Z19 alpha-zein. *J Agric Food Chem.* (2007) 55:439–45. doi: 10.1021/jf061002r

31. Dexter AF, Middelberg APJ. Peptides as functional surfactants. *Ind Eng Chem Res.* (2008) 47:6391–8. doi: 10.1021/ie800127f

32. Xu Q, Hong H, Wu J, Yan X. Bioavailability of bioactive peptides derived from food proteins across the intestinal epithelial membrane: a review. *Trends Food Sci Technol.* (2019) 86:399–411. doi: 10.1016/j.tifs.2019.02.050

33. Zhang Z, Wang J, Ding Y, Dai X, Li Y. Oral administration of marine collagen peptides from Chum Salmon skin enhances cutaneous wound healing and angiogenesis in rats. *J Sci Food Agric.* (2011) 91:2173–9. doi: 10.1002/jsfa.4435

34. Mei F, Liu J, Wu J, Duan Z, Chen M, Meng K, et al. Collagen peptides isolated from *salmo salar* and *tilapia nilotica* skin accelerate wound healing by altering cutaneous microbiome colonization *via* upregulated NOD2 and BD14. *J Agric Food Chem.* (2020) 68:1621–33. doi: 10.1021/acs.jafc.9b08002

35. Song H, Zhang S, Li B. Ingestion of collagen peptides prevents bone loss and improves bone microarchitecture in chronologically aged

mice—Science Direct. *J Funct Foods.* (2019). 52:1–7. doi: 10.1016/j.jff.2018.10.026

36. Lee EJ, Hur J, Ham SA, Jo Y, Lee S, Choi M-J, et al. Fish collagen peptide inhibits the adipogenic differentiation of preadipocytes and ameliorates obesity in high fat diet-fed mice. *Int J Biol Macromol.* (2017) 104:281–6. doi: 10.1016/j.ijbiomac.2017.05.151

37. O'Keeffe MB, Norris R, Alashi MA, Aluko RE, FitzGerald RJ. Peptide identification in a porcine gelatin prolyl endoproteinase hydrolysate with angiotensin converting enzyme (ACE) inhibitory and hypotensive activity. *J Funct Foods.* (2017) 34:77–88. doi: 10.1016/j.jff.2017.04.018

38. Mei F, Duan Z, Chen M, Lu J, Zhao M, Li L, et al. Effect of a high-collagen peptide diet on the gut microbiota and short-chain fatty acid metabolism. *J Funct Foods.* (2020) 75:104278. doi: 10.1016/j.jff.2020.104278

39. Blachier F, Beaumont M, Portune KJ, Steuer N, Lan A, Audebert M, et al. High-protein diets for weight management: Interactions with the intestinal microbiota and consequences for gut health. A position paper by the my new gut study group. *Clin Nutr.* (2019) 38:1012–22. doi: 10.1016/j.clnu.2018.09.016

40. Joint FAO/WHO/UNU Expert Consultation on Protein and Amino Acid Requirements in Human Nutrition 2002 : Geneva S, Nations F and AO of the U, Organization WH, University UN. Protein and amino acid requirements in human nutrition : report of a joint FAO/WHO/UNU expert consultation. World Health Organization (2007). xi, 265 p. Available online at: https://apps.who.int/iris/handle/10665/43411 (accessed August 1, 2022).

41. Markets R. *Global Collagen Peptides Market Report 2021: Market to Reach $822.9 Million by 2027 - Functional Foods and Immune Boosters Gain Prominence. GlobeNewswire News Room.* (2021). Available online at: https://www.globenewswire.com/en/news-release/2021/08/26/2286933/28124/en/Global-Collagen-Peptides-Market-Report-2021-Market-to-Reach-822-9-Million-by-2027-Functional-Foods-and-Immune-Boosters-Gain-Prominence.html (accessed August 1, 2022).

42. Lacerda Sanches V, Alves Peixoto RR, Cadore S. Phosphorus and zinc are less bioaccessible in soy-based-beverages in comparison to bovine milk. *J Funct Foods.* (2020) 65:103728. doi: 10.1016/j.jff.2019.103728

43. Silanikove N, Leitner G, Merin U. The interrelationships between lactose intolerance and the modern dairy industry: global perspectives in evolutional and historical backgrounds. *Nutrients.* (2015) 7: 7312–31. doi: 10.3390/nu7095340

44. Ugidos-Rodríguez S, Matallana-González MC, Sánchez-Mata MC. Lactose malabsorption and intolerance: a review. *Food Funct.* (2018) 9:4056–68. doi: 10.1039/C8FO00555A

45. Flom JD, Sicherer SH. Epidemiology of cow's milk allergy. *Nutrients.* (2019) 11:1051. doi: 10.3390/nu11051051

46. Jo J, Garssen J, Knippels L, Sandalova E. Role of cellular immunity in cow's milk allergy: pathogenesis, tolerance induction, and beyond. *Mediators Inflamm.* (2014) 2014:1–10. doi: 10.1155/2014/249784

47. Seves SM, Verkaik-Kloosterman J, Biesbroek S, Temme EH. Are more environmentally sustainable diets with less meat and dairy nutritionally adequate? *Public Health Nutr.* (2017) 20:2050–62. doi: 10.1017/S1368980017000763

48. Avirineni BS, Singh A, Zapata RC, Phillips CD, Chelikani PK. Dietary whey and egg proteins interact with inulin fiber to modulate energy balance and gut microbiota in obese rats. *J Nutr Biochem.* (2022) 99:108860. doi: 10.1016/j.jnutbio.2021.108860

49. Dávalos A, Miguel M, Bartolomé B, López-Fandino R. Antioxidant activity of peptides derived from egg white proteins by enzymatic hydrolysis. *J Food Prot.* (2004) 67:1939–44. doi: 10.4315/0362-028X-67.9.1939

50. You S-J, Udenigwe CC, Aluko RE, Wu J. Multifunctional peptides from egg white lysozyme. *Food Res Int.* (2010) 43:848–55. doi: 10.1016/j.foodres.2009.12.004

51. Albenzio M, Santillo A, Caroprese M, Della Malva A, Marino R. Bioactive peptides in animal food products. *Foods.* (2017)6:35. doi: 10.3390/foods6050035

52. ToTu beverage egg white product|capriovus. Available online at: https://capriovus.eu/en/totu-beverage-egg-white-product/ (accessed July 27, 2022).

53. Wang J, Chi Y, Cheng Y, Zhao Y. Physicochemical properties, in vitro digestibility and antioxidant activity of dry-heated egg white protein. *Food Chem.* (2018) 246:18–25. doi: 10.1016/j.foodchem.2017.10.128

54. Yuan S. Ming-wei L, Qi-qiang H, Larsson SC. Egg, cholesterol and protein intake and incident type 2 diabetes mellitus: Results of repeated measurements from a prospective cohort study. *Clin Nutr.* (2021) 40:4180–6. doi: 10.1016/j.clnu.2021.01.041

55. Bayram HM, Ozturkcan A. Added sugars and non-nutritive sweeteners in the food supply: Are they a threat for consumers? *Clin Nutr ESPEN.* (2022) 49:442–8. doi: 10.1016/j.clnesp.2022.03.006

56. Moyer RA, Hummer KE, Finn CE, Frei B, Wrolstad RE. Anthocyanins, phenolics, and antioxidant capacity in diverse small fruits: vaccinium, rubus, and ribes. *J Agric Food Chem.* (2002) 50:519–25. doi: 10.1021/jf011062r

57. Hidas KI, Németh C, Nguyen LLP, Visy A, Tóth A, Barkó A, et al. Effect of cryogenic freezing on the rheological and calorimetric properties of pasteurized liquid egg yolk. *Czech J Food Sci.* (2021) 39:181–8. doi: 10.17221/37/2021-CJFS

58. Ahmed J. "Chapter 15 - Rheological Properties of Gelatin and Advances in Measurement.," *Advances in Food Rheology and its Applications*. Woodhead Publishing Series in Food Science, Technology and Nutrition. Woodhead Publishing (2017). p. 377–404 doi: 10.1016/B978-0-08-100431-9.00015-2

59. Ahmed J, Ptaszek P, Basu S. "Chapter 1 - Food Rheology: Scientific Development and Importance to Food Industry.," *Advances in Food Rheology and its Applications*. Woodhead Publishing Series in Food Science, Technology and Nutrition. Woodhead Publishing (2017). p. 1–4 doi: 10.1016/B978-0-08-100431-9.00001-2

60. Herschel WH, Bulkley R. Konsistenzmessungen von Gummi-Benzollösungen. *Kolloid-Z.* (1926) 39:291–300. doi: 10.1007/BF01432034

61. Lee J, Durst RW, Wrolstad RE. Collaborators: determination of total monomeric anthocyanin pigment content of fruit juices, beverages, natural colorants, and wines by the pH differential method: collaborative study. *J AOAC Int.* (2005) 88:1269–78. doi: 10.1093/jaoac/88.5.1269

62. Taghavi T, Patel H, Akande OE, Galam DCA. Total anthocyanin content of strawberry and the profile changes by extraction methods and sample processing. *Foods.* (2022) 11:1072. doi: 10.3390/foods11081072

63. Moure A, Pazos M, Medina I, Domínguez H, Parajó JC. Antioxidant activity of extracts produced by solvent extraction of almond shells acid hydrolysates. *Food Chem.* (2007) 101:193–201. doi: 10.1016/j.foodchem.2006.01.017

64. Carletti A, Cardoso C, Lobo-Arteaga J, Sales S, Juliao D, Ferreira I, et al. Antioxidant and anti-inflammatory extracts from sea cucumbers and tunicates induce a pro-osteogenic effect in *Zebrafish Larvae*. *Front Nutr.* (2022) 9:833. doi: 10.3389/fnut.2022.888360

65. Rumbaoa RGO, Cornago DF, Geronimo IM. Phenolic content and antioxidant capacity of Philippine sweet potato (*Ipomoea batatas*) varieties. *Food Chem.* (2009) 113:1133–8. doi: 10.1016/j.foodchem.2008.08.088

66. Musilova J, Lidikova J, Vollmannova A, Frankova H, Urminska D, Bojnanska T. Toth T. Influence of heat treatments on the content of bioactive substances and antioxidant properties of sweet potato *(Ipomoea batatas L). Tubers J Food Qual.* (2020) 2020:e8856260. doi: 10.1155/2020/8856260

67. Box GEP, Draper NR. *Empirical Model-Building and Response Surfaces*. New York: Wiley. (1987).

68. Holdsworth SD. Applicability of rheological models to the interpretation of flow and processing behaviour of fluid food products. *J Texture Stud.* (1971) 2:393–418. doi: 10.1111/j.1745-4603.1971.tb00589.x

69. Glicksman M. *Gum Technology in the Food Industry*. Cambridge: Academic Press (1969).

70. Wang H, Wang CN, Guo MR. Effects of addition of strawberry juice pre- or postfermentation on physiochemical and sensory properties of fermented goat milk. *J Dairy Sci.* (2019) 102:4978–88. doi: 10.3168/jds.2018-15750

71. Penna ALB, Sivieri K, Oliveira MN. Relation between quality and rheological properties of lactic beverages. *J Food Eng.* (2001) 49:7–13. doi: 10.1016/S0260-8774(00)00179-5

72. Dogaru DV, Poiana M-A, Mateescu C, Moigradean D, Stoin D, Costescu C, et al. Rheological behavior of some berry milk-based-beverages with enhanced functionality. *J Agroaliment Process Technol.* (2014) 20:376–82. Available online at: https://www.semanticscholar.org/paper/Rheological-behavior-of-some-berry-milk-based-with-Dogaru-Poiana/0f5e006a7a4abff750e0bdc232d9091dc6a4e1c0

73. Domagala J, Sady M, Grega T, Bonczar G. The influence of storage time on rheological properties and texture of yoghurts with the addition of oat-maltodextrin as the fat substitute. *Int J Food Prop.* (2005) 8:395–404. doi: 10.1081/JFP-200059497

74. Koca I, Karadeniz B. Antioxidant properties of blackberry and blueberry fruits grown in the black sea region of turkey. *Sci Hortic.* (2009) 121:447–50. doi: 10.1016/j.scienta.2009.03.015

75. Trigueros L, Wojdyło A. Sendra E. Antioxidant activity and protein–polyphenol interactions in a pomegranate *(Punica granatum L). Yogurt J Agric Food Chem.* (2014) 62:6417–25. doi: 10.1021/jf501503h

76. Raikos V, Ni H, Hayes H, Ranawana V. Antioxidant properties of a yogurt beverage enriched with salal (*Gaultheria shallon*) berries and blackcurrant (*Ribes nigrum*) Pomace during Cold Storage. *Beverages.* (2019) 5:2. doi: 10.3390/beverages5010002

77. Mustafa AM, Angeloni S, Abouelenein D, Acquaticci L, Xiao J, Sagratini G, et al. new HPLC-MS/MS method for the simultaneous determination of 36 polyphenols in blueberry, strawberry and their commercial products and determination of antioxidant activity. *Food Chem.* (2022) 367:130743. doi: 10.1016/j.foodchem.2021.130743

78. Wang H, Cao G, Prior RL. Total antioxidant capacity of fruits. *J Agric Food Chem.* (1996) 44:701–5. doi: 10.1021/jf950579y

79. Rojas-Ocampo E, Torrejón-Valqui L, Muñóz-Astecker LD, Medina-Mendoza M, Mori-Mestanza D, Castro-Alayo EM. Antioxidant capacity, total phenolic content and phenolic compounds of pulp and bagasse of four Peruvian berries. *Heliyon.* (2021) 7:e07787. doi: 10.1016/j.heliyon.2021.e07787

80. Žlabur JŠ, Mikulec N, DoŽdor L, Duralija B, Galić A, Voća S. Preservation of biologically active compounds and nutritional potential of quick-frozen berry fruits of the genus rubus. *Processes.* (2021) 9:1940. doi: 10.3390/pr9111940

81. Yazdizadeh Shotorbani N, Jamei R, Heidari R. Antioxidant activities of two sweet pepper *Capsicum annuum L.* varieties phenolic extracts and the effects of thermal treatment Avicenna. *J Phytomedicine.* (2013) 3:25–34. Available online at: https://pubmed.ncbi.nlm.nih.gov/25050256/

82. López J, Uribe E, Vega-Gálvez A, Miranda M, Vergara J, Gonzalez E, et al. Effect of air temperature on drying kinetics, vitamin C, antioxidant activity, total phenolic content, non-enzymatic browning and firmness of blueberries variety O'Neil. *Food Bioprocess Technol.* (2010) 3:772–7. doi: 10.1007/s11947-009-0306-8

Frontiers in Nutrition

Explores what and how we eat in the context of health, sustainability and 21st century food science

A multidisciplinary journal that integrates research on dietary behavior, agronomy and 21st century food science with a focus on human health.

Discover the latest Research Topics

See more →

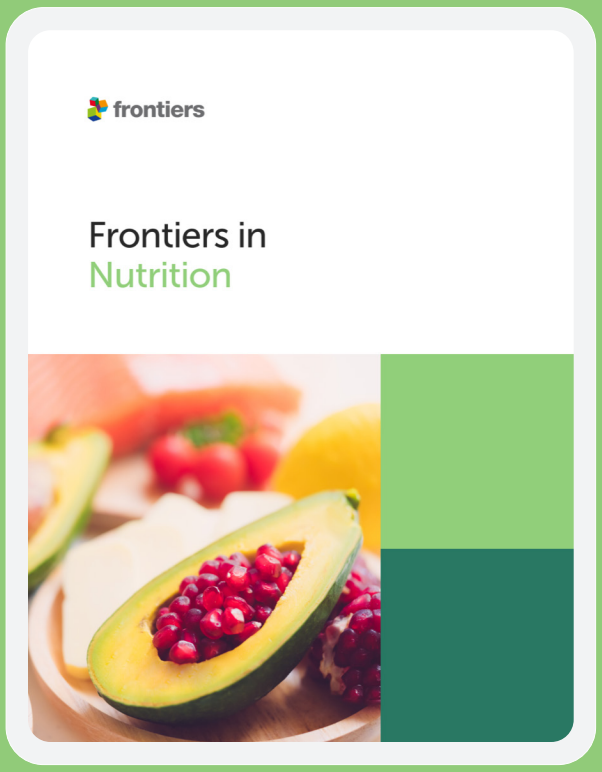

Frontiers

Avenue du Tribunal-Fédéral 34
1005 Lausanne, Switzerland
frontiersin.org

Contact us

+41 (0)21 510 17 00
frontiersin.org/about/contact